



Dipl.-Ing. David Steyrl

**Improving the quality of the
electroencephalogram
simultaneously recorded with
functional magnetic resonance
imaging**

Dissertation

at

Graz University of Technology

Supervisor

Univ.-Prof. Dipl.-Ing. Dr.techn. Gernot R. Müller-Putz

Institute of Neural Engineering

Faculty of Computer Science and Biomedical Engineering

Graz, October 2018

Eidensstattliche Erklärung

Affidavit

Ich erkläre an Eides statt, dass ich die vorliegende Arbeit selbständig verfasst, andere als die angegebenen Quellen/Hilfsmittel nicht benutzt, und die den benutzten Quellen wörtlich und inhaltlich entnommenen Stellen als solche kenntlich gemacht habe. Das in TUGRAZonline hochgeladene Textdokument ist mit der vorliegenden Dissertation identisch.

I declare that I have authored this thesis independently, that I have not used other than the declared sources/resources, and that I have explicitly indicated all material which has been quoted either literally or by content from the sources used. The text document uploaded to the TUGRAZonline is identical to the present doctoral dissertation.

15.10.2018

Datum / Date



Unterschrift / Signature

Acknowledgments

At this place I want to thank all the people who directly or indirectly helped and supported me to finish this thesis.

Gernot, for your trust in me and my abilities to do a PhD, for your guidance, support and patience throughout the years, for the discussions we had, and for the years I was allowed to work as your assistant.

Reini, for infecting me with the “science virus” during my Master’s, for insightful comments and encouragement, for conversations on music, and above all on “*life, the universe and everything*”.

Josef and **Martin**, for the great time with you sharing an office, for feedback on the work, for productive discussions on more than only work, and also for the time out of office.

A special gratitude goes to everyone working and studying at the BCI lab, for sharing a great time and many hours of fruitful discussion. I wish you all the best for your research!

Mum, Dad, Matthias, and all my friends, simply for being there and for providing moral and emotional support in my life. It is important to know that there is always a place for oneself.

The Graz and the Vienna “Das Schwarze Auge” groups for many hours of joyful playing, and for listening to my PhD stories.

Dearest **Margarita**, for becoming part of my life, for helping me endure, and for enduring me in the more difficult moments.

Thank you so much!

Abstract

The concurrent recording of the electroencephalogram (EEG) with functional magnetic resonance imaging (fMRI) allows the simultaneous study of the electrophysiology, the blood oxygen level dependent signal, and particularly also their interplay. However, the EEG is affected by a large number of fMRI-related, partly repetitive, artifacts. Average artifact subtraction (AAS) – the most frequently used artifact reduction technique – computes artifact templates from artifact repetitions and subtracts them from the EEG. This effectively reduces repetitive, invariant artifacts, but serious artifact residuals remain. Therefore, this thesis pursued two objectives: analysis of the artifact residuals and development of a new technique for the reduction of the residuals.

The inherent variability of artifacts is known to cause residuals after the AAS method, because the subtraction template does not fit the actual artifact. In this thesis, an additional cause of artifact residuals was identified. An intrinsic vulnerability of the AAS technique to correlated artifacts leads to artifact contaminated subtraction templates and consequently to artifact residuals in the EEG. The new artifact reduction technique uses recordings of artifact residuals from a reference-layer EEG cap combined with adaptive filtering to remove the residuals from the EEG and is referred to as reference-layer adaptive filtering (RLAF). The RLAF method is highly effective in offline and online application scenarios. It improves the signal-to-noise-ratio as well as the classification accuracy of physiological EEG components substantially. The RLAF technique's ability to reduce all kinds of artifact residuals – including non-stationary and varying components – in combination with its easy handling, makes it a candidate for a future gold standard method.

Kurzfassung

Die simultane Aufzeichnung des Elektroenzephalograms (EEG) mit funktioneller Magnetresonanztomographie (fMRT) ermöglicht eine gleichzeitige Untersuchung der Elektrophysiologie, des blutsauerstoffabhängigen Signals und vor allem deren Zusammenspiel. Allerdings ist das EEG von einer Vielzahl von teilweise sich wiederholenden, fMRT-bezogenen Artefakten betroffen. Average Artifact Subtraction (AAS) – die am häufigsten verwendete Technik zur Artefaktreduktion – berechnet Artefaktvorlagen aus Artefaktwiederholungen und subtrahiert sie vom EEG. Diese Methode reduziert repetitive, invariante Artefakte effektiv, aber es bleiben gravierende Artefaktreste zurück. Diese Arbeit verfolgte daher zwei Ziele: Die Analyse der Artefaktreste und die Entwicklung einer neuen Technik zur Reduktion der Artefaktresiduen.

Die inhärente Variabilität von Artefakten ist bekannt Artefaktresiduen nach der AAS-Methode zu verursachen, da die Subtraktionsschablone nicht zum eigentlichen Artefakt passt. In dieser Arbeit wurde eine zusätzliche Ursache für Artefaktreste identifiziert. Eine intrinsische Anfälligkeit der AAS-Technik gegenüber korrelierten Artefakten führt zu artefaktkontaminierten Subtraktionsvorlagen und damit zu Artefaktresiduen im EEG. Die neue Artefaktreduktionstechnik verwendet Messungen der Artefaktreste aus einer Referenzschicht EEG Kappe kombiniert mit adaptiver Filterung, um die Artefaktresiduen aus dem EEG zu entfernen und wird als Reference-Layer Adaptive Filtering (RLAF) bezeichnet. Die RLAF-Methode ist sowohl in Offline- und als auch in Online-Anwendungsszenarien sehr effektiv. Das Signal-Rausch-Verhältnis sowie die Klassifikationsgenauigkeit der physiologischen EEG-Komponenten werden deutlich verbessert. Die Fähigkeit, alle Arten von Rückständen – auch nicht stationäre und variable Komponenten – zu reduzieren, in Kombination mit seiner einfachen Handhabung, macht die RLAF-Technik zu einem Kandidaten für eine zukünftige Goldstandard-Methode.

Contents

1 Introduction.....	1
1.1 The challenge of understanding the human brain.....	2
1.2 Functional neuroimaging.....	3
1.3 Multimodal neuroimaging.....	6
1.4 Simultaneous EEG-fMRI.....	8
1.5 Artifacts in simultaneous EEG-fMRI.....	12
1.6 State-of-the-art in artifact reduction.....	18
1.7 Motivation, aim and structure of this thesis.....	25
2 Materials and methods.....	27
2.1 Primary publication 1: Artifacts in EEG of simultaneous EEG-fMRI: Pulse artifact remainders in the gradient artifact template are a source of artifact residuals after average artifact subtraction.....	28
2.1.1 Introduction.....	29
2.1.2 Methods.....	32
2.1.3 Results.....	36
2.1.4 Discussion.....	39
2.2 Primary publication 2: Reduction of EEG Artifacts in Simultaneous EEG- fMRI: Reference Layer Adaptive Filtering (RLAF).....	44
2.3 Primary publication 3: Reference layer adaptive filtering (RLAF) for EEG artifact reduction in simultaneous EEG-fMRI.....	46
2.4 Primary publication 4: Online reduction of artifacts in EEG of simultane- ous EEG-fMRI using reference layer adaptive filtering (RLAF).....	48
2.5 Secondary publication: Single trial Motor Imagery classification in EEG measured during fMRI image acquisition – a first glance.....	50
3 Discussion.....	51
3.1 Overview.....	52
3.2 Remaining artifacts after applying the AAS technique.....	52

3.3 From remaining artifacts to reference-layer adaptive filtering.....	53
3.4 The reference-layer EEG cap prototypes.....	54
3.5 Reference-layer adaptive filtering in action and its relation to the state-of-the-art.....	55
3.6 Summary and Conclusions.....	57
3.7 Outlook.....	57
4 References.....	59
5 Appendix.....	81
5.1 Publications.....	82
5.2 CV.....	130

List of Figures

1.1 Local blood flow changes during neural activity.....	4
1.2 Sketch of the EEG source.....	6
1.3 Spatial and temporal resolution of neuroimaging methods.....	7
1.4 The gradient artifact in time and frequency domain.....	14
1.5 The pulse artifact in time and frequency domain.....	15
1.6 Schematics of adaptive filters.....	23
1.7 Spectra of EEG recorded inside and outside an MRI scanner.....	26
2.1 Spectra of EEG recorded in lab and inside an MRI scanner.....	32
2.2 Artificial EEG component.....	34
2.3 Artificial gradient artifact component.....	35
2.4 Artificial pulse artifact component.....	36
2.5 Comparison of the artificial EEG with the reconstructed.....	37
2.6 Comparison of the spectra of the artificial EEG with the reconstructed.....	38
2.7 Reference-layer EEG cap prototype.....	45
2.8 Signal processing of the different evaluation settings.....	47
2.9 Representative example of visually evoked potentials.....	49
2.10 Sensory-motor rhythm patterns in the EEG.....	50

Acronyms

AAS	average artifact subtraction
BCI	brain-computer interface
BOLD	blood-oxygenation-level-dependent
ECG	electrocardiography
EEG	electroencephalography
EPI	echo planar imaging
FASTR	fMRI artifact slice template removal
fMRI	functional magnetic resonance imaging
GA	gradient artifact
HPA	helium pump artifact
ICA	independent component analysis
LMS	least mean square
MA	motion artifact
MBRLAF	multi band reference-layer adaptive filtering
MRI	magnetic resonance imaging
PA	pulse artifact
PCA	principal component analysis
PET	positron emission tomography
RF	radio frequency
RLAF	reference-layer adaptive filtering
RLAS	reference-layer artifact subtraction
SNR	signal-to-noise-ratio
TR	time of repetition
VA	ventilation artifact

1 Introduction

“Everything we do, every thought we’ve ever had, is produced by the human brain. But exactly how it operates remains one of the biggest unsolved mysteries, and it seems the more we probe its secrets, the more surprises we find.”

– Neil de Grasse Tyson

1.1 The challenge of understanding the human brain

The brain is a fascinating organ. It serves as the center of the nervous system in most higher developed animals as well as in humans. It is capable of generating sophisticated purposeful control signals that allow quick and coordinated reactions to complex stimuli, even in situations never experienced before. These reactions are commonly summarized under the term behavior (Vargas 2015). However, the brain is not limited to reactions. The brain stores the outcomes of its behavior in order to generate models of stimuli-behavior-outcomes experiences. With these models, the brain anticipates possible outcomes and actively adapts its behavior to achieve desired outcomes. At the same time, the brain adapts the models that are used for this prediction. These adaptations to anticipated outcomes lead to non-causal behavior, since the behavior is influenced by outcomes that never take place (vonGlaserfeld 1995).

The complex non-causal behavior of humans is very hard to probe. To allow any investigations, scientists often divide behavior into individual cognitive tasks, for instance visual recognition, action selection, or motor control. Neuroscience is the discipline that studies the brain on various levels to understand how the brain processes cognitive tasks (Kandel 2013). The ultimate goal of neuroscience is to develop a comprehensive understanding of the human brain that encompasses all facets of human behavior. Although neuroscience has made considerable progress in many directions in recent decades, this goal has not yet been achieved (Adolphs 2015, Lisman 2015).

The incredible complexity of the human brain poses a serious obstacle to this goal (DeFelipe 2015). The human brain consists of approximately $1.9-2.6 \times 10^{10}$ neocortical neurons and $2.8-3.9 \times 10^{10}$ glial cells (Pakkenberg 2001, Pelvig 2008). Every neocortical neuron forms a large number of synapses to contact other neurons. On average, the human brain has approximately 1.64×10^{14} synapses (Tang 2001). For comparison, our galaxy – the milky way – consists of approximately 1×10^{12} stars only (Odenwald 2017). Due to this tremendous complexity, it is nowadays impossible to measure every single brain cell activity and to construct a model that includes all of these activities. However, it is possible to measure the activity of a very limited number of neurons or to measure the aggregated activity of brain areas by applying functional neuroimaging techniques (Raichle 1998, Shibasaki 2008).

Consequently, the challenge is to understand an incredibly complex organ that exhibits non-causal cognitive functions while only very limited information about its activity is accessible.

1.2 Functional neuroimaging

First theories about how the human brain processes tasks were developed through studies of the brain's anatomy or in particular, through studies of anatomical abnormalities of the brain. It was found that the same brain lesions can lead to the same cognitive deficits, for instance lesions in a certain brain area – the Broca's area – were associated with a loss of the speech ability (Dronkers 2007).

One step further was to probe the active human brain. The term functional neuroimaging refers to a wide range of techniques that image the activity of human brains in vivo (Cabeza 2001). Functional neuroimaging research started more than 130 years ago. It is assumed that Angelo Mosso, a versatile Italian researcher, was the first who developed a functional neuroimaging technique (Sandrone 2014). He invented the plethysmograph, a device that measures cerebral blood flow variations by capturing brain pulsations in volunteers with skull defects (Cabeza 2001). He observed that these pulsations increased regionally during cognitive tasks and he formulated the idea that a cognitive task can locally change the blood flow in the brain (Raichle 1998).

Nowadays, this relationship is referred to as neurovascular coupling (Girouard 2006). Cognitive tasks are processed by neurons and the processing requires energy. Different cognitive tasks require different processing and, thus, consume different amounts of energy. Therefore, the brain must adapt its local energy supply to the cognitive task. One parameter that is controlled to achieve the adaptation of the supply is the local cerebral blood flow (Kandel 2013, Iadecola 2017). Although the existence of the blood flow adaptation is not doubted, its cellular basis is largely unclear (Raichle 1998). The local blood flow adaptation serves as basis for a group of neuroimaging techniques, with functional magnetic resonance imaging (fMRI) being the most popular representative (Ogawa 1990, Raichle 1998, Norris 2006, Otte 2006, Shibasaki 2008). The fMRI concept builds on the shift in relative blood oxygenation due to the blood flow adaptation. A higher blood flow comes along with a higher relative oxygenation of the blood (Figure 1.1). Generally, MRI use a strong static magnetic field to align nuclei in the tissue of interested that show a magnetic moment (e.g. Hydrogen atoms). Two dynamic magnetic fields – the gradient field and the radio frequency (RF) field – are used to spatially locate nuclei and to temporary disturb the alignment of the nuclei. After removing the RF field, the nuclei realign because of the static magnetic field. The duration of realignment is depending on the tissue that surrounds the nuclei and can be used to compute a picture of the tissue (Huetzel 2004). It was found that blood exhibits different magnetic properties depending on its oxygenation state. Oxygenated blood is diamagnetic (repelled by a magnetic field) and deoxygenated blood is paramagnetic (attracted by a magnetic field). The

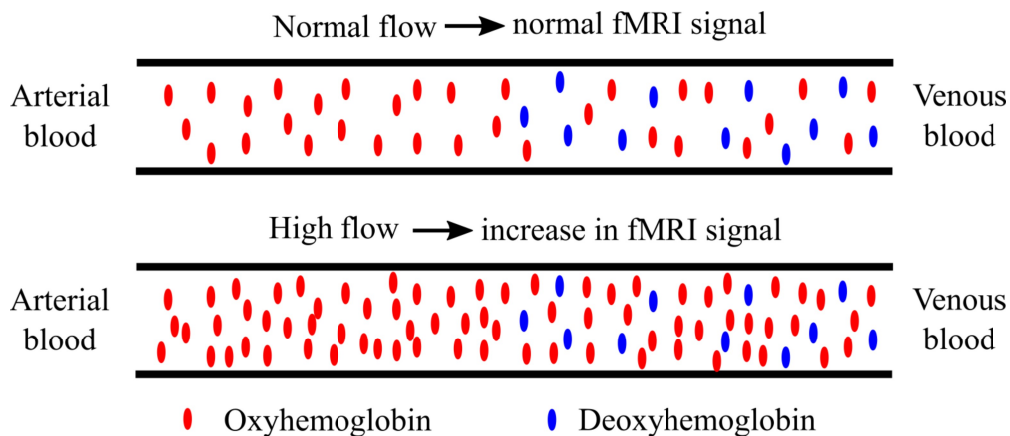


Figure 1.1: The local blood flow increases during neuronal activity while oxygen consumption stays approximately constant. As a consequence, the relative blood oxygenation of the venous blood is elevated, resulting in an increase in the MRI signal (adapted from Ogawa 1990).

duration of nuclei realignment is therefore also depending on the local relative blood oxygenation as the diamagnetic blood interferes less with the MR signal. Removing the tissue related MRI signal leads to a blood-oxygenation-level-dependent (BOLD) signal (Figure 1.1), i.e. a signal that reflects neural activity via the mechanism of neurovascular coupling (Ogawa 1990, Huettel 2004).

Another important non-invasive neuroimaging technique that bases on neurovascular coupling is functional near infrared spectroscopy (Joebsis 1977, Ferrari 2012). This technique makes use of differences in light dispersion between oxygenated and deoxygenated blood to measure a neural activity related signal (Shin 2016).

A second group of neuroimaging techniques directly utilize the change in energy consumption to image brain activity (Otte 2006). One popular example of that group is positron emission tomography (PET) (Reivich 1979, Otte 2006). PET uses radioactively labeled glucose to trace changes in glucose consumption. This changes in energy consumption are directly related to brain activity, as glucose is the main source of energy in neurons (Reivich 1979).

The neurovascular coupling based methods as well as the energy consumption based techniques rely on indirect measurements of brain activity, since they measure changes in the metabolism. The actual processing of a cognitive tasks, however, is performed electro-chemically by neurons (Kandel 2013). The direct measurement of electrical potentials serves as basis for another group of neuroimaging techniques. These techniques measure the electrical potentials at different levels with a high temporal resolution. Micro-electrode arrays with many small pin electrodes on an area of approximately $3 \times 3 \text{ mm}^2$ are used to record action potentials as well as local extracellular potential changes directly in the brain tissue at neuron level (Cheung 2007). In electrocorticography, electrodes are placed one level above, on the exposed surface

of the brain or on top of the dura. This technique measures the aggregated electrical activity of a brain area of approximately $4 \times 4 \text{ mm}^2$ per electrode (Miller 2007). Finally, electroencephalography (EEG) captures electrical potentials non-invasively at scalp level (Niedermeyer 2005). The electro-chemical activity of neurons generates ionic membrane currents. The membrane currents in turn cause local extracellular potential changes in the brain tissue. The superposition of the potentials is termed local field potential. The local field potentials finally form the scalp potentials measured by the EEG (Buzsáki 2012). However, the local field potentials cannot be measured directly, only a modified version of the local field potentials propagates to the scalp level (Buzsáki 2012). The modification has at least two causes: firstly, the electric field decays with the square of the distance. Therefore, the local field potentials are subject to substantial attenuation until they reach the electrodes at the scalp; secondly, volume conduction of the head tissues (brain, cerebral fluid, skull, scalp) cause spatial smoothing over an area of some cm^2 (Buzsáki 2012). Due to the attenuation and smoothing, only synchronous and spatially aligned local field potentials, meaning electrical brain activity that sum up over brain areas, can be measured at scalp level. One prominent example is the visual alpha rhythm at 8-12 Hz that occurs over the occipital brain areas (Niedermeyer 2005). Synchronous and spatially aligned local field potentials are mainly caused by correlated synaptic transmissions that form neural dipoles in parallel – spatially aligned – pyramidal cells (Figure 1.2) (Buzsáki 2012, Einevoll 2013). Action potentials cause synaptic transmissions, but information coded in action potential spike trains are not one-to-one equivalent to information in the local field potentials (Einevoll 2013). In fact, the connection from action potentials via synaptic transmissions to local field potentials is not entirely understood yet. Ionic trans-membrane currents can be well described by models, however, influences like the feedback of local field potentials to the activity of surrounding cells and also random effects as synaptic transport failure limit our understanding of that connection (Hodgkin 1952, Goldman 2004, Einevoll 2013). In short, action potentials of afferent fibers in the cortex can cause synaptic transmissions and as a consequence local field potentials. If the local field potentials occur synchronously and spatially aligned, as it is the case with the dipole potentials at pyramidal cells, then the sum of the local field potentials is strong enough to be measured at the scalp level. The occurring scalp potentials are referred to as EEG (Niedermeyer 2005). Initially the spatial resolution of the EEG is low, since each sensor measures the aggregated brain activity of some cm^2 . However, the resolution can be improved significantly through the application of source imaging techniques (Michel 2004, He 2011, Michel 2012).

It is also possible to directly measure the magnetic fields of the electrical brain activity at scalp level. This method is named magnetoencephalography (Williamson 1991). Magnetoencephalography uses superconducting quantum inter-

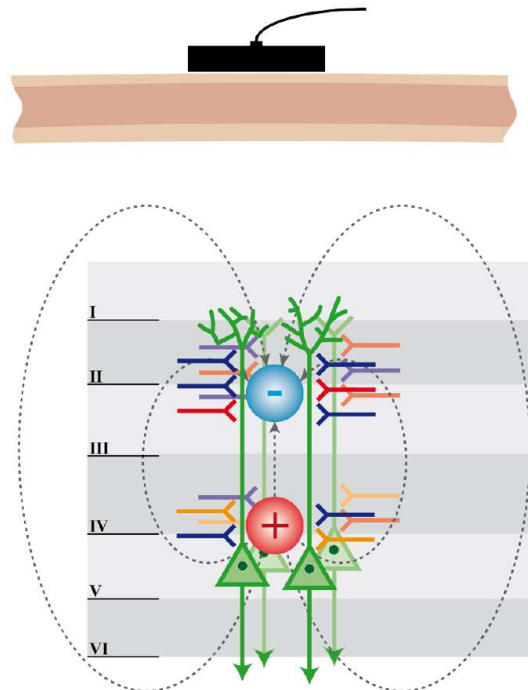


Figure 1.2: Sketch of EEG sources. I-IV mark the cortical layers. Cortical layer 5 and 6 pyramidal cells are depicted in green. The spatial and temporal dendritic integration leads to the formation of electrical dipoles. If many pyramidal neurons receive synchronous basal or apical synaptic transmissions, then the resulting electrical field propagates over large distances and is even detectable at the scalp where it is referred to as EEG (Steyrl 2016a).

ference sensors to directly measure the very small (10^1 - 10^3 fT) magnetic fields that are generated by the electrical brain activity. To determine the source of the electric field in the brain it is necessary to solve the inverse problem (Salmelin 2009).

In a nutshell, functional neuroimaging techniques are essential in neuroscience to develop a better understanding of how the brain process tasks, because they allow to study the relationships between cognitive tasks and the related activities in certain brain areas, but also to study intrinsic variations in brain activities. A variety of neuroimaging techniques based on different physiological parameters are available.

1.3 Multimodal neuroimaging

Many achievements in neuroscience of recent decades were driven by advances in functional neuroimaging techniques (Filler 2009). However, one can not expect to fully understand the function of a complex system such as the human brain by investigating changes in a single physiological parameter. Therefore, it has been proposed to probe cognitive tasks with different functional neuroimaging techniques and inte-

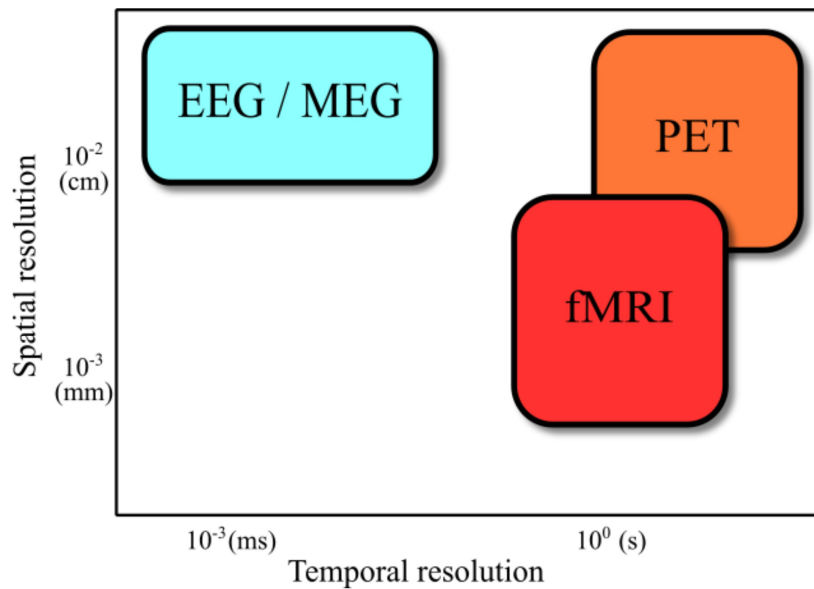


Figure 1.3: Classification of neuroimaging methods by their spatial and temporal resolution (He 2012, Sejnowski 2014).

grate the information into a comprehensive picture of the human brain activity (Mulert 2010, Uludag 2014). Each technique adds its unique view to the overall picture. For instance, functional neuroimaging techniques have different temporal and spatial resolutions (Figure 1.3). Hence, a technique with a high temporal resolution is necessary to track fast, transient brain activities, while a technique with a high spatial resolution is necessary to locate these activities.

Multimodal functional neuroimaging can be realized by a separate or a simultaneous application of two or more neuroimaging techniques (Uludag 2014). Separate means that one neuroimaging technique is used during one experiment and later, another neuroimaging technique is used during a second experiment. Often the paradigms of the two experiments are the same. Simultaneous means that the neuroimaging techniques are applied concurrently during one experiment. It depends on the research question and the data analysis techniques, whether the one or the other approach is appropriate. For instance, if it can be assumed that the brain activities of interest are stereotypical to a cognitive task and that movements of the study participants between two experiments have no influence, then a separate application of the neuroimaging techniques is sufficient. However, if the brain activity is transient and will not reoccur, for instance due to surprising effects in the experimental paradigm, then a simultaneous application of neuroimaging techniques is required (Debener 2005).

Multimodal neuroimaging requires methods to fuse the data of the different techniques into one common analysis. The challenge of the common analysis is that each neuroimaging technique acquires data in its own recording space (Uludag 2014). For

example, one technique records a time-series of data per volume and the other collect a time-series of data per surface position. In this example, the recording spaces differ in the spatial dimension (volume vs. surface), but generally they can differ in any dimension and often they differ in more than one. Therefore, various approaches have been developed to fuse the data at different levels of abstraction. Accordingly, some methods work at pure data level, others work at highly abstracted levels such as classes of performed cognitive tasks. The various approaches of data fusion methods and their selection have been the subject of books, review papers, and special issues in journals (Mulert 2010, Uludag 2014, Ritter 2006, Rosa 2010, Biessmann 2011, Huster 2012, Calhoun 2014, Dahne 2015, Abreu 2018). It is again the research question that determines the appropriate method.

Multimodal functional neuroimaging commonly involves two different techniques, particularly when they are applied simultaneously (Calhoun 2014). However, recently simultaneous trimodal neuroimaging results were published (Shah 2017, Rajkumar 2017). In theory, all combinations of functional neuroimaging techniques are possible and also the technical feasibility was demonstrated for many combinations (Ives 1993, Kleinschmidt 1996, Zotev 2008, Sadato 1998, Catana 2008, Hoshi 1994). However, some combinations of functional neuroimaging techniques are more advantageous than others. In particular, combinations that fuse neuroimaging techniques with different characteristics are favorable, because then one technique compensates disadvantages of the other and vice versa. Furthermore, such combinations avoid redundancy effects. This advantageous combinations proved their usefulness in numerous research and clinical applications (Krakow 1999, Moosmann 2003, Niessing 2005, Debener 2006, Gotman 2006, Hamandi 2006, deMuck 2007, Tiege 2007, Fazli 2012, Moeller 2013, Mulert 2013, Baumeister 2014, Kay 2014, Liu 2015, OHalloran 2016, Case 2017, Hahn 2017, Mano 2017, Nemtsas 2017, Perronnet 2017, Rausch 2017, Tarantino 2017).

In essence, multimodal functional neuroimaging integrates the information of two or more neuroimaging techniques to generate a comprehensive picture of brain activity related to cognitive tasks. The combination of neuroimaging techniques with different characteristics is beneficial to compensate weaknesses of techniques and to avoid redundancy effects.

1.4 Simultaneous EEG-fMRI

A successful multimodal functional neuroimaging technique is simultaneous EEG-fMRI, thus, the concurrent application of electroencephalography and functional magnetic resonance imaging (Mulert 2010, Laufs 2012). This combination is advantageous because the two techniques have very different characteristics. Firstly, they

differ in terms of the captured physiological parameter. The EEG measures electrical potentials at the scalp which represent summations in time and space of the electrical brain activity, whereas fMRI captures blood-oxygenation-level-dependent signals in the brain that are correlated with brain activity due to the cardiovascular coupling (Niedermeyer 2005, Ogawa 1990). Therefore, simultaneous EEG-fMRI allows comprehensive studies of the same brain activity from the electrophysiological and from the metabolic/vascular point of view, including the electrophysiological metabolic/vascular interaction (Uludag 2014, Ritter 2006). Secondly, they differ in terms of their time resolution. The EEG has a time resolution of ~ 1 ms, in contrast, the time resolution of fMRI is ~ 1 s (Horwitz 2002, Grova 2008, Michel 2012). Thirdly, EEG and fMRI also differ in terms of their spatial resolution. The raw spatial resolution of the EEG is limited to ~ 2 cm because of the volume conduction of tissue, whereas fMRI has a spatial resolution of ~ 2 mm (Grova 2008, Michel 2012). The combination of the two techniques – simultaneous EEG-fMRI – allows to investigate the temporal dynamics of brain activity through the EEG with a high temporal resolution, while fMRI can be used to locate the brain activity with a high spatial resolution.

The history of simultaneous EEG-fMRI started in the early nineties in epilepsy research with the problem of locating transient epileptic brain activity (Ives 1993). Patients with severe focal epilepsy have the option of having their epileptic brain zones removed, if no more pharmacological options are available (Grova 2008). For this purpose, it is important to determine the exact location of the epileptic zone. Unfortunately, an application of neuroimaging techniques during an epileptic seizure is hardly possible due to the occurring motions. However, epileptic spikes can occur also between seizures without producing clinical signs. These spikes are referred to as interictal spikes (Grova 2008). Interictal spikes are in general unpredictable, they can not be reliably induced by external stimuli, and they are relatively short-lived (Laufs 2012). Hence, it is necessary to detect their occurrence with a neuroimaging technique. The EEG is perfectly suited for the detection due to its high temporal resolution. However, the low spatial resolution of the EEG limits its ability to locate the epileptic zone (Grova 2008, Michel 2012). On the other hand, fMRI offers a high spatial resolution that allows to precisely locate the epileptic zone, but its temporal resolution is too low to determine the occurrence of interictal spikes (Horwitz 2002, Grova 2008). Simultaneous EEG-fMRI was introduced to close that gap (Ives 1993). After the successful demonstration of the feasibility of safe simultaneous EEG-fMRI by John Ives, Steve Warach and Franz Schmitt in 1992, it took almost 10 years until commercial systems became available, e.g. the “Opti-Link” system from Neuro Scan Labs (Charlotte, NC, U.S.A.), or the “BrainAmp MR” system from Brainproducts (Munich, Germany) (Ives 1993, Laufs 2012). Nowadays, simultaneous EEG-fMRI is applied to investigate a wide range of neuroscientific questions. Selected applications are presented below.

Simultaneous EEG-fMRI and epilepsy research

Simultaneous EEG-fMRI has been applied to patient groups – including children – with different epilepsy types in order to provide useful clinical information on the location of seizure onset zones during pre-surgical evaluations (Rosenow 2001). Feasibility studies (Gotman 2006, Hamandi 2004, Lemieux 2004, Salek-Haddadi 2002, Stern 2006) and studies that investigated cohorts of patients (Al-Asmi 2003, Krakow 1999, Patel 1999, Salek-Haddadi 2006) led to the conclusion that interictal spike correlated BOLD signals do not reliably and always reflect the epileptic sources (Laufs 2007). It seems that interictal spike correlated BOLD signals often reflect the propagation of epileptic spikes rather than their source (DeTiege 2007, Hamandi 2008, LeVan 2010). This is plausible, since the propagation of interictal spikes takes up to a few seconds and that is the same time scale as the time resolution of fMRI (Gotz-Trabert 2008, Laufs 2012). Other studies showed however, that simultaneous EEG-fMRI adds important information in pre-surgical evaluations when improved analysis methods are used (Rosenkranz 2010, Thornton 2010, Zijlmans 2007, vanGraan 2015, Bagarinao 2018). Nowadays, advanced epilepsy centers regularly include simultaneous EEG-fMRI results in their pre-surgical evaluations (vanGraan 2015).

Simultaneous EEG-fMRI and oscillatory EEG activity

In 1929, Hans Berger discovered that the EEG amplitude of occipital electrode positions changes inversely with opened and closed eyes (Berger 1929). The changes occur primarily in a narrow frequency range of 8-12 Hz. This specific amplitude change is referred to as the alpha rhythm (Niedermeyer 2005). Studies have shown that this rhythm is also present in other brain regions and that it reflects the idle state of a region (Pfurtscheller 1999, Niedermeyer 2005). The correlation of the alpha rhythm with the fMRI BOLD signal was among the first issues outside the epilepsy field that was investigated with simultaneous EEG-fMRI (Goldman 2002, Laufs 2003, Moosmann 2003). The initial results are ambiguous and partly contradictory, because both positive and negative correlations of the alpha rhythm amplitude with BOLD signals were found. Drowsiness and attention of the study participants, but also individual behavior were identified to be factors that explain the ambiguous findings (Kjaer 2002, Laufs 2006, deMuck 2008, DiFrancesco 2008, Sadaghiani 2010). Other studies investigated the effects of the alpha rhythm on evoked BOLD responses. It was discovered that the alpha rhythm is a factor that modulates evoked BOLD responses (Becker 2011, Mullinger 2017). Interestingly, this results provide evidence that the origin of the post-stimulus BOLD undershoot of evoked BOLD responses is neural and not vascular, a topic that has been discussed for years (Mullinger 2017). Further studies investigated the correlations of other EEG frequency ranges and phenomena, like the beta rhythm, the post movement beta

event-related synchronization, and the low gamma rhythm with fMRI BOLD signals (Parkes 2006, Tyvaert 2008, Pfurtscheller 1998, Ritter 2009, Scheeringa 2011, Gompf 2017, Green 2017). It was shown that the gamma rhythm is linked to enhanced neural communication, while the alpha rhythm is related to functional inhibition, supporting previous findings that were based on EEG research only (Pfurtscheller 2003, Niedermeyer 2005, Scheeringa 2011). Generally, task dependent non-linear relationships were found between EEG rhythms and fMRI BOLD signals, suggesting complex and not yet understood interactions (Gompf 2017).

Simultaneous EEG-fMRI and fMRI resting state networks

The discovery of resting state brain activity in fMRI data was controversial in the beginning, but its existence is now widely accepted and a whole new field of research has opened up (Biswal 1995, Biswal 2010, Biswal 2012). Resting state activity in the fMRI is characterized by network like interactions between brain regions and thus, the resting state activity is termed resting state networks. Several different networks have been described over the past years. For instance, one network seems to be responsible for motor control (Biswal 2012). Also, the EEG shows activity when the human brain is at rest and it is assumed that this activity has important roles, for instance, in perception and again motor control (Pfurtscheller 1999, Engel 2001). In the EEG, resting state activity is often characterized by rhythmic activity in the 8-13 Hz range, for instance the alpha rhythm at occipital head positions or the sensory motor rhythm's at the motor cortex (Berger 1929, Pfurtscheller 1999). The study of the relationship between these two resting state characterizations is another research area where simultaneous EEG-fMRI is applied. Investigations showed correlations of fMRI resting state networks with EEG rhythms and their spatial distribution, but also with the EEG-based connectome (Mantini 2007a, Jann 2010, Deligianni 2014, Tsuchimoto 2017). The results supports the neuronal origin of the resting state networks and the assumption that EEG rhythms and their topographies are electrophysiological signatures of distributed neuronal networks (Jann 2010). Abnormalities in the resting state networks were observed in several diseases, for instance in Alzheimer's disease patients. Therefore, the associations between the default mode network and occipital alpha rhythm power was investigated in early stage Alzheimer's disease patients in comparison to healthy controls (Brueggen 2017). A decrease in this correlation was found, pointing at a potential application of simultaneous EEG-fMRI in Alzheimer's disease research (Brueggen 2017).

Simultaneous EEG-fMRI and brain-computer interface research

A brain-computer interface (BCI) is a devices that translate thought correlated brain activities into commands for computers and other devices (Wolpaw 2002, Milán 2010). Hence, BCIs bypass the normal human neural output paths and allow

users to perform actions by voluntarily modulated brain activity. In most non-invasive BCIs, the EEG is utilized to capture brain activity, because the EEG has several advantages in regard to BCI control. For instance, some brain activity changes are reflected quickly in the EEG which allows a relative low delay of around 1 s between intention and command (Steyrl 2016b). Unfortunately, BCIs work unsatisfactory in about one third of users (Blankertz 2010, Hammer 2012). Simultaneous EEG-fMRI was applied to study the vascular aspects of EEG-based BCI usage and different groups of users where BCIs do not work satisfactorily were identified, suggesting that the reliability problem of BCIs is multi-factorial (Zich 2015). Some researchers expect BCIs to be more reliable if multimodal neuroimaging is used to capture brain activity. The feasibility, a framework, and first results of such a new type of BCIs that rely on online feedback of simultaneous EEG-fMRI were demonstrated (Zotev 2008, Mano 2017, Perronnet 2017).

In conclusion, with simultaneous EEG-fMRI it is possible to study the same brain activities from the electrophysiological and from the metabolic/vascular point of view, including the interactions between electrophysiology and metabolism. Simultaneous EEG-fMRI is successfully applied in a variety of scientific research fields, but also in the clinical routine.

1.5 Artifacts in simultaneous EEG-fMRI

Simultaneous EEG-fMRI is used in a variety of scientific fields; however, its actual application is a challenge (He 2011). Beside safety of application, the main technical challenge is the existence of a complex mutual interference between the EEG and fMRI during their simultaneous application. The interference causes a substantial loss of data quality in both techniques (Mulert 2010). The quality of fMRI-data is degraded, because the EEG recording hardware inside the MRI scanner bore interferes with the static magnetic field, the gradient fields, and the radio frequency fields of the MRI scanner (Bonmassar 2001, Mulert 2010, Luo 2012, Jorge 2015a). The interference causes field inhomogeneities and field signal losses, which subsequently leads to visible artifacts in the fMRI data. The actual quality loss depends on the head region and varies between negligible and severe. Fortunately, the quality loss does not prevent a meaningful analyses of the fMRI-data (Bonmassar 2001, Luo 2012, Jorge 2015a). However, also the quality of the EEG-data is critically impaired due to the interference with the MRI scanner environment (Mulert 2010, Mullinger 2011a). The EEG is affected by a variety of artifact voltages that are induced into the EEG measurement setup. The induction of a voltage in electrical circuits is mathematically described by Faraday's law of induction:

$$\varepsilon = - \frac{d\Phi_B}{dt}, \quad (1)$$

where ε is the induced electromotive force and Φ_B is the magnetic flux, that is given by:

$$\Phi_B = \iint_{\Sigma(t)} \mathbf{B}(\mathbf{r}, t) \cdot d\mathbf{A}. \quad (2)$$

In this equation, $d\mathbf{A}$ stands for an element of the time dependent surface $\Sigma(t)$ and $\mathbf{B}(\mathbf{r}, t)$ stands for the space and time dependent magnetic field. Equation (1) and (2) describe that the induced artifact voltage ε is proportional to the rate of change of the magnetic flux Φ_B , which in turn is defined by the magnetic field $\mathbf{B}(\mathbf{r}, t)$ that passes through the surface $\Sigma(t)$. Hence, an artifact can be induced because of two principles. Firstly, because of a change in the strength of a magnetic field $\mathbf{B}(\mathbf{r}, t)$, and secondly, because of a change of the surface enclosed by a wire loop $\Sigma(t)$ (Yan 2010). The artifacts occurring are up to 1000 times larger than the EEG amplitudes and effectively prevent any meaningful direct EEG-data analysis. Important artifacts are described below.

The gradient artifact

An MRI scanner applies a sequence of electromagnetic fields to record signals of the brain. The common type of sequence used for the recording of BOLD signals is echo planar imaging (EPI). This sequence is usually repeated every 1.5 to 2.5 s to record a time series of BOLD signals per voxel. During an EPI sequence, the gradient fields, and the RF fields of the MRI scanner are switched on and off. Changing electromagnetic fields cause electromotive force and consequently voltage in electrically conducting materials, as described above in equation (1) and (2). The actual magnitude and shape of the induced voltages depend on the EEG electrode's position and orientation, the cable length and routing, and on the slew rate of the electromagnetic fields, thus, the induced voltage has an individual, generally not predictable, shape at each EEG channel (Yan 2009, Mullinger 2011b, Asseconi 2016). Voltages induced by RF fields are typically blocked with special low pass filters, since the frequency range of RF fields is usually between 30 kHz and 30 GHz and thus much higher than the EEG frequency range of 0 to 1000 Hz (Laufs 2012). However, the voltages induced by the changing gradient fields cannot be filtered out, because their frequency range overlap with the EEG frequency range. This voltages interfere with the EEG signals and are referred to as the gradient artifact (GA) or sometimes as the scanner artifact or the imaging artifact (Allen 2000, Grouiller 2007, Yan 2009). A GA example is depicted in Figure 1.4. The GA repeats with every repetition of the EPI sequence and, hence, it can be divided into epochs. The GA is almost identical between epochs due to its technical nature; however, head motions that change the position or

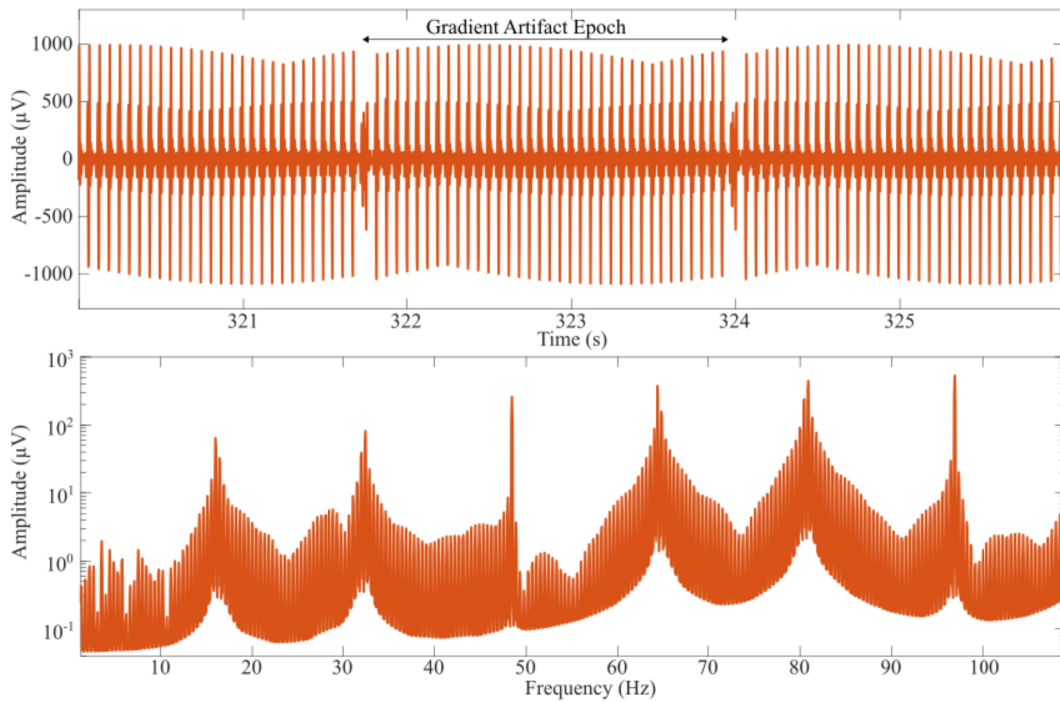


Figure 1.4: Gradient artifact example, measured at electrode position POz. Top: time course of the gradient artifact. Bottom: spectrum of the gradient artifact.

orientation of EEG electrodes and cables alter the shape of the GA permanently (Allen 2000, Yan 2009). Frequency domain analyses show that the GA covers the whole EEG frequency range, but the artifact's power is higher at single frequencies (e.g. 16 Hz, 32 Hz, 48 Hz, 64 Hz, 80 Hz, 96 Hz, compare Figure 1.4). The artifact's power is generally lower below 12 Hz (Figure 1.4). Generally, the exact spectrum of the GA depends on the MRI scanner manufacturer and the applied sequence. Among all artifacts that occur in the EEG of simultaneous EEG-fMRI, the GA has the highest amplitudes (Mulert 2010). Usually, the amplitudes are between 500 and 15000 μV , thus up to 1000 times higher than EEG amplitudes (Allen 2000, Yan 2009, Mullinger 2011b). An axial repositioning of the subjects head out of the MRI scanner's iso-center helps to reduce the amplitudes of the GA; however, it is not yet possible to avoid the artifact (Mullinger 2011b, Jorge 2015a). Signal processing based GA reduction techniques are strictly mandatory in order to obtain acceptable EEG signal quality and to allow any meaningful analyses (Allen 2000, Mulert 2010).

The pulse artifact

Another severe artifact is repetitive with the human cardiac-cycle and is referred to as the pulse artifact (PA) or ballistocardiogram artifact (Allen 1998, Debener 2007, Debener 2008, Yan 2010, Mullinger 2013a, Marino 2018a). An example of the PA is

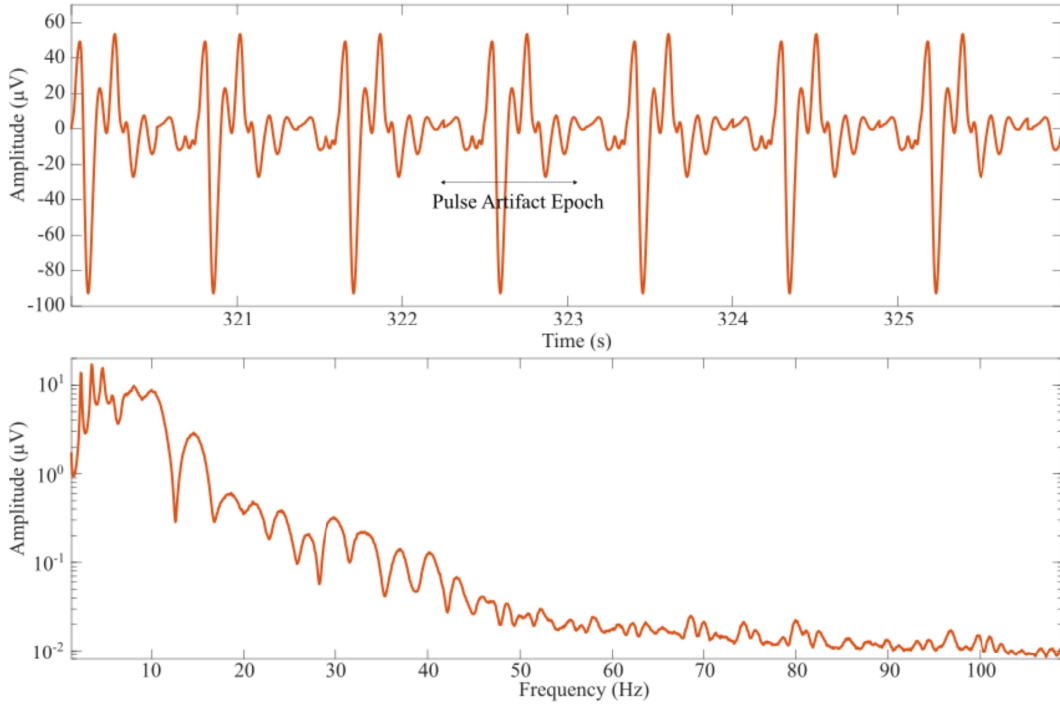


Figure 1.5: Pulse artifact example, measured at position POz. Top: time course of the pulse artifact. Bottom: spectrum of the pulse artifact.

depicted in Figure 1.5. The PA is a mixture of at least three different artifacts that are all related to the cardiac-cycle (Bonmassar 2002, Nakamura 2006, Debener 2008, Yan 2010, Mullinger 2013a). The main component of the PA amplitude is caused by cardiac-pulse-driven head rotation or nodding (Mullinger 2013a). The change in direction of the blood flow in the human head results in a mechanical impulse that causes small head rotations or nodding. This small motions of the head change the position of the EEG electrodes and consequently, the surface area of the conducting loop $\Sigma(t)$ in Faraday's law of induction, which causes voltage induction, see equation (1) and (2). The induced artifact amplitude is directly proportional to the motion amplitude and the strength of the static magnetic field of the MRI scanner (Debener 2008, Yan 2010). The second component of the PA amplitude is also caused by motion, but in this case, motions of the EEG electrodes due to the expansion and contraction of blood vessels below the respective EEG electrode (Bonmassar 2002, Mullinger 2013a). The amplitude of this component is also dependent on the static magnetic field strength. The third component of the PA amplitude is related to the electromagnetic properties of blood. Blood is electrically conductive and therefore, surrounded by an electromagnetic field, when accelerated in a magnetic field. This electromagnetic field is proportional to the acceleration of the blood and thus, it changes with the cardiac-cycle. The changing electromagnetic field induces artifact voltages in the EEG. This voltage is known as Hall voltage and depends on the static

magnetic field strength (Bonmassar 2002, Mullinger 2013a). This three contributors together form the shape of the PA. The exact shape depends on the field strength and on the electrodes positions and orientations on the head (Debener 2008, Yan 2010, Mullinger 2013a, Marino 2018a). As a consequence, head motions that alter the position and orientation of EEG electrodes change the shape of a PA permanently. The PA is repetitive with the cardiac-cycle, but the cardiac-pulse-cycle varies inherently in terms of its amplitude and timing. Therefore, the PA shape between epochs is similar, but not identical. Investigations show that the blood vessel expansion component and the Hall voltage component contribute significantly to the PA variability although they are generally smaller in terms of their amplitude than the head nodding component (Nakamura 2006, Debener 2008, Yan 2010, Mullinger 2013a). The field strength dependency of the PA is an issue that aggravated over the years. The signal-to-noise-ratio (SNR) of MRI signals and thus, the obtained fMRI data quality, is proportional to the static magnetic field strength of the MRI scanner. Therefore, modern MRI scanners tend to utilize very strong static magnetic fields of 3-7 T and consequently, the PA amplitudes are significantly increased in modern MRI scanners (Debener 2008, Yan 2010). The amplitudes are usually within a range of approximately 20-150 μV at 3 T field strength, with larger amplitudes at frontal electrode positions and smaller at occipital positions. Generally, the PA amplitudes are in the same range as EEG amplitudes. Analyses in the frequency domain show that the power of the artifact is highest between 1 and 35 Hz, which overlaps with the frequency range of the EEG (Figure 1.5). Signal processing based artifact reduction techniques are the only option to lower the impact of the PA on the EEG and to enable useful analyses.

Vibration related artifacts

Some MRI scanner subsystems require electric engines in order to fulfill their task. Two subsystems with electric engines are usually active during imaging: firstly, the helium pump of the cooling system for the superconducting magnet and secondly, the ventilation system for the patients. The electrical engines generate vibrations and thus, small motions of the EEG electrodes and cables. The motions change the surface area of the conducting loop – referred to as $\Sigma(t)$ in Faraday’s law of induction – and, as a consequence, induce artifact voltages in the EEG. The artifact due to the cooling system is often referred to as the helium pump artifact (HPA) and the artifact due to the patient ventilation system is commonly referred to as the ventilation artifact (VA) (Mulert 2010, Mullinger 2013b, Nierhaus 2013, Rothlübbers 2014, Kim 2015). Their amplitudes are typically below 20 μV , hence, smaller than the amplitudes of the GA or the PA (Nierhaus 2013). The exact properties of the artifacts, such as amplitude and frequency spectrum are presumably specific to a scanner brand or model and to the specific simultaneous EEG-fMRI setup. For instance, a

frequency analysis of HPA affected EEG-data, measured in a SIEMENS Magnetom scanner of the Tim Trio series (Siemens, Erlangen, Germany), showed that the artifact covers a frequency range of approximately 20 to 100 Hz (Nierhaus 2013). Whereas, a frequency analysis of HPA affected EEG, measured in a SIEMENS Magnetom scanner of the Verio series, showed that for this series, the HPA covers the frequency range of approximately 30 to 200 Hz, including several artifact free ranges in between (Nierhaus 2013). The properties of the VA depend also on the scanner model, but are additionally depending on the chosen ventilation level (Nierhaus 2013). In general, both artifacts have not been sufficiently studied yet and many of their properties are unknown. Due to this issue, and since it is possible to switch off the helium pump and the patient ventilation system to prevent these artifacts, it is not yet popular to use signal processing based techniques for their reduction. However, the use of such artifact reduction techniques would be preferable over deactivating the scanner subsystems, as the concerned MRI scanner subsystems play important roles for the safe operation of the MRI scanners and for the comfort of the study participants. At least two techniques the reduction of the HPA have been published (Rothlübbers 2014, Kim 2015). Unfortunately, it seems that no signal processing based artifact reduction technique is yet available for the VA.

Motions related artifact

Active motions of study participants are another source of artifacts (Bonmassar 2002, Masterton 2007, VanderMeer 2010, Jorge 2015b, Spencer 2018). The generating mechanism is the same as for the main component of the PA and for the vibration related artifacts. The motions change the EEG electrodes and cables positions, which alter the shape of the conducting loops, leading to artifact voltages in the EEG. This motion related artifact or simply motion artifact (MA), is problematic in three senses. Firstly, it is non-repetitive, non-stationary, and typically not predictable, since its occurrence and properties depend on the motions (Bonmassar 2002, Spencer 2018). Secondly, motions change the properties of the GA, the PA, and presumably also of the vibration related artifacts permanently, since the motions change the EEG electrodes and cables positions (Masterton 2007). This poses a serious obstacle to GA and PA reduction techniques that exploit the repetitiveness of these artifacts. Thirdly, motion artifacts can introduce spurious correlations in simultaneous EEG-fMRI data, that pretend to be plausible EEG effects and EEG-BOLD correlations (Fellner 2016). This effect can lead to wrong conclusion from simultaneous EEG-fMRI data. Best practice is to prevent the MA by restricting possible motions of the study participants with, for instance, vacuum cushion. However, also a variety of signal processing based artifact reduction techniques have been proposed.

In summary, severe artifacts occur in the EEG of simultaneous EEG-fMRI and an adequate handling of these artifacts is essential to enable any meaningful analysis of the

EEG-data. Two options of handling are available: prevention or signal processing based artifact reduction with appropriate techniques.

1.6 State-of-the-art in artifact reduction

In general, two approaches for artifact reduction in the EEG of simultaneous EEG-fMRI are feasible. On the one hand, in some cases it is possible to avoid or reduce artifacts by removing or minimizing the sources of the artifacts. Examples following this approach include switching off the helium pump to avoid the HPA, using sand bags to stabilize EEG cables consequently to reduce all artifacts caused by motions of EEG cables, or the application of shorter EEG cables to reduce the effective cable loop (Mullinger 2013b, Asseondi 2016). On the other hand, it is often possible to reduce the occurring artifacts by signal processing based artifact reduction techniques. Artifact reduction following the first approach is commonly limited, since most of the artifact sources are fundamental to a working MRI scanner (Mulert 2010). Therefore, artifact reduction following the second approach is typically the only way to achieve a quality of EEG-data that is usable. A variety of artifact reduction techniques have been developed in recent years. Unfortunately, a comprehensive and up-to-date review of the techniques is missing. The available reviews date back to 2007 and include selected techniques only (Grouiller 2007, Ritter 2007). As a consequence, various techniques are in use:

Average artifact subtraction

The average artifact subtraction (AAS) technique is among the best performing artifact reduction techniques and the de facto gold standard method for artifact reduction in simultaneous EEG-fMRI (Grouiller 2007). It is presumably the most often applied method as it is implemented in the software packages of commercial fMRI-compatible EEG systems, where it is often the standard method for the reduction of both, the GA and the PA (BrainAmp, BrainProducts, Munich, Germany; Geodesic EEG System, Electrical Geodesics, Inc., Eugene, OR, USA; NEURO PRAX System, neuroCare GmbH, Germany). Furthermore, AAS is used in other artifact reduction methods, e.g. as pre-processing technique before spatial filtering techniques (Niazy 2005, Chowdhury 2014). The AAS method was introduced by Allen et al., in order to reduce the PA (Allen 1998). Allen et al. observed that the PA repeats itself at EEG channel level with the cardiac-cycle and they developed a technique that exploits this repetitive nature of the artifact. They divided the EEG recordings in artifact epochs and calculated an individual artifact template per EEG channel and per artifact epoch by averaging over a sliding window of adjacent artifact epochs of the respective EEG channel. Subsequently, they subtracted the artifact template from the current artifact epoch to restore the underlying EEG. The AAS technique relies thereby on three im-

implicit assumptions: (i) The EEG has a mean value of zero. Consequently, no EEG remain in the templates after averaging over artifact epochs. (ii) The artifact is repetitive. Hence, one can partition the EEG into artifact epochs. (iii) The artifact remains constant across adjacent artifact epochs. Which means that averaging over epochs leads to an accurate artifact template. Assumptions (i) and (ii) are typically fulfilled by the PA. For instance, regarding the first assumption, one can achieve zero mean EEG by high pass filtering. Regarding assumption two, one can reliably divide the pulse artifact into epochs with the help of separate simultaneously recorded electrocardiographic (ECG) data (Allen 1998, Mullinger 2008). Assumption (iii), however, is commonly not fulfilled by the PA. The cardiac-pulse-cycle inherently varies in terms of its magnitude and timing. Furthermore, active head motions potentially alter the shape of the PA permanently. This violation of assumption (iii) leads to the following behavior of the AAS method: generally, the higher the number of artifact epochs included in the averaging process is, the higher is the template quality, since the remaining EEG in the template is lower. However, a higher number of artifact epochs also means that it takes longer to regain a clean template, after a change in the artifact shape occurred. Hence, the size of the sliding window, meaning the number of artifact epochs for averaging, is a trade off between the template quality and the adaptability to changes in the artifact shape. Allen et al. decided to include the pulse artifact epochs of 10 s of the preceding EEG relative to the current epoch into the averaging process to construct the template (Allen 1998). The AAS technique is also widely applied for the reduction of the GA. As described above, the GA is typically the dominant artifact and must be tackled first, before any other artifact reduction. Allen et al. introduced a modified AAS method for the reduction of the GA in 2000 (Allen 2000). The idea, as well as the three basic assumptions are the same as for the reduction of the PA. An artifact template is built by averaging over adjacent GA epochs. Subtracting the template from the current epoch uncovers the underlying signal. The three assumptions are: (i) The EEG-data have zero mean, (ii) the artifact is repetitive, and (iii) the adjacent epochs are similar. Due to the technical nature of the gradient artifact, all three assumptions are typically fulfilled (Yan 2009). The only exception are active head motions of the study participant, which are still highly problematic, since they alter the artifacts shapes permanently and therefore, cause a temporal violation of the third assumption. For the GA reduction process, Allen et al. adjusted the sliding window in the averaging procedure for the template construction. They argued that artifact reduction is often performed offline, hence, the data collection is already completed. Therefore, it is possible to include past artifact epochs as well as future artifact epochs in the sliding window when processing a certain epoch. Furthermore, they suggested an answer to the question of how many epochs should be included in the averaging process. They argued that signal components that occur in the EEG (artifacts and brain-signals) have amplitudes of 10-250 μV and, therefore,

it is necessary to adjust the sliding window size to include at least 25 epochs in the template construction process to ensure that the residual amplitudes of the largest components in the template are below the amplitudes of smallest components of the EEG. By combining these two enhancements, they decided to include twelve past artifact epochs, twelve future epochs and the current artifact epoch in the calculation of the artifact template for subtraction (Allen 2000). It must be noted that this suggestion regarding the number of epochs holds for single events in the EEG, for instance eye blinks, but it does not hold for repetitive or permanent components in the EEG. For instance, the brain activity related component of the EEG itself is present in every single epoch; therefore, the residual EEG amplitudes in the template are reduced by approximately a factor of square-root of the number of the epochs and not by the number of the epochs. Hence, using 25 epochs in the averaging step implies that EEG amplitudes are reduced by a factor of $\sqrt{25}$ (i.e., only by a factor of 5). In the past, one issue related to GA reduction with the AAS technique was that the time of the clocks of the EEG recording system and MRI scanners were not synchronized. As a consequence, single repetitions of the GA were sampled at slightly different time points. The subsequent averaging led to a blurred artifact template and, in turn, artifact reduction was impaired. This issue has been solved in modern EEG recording systems, as they offer the option to synchronize the clock of the EEG recording system with the clock of the MRI scanner through the use of a phase locked loop (Mullinger 2008).

fMRI artifact slice template removal

A second common artifact reduction technique is fMRI artifact slice template removal (FASTR). It was developed by Niazy et al. – partly based on work of Negishi et al. – for the reduction of the GA and is available as plug-in for the well-known EEGLAB platform (Niazy 2005, Negishi 2004, Delorme 2004). The FASTR method uses the same approach as the AAS technique: it constructs an artifact template and subtracts the template from the EEG to reduce the GA. However, the methods differ in how the templates are constructed. In FASTR, a unique template for each artifact is constructed of the local moving average plus a linear combination of basis functions that account for the variation of artifact residuals. The additional basis functions are the difference to the AAS method. The basis functions are obtained after the AAS method was applied by decomposing the spatio-temporal EEG matrix into orthogonal temporal components with temporal principal component analysis (PCA). It is assumed that the GA residuals are uncorrelated to neuronal activity and typically of higher amplitude. Therefore, they should usually be captured in the very first PCA components. These dominant components serve then as the set of basis functions. Furthermore, Niazy et al. propose the use of FASTR to reduce the PA, but without applying the AAS technique in the pre-processing step, thus only the use of basic

functions. They claim that the FASTR approach is superior to the AAS technique (Niazy 2005). However, in a comparison by Grouiller et al., the FASTR approach was not superior in general, but only in rare cases (Grouiller 2007).

Spatial principal component analysis and independent component analysis

Techniques based on the spatial decomposition of the EEG such as spatial PCA and independent component analysis (ICA) are also popular for artifact reduction. A large number of papers have been published that deal with the application of PCA and especially ICA to reduce the GA and the PA. (Benar 2003, Srivastava 2005, Briselli 2006, Nakamura 2006, Mantini 2007b, Ritter 2007, Vanderperren 2010, Abreu 2016). Some authors claim that in particular the ICA technique is superior to AAS; however, as Niazy et al. already pointed out “... *the identification of artifact components can be subjective and is usually done manually. Most importantly, spatial filters assume that all the sensors are contaminated by common sources, which is not the case. The BCG artifact [the PA] derives from sources that are rotating/moving, which contaminate different sensors at different points during the cardiac cycle with different effects.*” (Niazy 2005). This means that the quality of EEG after the application of the ICA technique depends on subjective selections and an over-fitting of the data cannot be ruled out. Furthermore, one of the basic assumptions of the ICA method is violated in terms of artifacts in the EEG recorded simultaneously with fMRI, namely that all EEG sensors are contaminated by common sources (Debener 2007, Marino 2018). Consequently, Grouiller et al. found in their review that the quality of EEG after the application of ICA is highly variable and typically worse than after the application of the AAS technique. Concerning the reduction of the GA they wrote: “... *ICA behaved badly in experimental data.*” and concerning the reduction of the PA they concluded: “*ICA showed poor results in removing cardiac artefacts both in experimental and simulated data*” (Grouiller 2007).

Techniques utilizing separate artifact measurements

Another group of artifact reduction techniques captures artifacts separately and subsequently, a forward model is used to estimate the impact of the artifacts on the EEG, to enable artifact reduction. Both parts of such techniques – the measurement of the artifacts and the forward model – are critical to reliably achieve a high EEG quality. Several methods to measure specific types of artifacts were proposed. For instance Bonmassar et al. used a piezoelectric motion sensor to capture motions of the study participants (Bonmassar 2002). Masterton et al. introduced cable loops attached to the EEG cap to measure motions, including the motions that cause vibration related artifacts (Masterton 2007, Abbot 2014). Van der Meer et al. utilized separate electromyographic recordings at the arm as motion indicators (VanderMeer 2010). Maziero et al. developed a fMRI compatible Moiré-phase grating sys-

tem in order to track motions (Maziero 2016). However, it is cumbersome and error-prone to capture each possible artifact separately. An appealing approach is to measure artifacts together – all at once if possible – in the same way as they influence EEG recordings (Xia 2013, Chowdhury 2014, Luo 2014, Jorge 2015b). This can be achieved by placing separate reference electrodes directly at the head of study participants. The reference electrodes are the same as the EEG electrodes, but isolated from the scalp. This approach dates back to a no longer existing company named Alatheia Ltd (Chantilly, VA, USA) and their ‘fEEG’ system (Dunseath 2009, McGlone 2009). Chowdhury et al. published a promising study on an advanced version of that approach (Chowdhury 2014). They used agar and PVC film to build a reference-layer for the whole head, which is electrically isolated from the scalp, but has similar electrical properties and shape. They utilized electrode pairs, where one electrode is capturing the artifact afflicted EEG at the scalp (scalp electrode), while the other is capturing the accompanying artifacts at the reference-layer (reference electrode). Electrodes of a pair are closely spaced, reference electrodes on top of scalp electrodes, separated by PVC film only. Hence, this setup enables individual artifact recordings per EEG electrode and it can be assumed that artifacts captured by an electrode pair are similar. Consequently, an artifact subtraction will reduce the artifacts in the EEG. It was demonstrated that this reference-layer artifact subtraction (RLAS) approach outperforms the AAS method in terms of GA and PA attenuation when MAs are present and that the RLAS approach is even more effective when combined with the AAS technique as pre-processing step (Chowdhury 2014). Despite the results, the RLAS approach of a separate reference-layer and paired electrodes was not pursued further. Especially the forward model was not improved. However, the applied forward model is the second critical part in methods that utilize separate artifact recordings. The forward model is responsible to establish a link between the measured artifacts and the artifacts in the EEG. In the case that the separately measured artifacts are identical to the artifacts in the EEG, a straight forward subtraction is the optimal solution. Usually, the artifacts are similar, however, not identical as the geometry of the surface enclosed by the respective wire loop and the orientation of the wire loop relative to the magnetic fields are not the same. As a result, a straight forward subtraction is generally sub-optimal. Due to Faraday’s law of induction, it is valid to assume a linear relationship between separately measured artifacts and artifacts in the EEG (Yan 2010, Jorge 2015b). Therefore, linear models are considered a good choice to establish a forward model (Bonmassar 2002, Master-ton 2007, Xia 2013, Abbot 2014, Luo 2014, Jorge 2015b). Unfortunately, the linear relationship is usually not stable over time as for instance, the impedances between electrodes and scalp change, or the geometry of the surfaces enclosed by the wire loops alter due to motions of the study participant (Yan 2010, Jorge 2015b). Hence, a one time fit of the linear models, for instance at the beginning of an experiment, is

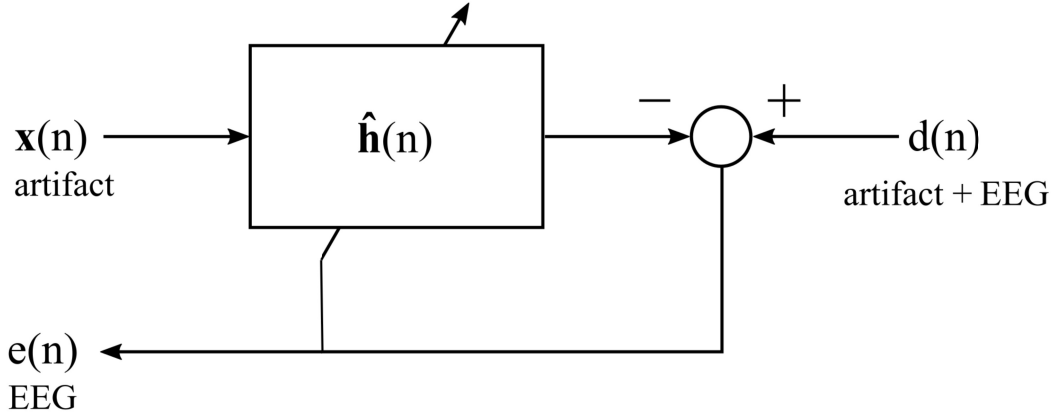


Figure 1.6: Schematics of adaptive filters. $\mathbf{x}(n)$ is the vector of separate artifact measurements, $d(n)$ is the EEG that is contaminated by artifacts, $e(n)$ is the residual after the subtraction of the filtered artifact vector, and $\hat{\mathbf{h}}(n)$ is the estimated filter, or estimated forward model.

insufficient. A continuous adaptation of the linear model is required. Adaptive filters provide such a functionality (Haykin 1996). A schematic representation of adaptive filters is shown in Figure 1.6. In general, adaptive filter algorithms work iteratively. Usually, each iteration is divided into two steps. Firstly, the forward model $\hat{\mathbf{h}}(n)$ is used to estimate the influence of the artifact $\mathbf{x}(n)$ on the artifact-contaminated EEG $d(n)$. The residuals of the estimated artifact influence and the contaminated EEG $d(n)$ is the cleaned EEG. In the adaptive filter notion, this signal is referred to as the error $e(n)$. Secondly, the forward model $\hat{\mathbf{h}}(n)$ is adapted to improve the estimation of the artifact influence. The adaptation direction is derived from the error signal $e(n)$. Several algorithms are available to perform the two steps (Haykin 1996). Popular examples are the least mean squares algorithm and the recursive least squares algorithm (Haykin 1996). Unfortunately, a systematic review on the application of adaptive filters for the artifact reduction in simultaneous EEG-fMRI is missing. Furthermore, the available results are not necessarily comparable, as they were obtained for different types of artifacts and different types of artifact measurement techniques (Bonmassar 2002, Masterton 2007, Jorge 2015b). Often, the least mean squares algorithm is applied. This algorithm minimizes the mean squared residuals, hence, $e^2(n)$. Mathematically the algorithm is described by the two following equations,

$$e(n) = d(n) - \hat{\mathbf{h}}^H(n) \cdot \mathbf{x}(n), \quad (3)$$

which is the forward model step and

$$\hat{\mathbf{h}}(n+1) = \hat{\mathbf{h}}(n) + \mu \cdot \mathbf{x}(n) \cdot e(n), \quad (4)$$

which is the update step. The variables are the same as above, additionally $\hat{\mathbf{h}}^H(n)$ is the Hermitian transpose of $\hat{\mathbf{h}}(n)$ and μ is the step width, a parameter that controls the convergence speed and the stability of the adaptation process (Haykin 1996). The

characteristics of the artifact input $\mathbf{x}(n)$ is critical for the performance of the adaptive filtering technique. If the separate artifact recording does not capture all aspects of the artifact in the EEG, then the adaptive filter will fail to reduce the artifact. Furthermore, if the separate artifact recording does contain EEG, then the adaptive filter will also remove EEG. So far, all applications of adaptive filtering were to some extent affected by one of the two problems. However, this approach is very appealing, as it conceptually allows to reduce all types of artifacts that can be captured by separate recordings.

Other artifact reduction techniques

In general, the field of techniques for artifact reduction in the EEG of simultaneous EEG-fMRI is very innovative. Apart of the techniques mentioned above, many others have been published. Some of them are related to the techniques already described. For instance, beam-formers are spatial filters, singular value decomposition can be interpreted as the generalization of the PCA, and independent vector analysis is an extension of ICA (Brookes 2008, Liu 2012, Acharjee 2015). Others are based on different principles. For instance, Ferdowsi et al. introduced a technique based on short term and long term linear predictors, and Abolghasemi and Ferdowsi presented a method based on dictionary learning (Ferdowsi 2013, Abolghasemi 2015). The authors of the papers are convinced that their techniques outperform the popular methods described above under certain conditions; however, independent confirmations are missing.

Online applicable artifact reduction techniques

The data quality of EEG recorded simultaneously with fMRI is one, but not the only important criterion for artifact reduction techniques. There is also growing interest in techniques that reduce artifacts online. The interest is based on neuroscientific experiments, where an immediate processing of the measured data is required. Examples of such experiments are: (i) Triggering visual stimulation depending on ongoing EEG and investigating the effects with fMRI (Becker 2011). (ii) Locating cerebral generators of epilepsy spikes online (Gotman 2006). (iii) Investigating brain activity with fMRI during the use of EEG neurofeedback (Zotev 2014, Zich 2014, Zich 2015). (iv) The construction of a new type of brain-computer interfaces that rely on the online feedback of two neuroimaging modalities. For instance, simultaneous EEG and fMRI feedback, to generate control signals for an application or for the paradigm itself (Brunner 2015, Mano 2017, Perronnet 2017). In the context of online artifact reduction, online refers to timely artifact reduction without knowing the future data. “*Timely*” does not specify a processing time, it means that the artifact reduction is fast enough for a particular application. The term “*without knowing the future data*” implies causal signal processing. Unfortunately, most artifact reduction techniques

are based on non-causal signal processing. They require future data to work properly and can therefore only be applied offline after the experiment. This led to the development of online applicable artifact reduction techniques. Commonly they are based on offline techniques, but utilize a window of current data only. For instance, Brain Products (Brain Products GmbH, Gilching, Germany) provide an online version of the AAS method for GA and PA reduction in their commercial RecView tool that is similar to the original AAS technique published by Allen et al. (Allen 1998). Other online capable artifact reduction methods use windowed versions of the FASTR technique or of ICA as basis. The online capable techniques have the same basic weaknesses as the equivalent offline techniques, but the weaknesses are often more pronounced due to the windowing (Wu 2016, Mayeli 2016, Wen 2016).

In short, there are many artifact reduction techniques available, with the AAS method, the FASTR technique, and spatial decomposition techniques being the most common. The approach of separate artifact measurements is not common, but appealing, since it conceptually allows to reduce all occurring artifacts at once. A possible online applicability is another important criterion for artifact reduction techniques and is a requirement for certain types of experiments.

1.7 Motivation, aim and structure of this thesis

At present, a variety of artifact reduction techniques are available. However, residual artifacts are still present after the application of these methods. The low quality of EEG recorded concurrently with fMRI is still a weakness of simultaneous EEG-fMRI and presents a major obstacle for a broader application of this technique in neuroscience. For instance, several studies reported that EEG recorded outside the MRI scanner is significantly different from EEG recorded inside the active MRI scanner, although GA and PA reduction was performed with state-of-the-art artifact reduction techniques (Benar 2003, Grouiller 2007, Ritter 2007). An example is depicted in Figure 1.7, where substantial differences are visible between the spectra of Lab EEG and inside the MRI scanner EEG. For instance, GA residuals are identifiable by their spectral signature (peaks in the spectrum at 16 Hz, 32 Hz, 48 Hz, 64 Hz, 80 Hz, 96 Hz, compare Figure 1.4). This observation is also reflected in studies where machine-learning techniques were used to classify brain tasks by EEG for the application in BCIs. The achieved classification accuracies were on average 10% points lower with EEG recorded simultaneously to fMRI compared to EEG that was recorded in a lab environment, although the AAS artifact reduction method was applied (Zich 2015). Consequently, the aim of this thesis is twofold: (i) Identification and analysis of the causes of the artifact residuals after the application of the AAS method. (ii) Development and analysis of a new technique to improve the quality of EEG recorded simultaneously with fMRI, to enable a broader application of simulta-

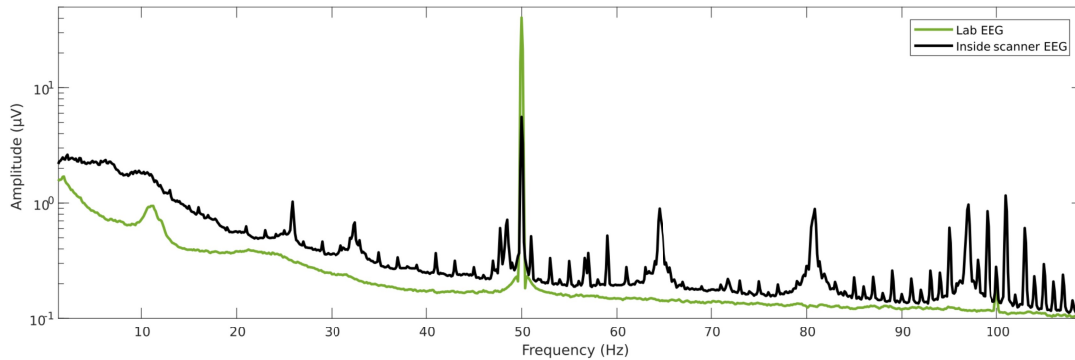


Figure 1.7: Spectrum of EEG recorded inside an MRI scanner, after artifact reduction with the AAS method (black). Spectrum of EEG recorded in a lab environment (green).

neous EEG-fMRI in the future. For this purpose, it was decided to develop a technique that deploy a reference-layer EEG cap (developed with GUGER TECHNOLOGIES OG, Graz, Austria) that enables separate artifact recordings per electrode by electrode pairs – as used in the RLAS technique – and to extend this approach by adaptive filtering. This approach is referred to as reference-layer adaptive filtering (RLAF).

The thesis starts with this introduction chapter. It gives an overview on multimodal neuroimaging, simultaneous EEG-fMRI, occurring artifacts, and associated artifact reduction techniques. The second chapter covers the materials and methods. It includes four primary scientific publications or studies, and one secondary. The first primary study presents an analysis of the causes of residual artifacts after the AAS method and points out possible enhancements. At the time of writing this thesis, this study was not yet published, therefore it is included in full text. The primary publications two, three, and four cover the introduction and evaluation of the new artifact reduction technique RLAF. The secondary publication reports on a pilot study in which a BCI experiment was performed inside an MRI scanner. The third chapter consist of a discussion that summarizes the results of the publications to set them into a big picture. Finally, the appendix contains copies of the published scientific papers.

2 Materials and Methods

“Measure what is measurable, and make measurable what is not so.”

– Antoine-Augustin Cournot and Thomas-Henri Martin

2.1 Primary publication 1: Artifacts in EEG of simultaneous EEG-fMRI: Pulse artifact remainders in the gradient artifact template are a source of artifact residuals after average artifact subtraction

[Steyrl 2018] Steyrl D, Müller-Putz GR (2018) Artifacts in EEG of simultaneous EEG-fMRI: Pulse artifact remainders in the gradient artifact template are a source of artifact residuals after average artifact subtraction. *Journal of Neural Engineering*. Accepted 29.10.2018

In accordance with the aims of this thesis, the first study was designed to answer the following two questions: (i) What are the causes of remaining artifacts after the application of the AAS technique? (ii) Are there possibilities to improve the AAS technique?

To answer this questions, the AAS technique was applied to artificial EEG-data that included simultaneous EEG-fMRI related artifacts. The use of artificial EEG facilitates the evaluation of artifact reduction methods, as it allows to compare clean EEG with EEG obtained after an application of artifact reduction techniques. This is not possible with real simultaneous EEG-fMRI recordings because the clean EEG is unknown in that case. The artificial EEG was compiled of single signal components, including artificial clean EEG, GA, and PA components. The artifact reduction was carried out under conditions that are optimal for the AAS method. Optimal means that all implicit prerequisites of the AAS technique were fulfilled: (i) the EEG had zero mean, (ii) the artifacts were repetitive, and (iii) the artifacts stayed constant across adjacent artifact epochs. The reconstructed EEG was compared with the clean EEG component to assess the quality of the reconstruction and to analyze the remaining artifacts.

At the time of writing this thesis, this study was accepted at *Journal of Neural Engineering* but not yet published. Therefore, the manuscript is included in this section.

Contribution to this thesis: This work reveals that the AAS technique is intrinsically prone to correlated artifacts. It shows that remaining PAs in the GA subtraction template adds artifacts to the EEG. The additional artifacts occur, although all prerequisites for the AAS technique were chosen optimal. Two options to improve the EEG quality are available: (i) Including a higher number of artifact epochs into the averaging process reduce the artifact residuals in the subtraction template. This approach, however, reduces the adaptability of the AAS technique. (ii) The application of additional post-processing techniques after the use of the AAS method to tackle the artifact residuals.

2.1.1 Introduction

In recent years electroencephalography (EEG) and functional magnetic resonance imaging (fMRI) have been applied simultaneously to study the active human brain concurrently from electrophysiological and metabolic/vascular perspectives (Ritter 2006, Mulert 2010, Rosa 2010, Huster 2012). The simultaneous application of the techniques allows the concurrent measurement of different brain signals and allows benefiting from their complementary features (Mulert 2010, Rosa 2010). For instance, EEG can capture signal changes in the range of milliseconds, but the exact locations of these changes remain difficult to determine (Niedermeyer 2005, Michel 2012). fMRI in turn can be used to determine the locations of signal changes with high precision, but the time resolution is limited to seconds (Ogawa 1990, Norris 2006). By combining these two techniques, the information collected with one technique can be supplemented by information from the other (Rosa 2010, Mullinger 2011, Huster 2012, Uludag 2014). One example of such an application is the EEG-informed fMRI analysis technique that is used to localize epileptic centers in the brain prior to a brain surgery (Ives 1993, Krakow 1999, Rosenow 2001, Laufs 2012).

However, EEG and fMRI are techniques that affect each other. On the one hand, the insertion of additional EEG equipment into the scanner bore results in degraded fMRI data quality, because it disturbs the magnetic field homogeneity and interferes with the radio frequency signals (Bonmassar 2001, Luo 2012). On the other hand, the presence of magnetic fields in MRI scanners introduce severe artifacts in the EEG. Dynamic magnetic fields induce electromagnetic force in the EEG cables according to Faraday's law. The static magnetic field of MRI scanners is also problematic, because small motions in the static magnet field – for instance by study participants – also induce significant electromagnetic force (Mullinger 2008, Mulert 2010). Typically, small motions cannot be avoided, because they may occur as a result of the human cardiac cycle or scanner vibrations (Bonmassar 2002, Mullinger 2013a, Nierhaus 2013, Rothlübbers 2014). Therefore, data obtained from the application of simultaneous EEG-fMRI are heavily affected by artifacts. In the case of fMRI, the data quality is reduced, but is usually sufficient to allow data analysis (Jorge 2015). In the case of EEG, however, the artifacts reduce the data quality so severely that artifact reduction methods based on signal processing are strongly advised (Mullinger 2013a).

Typically, two types of MRI related artifacts are dominant in the EEG and consequently, these artifacts are the main targets of artifact reduction techniques. The first type is caused by electromagnetic induction in the electrodes and the adjoining cables, due to the switching of the scanner's gradient field during the acquisition of fMRI data; this artifact type is often referred to as the gradient artifact (Yan 2009). It

is a broad-band artifact that covers the whole EEG relevant frequency range with amplitudes in the range of millivolts; hence, these amplitudes are roughly 1000 times higher than EEG amplitudes (Ritter 2007, Mulert 2010). The second artifact is mainly caused by motion of the EEG electrodes in the static magnetic field, due to cardiac-pulse-driven head nodding; this artifact type is often referred to as the pulse artifact (Debener 2008, Mullinger 2013b). It has maximum amplitudes of approximately 100 μV and is most prominent in the lower frequency range up to 30 Hz (Debener 2008, Mulert 2010, Mullinger 2013b).

Other MRI related artifacts are known, for instance, the helium pump artifact or the patient ventilation system related artifact (Nierhaus 2013, Rothl ubbers 2014). They are caused by vibrations introduced by the helium cooling system or the fans of the patient ventilation system. Although initial attempts to reduce these types of artifacts have been made, they are often not considered during the artifact reduction process, because they usually reduce data quality less than the gradient and pulse artifact and they are harder to remove due to their complex and non-repetitive structure.

A method that is often used to reduce the negative effects of the gradient artifact and the pulse artifact is the average artifact subtraction (AAS) technique (Allen 1998, Allen 2000). The method exploits the repetitive nature of both artifacts. An artifact template is calculated for the current artifact epoch by averaging over neighboring artifact epochs. The template is then subtracted from the current epoch to reduce the artifact. The method is typically applied twice: firstly, it is applied to reduce the effects of the gradient artifact, and secondly, to reduce the effects of the pulse artifact (Allen 1998, Allen 2000). The AAS technique relies on three implicit assumptions: (1) The EEG has zero mean. Hence, no EEG remains after averaging over EEG epochs. (2) The artifact is repetitive. Hence, one can partition the EEG data into artifact epochs. (3) The artifact remains constant across adjacent artifact epochs. Assumptions (1) and (2) are typically fulfilled for the gradient and pulse artifact. For instance, regarding the first assumption, one can achieve zero mean EEG by high pass filtering. Regarding assumption two, one can reliably divide the gradient artifact into epochs that are determined by the time of repetition of the MRI scanner sequence. The pulse artifact can be divided into epochs using separate simultaneously recorded ECG signals (Mullinger 2008). Assumption (3), however, is problematic. Firstly, any head motions induce artifacts and can potentially alter the shape of the gradient and pulse artifact permanently. Secondly, the cardiac pulse cycle inherently varies in terms of its magnitude and timing. This violation of assumption (3) leads to the following behavior of the AAS technique. In terms of gradient artifact reduction: the higher the number of artifact epochs included, the higher is the template quality, since the remaining signals in the template is low after averaging. However, a high number of artifact epochs also means that it takes longer to obtain a clean template again after a change in the artifact shape, for either a magnitude or timing, occur-

rence. Hence, this adaptivity to changes in the artifact is determined by the number of artifact epochs for averaging. In terms of pulse artifact reduction: the pulse artifact is inherently variable and a higher number of artifact epochs will not necessarily improve the template quality. However, the adaptivity of the AAS technique is still impaired by a higher number of artifact epochs. In their seminal paper on AAS for pulse artifact reduction, Allen et al. decided to include the pulse artifact epochs of 10 s of the preceding EEG signal relative to the current epoch into the averaging to construct the template (Allen 1998). Later, Allen et al. adjusted the averaging procedure. In their second paper on AAS – now for gradient artifact reduction – they argued that since artifact correction is often performed offline, it is possible to include not only past artifact epochs, but also future artifact epochs in the averaging (Allen 2000). Furthermore, they proposed an answer to the question of how many epochs should be included in the averaging process. They argued that signal components that occur in EEG (artifacts and brain-signals) have amplitudes of 10-250 μV and, therefore, it is necessary to include at least 25 epochs in the averaging to ensure that the residual amplitudes of the largest components in the template are below the amplitudes of the smallest components in the EEG signal. By combining these two enhancements, they decided to include twelve past artifact epochs, twelve future epochs and the current artifact epoch in the calculation of the artifact template (Allen 2000). The AAS technique is currently available in commercial fMRI-compatible EEG systems for the reduction of both the gradient and the pulse artifact. Examples of such systems are the BrainAmp system (BrainProducts, Munich, Germany), the Geodesic EEG system (Electrical Geodesics, Inc., Eugene, OR, USA), or the NEURO PRAX system (neuroCare GmbH, Germany). However, AAS is not only used as a stand-alone technique, but is often used as a pre-processing step before other techniques. For instance, as part of the optimal basis sets technique and before reference layer adaptive filtering (Niazy 2005, Steyrl 2017, Steyrl 2018). Furthermore, an on-line version of AAS is also available commercially (Allen 1998). Finally, it is also one of the best performing artifact reduction techniques (Garreffa 2003, Grouiller 2007, Ritter 2007). As a result, AAS is presumably the most frequently used artifact reduction technique in simultaneous EEG-fMRI.

Nevertheless, the results of several studies have shown that EEG recorded in a lab environment is significantly different from EEG recorded inside an MRI scanner, although the AAS technique was used to reduce the gradient and pulse artifact (Benar 2003, Grouiller 2007, Ritter 2007). An example is depicted in Figure 2.1. Figure 2.1 shows EEG spectra from the same study participants, first recorded in a lab environment and then inside an active MRI scanner with subsequent AAS. In the spectrum of EEG recorded inside the scanner, one can identify single peaks starting at around 25 Hz. These peaks seem to originate from gradient artifact residuals as well as from artifacts related to vibrations, i.e. those related to the cooling and patient

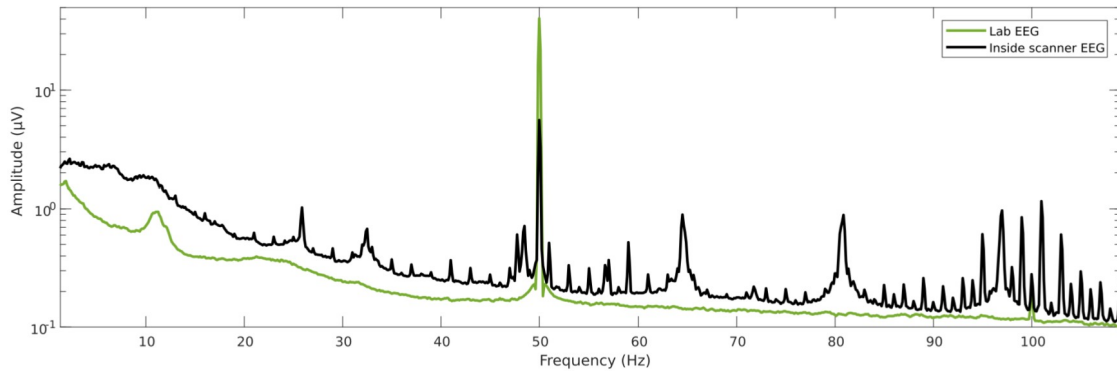


Figure 2.1: Spectra of EEG. Green: spectrum of EEG recorded in lab environment. Black: spectrum of EEG recorded inside the active MRI scanner after two subsequent applications of the AAS method for gradient and pulse artifact reduction. Channels with excessive power (mean ± 2 std) were excluded. The spectra were calculated with Welch’s method for each EEG channel separately (500 Hz sample rate, 1 Hz high pass, 125 Hz low pass, Kaiser window, window length 8 s, overlap approximately 50%) and were subsequently averaged over 6 participants.

ventilation systems. In addition to the artifact peaks, the amplitude of EEG recorded inside the MRI scanner is substantially higher across the frequency range from 1 Hz to approximately 40 Hz compared to the amplitude of EEG recorded in the lab. These artifact amplitudes overlay the typical peaks in the EEG spectrum that are associated with well-known and important brain rhythms; alpha rhythm at 8-13 Hz and beta rhythm at 13-30 Hz. To the best of our knowledge the cause of this broad band artifact has not yet been investigated.

Based on theoretical considerations, our hypothesis is that the AAS technique itself is a fundamental cause of this artifact. In this work, we apply the AAS technique to artificial EEG data to demonstrate that pulse artifact residuals in the AAS template during the gradient artifact reduction, add this artifact to the EEG.

2.1.2 Methods

An evaluation of artifact reduction techniques is problematic when artifacts and the signal of interest are available only as a mixture, as is the case with EEG of simultaneous EEG-fMRI. Inspired by a work of Grouiller et al., we use a procedure that is based on artificial signals to avoid the mixture problem (Grouiller 2007). The procedure uses a single artificial EEG channel that is built of known components. Three components are included: an artificial EEG component, an artificial gradient artifact component and an artificial pulse artifact component. The components serve as references in the evaluation. The procedure itself has three steps: (1) We generate representative artificial signal components and out of them, we create a single channel artificial EEG by summing up the components. The statistical properties of these artifi-

cial signal components are based on real simultaneous EEG-fMRI recordings from our previous work. Please refer to it for recording details (Steyrl 2018). Descriptions of the component generation are presented later in this section. (2) We apply the AAS technique two times. Firstly to reduce the gradient artifact (GA-AAS) and a secondly to reduce the pulse artifact (PA-AAS). In both, we include 25 artifact epochs in the template averaging step, 12 taken from before the current epoch, 12 taken from after the current epoch, and the current epoch; as recommended by Allen et al. (Allen 2000). (3) We compare the reconstructed EEG component after GA-AAS and PA-AAS with the original artificial EEG component to determine the effects of the applications of the AAS technique. Furthermore, this procedure allows the investigation of the single steps of the AAS technique. For instance, we investigate the quality of the artifact template in GA-AAS.

Artificial EEG component

The artifact-free EEG is the signal component of interest. We want to recover this component by applying the AAS technique. In order to create a realistic, representative, single-channel, artificial EEG component, we use the average spectrum of EEG that was recorded in a lab environment, see Figure 2.2 top (Steyrl 2018). This spectrum was calculated by averaging over the single channel spectra collected from 6 participants. Channels with excessive power (mean \pm 2 std) were excluded. The single spectra were calculated using Welch's method (500 Hz sample rate, 1 Hz high pass, 125 Hz low pass, Kaiser window, length 16 s, overlap approximately 50%). The 50 and 100 Hz peaks were removed by interpolating the average spectrum between 45 and 55 Hz, and between 99 and 101 Hz. A new frequency axis with a frequency resolution that is 420 times higher than the frequency resolution of the average spectrum was created, and the average spectrum was interpolated to fit to this new axis. The amplitudes were adjusted to fit Rayleigh's energy theorem (Oppenheim 2003). To create a time domain EEG signal from that spectrum, an inverse Fourier transform was applied to the spectrum. The result is an artificial EEG signal with a length of 2 h and a sample rate of 500 Hz (Figure 2.2 bottom). Its spectrum is similar to that of lab EEG (Figure 2.2 top).

Gradient artifact component

The gradient artifact is the most severe type of artifacts in terms of its amplitude. We chose an EEG channel with a representative gradient artifact to generate an artificial gradient artifact component (channel POz of participant 2 in Steyrl et al. 2018). The EEG channel was recorded with a sampling rate of 5000 Hz and activated synchronization between the EEG system clock and the MRI scanner clock. The time-of-repetition of the scanner was 2250 ms, an integer multiple of 20 μ s. Subsequently, the EEG channel was low pass filtered to avoid aliasing (12th order, second-order-structure, zero phase Butterworth low pass filter, 3 dB at 125 Hz) and down-sampled to

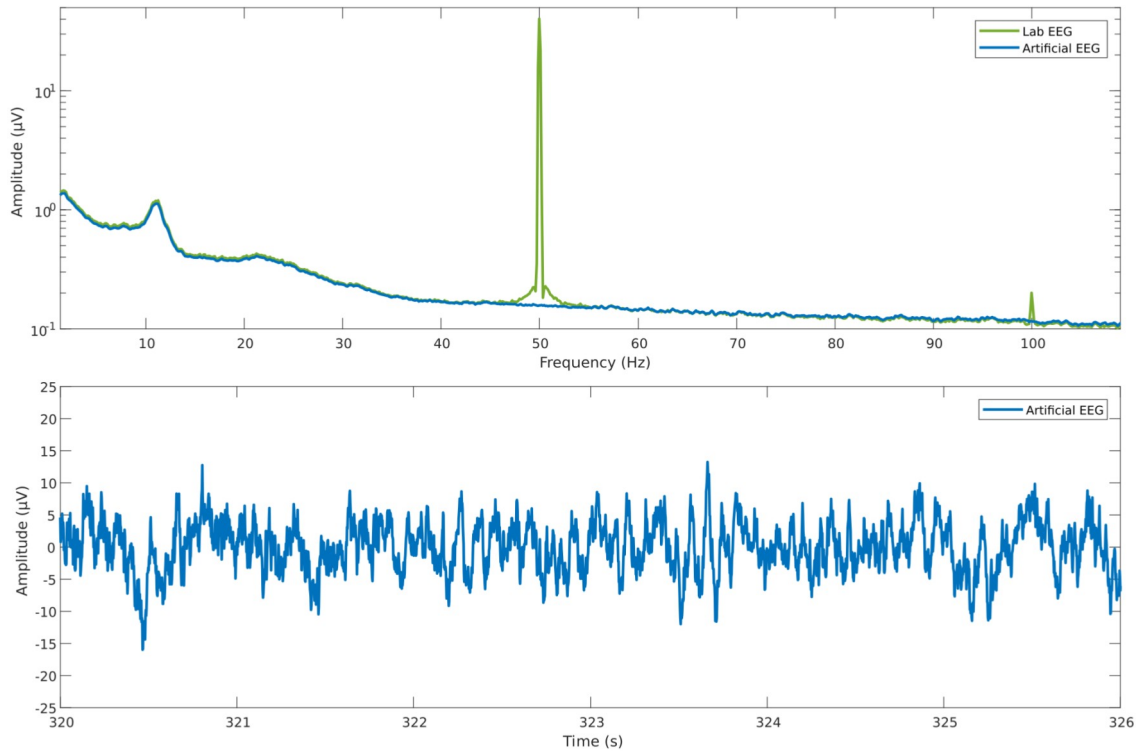


Figure 2.2: Top: spectrum of EEG recorded in a lab environment (green) and spectrum of the artificially generated EEG signal (blue). Bottom: example of time course of the artificial EEG signal.

500 Hz. We checked for an effect of the down-sampling on the gradient artifact reduction and found that the EEG quality was equal. The actual gradient artifact component was generated by repeating a gradient artifact template until the desired length of the component was reached. The template was obtained by averaging over gradient artifact epochs of the aforementioned EEG channel. Single gradient artifact epochs were removed before the averaging if they showed excessive power ($\text{mean} \pm 2 \text{ std}$). In total 464 gradient artifact epochs were included to calculate the gradient artifact template. The template was then repeated until a signal length of 2 h was reached (see Figure 2.3 top). The artificial gradient artifact component shows the typical spectral fingerprint of the gradient artifact: prominent peaks at 16 Hz, 32 Hz, 48 Hz, 64 Hz, 80 Hz, 96 Hz (see Figure 2.3 bottom). We decided to carry out our investigations under conditions that are optimal for the AAS technique, hence, the artificial gradient artifact component does not include any abrupt or slow changes over its entire duration.

Pulse artifact component

To create an artificial pulse artifact component, we used a similar approach as that for the gradient artifact component. Pulse artifact epochs of an EEG channel that shows representative pulse artifacts (channel POz of participant 2 in Steyrl 2018)

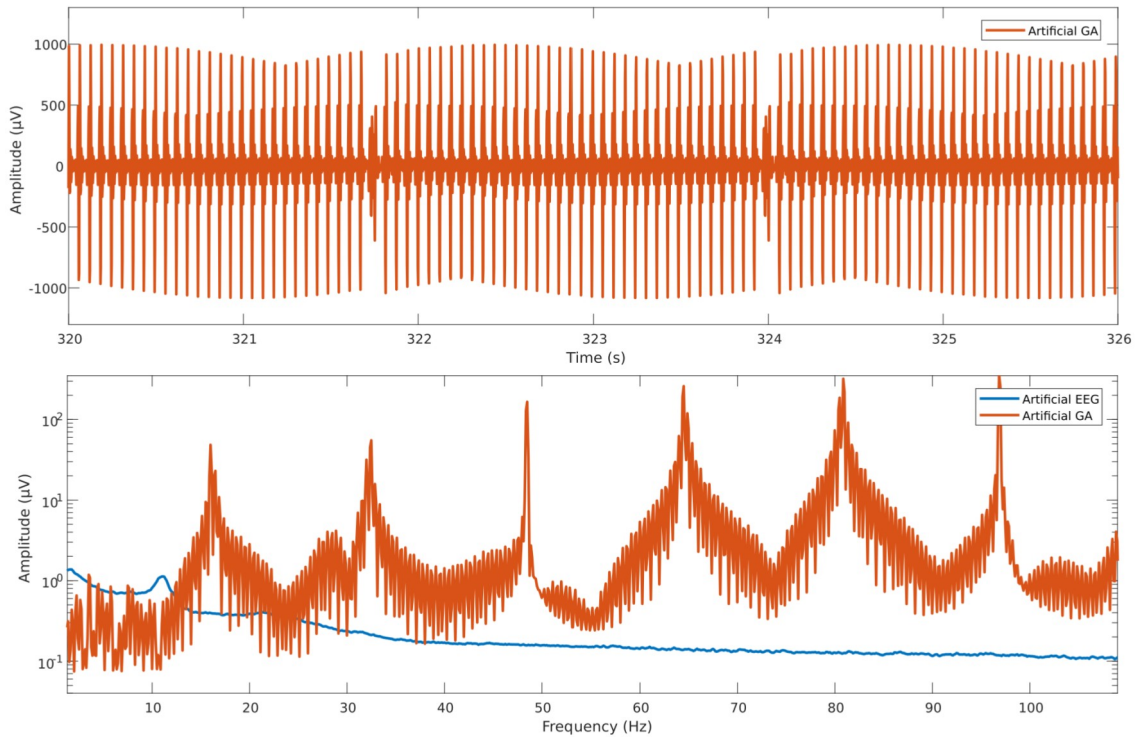


Figure 2.3: Top: repeated artifact template used to obtain a 2 h long artificial gradient artifact component. Bottom: comparison of spectrum of the artificial gradient artifact component (red) with that of the artificial EEG (blue).

were averaged to obtain a pulse artifact template. Epochs with excessive power (mean \pm 2 std) were removed. In total 914 pulse artifact epochs were included to calculate the pulse artifact template. To obtain an artificial 2 h pulse artifact signal, we lined up one artifact after another, but the duration between two successive artifacts was varied, to simulate the natural temporal variability of the pulse artifact occurrence. The gaps in between adjacent artifact epochs were filled with zeros. We adjusted the pulse artifact occurrence to match the measured average heart rate of participant 2 (see Figure 2.4 top). On average, a pulse artifact occurred every 0.86 s, which implied a heart rate of approximately 70 bpm. The standard deviation was 0.05 s. The artificial pulse artifact component shows the typical spectral signature of the pulse artifact: high power in the frequency range of 1-40 Hz and almost no power above 40 Hz. The pulse artifact amplitude was not modified over the course of the artificial pulse artifact component to ensure optimal conditions for AAS.

Performance metrics

We present a visual (time and frequency domain) comparison of the artificial EEG component, the reconstructed EEG after twice applying AAS (GA-AAS and PA-AAS), the artifact residuals in the reconstructed EEG, and the artifact residuals in the gradient artifact template. The artifact residuals of the reconstructed EEG were ob-

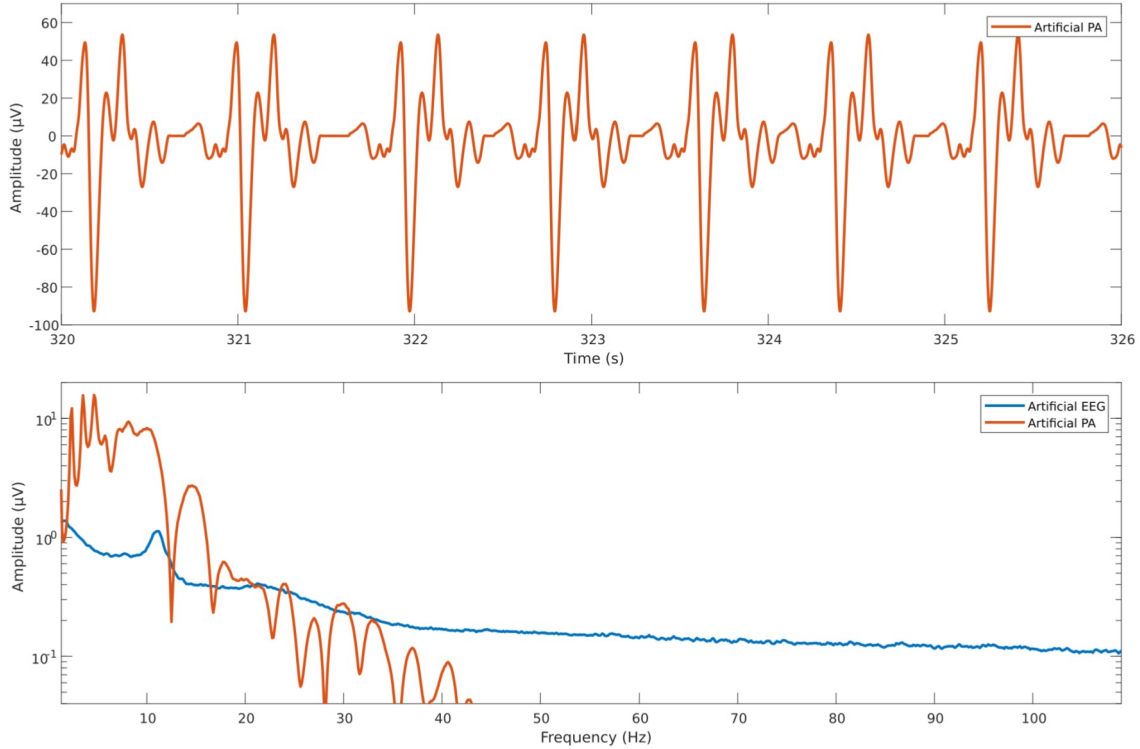


Figure 2.4: Top: repeated pulse artifact template to obtain a 2 h long artificial pulse artifact component. Bottom: comparison of spectrum of the artificial pulse artifact component (red) with that of the artificial EEG (blue).

tained by subtracting the artificial EEG component from the reconstructed EEG. The artifact residuals in the gradient artifact template were obtained by subtracting the gradient artifact component from the template.

A helpful metric that can be used to assess the similarity of signals is the Pearson correlation coefficient. This coefficient describes the difference between the original artificial EEG components and the reconstructed EEG component in the time domain; ideally, this coefficient is 1, implying that the signals are identical.

Furthermore, we calculate the signal-to-noise ratio (SNR) between the artificial EEG component and the artifact residuals in the reconstructed EEG to quantify the quality loss.

Computations were performed with Matlab (Mathworks Inc., Natick, MA, USA, Version 2017b).

2.1.3 Results

Figure 2.5 shows a representative period of: the artificial EEG component, the reconstructed EEG after GA-AAS and PA-AAS, the artifact residuals in the reconstructed EEG, and the artifact residuals in the gradient artifact template. The Pearson correla-

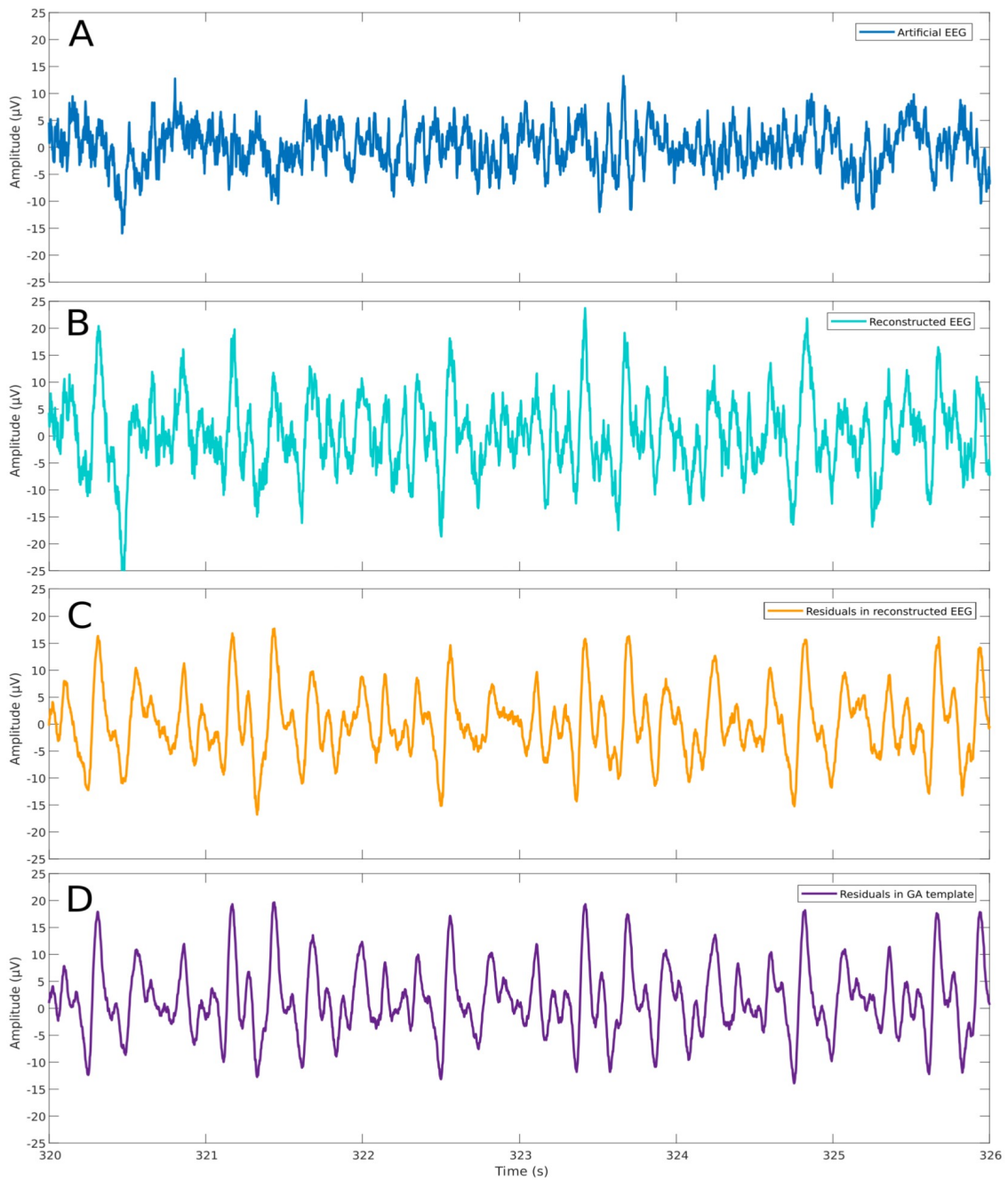


Figure 2.5: Comparison of: the artificial EEG component (A), the reconstructed EEG after two times AAS (GA-AAS and PA-AAS) (B), the artifact residuals in the reconstructed EEG (C), and the artifact residuals in the gradient artifact template (D).

tion coefficient between the artificial EEG component and the reconstructed EEG after two times AAS is 0.6. The SNR between the artificial EEG component and the artifact residuals in the reconstructed EEG is - 1.8 dB. The correlation coefficient between the residuals in the reconstructed EEG and the residuals in the gradient artifact template is 0.94.

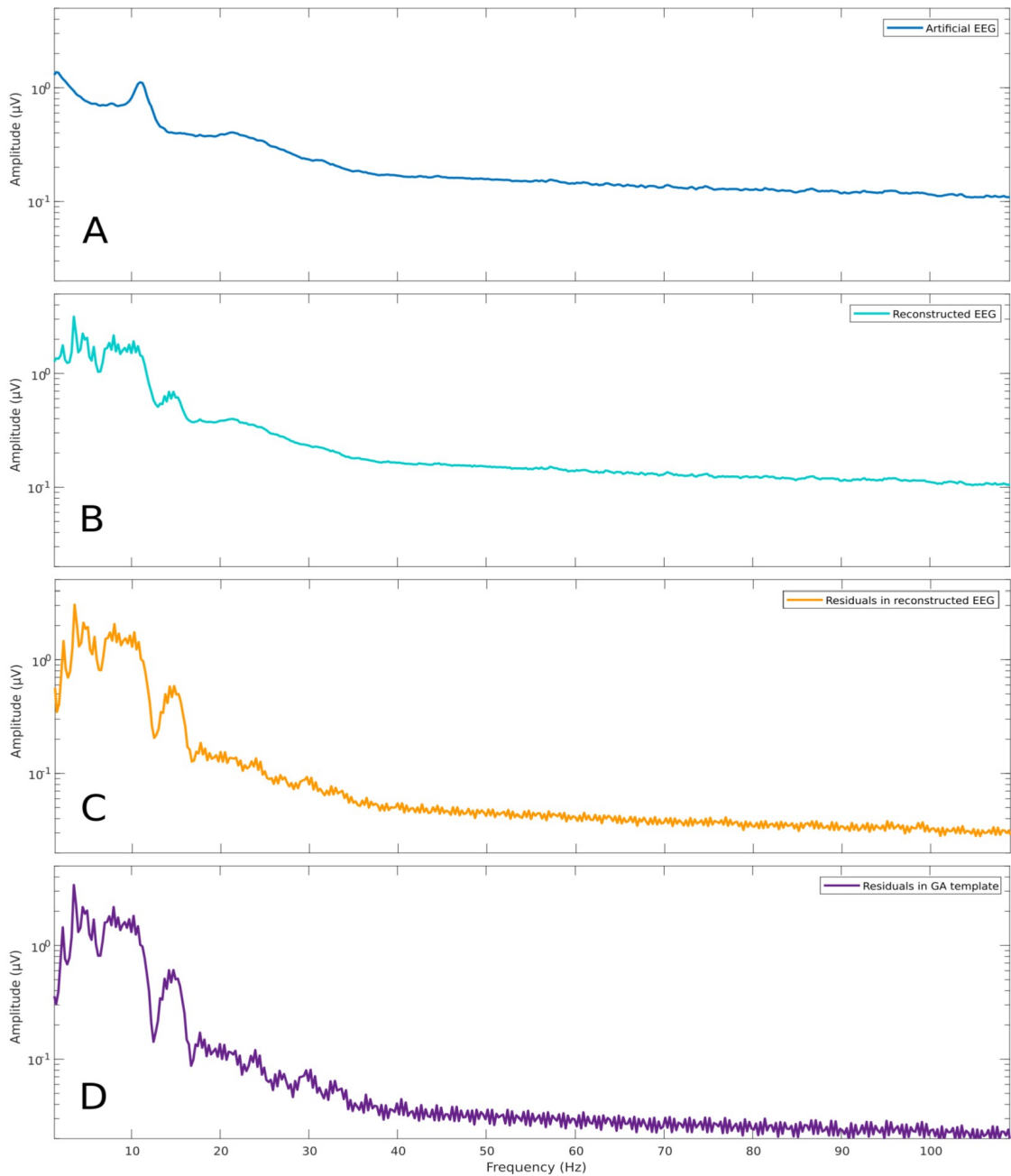


Figure 2.6: Comparison of the spectra of: the artificial EEG component (A), the reconstructed EEG after two times AAS (GA-AAS and PA-AAS) (B), the artifact residuals in the reconstructed EEG (C), and the artifact residuals in the gradient artifact template (D).

Figure 2.6 presents the spectra of: the artificial EEG component, the reconstructed EEG after GA-AAS and PA-AAS, the artifact residuals in the reconstructed EEG, and the artifact residuals in the gradient artifact template.

2.1.4 Discussion

Artifact reduction techniques are strongly advised as a rule prior to any analysis of EEG that was obtained during simultaneous EEG-fMRI. The artifacts represent a major problem for the analysis of the EEG, especially when oscillatory EEG components are under investigation or when only a small number of event-related potentials are available (Steyrl 2013, Zich 2015).

The AAS technique is one of the most frequently applied methods for artifact reduction and also one of the best performing compared to other available artifact reduction methods (Grouiller 2007). Nevertheless, some of the commonly investigated brain rhythms are typically masked by remaining artifacts appearing in the EEG although artifact reduction methods were applied. It is clear that some of these remaining artifacts are of a type that require a different reduction method, e.g. artifacts related to vibrations, as the helium pump artifact (Mullinger 2013a, Rothlübbers 2014). It is also clear, however, that artifact residuals of the gradient and the pulse artifact are still present after artifact reduction (Figure 2.1). Therefore, the question is: why is the AAS technique not able to completely remove the artifacts for which it was developed? One answer is that the assumption on the similarity of adjacent artifact epochs is violated, meaning that adjacent artifact epochs do not have the same timing and amplitude. In the case of the gradient artifact, small head motions change the shape of artifact epochs and leads to the introduction of gradient artifact residuals in the data (Yan 2009). In the case of the pulse artifact, the violation of the similarity assumption is even worse as this artifact is inherently variable and calculated templates are only approximations of the artifact epochs (Mullinger 2013b).

In this study, however, we created perfect conditions for the AAS technique in terms of gradient and pulse artifact reduction, because we constructed data without any artifact variation or additional artifacts as eye blink artifacts or power line artifacts. Nonetheless, we can still observe severe artifact residuals in the reconstructed EEG after the application of GA-AAS and PA-AAS. The reconstructed EEG clearly differs from the original artificial EEG in both, time and frequency domain (compare Figure 2.5 A, Figure 2.5 B and Figure 2.6 A, Figure 2.6 B). This impression is supported by the only moderate correlation coefficient of 0.6 between the artificial EEG and the reconstructed EEG. Furthermore, the SNR between the artificial EEG and the artifact residuals in the reconstructed EEG is -1.6 dB only. This negative SNR implies that the artifact residuals (Figure 2.5 C and Figure 2.6 C) are greater than the artificial EEG component, which explains the observation that important brain rhythms as the alpha rhythm are often not visible in EEG obtained during fMRI. These results are highly problematic since for EEG analysis we usually assume a correlation of near 1 and a high SNR, since we expect that the reconstructed EEG is the real EEG and draw our conclusions based on this assumption.

One example: The artifact residuals cover the alpha rhythm in the EEG. Although it is still possible to analyze the differences in alpha rhythm between two settings, the absolute amplitude cannot be used anymore.

Cause of the residual artifacts

A comparison of the spectral signatures of the pulse artifact (Figure 2.4 bottom) with the residual artifacts in the reconstructed EEG (Figure 2.6 C) indicates that the residual artifacts are remainders of the pulse artifact. Furthermore, the artifact residuals in the gradient artifact template during GA-AAS (Figure 2.5 D, Figure 2.6 D) are very similar to those in the reconstructed EEG in time domain as well as in frequency domain. For instance, their correlation coefficient in time domain is 0.95. Hence, pulse artifact remainders are present in the gradient artifact template and consequently, the remainders are added to the reconstructed EEG during gradient artifact template subtraction. Consequently, template corruption is indeed the cause of the artifact residuals in the reconstructed EEG. The pulse artifact component in our study has a maximum amplitude of about 100 μV . According to Allen et al. averaging over 25 epochs should reduce this amplitude to about 4 μV in the template (Allen 2000). However, about three pulse artifact epochs are present in every epoch of the gradient artifact. These single pulse artifact epochs may add up with the pulse artifact epochs of other gradient artifact epochs during the gradient artifact template construction, because they are aligned by chance during averaging. This increases the residual pulse artifact observed in the template by the number of aligned artifacts. We observed residual pulse artifact amplitudes of up to 20 μV instead of the expected residual pulse artifact amplitudes of about 4 μV .

Allen et al. suggested the use of 25 artifact epochs to calculate the artifact templates (Allen 2000). Their reason for that number was that 25 epochs should be enough to reduce artifact residuals in the template to be smaller than the EEG component of interest. However, the number of 25 epochs holds only for single artifacts, for instance eye blinks, but it does not hold for repetitive artifacts, if they are correlated – at least temporarily – with the gradient artifact epochs. During GA-AAS, pulse artifacts are present in every single gradient artifact epoch; therefore, the residual pulse artifact amplitudes in the gradient artifact template are reduced by approximately a factor of square-root of the number of the epochs and not by the number of the epochs. Hence, using 25 epochs in the averaging step implies that pulse artifact amplitudes in the gradient artifact template are reduced by a factor of $\sqrt{25}$ (i.e., only by a factor of 5) and this leads to the residual pulse artifact amplitudes of up to 20 μV that we identified in the reconstructed EEG.

Reducing pulse artifact residuals in the gradient artifact template by higher numbers of epochs

An obvious solution of the problem of the pulse artifact residuals in the gradient artifact template is to use more gradient artifact epochs in the template construction process during GA-AAS. For example, we tested 101 gradient artifact epochs and found a substantial reduction of artifact residuals. The correlation coefficient of artificial EEG and reconstructed EEG improved to 0.84. The SNR of artificial EEG and residual artifacts in the reconstructed EEG improved to 3.8 dB. However, the increased number of gradient artifact epochs reduces the adaptivity of the AAS technique. For example, 101 epochs and a scanner time-of-repetition of 2.5 s implies that 4.2 minutes of EEG are included in the averaging for the template creation. Hence, if motion occurs during that time, all templates that include the gradient artifact epochs in which the motion occurs will be distorted by the permanent artifact change due to the motion. Consequently, in real AAS applications with motions of the study participants, the quality of the artifact template would increase with the number of epochs up to a certain point and then degrade again. One could formulate this situation as an optimization problem, dependent on the frequency of the motion. However, an individual optimization step per study participant would be necessary, which may be impracticable.

Variant of AAS

Interestingly, modifications of the AAS technique that aim at improving the template quality have already been proposed. Sijbers et al. suggested using median filtering instead of averaging for the template creation (Sijbers 2000). The median filtering should mitigate the effects of artifacts in the template. Our experience, however, is that this method is somewhat advantageous in the lower frequency range, but increases the gradient artifact residuals in the upper frequency range and as a result we found no overall benefit.

Gonçalves et al. proposed another modification: weighting epochs by their variance in the averaging step (Gonçalves 2007). The idea behind this approach is that the artifact affected EEG epochs have a higher variance than those without artifacts. This method is possibly beneficial if single artifacts are present, but we identified the pulse artifact as the main contributor to the artifact residuals in the template. The pulse artifact is present at all times and constantly contributes to the variance. Therefore, the weighting step has virtually no influence on the pulse artifact residuals found in the gradient artifact template.

Post AAS techniques to improve EEG quality

Beside improving the AAS technique, it is also an option to use additional artifact reduction methods after the AAS technique to improve the EEG quality. Different

methods were proposed. One example are linear signal decomposition based techniques. For instance, temporal principal component analysis can be applied to find and remove residual of the gradient and pulse artifact in the reconstructed EEG (Niazy 2005). This method is known as optimal basis sets technique and it seems that in comparison to the AAS technique, it is beneficial at lower sampling rates, but it is less effective for interictal spikes reconstruction (Grouiller 2007). Other linear signal decomposition techniques are spatial principal component analysis or independent component analysis (Benar 2003, Srivastava 2005). However, as Niazy et al. already pointed out *“One problem with these approaches is that they necessitate the presence of a large number of sensors. Also, the identification of artifact components can be subjective and is usually done manually. Most importantly, spatial filters assume that all the sensors are contaminated by common sources, which is not the case. The BCG artifact [pulse artifact] derives from sources that are rotating/moving, which contaminate different sensors at different points during the cardiac cycle with different effects.”* (Niazy 2005). A different approach to improve the EEG quality is based on adaptive filtering. Independent recordings of the artifacts or the artifact residuals are used as input for an adaptive filter to reduce the artifact residuals further. This approach showed very promising results, but additional hardware – often only available as a prototype – is necessary and is therefore limiting this approach (Bonmassar 2002, Masterton 2007, Abbott 2014, Steyrl 2017, Steyrl 2018).

Conclusions

Our results reveal a previously unknown source of artifact residuals in EEG of simultaneous EEG-fMRI. The AAS technique itself adds artifact residuals to the EEG, although we created optimal conditions for the AAS technique. In particular, pulse artifact residuals that remain in the gradient artifact template are added to the reconstructed EEG. The artifact residuals mask the commonly analyzed alpha and beta rhythms of the EEG. Therefore, researchers should be aware that the AAS method can substantially contaminate the EEG data. In theory, the pulse artifact residuals in the gradient artifact template can be reduced by using a higher number of gradient artifact epochs in the averaging procedure. However, this comes at the cost of adaptivity of the AAS technique. Adaptivity is important in real AAS applications, where study participants move their heads. The optimal number of epochs for the template calculation is thus difficult to define. However, using 25 epochs in the averaging step, as suggested by Allen et al., results in a low EEG quality. We recommend using a higher number of gradient artifact epochs. To avoid the loss in adaptivity, we suggest using a shorter time-of-repetition in the MRI scanner sequence. However, a shorter time-of-repetition potentially leads to unwanted heating of the body tissue or the EEG equipment and therefore further investigations of this approach are necessary.

Acknowledgments

This work was partly supported by the ERC Consolidator Grant 681231 ‘Feel Your Reach’.

2.2 Primary publication 2: Reduction of EEG Artifacts in Simultaneous EEG-fMRI: Reference Layer Adaptive Filtering (RLAF)

[Steyrl 2015] Steyrl D, Patz F, Krausz G, Edlinger G, Müller-Putz GR (2015) Reduction of EEG Artifacts in Simultaneous EEG-fMRI: Reference Layer Adaptive Filtering (RLAF). In: Proceedings of the 37th Annual International Conference of the IEEE Engineering in Medicine and Biology Society, EMBC15, Milano, Italy, August 25-29, pp.3803-3806. <https://doi.org/10.1109/EMBC.2015.7319222>

As shown in primary publication 1, residual artifacts are still present in the EEG after applying the AAS method. In fact, the AAS technique is vulnerable to correlated artifacts and adds artifacts to the EEG due to PA remainders in the GA subtraction templates. Chowdhury et al demonstrated that applying the RLAS technique after the AAS method reduces artifact residuals substantially (Chowdhury 2014). This is plausible as the artifact residuals in the reference-layer recordings are presumably similar to the artifact residuals in the EEG and a subtraction of the reference-layer signals from the EEG will mitigate the residual artifacts. However, the reference-layer construction used by Chowdhury et al is not reusable and the entire construction is fragile and cumbersome (Chowdhury 2014). Furthermore, they did not take into account possible differences between the artifact residuals of the reference-layer and the EEG. Therefore, in accordance with the second aim of this thesis, a new artifact reduction technique was developed that combines a robust EEG cap prototype (GUGER TECHNOLOGIES OG, Graz, Austria) with a built in reference-layer that allows to record artifacts and EEG with narrow spaced mechanically coupled double layer electrode pairs (Figure 2.7, A and B) and adaptive filtering to compensate possible differences. The new technique is referred to as RLAF and – similar to the RLAS method – it is applied in an additional signal processing step after the AAS method.

The primary publication 2 is the first publication of a series of three that introduce and evaluate the RLAF technique. The study had four objectives: (i) To test the handling of the reference-layer EEG cap prototype. (ii) To present the idea of the RLAF method. (iii) To demonstrate the general feasibility of the RLAF technique. (iv) To validate the finding of Chowdhury et al regarding the application sequence of the AAS technique and the RLAS technique and to test whether this findings also apply to the RLAF method (Chowdhury 2014). Therefore, test measurements were carried out inside an MRI scanner during fMRI acquisition. The EEG cap prototype was fixed on a spherical MRI phantom. Artifact reduction was carried out in 5 different settings. In settings 1 to 3, the artifact reduction techniques AAS, RLAS, and RLAF

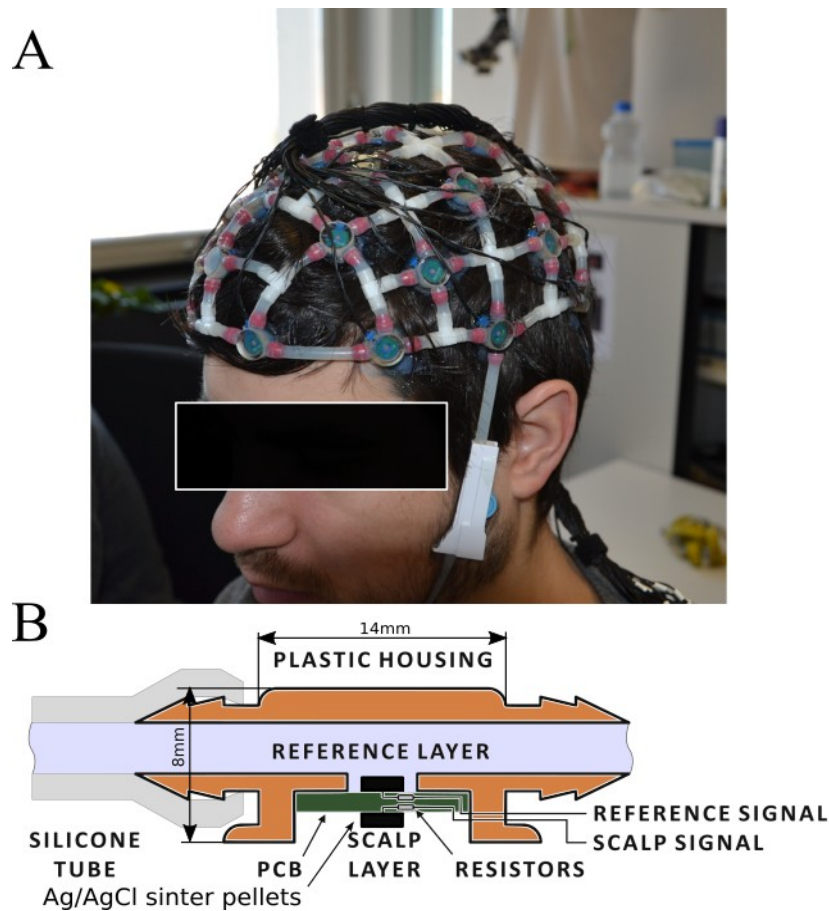


Figure 2.7: Reference layer cap prototype. A: Cap prototype mounted on a head, B: schematics of a reference layer electrode pair.

were directly applied to the test-data. In settings 4 and 5, techniques were combined. In setting 4, the RLAS technique was applied after the AAS method, and in setting 5, the RLAF technique was applied after the AAS method. Artifact reduction efficacy was evaluated by the residual power in the test-data after artifact reduction. The MRI phantom can not emit electromagnetic signals, hence, all signals measured with the EEG system are artifacts from the MRI scanner. Meaning, the smaller the residual artifact power, the better the artifact reduction method.

Contribution to this thesis: This study shows that the reference-layer EEG-cap prototype can be applied multiple times. It successfully demonstrates the feasibility of the RLAF technique and shows that the finding of Chowdhury et al regarding the application sequence of RLAS is also valid for the RLAF technique (Chowdhury 2014). Finally, the study demonstrates that the RLAF method reduces artifacts more effective than the RLAS technique, at least with the test-data recorded at the fMRI phantom.

2.3 Primary publication 3: Reference layer adaptive filtering (RLAF) for EEG artifact reduction in simultaneous EEG-fMRI

[Steyrl 2017] Steyrl D, Krausz G, Koschutnig K, Edlinger G, Müller-Putz GR (2017) Reference layer adaptive filtering (RLAF) for EEG artifact reduction in simultaneous EEG-fMRI. *Journal of Neural Engineering* 14(2):026003. <https://doi.org/10.1088/1741-2552/14/2/026003>

After the first successful application of the RLAF method with test-data, the next step was to evaluate the method on the human EEG. However, insightful evaluations of artifact reduction techniques with human EEG-data is tricky, since the clean EEG is not known. Furthermore, an evaluation on humans require the equipment to be safe. In the case of simultaneous EEG-fMRI, the possible heating of metal objects in the RF field of the MRI scanner is problematic and it must be ruled out that the heating is harmful in any way.

The primary publication 3 is the second publication that introduce and evaluate the RLAF technique and it had the following two objectives: (i) To assess the heating of the EEG electrodes of the reference-layer EEG cap prototype. (ii) To evaluate the performance of the RLAF technique in human EEG. For the assessment of the heating, temperature measurements were carried out inside the MRI scanner. During the temperature measurements, MRI sequences with a high specific absorption rate were applied to establish a worst case scenario. For the evaluation of the artifact reduction performance in human EEG, it is possible to use the SNRs of well-known EEG activity after applying artifact reduction techniques as performance metric. For instance, in primary publication 3, the first EEG activity used as performance metric was occipital alpha rhythm change induced by closing the eyes. The second was visually evoked potentials induced by a checkerboard stimulation. A higher SNR means that the EEG activity is preserved while residual artifacts and noise are reduced. A second possibility is to use machine-learning techniques to classify EEG activity in the EEG after artifact reduction and to use the classification accuracy as a measure for EEG quality. Both approaches does not require clean EEG. Furthermore, in this publication, an enhanced version of the RLAF technique is introduced. This method uses a filter-bank to split the EEG into predefined frequency bands and performs the RLAF method then separately for each frequency band. The individual frequency bands are combined again to obtain EEG with full bandwidth. This method is referred to as multi band RLAF (MBRLAF). The evaluation was carried out by computing the SNRs and the classification accuracies for 4 different settings (Figure 2.8). Setting 1 used the EEG after the application of only the AAS technique. Setting 2 in-

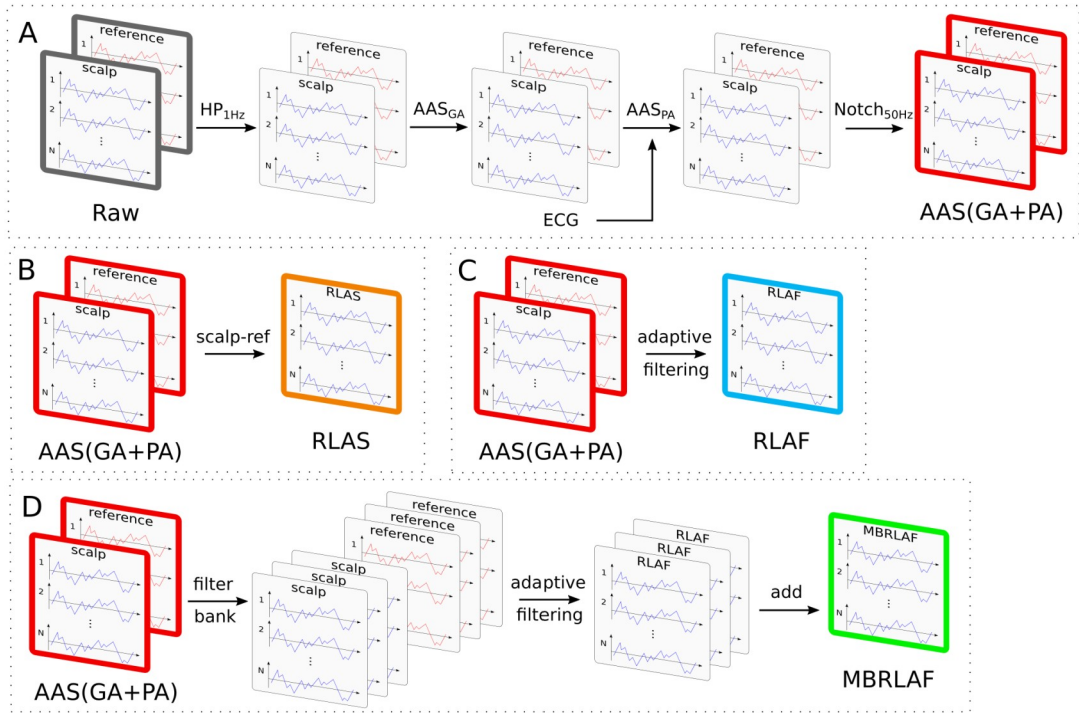


Figure 2.8: Signal processing of the different evaluation settings. Panel A: Setting 1, average artifact subtraction (AAS) of the gradient artifact (GA), AAS of the pulse artifact (PA) with support of electrocardiogram (ECG). Panel B: Setting 2, RLAS method. Panel C: Setting 3, RLAF technique, reference channels were adaptively scaled before being subtracted from the scalp channels. Panel D: Setting 4, MBRLAF method.

cluded the EEG after the application of the AAS technique and a subsequent application of the RLAS method. Setting 3 used the EEG obtained after the application of the AAS technique and a subsequent application of the RLAF method. Setting 4 included the EEG after the application of the AAS technique and a subsequent application of the MBRLAF method.

Contribution to this thesis: The temperature measurements confirm the safety of the reference-layer EEG cap prototype in terms of heating. The investigations of EEG activity show that all investigated add-on techniques (RLAS, RLAF, MBRLAF) successfully reduce remaining fMRI related artifacts in human EEG after the application of the AAS technique. In a direct comparison, the combination of AAS and MBRLAF performed best in terms of SNR and classification accuracy, followed by the combination of AAS with RLAF, and by AAS with RLAS.

2.4 Primary publication 4: Online reduction of artifacts in EEG of simultaneous EEG-fMRI using reference layer adaptive filtering (RLAF)

[Steyrl 2018] Steyrl D, Krausz G, Koschutnig K, Edlinger G, Müller-Putz GR (2018) Online reduction of artifacts in EEG of simultaneous EEG-fMRI using reference layer adaptive filtering (RLAF). *Brain Topography* 31(1):129-149. <https://doi.org/10.1007/s10548-017-0606-7>

The previous study showed that the RLAF technique is an effective method for the reduction of artifact residuals that remain in human EEG after the application of the AAS method. To conclude the comprehensive evaluation of the RLAF technique two subjects were remaining. Firstly, the online applicability of the RLAF technique was not yet demonstrated and evaluated and secondly, a comparison with the quality of EEG obtained in a lab environment (outside the MRI scanner) was missing.

The primary publication 4 is the last publication that introduce and evaluate the RLAF technique and had the objective to answer the following two questions: (i) Is it possible to use the RLAF technique for online artifact reduction and what is the quality of the obtained EEG compared to an offline artifact reduction? (ii) What is the quality of the obtained EEG compared to EEG recorded in the lab? The study protocol of primary publication 3 was modified to answer this questions. The main modification was to record EEG activity twice, first outside the MRI scanner in the lab and then inside the MRI scanner. Furthermore, the whole signal processing was implemented for online operation. As in primary publication 3, the SNRs of EEG activities after artifact reduction were used to evaluate the performance of the techniques. Four different setting were evaluated. Setting 1 included the EEG recorded in the lab. Setting 2 used the EEG after the application the offline variant of the AAS technique. Setting 3 included the EEG obtained by the online variant of AAS technique. Setting 4 used the EEG obtained by the online version of the AAS technique and a subsequent online application of the RLAF method. Furthermore, a new version of the reference-layer EEG cap prototype was used, that was built with more robust electrodes.

Contribution to this thesis: This study shows that the additional application of the online RLAF technique after the online AAS method improves the EEG quality substantially and that EEG activity of physiological brain signals are preserved with improved SNR (Figure 2.9). Occasionally, the combination of online AAS and online RLAF is even able to surpass the EEG quality of the offline AAS technique. Despite this undoubted progress in the EEG data quality, this publication showed that the

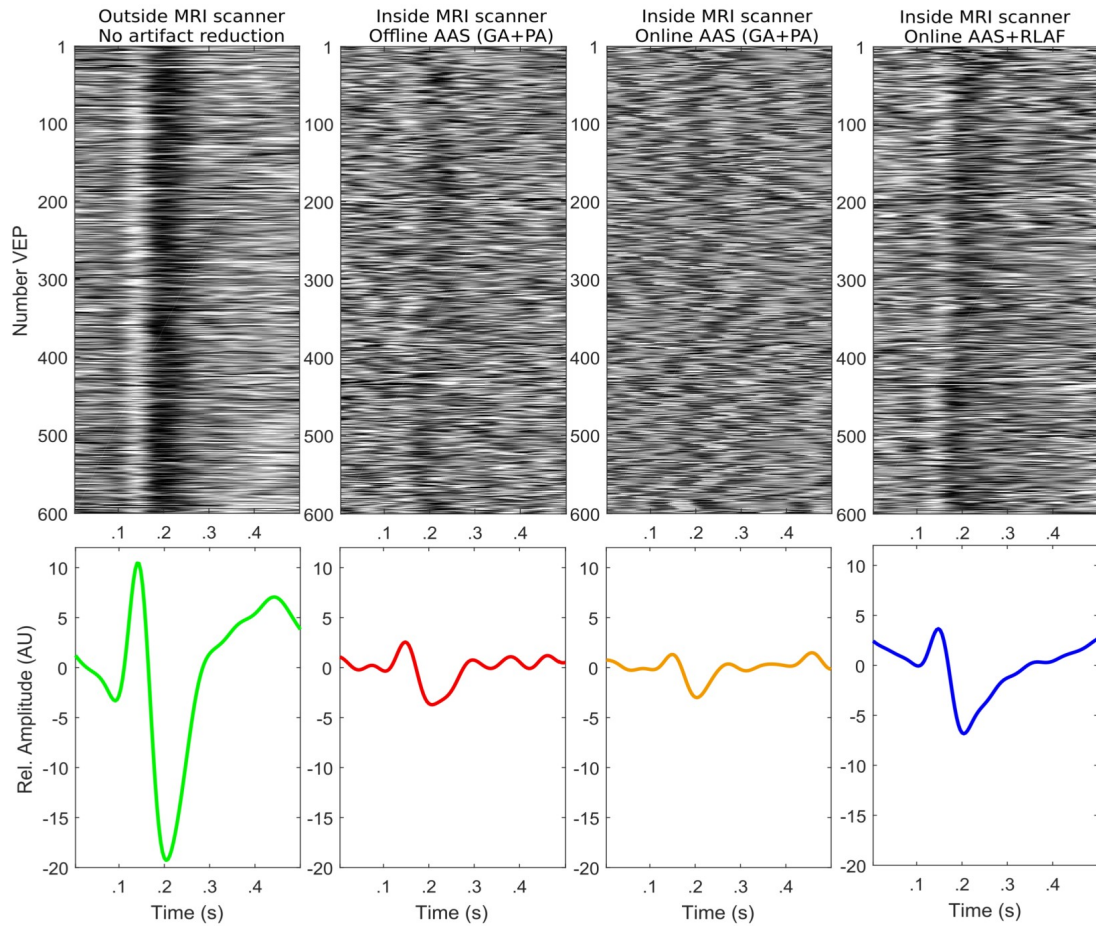


Figure 2.9: Representative examples of visually evoked potentials (VEPs) for different pre-processing and artifact reduction procedures (average artifact subtraction AAS, reference layer adaptive filtering RLAF). Examples are from participant 4 at electrode POZ. Upper row: single VEPs at electrode POZ (1-15 Hz). Bottom row: average VEPs at electrode POZ scaled to the EEG noise amplitude. Hence, VEP amplitude divided by the root-mean-square value of the (\pm) reference

quality of EEG recorded inside the MRI scanner is still not reaching the quality of EEG recorded in the lab.

2.5 Secondary publication: Single trial Motor Imagery classification in EEG measured during fMRI image acquisition – a first glance

[Steyrl 2013] Steyrl D, Wriessnegger SC, Müller-Putz GR (2013) Single trial Motor Imagery classification in EEG measured during fMRI image acquisition – a first glance. *Biomedical Engineering / Biomedizinische Technik* 58(Suppl.1):1-2. <https://doi.org/10.1515/bmt-2013-4450>

Motor-imagery allows the intentional modulation of sensory-motor rhythms in the EEG. An accurate classification of the sensory-motor rhythm modulations establishes a non-muscular path from the brain to the environment for communication and control purposes. This work is a pilot study that was conducted to explore the feasibility of sensory-motor rhythm classification from EEG recorded during concurrent fMRI to investigate EEG-based BCI control with fMRI. This study had two aims: (i) Comparison of the motor-imagery patterns in EEG recorded in a lab environment and in EEG recorded concurrently with fMRI. (ii) Comparison of the motor-imagery classification accuracy of EEG recorded in a lab environment and of EEG recorded concurrently with fMRI.

Contribution to this thesis: This study shows that for the single study participant, the classification accuracy of sensory-motor rhythm modulations is 22% points lower in EEG that was recorded inside the MRI scanner, compared to the classification accuracy in EEG that was recorded outside the MRI scanner. This result is also reflected in the motor-imagery patterns (Figure 2.10). The patterns are substantially weaker in the EEG recorded concurrently with fMRI.

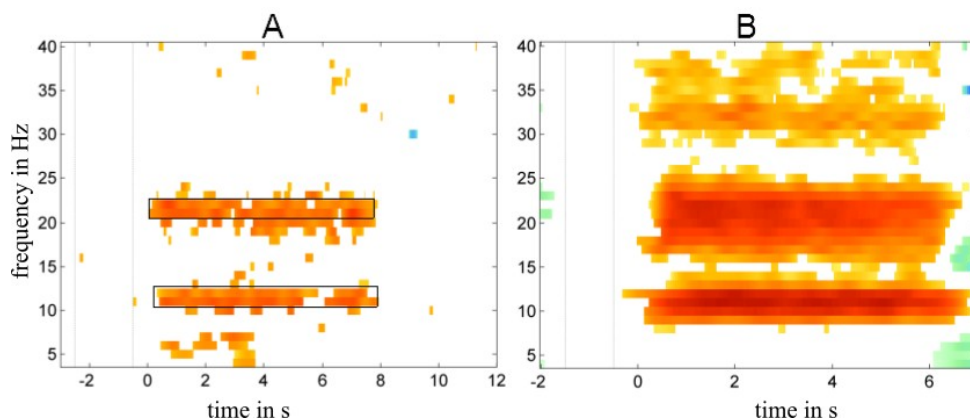


Figure 2.10: Sensory-motor rhythm patterns in the EEG. Time 0 indicate start of motor-imagery. Yellow to red indicate significant less power between right hand and feet motor-imagery (Lap C3, Bootstrap significance test $\alpha=0.01$). A: Patterns in EEG recorded concurrently with fMRI. B: Patterns in EEG recorded in the lab environment.

3 Discussion

*“All truths are easy to understand once they are discovered;
the point is to discover them.”*

– attributed to Galileo Galilei

3.1 Overview

This thesis pursued two research objectives. Firstly, identification and analysis of the causes of remaining artifacts after the application of the AAS method. Secondly, the development and evaluation of a new artifact reduction technique that is able to reduce the remaining artifacts to improve the data quality of EEG recorded simultaneously with fMRI. The new method is referred to as RLAF. The results of the analyses, hence, the contributions of the thesis to the existing body of knowledge, are presented in four primary publication and can be summarized in the following points:

1. Insights into the remaining artifacts after application of the AAS technique and possibilities for their reduction.
2. Empirical knowledge on handling and safety of the EEG cap prototype with built in reference-layer and tightly coupled EEG electrodes.
3. Introduction and comprehensive evaluation of the RLAF technique in terms of its feasibility, application to the EEG, online applicability, and artifact reduction efficiency.

3.2 Remaining artifacts after applying the AAS technique

Remainders of fMRI related artifacts are still present in the EEG after the application of any of the available artifact reduction method. This holds also true for the most common artifact reduction technique AAS. The AAS technique was designed to reduce repetitive artifacts as the GA and the PA. However, especially PA residuals remain in the EEG. For instance, the inherent variability of the PA is one cause for PA remainders, as it leads to a subtraction template misfit and consequently to artifact residuals. A recent study tackles the PA variability problem by adaptive optimal basis sets (Marino 2018b). Aside of the residuals caused by the PA variability, the first study of this thesis revealed a second previously unknown cause of PA residuals after the AAS method: PA remainders contaminate the subtraction templates during GA reduction and cause artifact residuals in the EEG because they are added to the EEG by the subtraction of the templates. During the GA template construction it occurs that single PA repetitions sum up and remain in the GA templates instead of being removed by averaging. This happens since the GA epoch length is often roughly a fixed multiple of the PA epoch length. Thus, the GA and the PA are temporary correlated and the correlation cause a violation of the assumption that averaging can produce a clean artifact template. Hence, the artifact residuals found in this study are explicitly not caused by the intrinsic variability of the PA, but origin from PA remainders in the GA template due to a temporary correlation of the GA and the PA. One

possibility to significantly reduce the artifact residuals in the GA subtraction template is to include more artifact epochs in the computation of the template, because more epochs reduce the effect of a few aligned PA epochs. However, this approach has the disadvantage that the AAS method loses its adaptability to changes in the artifact shape the more artifact epochs are included in the averaging (Allen 2000). Interestingly, several modifications of the AAS technique that aim at reducing artifacts in the GA and PA templates were proposed in the past already. For example, Sijbers et al. proposed the use of median filtering instead of averaging for the template computation (Sijbers 2000). The median filtering should mitigate the effects of single high power artifacts in the GA or PA epochs. Preliminary studies in the course of this thesis showed that the median filtering does not remove the PA residuals in the subtraction template. Gonçalves et al. proposed another modification: weighting epochs by the inverse of their variance in the averaging step (Gonçalves 2007). The idea behind this approach is that if epochs of the GA or the PA are affected by additional artifacts then they have a higher variance compared to those without additional artifacts. This technique is possibly beneficial if single additional artifacts are present; however, preliminary studies carried out as part of this thesis showed no benefit in applying this modification in regard to the PA contaminated templates.

3.3 From remaining artifacts to reference-layer adaptive filtering

Although the AAS technique has certain weaknesses, it is still one of the most efficient techniques available to reduce the GA and the PA (Grouiller 2007). Modifications of the AAS technique were presented that try to overcome some of its limitations (Freyer 2009, Marino 2018b). Usually, it is tried to cope with the inherent variability of the PA. Unfortunately, the modifications are often mutually exclusive. Furthermore, other artifacts e.g. the MA, can not be reduced by the AAS technique by concept. Therefore, add-on techniques were presented to tackle the remaining artifacts after an application of the AAS technique. One example of a very promising add-on technique is the RLAS method (Chowdhury 2014). Initially, the method was developed as stand alone technique and became an add-on technique afterwards, as investigations by Chowdhury et al. showed that this method is very effective in reducing remaining artifacts. What makes the RLAS method particularly interesting is its capability to reduce any artifact that is represented in the reference-layer recordings. This applies to non-repetitive artifacts as well as to residuals of the PA due to their inherent variability, but also to the PA residuals identified in the first study, because when the AAS technique is also applied to the reference-layer recordings then AAS adds the same PA residuals to the reference-layer recordings as to the EEG and the subsequent subtraction will reduce them. Therefore, it was decided to pursue this

approach for the new method RLAF, but to enhance it in two important aspects. Firstly, a new reference-layer EEG cap prototype was used that has a robust built in reference-layer, mechanically tightly coupled electrode pairs and that can be applied several times. Secondly, the subtraction was replaced by adaptive filtering, to compensate possible artifact mismatches between the reference-layer and the EEG.

3.4 The reference-layer EEG cap prototypes

Two versions of the reference-layer EEG cap prototype were deployed in the three studies regarding the RLAF technique. The first version was developed and constructed by GUGER TECHNOLOGIES OG, Graz, Austria and was applied first time by Hermans et al. in a comparison of reference-signal based methods for the removal of movement related artifacts (Hermans 2016). In the course of this thesis, this cap was used for the measurements on the MRI phantom and in the first study with human EEG – primary publications two and three in this thesis. Unfortunately the cap became unusable afterwards, because the abrasive EEG gel removed the silver layer of some EEG electrodes and the underlying copper and the remaining silver formed a half-cell potential that led to a permanent saturation of the EEG amplifier. In cooperation with GUGER TECHNOLOGIES, a second version of the EEG cap prototype was constructed that use robust silver/silver-chloride sintered electrodes instead of the silver coating. This version of the EEG cap was deployed in the second study with human EEG-data – primary publication 4 of this thesis. The design of the cap prototypes pursued the following goals: safe in terms of heating, reusable reference-layer for short preparation times, and mechanically close coupling of the electrode pairs to prevent additional artifacts. In terms of heating through RF-energy absorption, the cap-prototypes can be considered safe, since the temperature measurements showed a maximum heating of approximately 1 °C and no study participant reported a heating of the electrodes. The studies confirmed that the reference-layer construction is reusable. The reference-layer made of saline water filled tubes effectively eliminates the time-consuming construction of a separate agar-gel reference-layers for every participant as it was deployed by Chowdhury et al. (Chowdhury 2014). In fact, using the reference-layer caps did not extend the preparation time of the study participants compared to the preparation time with a standard MRI compatible EEG cap. The newly designed double-layer electrodes are mechanically tightly coupled which prohibits any relative motions between the electrodes. No additional artifacts were found in the course of the studies. Therefore, the design goals for the caps were achieved.

3.5 Reference-layer adaptive filtering in action and its relation to the state-of-the-art

All studies conducted in the course of this thesis confirm that the RLAF technique reduces remaining artifacts in test-data as well as in human EEG substantially, both offline and online (Steyrl 2015, Steyrl 2017, Steyrl 2018). The found EEG quality improvement was both significant ($p < 0.01$) and relevant (Steyrl 2017). For instance, an offline application of the AAS technique yields typically a higher EEG quality as an online application, because in an offline application future EEG-data can be included in the template construction. However, the combination of online AAS and online RLAF led to an EEG quality that is comparable with those after an offline application of the AAS technique. This EEG quality improvement is an important step towards EEG based neurofeedback and BCIs studies inside an MRI scanner.

The RLAF method does not remove physiological EEG components. On the contrary, the SNR as well as the classification accuracy of physiological EEG components are improved by the RLAF technique (Steyrl 2017, Steyrl 2018). High quality physiological components are very important in terms of reliable data processing, study replicability, study duration (necessary repetitions), and they hold the potential of new findings. Using the RLAF method is convenient and practical. The only hyper-parameter that must be set is the step-size of the adaptive filters. A fixed value of 8×10^{-7} was found to be a good compromise between adaptation speed and stability of the adaptive filtering (Steyrl 2018). The chosen step-size allowed the adaptive filters to successfully adjust the forward model to compensate fast and slow changes in the relation between artifacts in the reference-signal and in the EEG. Furthermore, the fast as well as slow changes illustrate again that a one time fit of the forward model is not sufficient and that the adaptive filtering (scaling) is indeed necessary (Steyrl 2017).

In the course of this thesis, the RLAF technique was tested in its ability to improve the overall EEG quality. It was not investigated how improvements in single artifact residuals contribute to the overall improvement. However, Spencer et al. analyzed MAs and found that they are successfully reduced by the RLAS technique (Spencer 2018). Furthermore, Hermans et al. investigated PA residuals and found that reference-layer methods successfully reduce PA remainders (Hermans 2016). As RLAF is also a reference-layer based technique it can be assumed that these findings are also valid for the RLAF technique. Consequently, the EEG quality improvement by the RLAF technique is very likely the results of a combination of improvements in single remaining artifact. This is backed up by the fact that reference-layer techniques are conceptually able to reduce all types of artifacts that are represented in the reference-layer.

A comprehensive comparison or review of state-of-the-art artifact reduction methods would be very important for – and highly appreciated by – the simultaneous EEG-fMRI community. However, many techniques are in prototype state and require special hardware that is often available in one lab only. Furthermore, no standardized testing protocol for new artifact reduction techniques is available. Finally, test results can differ between MRI scanner models. Therefore, such a comparison is missing. However, in the course of this thesis the RLAF method was compared with the AAS technique (offline and online) and the RLAS technique (offline) (Steyrl 2017, Steyrl 2018, Allen 1998, Allen 2000, Chowdhury 2014). As already mentioned, the application of the RLAF method after the AAS technique yields a substantially improved EEG quality. Furthermore, the RLAF technique is generally also superior to the predecessor technique RLAS, with one exception: the RLAS method showed slightly better artifact reduction results in the gamma frequency range (Steyrl 2017). This is caused by a general problematic behavior of time domain least-mean-square (LMS) adaptive filters when applied to the EEG. The EEG has a $1/f$ distribution in the frequency domain, meaning that the most signal power is in the lower frequency range. LMS adaptive filters minimize the signal power of the error signal – which is the EEG signal in the RLAF case – and therefore, LMS adaptive filters will fit their filter weights to the lower frequency range. Especially when the EEG is contaminated by PA residuals, because the power of the residuals is also higher in the frequency range below 20 Hz. The adaptation to the lower frequency range can lead to a misfit in the gamma range and to a slightly lower EEG quality in that range compared to a straight forward subtraction. The use of higher order adaptive filters instead of the deployed first order filters does not provide a solution. An adaptive filter with order > 1 represents an adaptive band-pass filter that is applied to the artifact signal (the signal from the reference-layer) before the subtraction. Therefore, adaptive filters of a higher order learn a band-pass filter for the lower frequency range when applied to the EEG and remove the higher frequency components from the reference-layer signal. The higher frequency components of the reference-layer signal (the artifacts with higher frequency) are subsequently missing for subtraction and will stay in the EEG. The MBRLAF technique was developed to compensate this weakness. This method divides the EEG of each electrode and the associated artifact signal from the reference-layer into frequency bands and applies a separate adaptive filter per frequency band. This approach ensures an optimal scaling for each frequency band and was the best performing technique in the conducted comparisons (Steyrl 2017). However, the improvement comes at the cost of computational complexity. Therefore, this approach was not used in assessing the online capabilities of the RLAF approach.

3.6 Summary and Conclusions

PA residuals in the subtraction templates during GA reduction were found to cause substantial artifact residuals in the EEG when the AAS method is applied. This cause was previously unknown and is not a result of artifact variability, but results from an intrinsic weakness of the AAS technique with correlated artifacts. The studies of this thesis showed that the RLAF method is an effective technique to substantially reduce this and other types of artifact residuals in the EEG. The RLAF method improves the SNR as well as the classification accuracy of physiological EEG components in off-line and online applications. The ability to reduce all kinds of occurring artifacts in combination with its easy handling – only small extension of the preparation time, only one hyper-parameter that does not need tuning – makes the RLAF technique a candidate for a future gold standard method for artifact reduction in EEG concurrently recorded with fMRI.

3.7 Outlook

It is clear that not only the variability of the PA is a major problem for the AAS method, but also the PA remainders in the GA template. Although it is not yet clear how to use that knowledge, at least it provides a new starting point for an improvement of the AAS technique.

Currently, the reference-layer EEG cap is available in one size only and the cap is not adjustable to different head sizes and shapes, as the silicone tubes that establish the reference-layer have limited flexibility. A customizable design would be highly welcome. Furthermore, filling the cap with saline water is currently cumbersome since air bubbles can stay in the reference layer. The air bubbles can restrict the contact between the saline water and the electrode which potentially prohibits the interdependent artifact measurement for single electrode pair. An improved method for filling the reference-layer would save time.

At time of writing this thesis only one working reference-layer EEG cap prototype is available which prohibits a broad application of the RLAF method. However, the cap prototype was designed to be compatible with different EEG recording systems and the actual adaptive filtering can be implemented in the respective recording software of the EEG systems. Consequently, if the reference-layer EEG cap is once commercially available, the RLAF technique can spread fast as existing MRI compatible EEG recording systems can be upgraded with the RLAF technique.

The MBRLAF technique was developed to overcome the gamma range weakness of the RLAF method. Due to the higher computational demand, this method was not applied online. However, consequent parallelization of the band pass filtering and the

adaptive filtering in the MBRLAF technique should allow an online application in future. Another option to implements the MBRLAF technique present the use of frequency-domain adaptive filters instead of band-pass filtering and time-domain adaptive filters (Shynk 1992). Frequency-domain adaptive filters can provide the same functionality, but are computationally more effective due to efficient implementations of the Fourier transformation (Shynk 1992). Hence, signal processing holds the potential to improve the (MB)RLAF technique further.

4 References

“S: How many references do I need to include? P: Well, too few let people think you’re making things up, too many let people think you’re unoriginal. S: So what is the optimal number? P: A few.”

– freely adapted from PhD comics

References

- [Abbot 2014] Abbott DF, Masterton RAJ, Archer JS, Fleming SW, Warren AEL, Jackson GD (2014) Constructing carbon fiber motion-detection loops for simultaneous EEG–fMRI. *Front Neurol* 5:260. <https://doi.org/10.3389/fneur.2014.00260>
- [Abolghasemi 2015] Abolghasemi V, Ferdowsi S (2015) EEG-fMRI: dictionary learning for removal of ballistocardiogram artifact from EEG. *Biomed. Signal Process. Control* 18:186-94. <https://doi.org/10.1016/j.bspc.2015.01.001>
- [Abreu 2016] Abreu R, Leite M, Jorge J, Grouiller F, van der Zwaag W, Leal A, Figueiredo P (2016) Ballistocardiogram artefact correction taking into account physiological signal preservation in simultaneous EEG-fMRI. *NeuroImage* 15:45-63. <https://doi.org/10.1016/j.neuroimage.2016.03.034>
- [Abreu 2018] Abreu R, Leal A, Figueiredo P (2018) EEG-Informed fMRI: A Review of Data Analysis Methods. *Front. Hum. Neurosci.* 12:29. <https://doi.org/10.3389/fnhum.2018.00029>
- [Acharjee 2015] Acharjee PP, Phlypo R, Wu L, Calhoun VD, Adali T (2015) Independent vector analysis for gradient artifact removal in concurrent EEG-fMRI Data. *IEEE Trans. Biomed. Eng.* 62:1750-8. <https://doi.org/10.1109/TBME.2015.2403298>
- [Adolphs 2015] Adolphs R (2015) The unsolved problems of neuroscience. *Trends Cogn Sci.* 19(4):173-175. <https://doi.org/10.1016/j.tics.2015.01.007>
- [Al-Asmi 2003] Al-Asmi A, Benar CG, Gross DW, Khani YA, Andermann F, Pike B, Dubeau F, Gotman J (2003) fMRI activation in continuous and spike-triggered EEG–fMRI studies of epileptic spikes. *Epilepsia* 44:1328-1339. <https://doi.org/10.1046/j.1528-1157.2003.01003.x>
- [Allen 1998] Allen PJ, Polizzi G, Krakow K, Fish DR, Lemieux L (1998) Identification of EEG events in the MR scanner: the problem of pulse artifact and a method for its subtraction. *Neuroimage* 8(3):229-239. <https://doi.org/10.1006/nimg.1998.0361>
- [Allen 2000] Allen PJ, Josephs O, Turner R (2000) A method for removing imaging artifact from continuous EEG recorded during functional MRI. *Neuroimage* 12(2):230-239. <https://doi.org/10.1006/nimg.2000.0599>
- [Asseondi 2016] Asseondi S, Lavallee C, Ferrari P, Jovicich J (2016) Length matters: improved high field EEG-fMRI recordings using shorter EEG cables. *J Neurosci Methods* 269:74-87. <https://doi.org/10.1016/j.jneumeth.2016.05.014>

References

- [Bagarinao 2018] Bagarinao E, Maesawa S, Ito Y, Usui N, Natsume J, Watanabe H, Hoshiyama M, Wakabayashi T, Sobue G, Naganawa S, Isoda H (2018) Detecting sub-second changes in brain activation patterns during interictal epileptic spike using simultaneous EEG-fMRI. *Clinical Neurophysiology* 129(2):377-389. <https://doi.org/10.1016/j.clinph.2017.11.018>
- [Baumeister 2014] Baumeister S, Hohmann S, Wolf I, Plichta M, Rechtsteiner S, Zangl M, Ruf M, Holz N, Boecker R, Meyer-Lindenberg A, Holtmann M, Laucht M, Banaschewski T, Brandeis D (2014) Sequential inhibitory control processes assessed through simultaneous EEG-fMRI. *NeuroImage* 94:349-359. <https://doi.org/10.1016/j.neuroimage.2014.01.023>
- [Becker 2011] Becker R, Reinacher M, Freyer F, Villringer A, Ritter P (2011) How ongoing neuronal oscillations account for evoked fMRI variability. *J. Neurosci.* 31:11016-11027. <https://doi.org/10.1523/JNEUROSCI.0210-11.2011>
- [Benar 2003] Bénar CG, Aghakhani Y, Wang Y, Izenberg A, Al-Asmi A, Dubeau F, Gotman J (2003) Quality of EEG in simultaneous EEG-fMRI for epilepsy. *Clinical Neurophysiology* 114(3):569-580. [https://doi.org/10.1016/S1388-2457\(02\)00383-8](https://doi.org/10.1016/S1388-2457(02)00383-8)
- [Berger 1929] Berger H (1929) Über das Elektrenkephalogramm des Menschen. *Arch. Psychiatr. Nervenkr.* 87:527-570. <https://doi.org/10.1007/BF01797193>
- [Biessmann 2011] Bießmann F, Plis S, Meinecke FC, Eichele T, Müller KR (2011) Analysis of Multimodal Neuroimaging Data, *IEEE Reviews in Biomedical Engineering* 4:26-58. <https://doi.org/10.1109/RBME.2011.2170675>
- [Biswal 1995] Biswal BB, Yetkin FZ, Haughton VM, Hyde JS (1995) Functional connectivity in the motor cortex of resting human brain using echo-planar MRI. *Magn. Reson. Med.* 34(4):537-541. <https://doi.org/10.1002/mrm.1910340409>
- [Biswal 2010] Biswal BB, Mennes M, Zuo XN, Gohel S, Kelly C, Smith SM, Beckmann CF, Adelstein JS, Buckner RL, Colcombe S, Dogonowski AM, Ernst M, Fair D, Hampson M, Hoptman MJ, Hyde JS, Kiviniemi VJ, Kötter R, Li SJ, Lin CP, Lowe MJ, Mackay C, Madden DJ, Madsen KH, Margulies DS, Mayberg HS, McMahon K, Monk CS, Mostofsky SH, Nagel BJ, Pekar JJ, Peltier SJ, Petersen SE, Riedl V, Rombouts SA, Rypma B, Schlaggar BL, Schmidt S, Seidler RD, Siegle GJ, Sorg C, Teng GJ, Vejjola J, Villringer A, Walter M, Wang L, Weng XC, Whitfield-Gabrieli S, Williamson P, Windischberger C, Zang YF, Zhang HY, Castellanos FX, Milham MP (2010) Toward discovery science of human brain function. *Proc. Natl. Acad. Sci. U. S. A.* 107(10):4734-4739. <https://doi.org/10.1073/pnas.0911855107>
- [Biswal 2012] Biswal BB (2012) Resting state fMRI: A personal history. *NeuroImage* 62(2):938-944. <https://doi.org/10.1016/j.neuroimage.2012.01.090>

References

- [Blankertz 2010] Blankertz B, Sannelli C, Halder S, Eva MEM, Kübler A, Müller KR, Curio G, Dickhaus T (2010) Neurophysiological predictor of SMR-based BCI performance. *NeuroImage* 51(4):1303-1309. <https://doi.org/10.1016/j.neuroimage.2010.03.022>
- [Bonmassar 2001] Bonmassar G, Hadjikhani N, Ives JR, Hinton D, Belliveau JW (2001) Influence of EEG electrodes on the BOLD fMRI signal. *Hum Brain Mapp* 14:108-115. <https://doi.org/10.1002/hbm.1045>
- [Bonmassar 2002] Bonmassar G, Purdon PL, Jääskeläinen IP, Chiappa K, Solo V, Brown EN, Belliveau JW (2002) Motion and ballistocardiogram artifact removal for interleaved recording of EEG and EPs during MRI. *NeuroImage* 16:1127-1141. <https://doi.org/10.1006/nimg.2002.1125>
- [Briselli 2006] Briselli E, Garreffa G, Bianchi L, Bianciardi M, Macaluso E, Abbafati M, Marciani MG, Maraviglia B (2006) An independent component analysis-based approach on ballistocardiogram artifact removing. *Magn. Reson. Imaging* 24:393-400. <https://doi.org/10.1016/j.mri.2006.01.008>
- [Brookes 2008] Brookes MJ, Mullinger KJ, Stevenson CM, Morris PG, Bowtell R (2008) Simultaneous EEG source localisation and artifact rejection during concurrent fMRI by means of spatial filtering. *NeuroImage* 40:1090-104. <https://doi.org/10.1016/j.neuroimage.2007.12.030>
- [Brueggen 2017] Brueggen K, Fiala C, Berger C, Ochmann S, Babiloni C, Teipel SJ (2017) Early Changes in Alpha Band Power and DMN BOLD Activity in Alzheimer's Disease: A Simultaneous Resting State EEG-fMRI Study. *Frontiers in Aging Neuroscience* 9(319). <https://doi.org/10.3389/fnagi.2017.00319>
- [Brunner 2015] Brunner C, Birbaumer N, Blankertz B, Guger C, Kübler K, Mattia D, del Millán JR, Miralles F, Nijholt A, Opisso E, Ramsey N, Salomon P, Müller-Putz GR (2015) BNCI horizon 2020: towards a roadmap for the BCI community. *Brain Comput Interfaces* 2(1):1-10. <https://doi.org/10.1080/2326263X.2015.1008956>
- [Buzsáki 2012] Buzsáki G, Anastassiou CA, Koch C (2012) The Origin of Extracellular Fields and Currents – EEG, EcoG, LFP and Spikes. *Nature Reviews Neuroscience* 13:407-420. <https://doi.org/10.1038/nrn3241>
- [Cabeza 2001] Cabeza R, Kingstone A (2001) *Handbook of functional neuroimaging of cognition*. Cambridge The MIT Press p. 5
- [Calhoun 2014] Calhoun VD, Lemieux L (2014) *Neuroimage: Special issue on multimodal data fusion*. *Neuroimage* 102(1):1-2. <https://doi.org/10.1016/j.neuroimage.2014.04.070>

References

- [Case 2017] Case M, Zhang H, Mundahl J, Datta Y, Nelson S, Gupta K, He B (2017) Characterization of functional brain activity and connectivity using EEG and fMRI in patients with sickle cell disease. *NeuroImage: Clinical* 14:1-17. <https://doi.org/10.1016/j.nicl.2016.12.024>
- [Catana 2008] Catana C, Procissi D, Wu Y, Judenhofer MS, Qi J, Pichler BJ, Jacobs RE, Cherry SR (2008) Simultaneous in vivo positron emission tomography and magnetic resonance imaging. *Proceedings of the National Academy of Sciences* 105(10):3705-3710. <https://doi.org/10.1073/pnas.0711622105>
- [Cheung 2007] Cheung KC (2007) Implantable microscale neural interfaces. *Bio-medical Microdevices* 9:923-38. <https://doi.org/10.1007/s10544-006-9045-z>
- [Chowdhury 2014] Chowdhury ME, Mullinger KJ, Glover P, Bowtell R (2014) Reference layer artefact subtraction (RLAS): a novel method of minimizing EEG artefacts during simultaneous fMRI. *NeuroImage* 84:307-19. <https://doi.org/10.1016/j.neuroimage.2013.08.039>
- [Dahne 2015] Dähne S, Bießmann F, Samek W, Haufe S, Goltz D, Gundlach C, Villringer A, Fazli S, Müller KR (2015) Multivariate Machine Learning Methods for Fusing Multimodal Functional Neuroimaging Data. *Proceedings of the IEEE* 103(9):1507-1530. <https://doi.org/10.1109/JPROC.2015.2425807>
- [Debener 2005] Debener S, Ullsperger M, Siegel M, Fiehler K, von Cramon DY, Engel AK (2005) Trial-by-trial coupling of concurrent electroencephalogram and functional magnetic resonance imaging identifies the dynamics of performance monitoring. *J. Neurosci.* 25:11730-11737. <https://doi.org/10.1523/JNEUROSCI.3286-05.2005>
- [Debener 2006] Debener S, Ullsperger M, Siegel M, Engel AK (2006) Single-trial EEG-fMRI reveals the dynamics of cognitive function. *Trends Cogn Sci* 10(12):558-563. <https://doi.org/10.1016/j.tics.2006.09.010>
- [Debener 2007] Debener S, Strobel A, Sorger B, Peters J, Kranczioch C, Engel AK (2007) Improved quality of auditory event-related potentials recorded simultaneously with 3-T fMRI: removal of the ballistocardiogram artefact. *Neuroimage* 34:587-597. <https://doi.org/10.1016/j.neuroimage.2006.09.031>
- [Debener 2008] Debener S, Mullinger KJ, Niazy RK, Bowtell RW (2008) Properties of the ballistocardiogram artefact as revealed by EEG recordings at 1.5, 3 and 7 T static magnetic field strength. *Int J Psychophysiol* 67(3):189-199. <https://doi.org/10.1016/j.ijpsycho.2007.05.015>

References

- [DeFelipe 2015] DeFelipe J (2015) The anatomical problem posed by brain complexity and size: a potential solution. *Frontiers in Neuroanatomy* 9:104. <https://doi.org/10.3389/fnana.2015.00104>
- [Deligianni 2014] Deligianni F, Centeno M, Carmichael DW, Clayden JD (2014) Relating resting-state fMRI and EEG whole-brain connectomes across frequency bands. *Frontiers in Neuroscience* 8(258). <https://doi.org/10.3389/fnins.2014.00258>
- [Delorme 2004] Delorme A, Makeig S (2004) EEGLAB: an open source toolbox for analysis of single-trial EEG dynamics including independent component analysis. *J. Neurosci. Methods* 134(1):9-21. <https://doi.org/10.1016/j.jneumeth.2003.10.009>
- [deMuck 2007] de Munck JC, Gonçalves SI, Huijboom L, Kuijer JPA, Pouwels PJW, Heethaar RM, Lopes da Silva FH (2007) The hemodynamic response of the alpha rhythm: An EEG/fMRI study. *NeuroImage* 35(3):1142-1151. <https://doi.org/10.1016/j.neuroimage.2007.01.022>
- [deMuck 2008] de Munck JC, Goncalves SI, Faes TJ, Kuijer JP, Pouwels PJ, Heethaar RM, Lopes da Silva FH (2008) A study of the brain's resting state based on alpha band power, heart rate and fMRI. *Neuroimage* 42:112-121. <https://doi.org/10.1016/j.neuroimage.2008.04.244>
- [DeTiege 2007] De Tiege X, Harrison S, Laufs H, Boyd SG, Clark CA, Allen P, Neville BG, Vargha-Khadem F, Cross JH (2007) Impact of interictal epileptic activity on normal brain function in epileptic encephalopathy: an electroencephalography-functional magnetic resonance imaging study. *Epilepsy Behav.* 11:460-465. <https://doi.org/10.1016/j.yebeh.2007.06.001>
- [Difrancesco 2008] Difrancesco MW, Holland SK, Szaflarski JP (2008) Simultaneous EEG/functional magnetic resonance imaging at 4 Tesla: correlates of brain activity to spontaneous alpha rhythm during relaxation. *J. Clin. Neurophysiol.* 25:255-264. <https://doi.org/10.1097/WNP.0b013e3181879d56>
- [Dronkers 2007] Dronkers NF, Plaisant O, Iba-Zizen MT, Cabanis EA (2007) Paul Broca's historic cases: high resolution MR imaging of the brains of Leborgne and Le-long. *Brain* 130(5):1432-41. <https://doi.org/10.1093/brain/awm042>
- [Dunseath 2009] Dunseath WJR, Alden TA (2009) Electrode Cap for Obtaining Electrophysiological Measurement Signals from Head of Subject, has Measurement Signal Electrodes Extended through Electrically Conductive Layer and Insulating Layer for Contacting Head of Subject. US Patent Specification 2009/0099473 USA

References

[Einevoll 2013] Einevoll GT, Kayser C, Logothetis NK, Panzeri S (2013) Modelling and Analysis of Local Field Potentials for Studying the Function of Cortical Circuits. *Nature Reviews Neuroscience* 14:770-785. <https://doi.org/10.1038/nrn3599>

[Engel 2001] Engel AK, Fries P, Singer W (2001) Dynamic predictions: Oscillations and synchrony in top-down processing. *Nature Reviews Neuroscience* 2:704-716. <https://doi.org/10.1038/35094565>

[Fazli 2012] Fazli S, Mehnert J, Steinbrink J, Curio G, Villringer A, Müller KR, Blankertz B (2012) Enhanced performance by a hybrid NIRS-EEG brain computer interface. *NeuroImage* 59(1):519-529. <https://doi.org/10.1016/j.neuroimage.2011.07.084>

[Fellner 2016] Fellner M-C, Volberg G, Mullinger KJ, Goldhacker M, Wimber M, Greenlee MW, Hanslmayr S (2016) Spurious correlations in simultaneous EEG-fMRI driven by in-scanner movement. *NeuroImage* 133:354-366. <https://doi.org/10.1016/j.neuroimage.2016.03.031>

[Ferrari 2012] Ferrari M, Quaresima V (2012) A brief review on the history of human functional near-infrared spectroscopy (fNIRS) development and fields of application. *NeuroImage* 63(2):921-935. <https://doi.org/10.1016/j.neuroimage.2012.03.049>.

[Ferdowsi 2013] Ferdowsi S, Sanei S, Abolghasemi V, Nottage J, O'Daly O (2013) Removing Ballistocardiogram artifact from EEG using short- and long-term linear predictor. *IEEE Trans. Biomed. Eng.* 60:1900-11. <https://doi.org/10.1109/TBME.2013.2244888>

[Filler 2009] Filler AG (2009) The History, Development and Impact of Computed Imaging in Neurological Diagnosis and Neurosurgery: CT, MRI, and DTI. *Nature Precedings* 7(1):1-85. <https://doi.org/10.1038/npre.2009.3267.5>

[Freyer 2009] Freyer F, Becker R, Anami K, Curio G, Villringer A, Ritter P (2009) Ultrahighfrequency EEG during fMRI: pushing the limits of imaging-artifact correction. *NeuroImage* 48(1):94-108. <https://doi.org/10.1016/j.neuroimage.2009.06.022>

[Garreffa 2003] Garreffa G, Carnì M, Gualniera G, Ricci GB, Bozzao L, De Carli D, Morasso P, Pantano P, Colonnese C, Roma V, Maraviglia B (2003) Real-time MR artifacts filtering during continuous EEG/fMRI acquisition. *Magnetic Resonance Imaging* 21(10):1175-1189. <https://doi.org/10.1016/j.mri.2003.08.019>

[Girouard 2006] Girouard H, Iadecola C (2006) Neurovascular coupling in the normal brain and in hypertension, stroke, and Alzheimer disease. *Journal of Applied Physiology* 100:328-335. <https://doi.org/10.1152/jappphysiol.00966.2005>

References

- [Goldman 2002] Goldman RI, Stern JM, Engel JJ, Cohen MS (2002) Simultaneous EEG and fMRI of the alpha rhythm. *Neuroreport* 13, 2487-2492. <https://doi.org/10.1097/01.wnr.0000047685.08940.d0>
- [Goldman 2004] Goldman MS (2004) Enhancement of Information Transmission Efficiency by Synaptic Failures. *Neural Computation* 16:1137-1162. <https://doi.org/10.1162/089976604773717568>
- [Gompf 2017] Gompf F, Pflug A, Laufs H, Kell CA (2017) Non-linear Relationship between BOLD Activation and Amplitude of Beta Oscillations in the Supplementary Motor Area during Rhythmic Finger Tapping and Internal Timing, *Frontiers in Human Neuroscience* 11:582. <https://doi.org/10.3389/fnhum.2017.00582>
- [Gonçalves 2007] Gonçalves SI, Pouwels PJW, Kuijter JPA, Heethaar RM, de Munck JC (2007) Artifact removal in co-registered EEG/fMRI by selective average subtraction. *Clinical Neurophysiology* 118(11):2437-2450. <https://doi.org/10.1016/j.clinph.2007.08.017>
- [Gotman 2006] Gotman J, Kobayashi E, Bagshaw AP, Bénar CG, Dubeau F (2006) Combining EEG and fMRI: A multimodal tool for epilepsy research. *Journal of Magnetic Resonance Imaging* 23(6):1522-2586. <https://doi.org/10.1002/jmri.20577>
- [Gotz-Trabert 2008] Gotz-Trabert K, Hauck C, Wagner K, Fauser S, Schulze-Bonhage A (2008) Spread of ictal activity in focal epilepsy. *Epilepsia* 49, 1594-1601. <https://doi.org/10.1111/j.1528-1167.2008.01627.x>
- [Green 2017] Green JJ, Boehler CN, Roberts KC, Chen LC, Krebs RM, Song AW, Woldorff MG (2017) Cortical and Subcortical Coordination of Visual Spatial Attention Revealed by Simultaneous EEG-fMRI Recording. *Journal of Neuroscience* 37(33):7803-7810. <https://doi.org/10.1523/JNEUROSCI.0326-17.2017>
- [Grouiller 2007] Grouiller F, Vercueil L, Krainik A, Segebarth C, Kahane P, David O (2007) A comparative study of different artefact removal algorithms for EEG signals acquired during functional MRI, *NeuroImage* 38:124-137. <https://doi.org/10.1016/j.neuroimage.2007.07.025>
- [Grova 2008] Grova C, Daunizeau J, Kobayashi E, Bagshaw AP, Lina JM, Dubeau F, Gotman J (2008) Concordance between distributed EEG source localization and simultaneous EEG-fMRI studies of epileptic spikes. *NeuroImage* 39(2):755-774. <https://doi.org/10.1016/j.neuroimage.2007.08.020>

References

[Hahn 2017] Hahn A, Gryglewski G, Nics L, Rischka L, Ganger S, Sigurdardottir H, Vranka C, Silberbauer L, Vanicek T, Kautzky A, Wadsak W, Mitterhauser M, Hartenbach M, Hacker M, Kasper S, Lanzenberger R (2017) Task-relevant brain networks identified with simultaneous PET/MR imaging of metabolism and connectivity. *Brain Struct Funct.* <https://doi.org/10.1007/s00429-017-1558-0>

[Hamandi 2004] Hamandi K, Salek-Haddadi A, Fish DR, Lemieux L (2004) EEG/functional MRI in epilepsy: the Queen Square experience. *J. Clin. Neurophysiol.* 21:241-248.

[Hamandi 2006] Hamandi K, Salek-Haddadi A, Laufs H, Liston A, Friston K, Fish DR, Duncan JS, Lemieux L (2006) EEG-fMRI of idiopathic and secondarily generalized epilepsies. *NeuroImage* 31(4):1700-1710. <https://doi.org/10.1016/j.neuroimage.2006.02.016>

[Hamandi 2008] Hamandi K, Duncan JS (2008) fMRI in the evaluation of the ictal onset zone. In: Lüders, H.O. (Ed.), *Textbook of Epilepsy Surgery*. Informa Healthcare, p. Chapter 80.

[Hammer 2012] Hammer EM, Halder S, Blankertz B, Sannelli C, Dickhaus T, Kleih S, Müller KR, Kübler A (2012) Psychological predictors of SMR-BCI performance. *Biological Psychology* 89(1):80-86. <https://doi.org/10.1016/j.biopsycho.2011.09.006>

[Haykin 1996] Haykin S (1996) *Adaptive Filter Theory*. Prentice Hall, Upper Saddle River, NJ.

[He 2011] He B, Yang L, Wilke C, Yuan H (2011) Electrophysiological imaging of brain activity and connectivity – challenges and opportunities. *IEEE Trans Biomed Eng* 58(7):1918-1931. <https://doi.org/10.1109/TBME.2011.2139210>

[Hermans 2016] Hermans K, de Munck JC, Verdaasdonk R, Boon P, Krausz G, Prueckl R, Ossenblok P (2016) Effectiveness of Reference Signal-Based Methods for Removal of EEG Artifacts Due to Subtle Movements During fMRI Scanning. *IEEE Trans Biomed Eng* 63(12):2638-2646. <https://doi.org/10.1109/TBME.2016.2602038>

[Hodgkin 1952] Hodgkin AL, Huxley AF (1952) A Quantitative Description of Membrane Current and Its Application to Conduction and Excitation in Nerve. *The Journal of physiology* 117:500-544. <https://doi.org/10.1113/jphysiol.1952.sp004764>

[Horwitz 2002] Horwitz B, Poeppel D (2002) How can EEG/MEG and fMRI/PET data be combined? *Hum. Brain Mapp.* 17(1):1-3. <https://doi.org/10.1002/hbm.10057>

References

- [Hoshi 1994] Hoshi Y, Mizukami S, Tamura M (1994) Dynamic features of hemodynamic and metabolic changes in the human brain during all-night sleep as revealed by near-infrared spectroscopy. *Brain Research* 652(2):257-262. [https://doi.org/10.1016/0006-8993\(94\)90235-6](https://doi.org/10.1016/0006-8993(94)90235-6)
- [Huettel 2004] Huettel SA, Song AW, McCarthy G (2004) *Functional magnetic resonance imaging (Vol. 2)*. Sunderland, MA: Sinauer Associates, ISBN 978-0-87893-286-3
- [Huster 2012] Huster RJ, Debener S, Eichele T and Herrmann CS (2012) Methods for simultaneous EEG-fMRI: an introductory review. *J. Neurosci.* 32:6053-60. <https://doi.org/10.1523/JNEUROSCI.0447-12.2012>
- [Iadecola 2017] Iadecola C (2017) The Neurovascular Unit Coming of Age: A Journey through Neurovascular Coupling in Health and Disease. *Neuron* 96(1):17-42. <https://doi.org/10.1016/j.neuron.2017.07.030>
- [Ives 1993] Ives JR, Warach S, Schmitt F, Edelman RR, Schomer DL (1993) Monitoring the patient's EEG during echo planar MRI. *Electroencephalography and Clinical Neurophysiology* 87(6):417-420. [https://doi.org/10.1016/0013-4694\(93\)90156-P](https://doi.org/10.1016/0013-4694(93)90156-P)
- [Jann 2010] Jann K, Kottlow M, Dierks T, Boesch C, Koenig T (2010) Topographic Electrophysiological Signatures of fMRI Resting State Networks. *PLoS ONE* 5(9): e12945. <https://doi.org/10.1371/journal.pone.0012945>
- [Joebis 1977] Jöbsis F. (1977) Non-invasive infrared monitoring of cerebral and myocardial oxygen sufficiency and circulatory parameters. *Science* 198:1264-1267. <https://doi.org/10.1126/science.929199>
- [Jorge 2015a] Jorge J, Grouiller F, Ipek Ö, Stoermer R, Michel CM, Figueiredo P, van der Zwaag W, Gruetter R (2015) Simultaneous EEGfMRI at ultra-high field: artifact prevention and safety assessment. *NeuroImage* 105:132-144. <https://doi.org/10.1016/j.neuroimage.2014.10.055>
- [Jorge 2015b] Jorge J, Grouiller F, Gruetter R, van der Zwaag W, Figueiredo P (2015) Towards high-quality simultaneous EEG-fMRI at 7 T: detection and reduction of EEG artifacts due to head motion. *NeuroImage* 120:143-53. <https://doi.org/10.1016/j.neuroimage.2015.07.020>
- [Kjaer 2002] Kjaer TW, Law I, Wiltschiotz G, Paulson OB, Madsen PL (2002) Regional cerebral blood flow during light sleep - a H(2)(15)O-PET study. *J. Sleep Res.* 11:201-207. <https://doi.org/10.1046/j.1365-2869.2002.00303.x>
- [Kandel 2013] Kandel ER, Schwartz JH, Jessell TM, Siegelbaum SA, Hudspeth AJ (2013) *Principles of Neural Science, Fifth Edition*. ISBN 978-0-07-139011-8

References

[Kay 2014] Kay B, Szaflarski JP (2014) EEG/fMRI contributions to our understanding of genetic generalized epilepsies. *Epilepsy & Behavior* 34:129-135. <https://doi.org/10.1016/j.yebeh.2014.02.030>.

[Kim 2015] Kim H, Yoo S, Lee J (2015) Recursive approach of EEG-segment-based principal component analysis substantially reduces cryogenic pump artifacts in simultaneous EEG-fMRI data. *Neuroimage* 104:437-451. <https://doi.org/10.1016/j.neuroimage.2014.09.049>

[Kleinschmidt 1996] Kleinschmidt A, Obrig H, Requardt M, Merboldt KD, Dirnagl U, Villringer A, Frahm J (1996) Simultaneous Recording of Cerebral Blood Oxygenation Changes during Human Brain Activation by Magnetic Resonance Imaging and Near-Infrared Spectroscopy. *Journal of Cerebral Blood Flow & Metabolism* 16(5):817-826. <https://doi.org/10.1097/00004647-199609000-00006>

[Krakow 1999] Krakow K, Woermann FG, Symms MR, Allen PJ, Lemieux L, Barker GJ, Duncan JS, Fish DR (1999) EEG-triggered functional MRI of interictal epileptiform activity in patients with partial seizures. *Brain* 122(9):1679-1688. <https://doi.org/10.1093/brain/122.9.1679>

[Laufs 2003] Laufs H, Kleinschmidt A, Beyerle A, Eger E, Salek-Haddadi A, Preibisch C, Krakow K (2003) EEG-correlated fMRI of human alpha activity. *Neuroimage* 19:1463-1476. [https://doi.org/10.1016/S1053-8119\(03\)00286-6](https://doi.org/10.1016/S1053-8119(03)00286-6)

[Laufs 2006] Laufs H, Holt JL, Elfont R, Krams M, Paul JS, Krakow K, Kleinschmidt A (2006) Where the BOLD signal goes when alpha EEG leaves. *Neuroimage* 31:1408-1418. <https://doi.org/10.1016/j.neuroimage.2006.02.002>

[Laufs 2007] Laufs H, Duncan JS (2007) Electroencephalography/functional MRI in human epilepsy: what it currently can and cannot do. *Curr. Opin. Neurol.* 20:417-423. <https://doi.org/10.1097/WCO.0b013e3282202b92>

[Laufs 2012] Laufs H 2012 A personalized history of EEG-fMRI integration. *NeuroImage* 62:1056-67. <https://doi.org/10.1016/j.neuroimage.2012.01.039>

[Lemieux 1997] Lemieux L, Allen PJ, Franconi F, Symms MR, Fish DK (1997) Recording of EEG during fMRI experiments: Patient safety. *Magnetic Resonance in Medicine* 38(6):943-952. <https://doi.org/10.1002/mrm.1910380614>

[Lemieux 2004] Lemieux L (2004) Electroencephalography-correlated functional MR imaging studies of epileptic activity. *Neuroimaging Clin. N. Am.* 14:487-506. <https://doi.org/10.1016/j.nic.2004.04.009>

References

- [LeVan 2010] LeVan P, Tyvaert L, Moeller F, Gotman J (2010) Independent component analysis reveals dynamic ictal BOLD responses in EEG-fMRI data from focal epilepsy patients. *Neuroimage* 49:366-378. <https://doi.org/10.1016/j.neuroimage.2009.07.064>
- [Lisman 2015] Lisman J (2015) The Challenge of Understanding the Brain: Where We Stand in 2015. *Neuron* 86:864-882. <https://doi.org/10.1016/j.neuron.2015.03.032>
- [Liu 2012] Liu Z, de Zwart JA, Van Gelderen P, Kuo LW, Duyn J H (2012) Statistical feature extraction for artifact removal from concurrent fMRI-EEG recordings. *NeuroImage* 59:2073-87. <https://doi.org/10.1016/j.neuroimage.2011.10.042>
- [Liu 2015] Liu S, Cai W, Liu S, Zhang F, Fulham M, Feng D, Pujol S, Kikinis R (2015) Multimodal neuroimaging computing: a review of the applications in neuropsychiatric disorders. *Brain Informatics* 2:167-180. <https://doi.org/10.1007/s40708-015-0019-x>
- [Luo 2012] Luo Q, Glover GH (2012) Influence of dense-array EEG cap on fMRI signal. *Magn Reson Med* 68:807-815. <https://doi.org/10.1002/mrm.23299>
- [Luo 2014] Luo Q, Huang X, Glover GH (2014) Ballistocardiogram artifact removal with a reference layer and standard EEG cap. *J. Neurosci. Methods* 233:137-49. <https://doi.org/10.1016/j.jneumeth.2014.06.021>
- [Mantini 2007a] Mantini D, Perrucci MG, Del Gratta C, Romani GL, Corbetta M (2007) Electrophysiological signatures of resting state networks in the human brain. *Proc. Natl. Acad. Sci. U.S.A.* 104:13170-13175. <https://doi.org/10.1073/pnas.0700668104>
- [Mantini 2007b] Mantini D, Perrucci MG, Cugini S, Ferretti A, Romani GL, Del Gratta C (2007) Complete artifact removal for EEG recorded during continuous fMRI using independent component analysis. *NeuroImage* 34:598-607. <https://doi.org/10.1016/j.neuroimage.2006.09.037>
- [Mano 2017] Mano M, Lécuyer A, Bannier E, Perronnet L, Noorzadeh S, Barillot C (2017) How to build a hybrid neurofeedback platform combining EEG and fMRI. *Front Neurosci.* <https://doi.org/10.3389/fnins.2017.00140>
- [Marino 2018a] Marino M, Liu Q, Del Castello M, Corsi C, Wenderoth N, Mantini D (2018) Heart-Brain Interactions in the MR Environment: Characterization of the Ballistocardiogram in EEG Signals Collected During Simultaneous fMRI. *Brain Topography.* <https://doi.org/10.1007/s10548-018-0631-1>

References

- [Marino 2018b] Marino M, Liu Q, Koudelka V, Porcaro C, Hlinka J, Wenderoth N, Mantini D (2018) Adaptive optimal basis set for BCG artifact removal in simultaneous EEG-fMRI. *Sci Rep* 8(1):8902. <https://doi.org/10.1038/s41598-018-27187-6>.
- [Masterton 2007] Masterton RA, Abbott DF, Fleming SW, Jackson GD (2007) Measurement and reduction of motion and ballistocardiogram artefacts from simultaneous EEG and fMRI recordings. *NeuroImage* 37:202-11. <https://doi.org/10.1016/j.neuroimage.2007.02.060>
- [Mayeli 2016] Mayeli A, Zotev V, Refai H, Bodurka J (2016) Real-time EEG artifact correction during fMRI using ICA. *J Neurosci Methods* 274:27-37. <https://doi.org/10.1016/j.jneumeth.2016.09.012>
- [Maziero 2016] Maziero D, Velasco TR, Hunt N, Payne E, Lemieux L, Salmon CEG, Carmichael DW (2016) Towards motion insensitive EEG-fMRI: Correcting motion-induced voltages and gradient artefact instability in EEG using an fMRI prospective motion correction (PMC) system. *NeuroImage* 138:13-27. <https://doi.org/10.1016/j.neuroimage.2016.05.003>
- [McGlone 2009] McGlone F, Dunseath R, Stern J (2009) Simultaneous EEG and functional MRI employing novel noise reduction. *Epilepsia* 50:82-2. <https://doi.org/10.1111/j.1528-1167.2009.02377.x>
- [Michel 2004] Michel CM, Murray MM, Lantz G, Gonzalez S, Spinelli L, Grave de Peralta R (2004) EEG source imaging. *Clin Neurophysiol* 115(10):2195-222. <https://doi.org/10.1016/j.clinph.2004.06.001>
- [Michel 2012] Michel CM, Murray MM (2012) Towards the utilization of EEG as a brain imaging tool. *NeuroImage* 61:371-385. <https://doi.org/10.1016/j.neuroimage.2011.12.039>
- [Millán 2010] Millán JD, Rupp R, Müller-Putz GR, Murray-Smith R, Giugliemma C, Tangermann M, Vidaurre C, Cincotti F, Kübler A, Leeb R, Neuper C, Müller KR, Mattia D (2010) Combining brain-computer interfaces and assistive technologies: state-of-the-art and challenges. *Front Neurosci* 4:161. <https://doi.org/10.3389/fnins.2010.00161>
- [Miller 2007] Miller KJ, denNijs M, Shenoy P, Miller JW (2007) Real-time functional brain mapping using electrocorticography. *NeuroImage*. 37(2):504-507. <https://doi.org/10.1016/j.neuroimage.2007.05.029>
- [Moeller 2013] Moeller F, Stephani U, Siniatchkin M (2013) Simultaneous EEG and fMRI recordings (EEG-fMRI) in children with epilepsy. *Epilepsia* 54(6):1528-1167. <https://doi.org/10.1111/epi.12197>

References

- [Moosmann 2003] Moosmann M, Ritter P, Krastel I, Brink A, Thees S, Blankenburg F, Taskin B, Obrig H, Villringer A (2003) Correlates of alpha rhythm in functional magnetic resonance imaging and near infrared spectroscopy. *NeuroImage* 20(1):145-158. [https://doi.org/10.1016/S1053-8119\(03\)00344-6](https://doi.org/10.1016/S1053-8119(03)00344-6)
- [Mulert 2010] Mulert C, Lemieux L (2010) EEG-fMRI physiological basics, technique, and applications. Springer, Heidelberg, ISBN:978-3-540-87918-3. <https://doi.org/10.1007/978-3-540-87919-0>
- [Mulert 2013] Mulert C (2013) Simultaneous EEG and fMRI: towards the characterization of structure and dynamics of brain networks *Dialogues Clin Neurosci.* 15:381-386.
- [Mullinger 2008] Mullinger KJ, Morgan PS, Bowtell RW (2008) Improved Artifact Correction for Combined Electroencephalography/Functional MRI by Means of Synchronization and Use of Vectorcardiogram Recordings. *Journal of Magnetic Resonance Imaging* 27:607-616. <https://doi.org/10.1002/jmri.21277>
- [Mullinger 2011a] Mullinger KJ, Bowtell R (2011) Combining EEG and fMRI. In Modo M, Bulte JWM (eds), *Magnetic resonance neuroimaging, methods in molecular biology*, vol 711, Springer Science + Business Media, Germany, pp 303-326. https://doi.org/10.1007/978-1-61737-992-5_15
- [Mullinger 2011b] Mullinger KJ, Yan WX, Bowtell R (2011) Reducing the gradient artefact in simultaneous EEG-fMRI by adjusting the subject's axial position. *Neuroimage* 54(3):1942-1950. <https://doi.org/10.1016/j.neuroimage.2010.09.079>
- [Mullinger 2013a] Mullinger KJ, Havenhand J, Bowtell R (2013) Identifying the sources of the pulse artefact in EEG recordings made inside an MR scanner. *Neuroimage* 7:75-83. <https://doi.org/10.1016/j.neuroimage.2012.12.070>
- [Mullinger 2013b] Mullinger KJ, Castellone P, Bowtell R (2013) Best current practice for obtaining high quality EEG data during simultaneous fMRI. *J. Vis. Exp.* 76:50283. <https://doi.org/10.3791/50283>
- [Mullinger 2017] Mullinger KJ, Cherukara MT, Buxton RB, Francis ST, Mayhew SD (2017) Post-stimulus fMRI and EEG responses: Evidence for a neuronal origin hypothesised to be inhibitory. *NeuroImage* 157:388-399. <https://doi.org/10.1016/j.neuroimage.2017.06.020>
- [Nakamura 2006] Nakamura W, Anami K, Mori T, Saitoh O, Cichocki A, Amari S (2006) Removal of ballistocardiogram artifacts from simultaneously recorded EEG and fMRI data using independent component analysis. *IEEE Trans Biomed Eng* 53(7):1294-1308. <https://doi.org/10.1109/TBME.2006.875718>

References

- [Negishi 2004] Negishi M, Abildgaard M, Nixon T, Constable RT (2004) Removal of time-varying gradient artifacts from EEG data acquired during continuous fMRI. *Clin. Neurophysiol.* 115:2181-2192. <https://doi.org/10.1016/j.clinph.2004.04.005>
- [Nemtsas 2017] Nemtsas P, Birot G, Pittau F, Michel CM, Schaller K, Vulliemoz S, Kimiskidis VK, Seeck M (2017) Source localization of ictal epileptic activity based on high-density scalp EEG data. *Epilepsia* 58(6):1528-1167. <https://doi.org/10.1111/epi.13749>
- [Niazy 2005] Niazy RK, Beckmann CF, Iannetti GD, Brady JM, Smith SM (2005) Removal of fMRI environment artifacts from EEG data using optimal basis sets. *Neuroimage* 28(3):720-737. <https://doi.org/10.1016/j.neuroimage.2005.06.067>
- [Niedermeyer 2005] Niedermeyer E, Lopes da Silva FH (2005) *Electroencephalography: Basic Principles, Clinical Applications, and Related Fields* 5th edn (Philadelphia: Williams & Wilkins)
- [Nierhaus 2013] Nierhaus T, Gundlach C, Goltz D, Thiel SD, Pleger B, Villringer A (2013) Internal ventilation system of MR scanners induces specific EEG artifact during simultaneous EEG-fMRI. *Neuroimage* 74:70-76. <https://doi.org/10.1016/j.neuroimage.2013.02.016>
- [Niessing 2005] Niessing J, Ebisch B, Schmidt KE, Niessing M, Singer W, Galuske RAW (2005) Hemodynamic Signals Correlate Tightly with Synchronized Gamma Oscillations. *Science* 309,(5736):948-951. <https://doi.org/10.1126/science.1110948>
- [Norris 2006] Norris DG (2006) Principles of magnetic resonance assessment of brain function. *J Magn Res Imaging* 23:794-807. <https://doi.org/10.1002/jmri.20587>
- [Odenwald 2017] Odenwald S (2017) https://www.huffingtonpost.com/dr-sten-odenwald/number-of-stars-in-the-milky-way_b_4976030.html visited 16.02.2018
- [Ogawa 1990] Ogawa S, Lee TM (1990) Brain magnetic resonance imaging with contrast dependent on blood oxygenation. *Proc Natl Acad Sci USA* 87(24): 9868-9872.
- [OHalloran 2016] O'Halloran R, Kopell BH, Sprooten E, Goodman WK, Frangou S (2016) Multimodal neuroimaging-informed clinical applications in neuropsychiatric Disorders. *Front. Psychiatry* 7:63. <https://doi.org/10.3389/fpsy.2016.00063>
- [Oppenheim 2003] Oppenheim AV, Schafer RW (2003) *Discrete-Time Signal Processing* (3rd Ed.). Prentice-Hall, Inc., Upper Saddle River, NJ, USA. ISBN:0131988425 9780131988422

References

- [Otte 2006] Otte A, Halsband U (2006) Brain imaging tools in neurosciences. *Journal of Physiology-Paris* 99(4-6):281-292. <https://doi.org/10.1016/j.jphysparis.2006.03.011>
- [Pakkenberg 2001] Pakkenberg B, Gundersen HJG (2001) Neocortical neuron number in humans: Effect of Sex and Age. *The Journal of comparative neurology* 384:312-320. [https://doi.org/10.1002/\(SICI\)1096-9861\(19970728\)384:2<312::AID-CNE10>3.0.CO;2-K](https://doi.org/10.1002/(SICI)1096-9861(19970728)384:2<312::AID-CNE10>3.0.CO;2-K)
- [Parkes 2006] Parkes LM, Bastiaansen MCM, Norris DG (2006) Combining EEG and fMRI to investigate the post-movement beta rebound. *NeuroImage* 29(3):685-696. <https://doi.org/10.1016/j.neuroimage.2005.08.018>
- [Patel 1999] Patel MR, Blum A, Pearlman JD, Yousuf N, Ives JR, Saeteng S, Schomer DL, Edelman RR (1999) Echo-planar functional MR imaging of epilepsy with concurrent EEG monitoring. *AJNR Am. J. Neuroradiol.* 20:1916-1919.
- [Pelvig 2008] Pelvig DP, Pakkenberg H, Stark AK, Pakkenberg B (2008) Neocortical glial cell numbers in human brains. *Neurobiology of Aging* 29:1754-1762. <https://doi.org/10.1016/j.neurobiolaging.2007.04.013>
- [Perronnet 2017] Perronnet L, Lécuyer A, Mano M, Bannier E, Lotte F, Clerc M, Barillot C (2017) Unimodal versus bimodal EEG-fMRI neurofeedback of a motor imagery task. *Front Hum Neurosci.* <https://doi.org/10.3389/fnhum.2017.00193>
- [Pfurtscheller 1998] Pfurtscheller G, Zalaudek K, Neuper C (1998) Event-related beta synchronization after wrist, finger and thumb movement. *Electroencephalography and Clinical Neurophysiology/Electromyography and Motor Control* 109(2):154-160. [https://doi.org/10.1016/S0924-980X\(97\)00070-2](https://doi.org/10.1016/S0924-980X(97)00070-2)
- [Pfurtscheller 1999] Pfurtscheller G, Lopes da Silva FH (1999) Event-related EEG/MEG synchronization and desynchronization: basic principles. *Clinical Neurophysiology* 110(11):1842-1857. [https://doi.org/10.1016/S1388-2457\(99\)00141-8](https://doi.org/10.1016/S1388-2457(99)00141-8)
- [Pfurtscheller 2003] Pfurtscheller G, Graimann B, Huggins JE, Levine SP, Schuh LA (2003) Spatiotemporal patterns of beta desynchronization and gamma synchronization in corticographic data during self-paced movement. *Clin Neurophysiol.* 114(7):1226-1236. [https://doi.org/10.1016/S1388-2457\(03\)00067-1](https://doi.org/10.1016/S1388-2457(03)00067-1)
- [Raichle 1998] Raichle ME (1998) Behind the scenes of functional brain imaging: a historical and physiological perspective. *Proc Natl Acad Sci USA* 95(3):765-772.

References

[Rajkumar 2017] Rajkumar R, Rota Kops E, Mauler J, Tellmann L, Lerche C, Herzog H, Shah NJ, Neuner I (2017) Simultaneous trimodal PET-MR-EEG imaging: Do EEG caps generate artefacts in PET images? PLOS. <https://doi.org/10.1371/journal.pone.0184743>

[Rausch 2017] Rausch I, Rischka L, Ladefoged CN, Furtner J, Fenchel M, Hahn A, Lanzenberger R, Mayerhoefer ME, Traub-Weidinger T, Beyer T (2017) PET/MRI for Oncologic Brain Imaging: A Comparison of Standard MR-Based Attenuation Corrections with a Model-Based Approach for the Siemens mMR PET/MR System. *J Nucl Med* 58(9):1519-1525. <https://doi.org/10.2967/jnumed.116.186148>

[Reivich 1979] Reivich M, Kuhl D, Wolf A, Greenberg J, Phelps M, Ido T, Casella V, Fowler J, Hoffman E, Alavi A, Som P, Sokoloff L (1979) The [¹⁸F]fluorodeoxyglucose method for the measurement of local cerebral glucose utilization in man. *Circulation Research* 44:127-137. <https://doi.org/10.1161/01.RES.44.1.127>

[Ritter 2006] Ritter P, Villringer A (2006) Simultaneous EEG-fMRI. *Neurosci. Biobehav. Rev.* 30:823-38. <https://doi.org/10.1016/j.neubiorev.2006.06.008>

[Ritter 2007] Ritter P, Becker R, Graefe C, Villringer A (2007) Evaluating gradient artifact correction of EEG data acquired simultaneously with fMRI. *Mag. Res. Imaging* 25:923-32. <https://doi.org/10.1016/j.mri.2007.03.005>

[Ritter 2009] Ritter P, Moosmann M, Villringer A (2009) Rolandic alpha and beta EEG rhythms' strengths are inversely related to fMRI-BOLD signal in primary somatosensory and motor cortex. *Human Brain Mapping* 30(4):1097-0193. <https://doi.org/10.1002/hbm.20585>

[Rosa 2010] Rosa MJ, Daunizeau J, Friston KJ 2010 EEG-fMRI integration: A critical review of biophysical modeling and data analysis approaches. *Journal of Integrative Neuroscience* 9(4):453-476. <https://doi.org/10.1142/S0219635210002512>

[Rosenow 2001] Rosenow F, Lüders H (2001) Presurgical evaluation of epilepsy. *Brain* 124(9):1683-1700. <https://doi.org/10.1093/brain/124.9.1683>

[Rosenkranz 2010] Rosenkranz K, Lemieux L (2010) Present and future of simultaneous EEG-fMRI. *Magn Reson Mater Phy* 23:309-316 <https://doi.org/10.1007/s10334-009-0196-9>

[Rothlübbers 2014] Rothlübbers S, Relvas V, Leal A, Murta T, Lemieux L, Figueiredo P (2014) Characterisation and reduction of the EEG artefact caused by the helium cooling pump in the MR environment: validation in epilepsy patient data. *Brain Topogr* 28(2):208-220. <https://doi.org/10.1007/s10548-014-0408-0>

References

- [Sadaghiani 2010] Sadaghiani S, Scheeringa R, Lehongre K, Morillon B, Giraud AL, Kleinschmidt A (2010) Intrinsic connectivity networks, alpha oscillations, and tonic alertness: a simultaneous electroencephalography/functional magnetic resonance imaging study. *J. Neurosci.* 30:10243-10250. <https://doi.org/10.1523/JNEUROSCI.1004-10.2010>
- [Salek-Haddadi 2002] Salek-Haddadi A, Merschhemke M, Lemieux L, Fish DR (2002) Simultaneous EEG correlated ictal fMRI. *Neuroimage* 16, 32-40. <https://doi.org/10.1006/nimg.2002.1073>
- [Salek-Haddadi 2006] Salek-Haddadi A, Diehl B, Hamandi K, Merschhemke M, Liston A, Friston K, Duncan JS, Fish DR, Lemieux L (2006) Hemodynamic correlates of epileptiform discharges: an EEG-fMRI study of 63 patients with focal epilepsy. *Brain Res.* 1088:148-166. <https://doi.org/10.1016/j.brainres.2006.02.098>
- [Salmelin 2009] Salmelin R, Baillet S (2009) Electromagnetic brain imaging. *Hum Brain Mapp* 30:1753-1757. <https://doi.org/10.1002/hbm.20795>
- [Sadato 1998] Sadato N, Nakamura S, Oohashi T, Nishina E, Fuwamoto Y, Waki A, Yonekura Y (1998) Neural networks for generation and suppression of alpha rhythm: a PET study. *NeuroReport.* 9(5):893-897.
- [Sandrone 2014] Sandrone S (2014) Weighing brain activity with the balance: Angelo Mosso's original manuscripts come to light. *Brain.* 137:621-633. <https://doi.org/10.1093/brain/awt091>
- [Scheeringa 2011] Scheeringa R, Fries P, Petersson KM, Oostenveld R, Grothe I, Norris DG, Hagoort P, Bastiaansen MCM (2011) Neuronal Dynamics Underlying High- and Low-Frequency EEG Oscillations Contribute Independently to the Human BOLD Signal. *Neuron* 69(3):572-583. <https://doi.org/10.1016/j.neuron.2010.11.044>
- [Sejnowski 2014] Sejnowski TJ, Churchland PS, Movshon JA (2014) Putting big data to good use in neuroscience. *Nature Neuroscience* 17:1440-1441. <https://doi.org/10.1038/nn.3839>
- [Shah 2017] Shah NJ, Arrubla J, Rajkumar R, Farrher E, Mauler J, Rota Kops E, Tellmann L, Scheins J, Boers F, Dammers J, Sripad P, Lerche C, K. Langen KJ, Herzog H, Neuner I (2017) Multimodal Fingerprints of Resting State Networks as assessed by Simultaneous Trimodal MR-PET-EEG Imaging. *Scientific Reports* 7:6452. <https://doi.org/10.1038/s41598-017-05484-w>
- [Shibasaki 2008] Shibasaki H (2008) Human brain mapping: Hemodynamic response and electrophysiology. *Clinical Neurophysiology* 119:731-743. <https://doi.org/10.1016/j.clinph.2007.10.026>

- [Shin 2016] Shin J, Müller KR, Hwang HJ (2016) Near-infrared spectroscopy (NIRS)-based eyes-closed brain-computer interface (BCI) using prefrontal cortex activation due to mental arithmetic. *Scientific Reports* 6:36203. <https://doi.org/10.1038/srep36203>
- [Shynk 1992] Shynk JJ (1992) Frequency-domain and multirate adaptive filtering. *IEEE Signal Processing Magazine* 9(1):14-37
- [Sijbers 2000] Sijbers J, Van Audekerke J, Verhoye M, Van der Linden A, Van Dyck D (2000) Reduction of ECG and gradient related artifacts in simultaneously recorded human EEG/MRI data. *Magnetic Resonance Imaging* 18(7):881-886. [https://doi.org/10.1016/S0730-725X\(00\)00178-8](https://doi.org/10.1016/S0730-725X(00)00178-8)
- [Spencer 2018] Spencer GS, Smith JA, Chowdhury MEH, Bowtell R, Mullinger KJ (2018) Exploring the origins of EEG motion artefacts during simultaneous fMRI acquisition: Implications for motion artefact correction. *NeuroImage* 173:188-198. <https://doi.org/10.1016/j.neuroimage.2018.02.034>.
- [Srivastava 2005] Srivastava G, Crottaz-Herbette S, Lau KM, Glover GH, Menon V (2005) ICA-based procedures for removing ballistocardiogram artifacts from EEG data acquired in the MRI scanner. *NeuroImage* 24:50-60. <https://doi.org/10.1016/j.neuroimage.2004.09.041>
- [Stern 2006] Stern JM (2006) Simultaneous electroencephalography and functional magnetic resonance imaging applied to epilepsy. *Epilepsy Behav.* 8:683-692. <https://doi.org/10.1016/j.yebeh.2006.03.002>
- [Steyrl 2013] Steyrl D, Wriessnegger SC, Müller-Putz GR (2013) Single trial Motor Imagery classification in EEG measured during fMRI image acquisition – a first glance. *Biomedical Engineering / Biomedizinische Technik* 58(Suppl.1):1-2. <https://doi.org/10.1515/bmt-2013-4450>
- [Steyrl 2015] Steyrl D, Patz F, Krausz G, Edlinger G, Müller-Putz GR (2015) Reduction of EEG Artifacts in Simultaneous EEG-fMRI: Reference Layer Adaptive Filtering (RLAF). In: *Proceedings of the 37th Annual International Conference of the IEEE Engineering in Medicine and Biology Society, EMBC15, Milano, Italy, August 25-29, pp.3803-3806.* <https://doi.org/10.1109/EMBC.2015.7319222>
- [Steyrl 2016a] Steyrl D, Kobler RJ, Müller-Putz GR (2016) On similarities and differences of invasive and non-invasive electrical brain signals in brain-computer interfacing. *Journal of Biomedical Science and Engineering* 9(8):393-398. <https://doi.org/10.4236/jbise.2016.98034>

References

- [Steyrl 2016b] Steyrl D, Scherer R, Faller J, Müller-Putz GR (2016) Random forests in non-invasive sensorimotor rhythm brain-computer interfaces: A practical and convenient non-linear classifier. *Biomedical Engineering / Biomedizinische Technik* 61(1):77-86. <https://doi.org/10.1515/bmt-2014-0117>
- [Steyrl 2017] Steyrl D, Krausz G, Koschutnig K, Edlinger G, Müller-Putz GR (2017) Reference layer adaptive filtering (RLAF) for EEG artifact reduction in simultaneous EEG-fMRI. *Journal of Neural Engineering* 14(2):026003. <https://doi.org/10.1088/1741-2552/14/2/026003>
- [Steyrl 2018] Steyrl D, Krausz G, Koschutnig K, Edlinger G, Müller-Putz GR (2018) Online reduction of artifacts in EEG of simultaneous EEG-fMRI using reference layer adaptive filtering (RLAF). *Brain Topography* 31(1):129-149. <https://doi.org/10.1007/s10548-017-0606-7>
- [Tang 2001] Tang Y, Nyengaard JR, de Groot DMG, Gundersen HJG (2001) Total Regional and Global Number of Synapses in the Human Brain Neocortex. *Synapse* 41:258-273. <https://doi.org/10.1002/syn.1083>
- [Tarantino 2017] Tarantino V, Mazzone I, Formica S, Causin F and Vallesi A (2017) The Neural Bases of Event Monitoring across Domains: a Simultaneous ERP-fMRI Study. *Front. Hum. Neurosci.* 11:376. <https://doi.org/10.3389/fnhum.2017.00376>
- [Thornton 2010] Thornton R, Laufs H, Rodionov R, Cannadathu S, Carmichael DW, Vulliemoz S, Salek-Haddadi A, McEvoy AW, Smith SM, Lhatoo S, Elwes RD, Guye M, Walker MC, Lemieux L, Duncan JS (2010) EEG correlated functional MRI and postoperative outcome in focal epilepsy. *J Neurol Neurosurg Psychiatry* 81:922-927. <https://doi.org/10.1136/jnnp.2009.196253>
- [Tiege 2007] De Tiège X, Harrison S, Laufs H, Boyd SG, Clark CA, Allen P, Neville BG, Vargha-Khadem F, Cross JH (2007) Impact of interictal epileptic activity on normal brain function in epileptic encephalopathy: An electroencephalography-functional magnetic resonance imaging study. *Epilepsy & Behavior* 11:460-465. <https://doi.org/10.1016/j.yebeh.2007.06.001>
- [Tsuchimoto 2017] Tsuchimoto S, Shibusawa S, Mizuguchi N, Kato K, Ebata H, Liu M, Hanakawa T, Ushiba J (2017) Resting-State Fluctuations of EEG Sensorimotor Rhythm Reflect BOLD Activities in the Pericentral Areas: A Simultaneous EEG-fMRI Study. *Frontiers in Human Neuroscience* 11:356. <https://doi.org/10.3389/fnhum.2017.00356>

References

- [Tyvaert 2008] Tyvaert L, Levan P, Grova C, Dubeau F, Gotman J (2008) Effects of fluctuating physiological rhythms during prolonged EEG-fMRI studies. *Clin. Neurophysiol.* 119:2762-2774. <https://doi.org/10.1016/j.clinph.2008.07.284>
- [Uludag 2014] Uludağ K, Roebroek A (2014) General overview on the merits of multimodal neuroimaging data fusion. *Neuroimage* 102:3-10. <https://doi.org/10.1016/j.neuroimage.2014.05.018>
- [VanderMeer 2010] Van der Meer JN, Tijssen MAJ, Bour LJ, Van Rootselaar AF, Nederveen AJ (2010) Robust EMG-fMRI artifact reduction for motion (FARM). *Clin Neurophysiol* 121(5):766–776. <https://doi.org/10.1016/j.clinph.2009.12.035>
- [Vanderperren 2010] Vanderperren K, De Vos M, Ramautar JR, Novitskiy N, Mennes M, Asseondi S, Vanrumste B, Stiers P, Van den Bergh BRH, Wagemans J, Lagae L, Sunaert S, Van Huffel S (2010) Removal of BCG artifacts from EEG recordings inside the MR scanner: a comparison of methodological and validation-related aspects. *NeuroImage* 50:920-34. <https://doi.org/10.1016/j.neuroimage.2010.01.010>
- [vanGraan 2015] van Graan LA, Lemieux L, Chaudhary UJ (2015) Methods and utility of EEG-fMRI in epilepsy. *Quantitative Imaging in Medicine and Surgery* 5(2):300-312. <https://doi.org/10.3978/j.issn.2223-4292.2015.02.04>
- [Vargas 2015] Vargas EA (2015) B. F. Skinner's theory of behavior. *European Journal of Behavior Analysis* 18(1)2-38. <https://doi.org/10.1080/15021149.2015.1065640>
- [vonGlaserfeld 1995] von Glasersfeld E (1995) *Radical Constructivism, A Way of Knowing and Learning*. Routledge. ISBN: 978-0750705721
- [Vulliemoz 2010] Vulliemoz S, Rodionov R, Carmichael DW, Thornton R, Guye M, Lhatoo SD, Michel CM, Duncan JS, Lemieux L (2010) Continuous EEG source imaging enhances analysis of EEG-fMRI in focal epilepsy. *Neuroimage* 49, 3219-3229. <https://doi.org/10.1016/j.neuroimage.2009.11.055>
- [Wen 2016] Wen X, Kang M, Yao L, Zhao X (2016) Real-time ballistocardiographic artifact reduction using the k-teager energy operator detector and multi-channel referenced adaptive noise cancelling. *Int J Imaging Syst Technol* 26:209–215. <https://doi.org/10.1002/ima.22178>
- [Williamson 1991] Williamson SJ, Lu ZL, Karron D, Kaufman L (1991) Advantages and limitations of magnetic source imaging. *Brain Topogr* 4:169-180. <https://doi.org/10.1007/BF01132773>
- [Wolpaw 2002] Wolpaw JR, Birbaumer N, McFarland DJ, Pfurtscheller G, Vaughan TM (2002) Brain-computer interfaces for communication and control. *Clin Neurophysiol* 113: 767-791. [https://doi.org/10.1016/S1388-2457\(02\)00057-3](https://doi.org/10.1016/S1388-2457(02)00057-3)

References

- [Wu 2016] Wu X, Wu T, Zhan Z, Yao L, Wen X (2016) A real-time method to reduce ballistocardiogram artifacts from EEG during fMRI based on optimal basis sets (OBS). *Comput Methods Progr Biomed.* <https://doi.org/10.1016/j.cmpb.2016.01.018>
- [Xia 2013] Xia H, Ruan D, Cohen MS (2013) BCG Artifact removal for reconstructing full-scalp EEG inside the MR scanner 2013 Int. Workshop on Pattern Recognition in Neuroimaging (PRNI) 178-81. <https://doi.org/10.1109/PRNI.2013.53>
- [Yan 2009] Yan WX, Mullinger KJ, Brookes MJ, Bowtell R (2009) Understanding gradient artefacts in simultaneous EEG/fMRI, *NeuroImage* 46(2):459-471. <https://doi.org/10.1016/j.neuroimage.2009.01.029>
- [Yan 2010] Yan W X, Mullinger K J, Geirsdottir G B and Bowtell R (2010) Physical modeling of pulse artefact sources in simultaneous EEG/fMRI *Hum. Brain Mapp.* 31 604-20. <https://doi.org/10.1002/hbm.20891>
- [Zich 2014] Zich C, Debener S, De Vos M, Kranczioch C, Gutberlet I (2014) Real-time artifact correction enables EEG-based feedback inside the fMRI scanner, In: proceedings of the 6th International BrainComputer Interface Conference 2014, Verlag der Technischen Universität Graz. <https://doi.org/10.3217/978-3-85125-378-8-25>
- [Zich 2015] Zich C, Debener S, Kranczioch C, Bleichner MG, Gutberlet I, De Vos M (2015) Real-time EEG feedback during simultaneous EEG-fMRI identifies the cortical signature of motor imagery. *NeuroImage* 114:438-447. <https://doi.org/10.1016/j.neuroimage.2015.04.020>
- [Zijlmans 2007] Zijlmans M, Huiskamp G, Hersevoort M, Seppenwoolde JH, van Huffelen AC, Leijten FS (2007) EEG-fMRI in the preoperative work-up for epilepsy surgery. *Brain* 130:2343-2353. <https://doi.org/10.1093/brain/awm141>
- [Zotev 2008] Zotev VS, Matlashov AN, Volegov PL, Savukov IM, Espy MA, Mosher JC, Gomez JJ, Kraus RH (2008) Microtesla MRI of the human brain combined with MEG. *Journal of Magnetic Resonance* 194(1):115-120. <https://doi.org/10.1016/j.jmr.2008.06.007>
- [Zotev 2014] Zotev V, Phillips R, Yuan H, Misaki M, Bodurka J (2014) Self-regulation of human brain activity using simultaneous real-time fMRI and EEG neurofeedback. *NeuroImage* 85:985-995. <https://doi.org/10.1016/j.neuroimage.2013.04.126>

5 Appendix

“That’s all folks!”

– Looney Tunes cartoons

5.1 Publications

This section lists the approximate amount of work each author has contributed to each of the publications and subsequently includes copies of the publications.

Primary Publications	Author	Work	Contribution
1	D. Steyrl	90%	idea, programming, analysis, writing
	G.R. Müller-Putz	10%	advice, discussion, proofreading
2	D. Steyrl	70%	idea, programming, measurements, analysis, writing
	F. Patz	10%	hardware, measurements, writing
	G. Krausz	10%	hardware, measurements, proofreading
	G. Edlinger	5%	hardware
	G.R. Müller-Putz	5%	advice, discussion, proofreading
3	D. Steyrl	75%	idea, programming, measurements, analysis, writing
	G. Krausz	5%	hardware, proofreading
	K. Koschutnig	5%	measurements, writing
	G. Edlinger	5%	hardware
4	G.R. Müller-Putz	10%	advice, discussion, proofreading
	D. Steyrl	75%	idea, programming, measurements, analysis, writing
	G. Krausz	5%	hardware, proofreading
	K. Koschutnig	5%	measurements, proofreading
Secondary Publication	G. Edlinger	5%	hardware
	G.R. Müller-Putz	10%	advice, discussion, proofreading
	D. Steyrl	60%	programming, measurements, analysis, writing
	S.C. Wriessnegger	20%	measurements, proofreading
1	G.R. Müller-Putz	20%	idea, advice, discussion, proofreading

Reduction of EEG Artifacts in Simultaneous EEG-fMRI: Reference Layer Adaptive Filtering (RLAF)*

David Steyrl^{1,2} *Student Member IEEE*, Franz Patz³, Gunther Krausz³,
Günter Edlinger³ *Member IEEE*, and Gernot R. Müller-Putz^{1,2} *Member IEEE*

Abstract—Although simultaneous measurement of electroencephalography (EEG) and functional magnetic resonance imaging (fMRI) is one of the most valuable methods for studying human brain activity non-invasively, it remains challenging to measure high quality EEG inside the MRI scanner. Recently, a new approach for minimizing residual MRI scanner artifacts in the EEG was presented: reference layer artifact subtraction (RLAS). Here, reference electrodes capture only the artifacts, which are subsequently subtracted from the measurement electrodes. With the present work we demonstrate that replacing the subtraction by adaptive filtering statistically significantly outperforms RLAS. Reference layer adaptive filtering (RLAF) attenuates the average artifact root-mean-square (RMS) voltage of the passive MRI scanner to $0.7 \mu V$ (-14.4 dB). RLAS achieves $0.78 \mu V$ (-13.5 dB). The combination of average artifact subtraction (AAS) and RLAF reduces the residual average gradient artifact RMS voltage to $2.3 \mu V$ (-49.2 dB). AAS alone achieves $5.7 \mu V$ (-39.0 dB). All measurements were conducted with an MRI phantom, as the reference layer cap available to us was a prototype.

I. INTRODUCTION

Over the last 20 years, simultaneous acquisition of the electroencephalogram (EEG) and functional magnetic resonance imaging (fMRI) has become a very beneficial technique for studying the human brain's function non-invasively [1], [2]. However, simultaneous EEG-fMRI is still challenging in terms of subject handling and comfort, measurement reliability, signal quality, signal processing and data integration [3], [4]. One reason for some of the challenges is that EEG acquired simultaneously to fMRI is afflicted by a variety of artifacts.

(1) The gradient artifact (GA) is the most prominent artifact, with amplitudes up to $5000 \mu V$ [5]. It is caused by the gradient switching of the MRI scanner during acquisition of data. Commonly, the GA is attenuated by average artifact subtraction (AAS) as proposed in [6]. AAS is especially successful when EEG data acquisition is synchronized with the MRI scanner to ensure that the artifact is always sampled at the same time. A re-positioning of the subject inside the MRI scanner can help to reduce this artifact [5]. However, residuals can easily overwhelm the brain signals of interest [5].

*This research has been partially supported by ENIAC Joint Undertaking Project DeNeCoR (No. 324257).

¹D. Steyrl and G. R. Müller-Putz are with the Institute for Knowledge Discovery, Laboratory of Brain-Computer Interfaces, University of Technology, 8010 Graz, Austria david.steyrl@tugraz.at, gernot.mueller@tugraz.at

²D. Steyrl and G. R. Müller-Putz are with BioTechMed-Graz, Austria

³F. Patz, G. Krausz and G. Edlinger are with GUGER TECHNOLOGIES OG, Herbersteinstrasse 60, 8020 Graz, Austria patz@gtec.at

(2) After attenuating the GA, a second artifact is visible: The pulse artifact (PA). It has typically smaller amplitudes than the GA, but is often more problematic due to its variability over cardiac cycles. Analyses of this artifact brought up that it is caused by cardiac-pulse-driven head rotation, local scalp movements due to the expansion and contraction of scalp arteries and blood-flow induced Hall voltage [7]. The problems with this artifact aggravate at higher static magnetic fields, as the amplitude is directly linked to the field strength. Again, the most common approach for reducing this artifact is AAS, but in this case triggered by the electrocardiogram (ECG) [8]. Like with the residual GA, the remaining PA can easily mask the brain signals of interest.

(3) Other artifacts also reduce the EEG signal quality. Electrical noise induced by the scanner's helium pump is well known. Further, the MRI scanner's internal ventilation system was recently identified to cause specific artifacts in the EEG [9]. One can circumnavigate this artifacts by temporarily switching the systems off. However, this is not desirable since the systems have important roles for a safe operation of the MRI scanner.

New approaches for reducing residual artifacts are required. One promising new approach is called reference layer artifact subtraction (RLAS) by Chowdhury et al. [10]. An electrode positioned at a reference layer, isolated from the skin but with similar material properties and form, records a similar artifact as an EEG measurement electrode, if the electrodes are near to each other (e.g. the reference electrode on top of the measurement electrode). A subsequent subtraction of the artifact from the EEG measurement electrode unveils the EEG. Chowdhury et al. showed that the GA as well as the PA can be attenuated and that this approach can be advantageously combined with the existing AAS method. However, they concluded that for broader use, "...it will be necessary to devise a more robust reference layer arrangement that is also easier to use...".

Another group continued with RLAS and presented a more practical approach with a reusable cap [11]. They showed that RLAS can outperform optimal basis set (OBS) artifact correction, which is beside AAS a second popular PA correction method [12]. However, their approach is still time consuming, as an individual reference layer construction is needed for each experiment. Further, the number of available electrode positions is reduced, since some of them are used for the PA reconstruction.

Both groups agreed that RLAS can improve EEG signal quality, especially when combined with AAS. However, a

limiting fact is that the positions of a EEG measurement electrode and the respective reference electrode are not the same. Hence, the reference electrode can not capture exactly the same artifact as the measurement electrode. As a result, residual artifacts are still present after subtraction. Here, we want to bring adaptive filtering into play [13]. Adaptive filters find an optimal scaling, in the least-mean-square sense, for the artifact to subtract. We hypothesize that residual artifacts should be smaller after adaptive filtering than after subtraction. We call this approach reference layer adaptive filtering (RLAF). In this work, we bring evidence for this hypotheses by presenting artifact correction results of simultaneous EEG-fMRI measurements with an MRI phantom.

II. METHODS

A. Reference Layer Cap Prototype

The reference layer cap is a prototype, designed for better usability and improved wearability compared to the already presented caps. Ideally, the setup provides enough flexibility to accommodate to a person's head, but also applies enough contact pressure to achieve good signal quality. Another main target was to provide a setup that is applicable to the subject within minutes, comparable to standard EEG cap solutions. To satisfy those requirements, associated scalp/reference electrodes (forming a pair for signal subtraction) are closely spaced and also located in a fixed distance to each other so that artifact inducing effects are similar in both electrodes. We achieve this by a custom plastics housing that accommodates both, the scalp and reference electrode, placed right on top of each other.

To our experience, the time span in which persons wear EEG caps during typical experiments is often long enough to aggravate the effect of perspiration, which in turn has an impact on the electrical interconnections between the electrodes and therefore leads to signal changes. Hence, we replaced the reference layer surface by an electrically conductive grid so that the head is only covered at the positions of the electrode pairs. Moreover, by using fluid inside the grid interconnections one should be able to change the electrical conductivity of the reference layer. Concerning the impact of abandoning the continuous reference layer, we follow the reasonable assumption that a fine-meshed grid should resemble the electrical properties of a continuous surface to a sufficiently high degree.

The used prototype for the presented experiments consists of a grid of scalp/reference layer electrode pairs, arranged in a traditional 10-20 system.

B. EEG Amplifier and MRI Scanner

A 32 channel MRI compatible EEG amplifier (BrainAmp MR plus, Brainproducts GmbH, Munich, Germany) was used for recording, which was synchronized with the gradient clock of the MRI scanner via TTL pulses to ensure a highly accurate GA sampling. The sampling rate was 5000 Hz. The cut off frequency of the high pass filter was set to 0.016 Hz and was set to 250 Hz for the low pass filter. Voltage range

was set to $\pm 16.384 mV$, resulting in a resolution of $0.5 \mu V$. Measurements were conducted inside a 3 T Skyra (Siemens, Erlangen, Germany) MRI scanner. The scanner was equipped with a standard 24 channels head coil. When the scanner was active, an echo planar imaging (EPI) sequence with a time of repetition (TR) of 2000 ms was running. The EEG amplifier was positioned at the head end of the scanner, inside the bore. The electrode cables were fixed with sand bags.

C. MRI Phantom

Since the reference layer cap available to us is a prototype, we present measurements with an MRI phantom. The phantom was a water filled plastic sphere and was positioned inside the MRI scanner in the head coil. The phantom was covered with electrolyte paste. The EEG cap was fixed on the sphere and the EEG measurement electrodes were connected with the electrolyte paste layer by using more electrolyte paste.

D. Experiments

First, background noise inside the MRI scanner was recorded (experiment A). The scanner was passive (no sequence running), the helium pump and the ventilation were running. 200 s of data were recorded.

In the second experiment (experiment B), the MRI scanner was active (fMRI sequence was running), the helium pump and the ventilation were running. 590 s of data were recorded.

E. Reference Layer Artifact Subtraction (RLAS)

In a first step, the raw signals were band pass filtered between 0.5 and 100 Hz (zero phase Butterworth of 8th order). Then a sample-by-sample subtraction of the reference electrodes signal from the corresponding measurement electrodes signal was performed.

F. Reference Layer Adaptive Filtering (RLAF)

A band pass filter was applied first (0.5 to 100 Hz, zero phase Butterworth of 8th order). Subsequently, the signal was adaptively filtered. A first order model was chosen to allow only an amplitude scaling. The most common least-mean-square algorithm was chosen for updating filter weights. To achieve a stable adaptation, the step width of the adaptive filter was adjusted to the signal amplitude and was chosen 10^{-4} for experiment A and 4×10^{-8} for experiment B. The desired input was the measurement electrodes signal, the reference input was the reference electrodes signal and the output of the filter was the residual error term.

G. Average Artifact Subtraction (AAS)

The ready to use implementation of AAS in BrainVision Analyzer 2.1 (BrainProducts GmbH, Munich, Germany) was used. Volume onsets were determined by the recorded TTL triggers. All recorded volumes were used for average template calculation.

Appendix

TABLE I

MEDIAN (MDN), AVERAGE (AVG) AND STANDARD DEVIATION (SD) OF THE 16 EEG MEASUREMENT ELECTRODES (EEG) RMS VOLTAGES, THE 16 REFERENCE ELECTRODES (REF) RMS VOLTAGES, AFTER SUBTRACTION OF THE RESPECTIVE REFERENCE FROM THE MEASUREMENT ELECTRODES (RLAS), AFTER ADAPTIVE FILTERING (RLAF) AND AFTER AVERAGE ARTIFACT SUBTRACTION (AAS). REDUCTION OF RMS VOLTAGES BETWEEN EEG MEASUREMENT ELECTRODES AND AFTER SUBTRACTION OF REFERENCE SIGNAL (RLAS/EEG) IN dB . REDUCTION OF RMS VOLTAGES BETWEEN EEG MEASUREMENT ELECTRODES AND AFTER ADAPTIVE FILTERING (RLAS/EEG) IN dB . REDUCTION OF RMS VOLTAGES BETWEEN EEG MEASUREMENT ELECTRODES AND AFTER AAS (AAS/EEG) IN dB .

		EEG	REF	RLAS	RLAF	AAS	RLAS/EEG	RLAF/EEG	AAS/EEG
		μV	dB	dB	dB				
Experiment A: Scanner passive	MDN	3.54	3.84	0.74	0.67	n.a.	-13.4	-14.0	n.a.
	AVG	3.88	4.00	0.78	0.70	n.a.	-13.6	-14.4	n.a.
	SD	1.47	1.57	0.14	0.09	n.a.	2.7	3.1	n.a.
Experiment B1: Scanner active	MDN	595.4	541.8	111.8	74.2	5.8	-17.2	-19.5	-40.6
	AVG	665.2	661.5	112.5	71.3	5.7	-13.5	-18.0	-39.0
	SD	470.6	420.3	50.2	36.2	2.2	10.0	10.5	6.3
Experiment B2: Scanner active, after ASS	MDN	5.8	4.8	2.5	2.4	n.a.	-6.7	-7.0	n.a.
	AVG	5.7	5.3	2.5	2.3	n.a.	-7.8	-8.4	n.a.
	SD	2.2	2.3	1.1	1.1	n.a.	4.7	4.7	n.a.

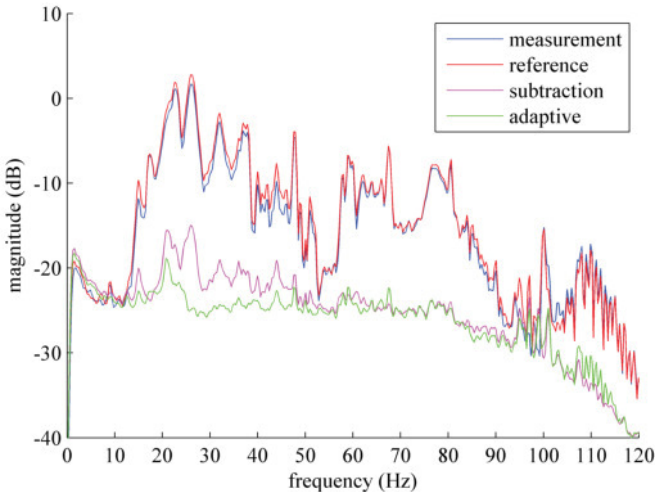


Fig. 1. Spectral density estimates for measurement channel at position C3, reference channel at position C3, after sample-by-sample subtraction (RLAS) and after adaptive filtering (RLAF). No MRI sequence was running (passive).

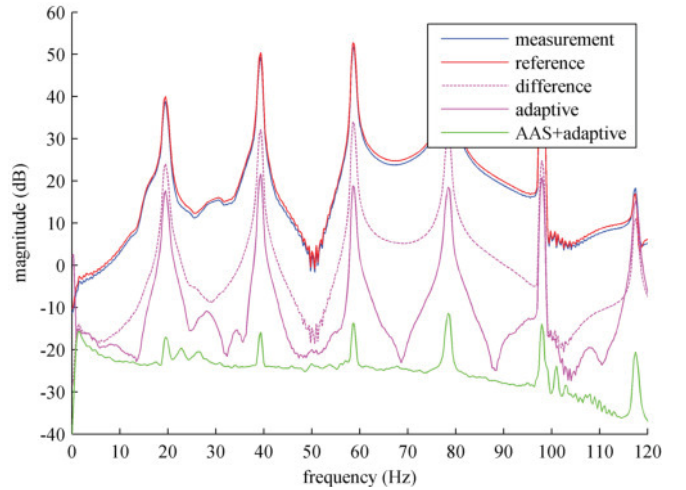


Fig. 2. Spectral density estimates for measurement channel at position Cz, reference channel at position Cz, after sample-by-sample subtraction (RLAS), after adaptive filtering (RLAF) and after ASS with subsequent adaptive filtering (AAS+RLAF). An fMRI sequence was running (active).

III. RESULTS

A. Experiment A

Root mean square (RMS) voltages of the recorded measurement channels were calculated. These values were compared to RMS voltages of the measurement channels after RLAS and after RLAF.

Table I summarizes the results. The difference between RLAS and RLAF (on average $0.8 dB$) is statistically significant (paired t-test, $p = 0.0012$, RLAS vs RLAF, experiment A, Table I). Fig. 1 shows representative spectral density estimates when no sequence was running (scanner was passive, channel C3).

B. Experiment B

RMS voltages of the recorded measurement channels were compared to RMS voltages of the measurement channels after RLAS and after RLAF (experiment B1). In a further comparison, the AAS was performed first and RLAS and RLAF were applied in a second step (experiment B2).

The results of experiment B1 are summarized in Table I and Fig. 2. The difference between RLAS and RLAF (on average $4.5 dB$) is statistically significant (paired t-test, $p = 0.0012$, Table I, experiment B1, RLAS vs RLAF).

Table I and Fig. 2 also show the results of Experiment B2. After AAS, the difference in subtraction and adaptive filtering (on average $0.6 dB$) is statistically significant (paired t-test, $p = 0.002$, Table I, experiment B2, RLAS vs RLAF).

IV. DISCUSSION

A. Experiment A

We measured the electromagnetic noise inside a passive MRI scanner (no sequence running) and found artifacts (see Fig. 1, starting at approximately 15 Hz) which seem to be identical with helium pump and ventilation artifacts [9]. These artifacts degrade the signal-to-noise-ratio (SNR) and hinder accurate EEG analysis of higher frequencies in simultaneous EEG-fMRI [9].

RLAS is a good starting point for attenuating the passive MRI scanner noise. It reduces the RMS voltage on average by -13.6 dB. Also when looking at the spectra (Fig. 1), the passive MRI scanner artifact is highly attenuated. Hence, RLAS is not only beneficial for reducing the GA and the PA [10], [11], but also for reducing passive MRI scanner noise.

However, adaptive filtering is able to reduce the passive scanner noise further. RLAF achieves an average artifact attenuation of -14.4 dB, which is an improvement of 0.8 dB over RLAS. As visible in Fig. 1, RLAF is more effective between 10 Hz and 50 Hz compared to subtraction. The first order adaptive filter model scales the reference signal to fit best to the measurement signal and therefore compensates for small differences between artifacts in measurement and reference channels caused by location differences. The performance of RLAF is impressive, as the residual artifact RMS voltage of 0.7 μ V is near to the amplifiers resolution of 0.5 μ V.

B. Experiment B

Artifacts induced by active MRI scanners (GA) are huge [6]. We perceived amplitudes up to 1500 μ V. The induced artifacts are similar in measurement and reference layer channels (see spectra in Fig. 2). RLAS reduces the artifacts average RMS voltage by -13.5 dB, which is similar to the reduction achieved in experiment A.

RLAF improves the artifact attenuation further and achieves a damping of -18.5 dB. This improvement is also visible in the spectra (see Fig. 2).

However, artifact attenuation achieved by RLAS or RLAF is not sufficient. A minimal average residual artifact RMS voltage of 71.3 μ V is too high for satisfactory EEG analyses. For example, AAS achieves 5.7 μ V. The reference layer approach alone is not able to reduce the GA to a level that EEG can be satisfactorily analyzed. This findings are in line with [10].

Luckily, RLAS and RLAF can be combined with AAS. Chowdhury et al. [10] demonstrated that combining AAS with RLAS is superior to AAS alone. Our results replicate their findings. AAS alone results in residual artifact RMS voltage of 5.7 μ V. A following RLAS improves the average residual artifact RMS voltage to 2.5 μ V. This average residual RMS voltage is even smaller than the average artifact's RMS voltage of a passive MRI scanner.

However, RLAF is able to improve the efficacy of RLAS again. AAS followed by RLAF reduces the average residual

artifact RMS voltage to 2.3 μ V. This is an improvement of 0.6 dB compared to RLAS and an overall attenuation of the average MRI artifacts of 49.2 dB (from 665.2 μ V to 2.3 μ V). Fig. 2 shows the artifact spectrum after combining AAS and RLAF for artifact suppression. Although the artifact is still visible, all frequency components of the artifact are now below -10 dB.

V. CONCLUSION

With this work, we show for the first time, that reference layer adaptive filtering (RLAF) statistically significantly improves the RLAS approach for reducing EEG artifacts during simultaneous fMRI. The efficacy of RLAF was shown for passive MRI scanner artifacts (helium pump and ventilation noise) and for the residual GA after AAS with measurements on an MRI phantom. The next step will be to make measurements with humans for investigating the influence of the RLAF approach on known EEG patterns.

REFERENCES

- [1] B. He, L. Yang, C. Wilke, and H. Yuan, Electrophysiological Imaging of Brain Activity and Connectivity - Challenges and Opportunities, IEEE Trans. Biomed. Eng., vol. 58(7), pp. 1918-31, 2011. doi:10.1109/TBME.2011.2139210
- [2] K. Uludağ, and A. Roebroeck, General overview on the merits of multimodal neuroimaging data fusion. Neuroimage, vol. 102, pp. 3-10, 2014. doi: 10.1016/j.neuroimage.2014.05.018
- [3] P. Ritter, and A. Villringer, Simultaneous EEG-fMRI. Neurosci. Biobehav. Rev., vol. 30(6), pp. 823-38, 2006.
- [4] D. Steyerl, S. C. Wriessnegger, and G. R. Müller-Putz, Single trial Motor Imagery classification in EEG measured during fMRI image acquisition - a first glance, Biomed Eng / Biomed Tech, vol. 58, 2013. doi: 10.1515/bmt-2013-4450
- [5] K. J. Mullinger, W. X. Yan, and R. Bowtell, Reducing the gradient artefact in simultaneous EEG-fMRI by adjusting the subject's axial position. Neuroimage, vol. 54(3), pp. 1942-50, 2011. doi: 10.1016/j.neuroimage.2010.09.079
- [6] P. J. Allen, O. Josephs, and R. Turner, A method for removing imaging artifact from continuous EEG recorded during functional MRI. Neuroimage, vol. 12(2), 230-9, 2000.
- [7] K. J. Mullinger, J. Havenhand, and R. Bowtell, Identifying the sources of the pulse artefact in EEG recordings made inside an MR scanner. Neuroimage, vol. 7, pp. 75-83, 2013. doi: 10.1016/j.neuroimage.2012.12.070
- [8] P. J. Allen, G. Polizzi, K. Krakow, D. R. Fish, and L. Lemieux, Identification of EEG events in the MR scanner: the problem of pulse artifact and a method for its subtraction. Neuroimage, vol. 8(3), pp. 229-39, 1998.
- [9] T. Nierhaus, C. Gundlach, D. Goltz, S. D. Thiel, B. Pleger, and A. Villringer, Internal ventilation system of MR scanners induces specific EEG artifact during simultaneous EEG-fMRI. Neuroimage, vol. 74, pp. 70-6, 2013. doi: 10.1016/j.neuroimage.2013.02.016
- [10] M. E. Chowdhury, K. J. Mullinger, P. Glover, and R. Bowtell, Reference layer artefact subtraction (RLAS): a novel method of minimizing EEG artefacts during simultaneous fMRI. Neuroimage, vol. 84, pp. 307-19, 2014. doi: 10.1016/j.neuroimage.2013.08.039
- [11] Q. Luo, X. Huang, and G. H. Glover, Ballistocardiogram artifact removal with a reference layer and standard EEG cap. J Neurosci Methods, vol. 233, pp. 137-49, 2014. doi: 10.1016/j.jneumeth.2014.06.021
- [12] R. K. Niazy, C. F. Beckmann, G. D. Iannetti, J. M. Brady, and S. M. Smith, Removal of FMRI environment artifacts from EEG data using optimal basis sets. Neuroimage, vol. 28(3), pp. 720-37, 2005.
- [13] S. Haykin, Adaptive Filter Theory, Prentice-Hall, 1986.

Reference layer adaptive filtering (RLAF) for EEG artifact reduction in simultaneous EEG-fMRI

David Steyrl^{1,4}, Gunther Krausz², Karl Koschutnig^{3,4}, Günter Edlinger² and Gernot R Müller-Putz^{1,4}

¹ Laboratory of Brain-Computer Interfaces, Institute of Neural Engineering, Graz University of Technology, Graz, Austria

² GUGER TECHNOLOGIES OG, Graz, Austria

³ Department of Psychology, University of Graz, Graz, Austria

⁴ BioTechMed-Graz, Graz, Austria

E-mail: gernot.mueller@tugraz.at

Received 21 September 2016, revised 23 November 2016

Accepted for publication 25 November 2016

Published 3 February 2017



CrossMark

Abstract

Objective. Simultaneous electroencephalography (EEG) and functional magnetic resonance imaging (fMRI) combines advantages of both methods, namely high temporal resolution of EEG and high spatial resolution of fMRI. However, EEG quality is limited due to severe artifacts caused by fMRI scanners. **Approach.** To improve EEG data quality substantially, we introduce methods that use a reusable reference layer EEG cap prototype in combination with adaptive filtering. The first method, reference layer adaptive filtering (RLAF), uses adaptive filtering with reference layer artifact data to optimize artifact subtraction from EEG. In the second method, multi band reference layer adaptive filtering (MBRLAF), adaptive filtering is performed on bandwidth limited sub-bands of the EEG and the reference channels. **Main results.** The results suggests that RLAF outperforms the baseline method, average artifact subtraction, in all settings and also its direct predecessor, reference layer artifact subtraction (RLAS), in lower (<35 Hz) frequency ranges. MBRLAF is computationally more demanding than RLAF, but highly effective in all EEG frequency ranges. Effectivity is determined by visual inspection, as well as root-mean-square voltage reduction and power reduction of EEG provided that physiological EEG components such as occipital EEG alpha power and visual evoked potentials (VEP) are preserved. We demonstrate that both, RLAF and MBRLAF, improve VEP quality. For that, we calculate the mean-squared-distance of single trial VEP to the mean VEP and estimate single trial VEP classification accuracies. We found that the average mean-squared-distance is lowest and the average classification accuracy is highest after MBLAF. RLAF was second best. **Significance.** In conclusion, the results suggests that RLAF and MBRLAF are potentially very effective in improving EEG quality of simultaneous EEG-fMRI.

Highlights

We present a new and reusable reference layer cap prototype for simultaneous EEG-fMRI

We introduce new algorithms for reducing EEG artifacts due to simultaneous fMRI

The algorithms combine a reference layer and adaptive filtering

Several evaluation criteria suggest superior effectivity in terms of artifact reduction

We demonstrate that physiological EEG components are preserved



Original content from this work may be used under the terms of the [Creative Commons Attribution 3.0 licence](https://creativecommons.org/licenses/by/3.0/). Any further distribution of this work must maintain attribution to the author(s) and the title of the work, journal citation and DOI.

Keywords: simultaneous EEG-fMRI, EEG artifact reduction, reference layer cap, adaptive filtering, reference layer adaptive filtering, multi band reference layer adaptive filtering

(Some figures may appear in colour only in the online journal)

Introduction

Electroencephalography (EEG) as well as functional magnetic resonance imaging (fMRI) are standard tools for non-invasive functional brain imaging (Michel and Murray 2012, Norris 2006). EEG captures electrical potentials at the scalp, whereas fMRI captures blood oxygenation level dependent (BOLD) signals in the brain (Ogawa et al 1990, Niedermeyer and Lopes da Silva 2005). These two techniques have complementary characteristics: EEG has a high temporal resolution in the range of milliseconds, while fMRI has a high spatial resolution in the range of millimeters and is also capable of measuring activity in deep brain regions (He et al 2011, Laufs 2012). Concurrent measurement of EEG and fMRI allows benefitting from the advantages of both methods (Huster et al 2012, Uludag and Roebroek 2014). This combination is often termed as simultaneous EEG-fMRI (Ritter and Villringer 2006).

Several aspects of simultaneous EEG-fMRI, however, remain challenging (He et al 2011). One technical challenge is the existence of a complex mutual influence of these two methods, when applied simultaneously. On the one hand, EEG electrodes reduce static magnetic field homogeneity of MRI scanners, which in turn influences MRI signal quality negatively. MRI signal quality is worsened on the scalp and in the brain, however, the impact is negligible on the fMRI BOLD signal (Bonmassar et al 2001, Luo and Glover 2012). On the other hand, MRI scanners cause several serious artifacts in EEG signals during standby and during their operation. EEG artifacts due to simultaneous fMRI can in principle be reduced by adequate signal processing methods. The means for obtaining high quality EEG in simultaneous EEG-fMRI, however, are still an issue of ongoing research (Mulert and Lemieux 2010, Mullinger and Bowtell 2011). In this work, we present a new EEG cap in combination with new artifact reduction methods to improve EEG signal quality substantially. Before we go into details of our work, we recap EEG artifact characteristics and illustrate difficulties which hinder a straightforward artifact reduction.

- (1) The most prominent artifact is the gradient artifact (GA).

It is caused by induction in the leads of EEG electrodes due to magnetic field gradient switching during fMRI data acquisition (Allen et al 2000). The GA amplitudes are 2–3 orders of magnitude higher than the underlying EEG which masks the EEG completely (Allen et al 2000, Mullinger et al 2011). Analysis in the frequency domain reveals a coverage of the whole frequency range. An axial repositioning of study participants out of the MRI scanner's iso-center as well as an optimized routing of leads to minimize loops help to reduce the impact of the GA (Mullinger et al 2011, Jorge et al 2015a). However, signal

processing based GA reduction is absolutely essential for achieving acceptable EEG signal quality. The most common GA reduction method is average artifact subtraction (AAS) (Allen et al 2000). It exploits the repetitive nature of the GA. For each EEG channel separately, EEG data are segmented into artefact epochs and subsequently, an artifact template is computed through averaging over artifact epochs. Finally, artifact templates are subtracted from each artifact epoch to unveil the underlying EEG signal. Synchronization of the EEG sampling with the MRI scanner clock ensures that the GA is always sampled at the same times per epoch and hence improves quality of artifact templates (Mullinger et al 2008). However, even a slight motion of the study participant alters the shape of the GA and therefore the template fit will be impaired. Hence, residuals of the GA with magnitudes in the range of EEG signals may occur even after AAS.

- (2) After attenuating the GA or when the MRI scanner is not operating, a second EEG distortion is visible, the ballisto-cardiogram artefact or pulse artifact: an artifact in synchrony with the cardiac-pulse-cycle. To emphasize its coupling with the cardiac-pulse-cycle, we stick to the name pulse artifact (PA) throughout this work. The PA has two main causes: on the one hand, slight electrode motions in the static magnetic field, like cardiac-pulse-driven head rotations and local scalp motions due to the expansion and contraction of scalp arteries, and on the other hand, blood-flow induced Hall voltage (Bonmassar et al 2002, Mullinger et al 2013a). The contribution of the Hall effect to the PA, however, is small compared to the contribution of electrode motions (Mullinger et al 2013a). Amplitudes of the PA increase with field strength, making the artifact more problematic in modern MRI scanners with their very strong static magnetic fields of 3–7 T (Debener et al 2008, Mullinger et al 2013a). The PA can have amplitudes greater than 50 μV at 3 T and has its largest components in lower frequency ranges up to ~ 30 Hz (Allen et al 1998, Debener et al 2007, Debener et al 2008). AAS is again the most common method to tackle this artifact (Allen et al 1998). Simultaneously recorded electrocardiogram (ECG) data are used to find epochs of the PA in EEG. Separate PA templates are computed for each EEG channel and subsequently subtracted from PA epochs. However, the cardiac cycle inherently varies over time, and therefore the PA varies too, which in turn limits the success of the AAS method, since artifact templates only approximately fit the PA. Like with residuals of the GA, PA residuals are in the same order of magnitude as EEG signals. Moreover, PA residuals mask brain signals more profoundly than GA residuals since they are in the same frequency band as the brain signals.

- (3) Another source of artifacts in the EEG of simultaneous EEG-fMRI is the helium pump of the coolant system of the MRI scanner (Mullinger *et al* 2013b, Nierhaus *et al* 2013). This helium pump artifact (HPA) has not been sufficiently studied yet. Its shape and strength varies and is heavily dependent on the MRI scanner itself (Nierhaus *et al* 2013, Rothl ubbers *et al* 2014). In frequency domain analysis, the HPA shows several prominent peaks with amplitudes of up to $\sim 1 \mu\text{V Hz}^{-1}$ ranging from ~ 45 Hz to ~ 55 Hz and from ~ 90 Hz to ~ 115 Hz. It is not yet popular to apply HPA reduction methods, although at least one method has been published (Rothl ubbers *et al* 2014).
- (4) The internal ventilation system of MRI scanners has recently been identified as an additional source of specific artifacts in the EEG (Nierhaus *et al* 2013). In frequency domain analysis, Nierhaus *et al* found prominent peaks at ~ 37 Hz and at ~ 42 Hz depending on the ventilation level of the MRI scanner. Amplitudes of up to $20 \mu\text{V}$ can occur (Nierhaus *et al* 2013). The exact shape of the ventilation artifact (VA) is most likely specific to a particular MR scanner make or model (Nierhaus *et al* 2013). To our knowledge, this artifact has not been well studied yet and therefore, no dedicated VA reduction method is available. Of course, it is possible to circumnavigate these two last mentioned artifact types (3, 4) by temporarily switching the helium pump and ventilation system off. However, this is not desirable, since these systems have important roles for a safe operation of the MRI scanner and for the comfort of the study participant.
- (5) The motions of study participants cause strong artifacts in the EEG due to Faraday’s law of induction in the static magnetic field of the MRI scanner. Shape and amplitudes of motion artifacts (MA) are not predictable and can easily superimpose EEG signals (van der Meer *et al* 2010). Several methods to reduce this kind of artifacts have been proposed (Bonmassar *et al* 2002, Masterton *et al* 2007, van der Meer *et al* 2010, Abbott *et al* 2014, Jorge *et al* 2015b). Most of them attempt to capture MA separately to subsequently subtract them from EEG. The motions of study participants are problematic in two senses. First, they induce artifacts. Second, they also limit the success of artifact reduction methods based on the repetitiveness of artifacts, because their shape will change with the position of the study participants.

These very different artifact characteristics combined with the need for EEG quality improvements have pushed the development of a variety of artifact reduction methods over the past decade. Beside AAS, optimal basis sets (OBS) artifact reduction (Niazy *et al* 2005, Wu *et al* 2016) and independent component analysis artifact reduction are also popular at the present time (Srivastava *et al* 2005, Briselli *et al* 2006, Mantini *et al* 2007, Ritter *et al* 2007, Vanderperren *et al* 2010, Abreu *et al* 2016). Other methods, for example based on beam former, singular value decomposition, linear predictors, independent vector analysis and dictionary learning, have been published and can outperform popular methods under certain conditions (Brookes *et al* 2008, Liu *et al* 2012, Ferdowsi *et al*

2013, Abolghasemi and Ferdowsi 2015, Acharjee *et al* 2015). Generally, each method has its merits and caveats and an optimal choice is tricky. Preferably, one would like to have a method at hand that reduces as many as possible of the aforementioned artifacts in one step.

Chowdhury *et al* published new investigations on a very promising approach that was invented by a no longer existing company named Alatheia Ltd (Chantilly, VA, USA) in their ‘fEEG’ system (Dunseath *et al* 2009, McGlone *et al* 2009, Chowdhury *et al* 2014). This approach is conceptually able to tackle all occurring artifacts at once. The idea is to capture all kinds of artifacts at the head at once and subtract them from the EEG. Chowdhury *et al* used agar and PVC film to build a reference layer for the head, which is electrically isolated from the scalp, but has similar electrical properties and shape. They used electrode pairs, where one electrode is capturing the artifact afflicted EEG at the scalp (scalp electrode), while the other is capturing artifacts at the reference layer (reference electrode). Electrodes of a pair are closely spaced, reference electrodes on top of scalp electrodes, separated by PVC film only. Hence, it can be assumed that artifacts captured by an electrode pair are similar and a subsequent subtraction of artifacts from the artifact afflicted EEG unveils the underlying true EEG. Since this approach makes use of a reference layer and subsequent artifact subtraction it is termed as reference layer artifact subtraction (RLAS). Generally, RLAS can effectively attenuate all kinds of artifacts that are captured by reference electrodes. It was demonstrated that RLAS outperforms AAS in terms of GA and PA attenuation when MA are present (~ 1 dB lower root-mean-square (RMS) voltages) and that RLAS is even more effective when combined with AAS as pre-processing step (min. ~ 7 dB lower RMS voltages) (Chowdhury *et al* 2014).

We identified two components of the RLAS approach that can be optimized. First, the reference layer itself was cumbersome, unstable and not reusable. Chowdhury *et al* concluded that for broader use, ‘...it will be necessary to devise a more robust reference layer arrangement that is also easier to use...’ (Chowdhury *et al* 2014). Second, artifacts captured by electrode pairs are similar, but not equal, because of the following reasons: (i) electrodes of a pair cannot be positioned at the exact same place, (ii) electrodes of a pair can move differently, since they are not mechanically coupled, (iii) the shape of the reference layer cannot be totally equal to the shape of the head of course, and (iv) impedances of electrode pairs can differ. Consequently, residuals are present after artifact subtraction. However, due to Faraday’s law of induction, it is valid to assume a linear relationship between artifacts captured at the reference layer and artifacts captured at the scalp, but the relationship can change over time, since for example the impedances can change (Yan *et al* 2010, Jorge *et al* 2015b). Adaptive filters, correctly applied, find an optimal scaling for the artifact to subtract and adapt the scaling over time to meet the optimization criterion (Haykin 1986).

Hence, we introduce a new reference layer cap prototype and present artifact reduction methods that replace the subtraction of the original RLAS approach with adaptive filtering. We name this approach reference layer adaptive filtering (RLAF).

We also incorporate ideas of other groups, but our approach is substantially different to already published methods. (i) In contrast to Xia *et al*, Luo *et al*, Chowdhury *et al*, we filter electrode pair signals adaptively (Xia *et al* 2013, Chowdhury *et al* 2014, Luo *et al* 2014). Hence, reference layer electrode signals are not only just subtracted from scalp electrode signals, but are adaptively scaled before subtraction. (ii) We introduce a new, truly reusable reference layer cap prototype, which is equipped with mechanically tightly coupled and narrow spaced electrode pairs. The coupling ensures that electrodes of a pair can only move together, meaning that all electrode motion related artifacts are equally captured by both electrodes. This is in contrast to Masterton *et al*, Xia *et al*, Luo *et al*, Jorge *et al* and van der Meer *et al*, where reference electrodes are able to move independently of the scalp electrodes due to their separate placing (Masterton *et al* 2007, Xia *et al* 2013, Luo *et al* 2014, Jorge *et al* 2015b, van der Meer *et al* 2016). (iii) the electrode pairs of our cap provide reference electrode signals without occupying scalp electrode positions, hence all EEG positions are available to enable high density EEG recording. In Xia *et al*, Luo *et al* and Jorge *et al* electrodes occupy scalp electrode positions (Xia *et al* 2013, Luo *et al* 2014, Jorge *et al* 2015b). (iv) The electrode pairs provide a dedicated reference electrode signal per scalp electrode and avoid a reference signal construction that is based on the assumption that individual reference signals can be calculated by a linear combination of a few distributed reference electrode signals, as assumed in Xia *et al* (2013), Luo *et al* (2014), Jorge *et al* (2015b) and van der Meer *et al* (2016).

We already presented a proof-of-concept of our RLAF approach with a spherical fMRI phantom in Steyrl *et al* (2015). Within this work, we present details on the reference layer cap prototype. We show that adaptive filtering instead of subtraction potentially improves the reference layer approach. We evaluate the RLAF artifact reduction method on simultaneous EEG-fMRI data of humans with regard to EEG data quality enhancement. For this purpose we show time courses of the EEG after artifact reduction methods, we analyze EEG root-mean-square voltage changes and EEG power reduction, we demonstrate that both, evoked and induced EEG activity are preserved, and that single-trial quality of event related potentials is improved. We compare our RLAF results with its direct predecessor RLAS and with the most common artifact reduction method AAS. And finally, we present a new extension of the RLAF approach named multi band reference layer adaptive filtering (MBRLAF), which performs adaptive filtering on bandwidth limited sub-bands of the EEG and the reference channels to potentially improve RLAF further.

Materials and methods

Participants

Two volunteers (both female, 25 and 23 years old) participated in this experiment which was performed in accordance with the Declaration of Helsinki and was approved by the local ethics committee. Participants had medical histories free of neurological problems and were not under medication.

They were fully informed about the objectives of the experiment and gave consent for participation before taking part.

Experiment description

The experiment was designed to evaluate evoked responses (visual evoked responses) and induced responses (alpha-rhythm changes). After EEG cap setup and instructions the participants lay in the MRI scanner, while looking at a monitor via a head coil mounted mirror. The monitor was positioned at the foot end of the scanner. The participants were asked to remain as still as possible during the experiment. In the first part of the experiment, the participants underwent inverse checkerboard stimuli to trigger visual evoked potentials (VEP). The checkerboard had 8×8 square black and white fields with a centered red dot, was scaled to the size of the monitor and was inverted after a randomized duration of 0.5s–0.6s. EEG data of 1200 inversions were collected, which lasted approximately 11 min. In the second part, 10 min of resting EEG was recorded to allow analysis of induced activity changes between eyes open and eyes closed. The participants were instructed to close their eyes, but not to fall asleep. The total duration of the experiment was approximately 70 min, including 40 min cap preparation and instructions, 20 min measurement, 10 min additional time for handling.

Reference layer cap prototype

The reference layer cap used in this study was a prototype developed by GUGER TECHNOLOGIES OG, Austria (patents pending), see figure 1 panel A and B. It consists of 30 double-layer electrode pairs and 2 additional ECG electrodes. Twenty-nine electrode pairs for capturing EEG and one electrode pair as common ground/reference electrode. Each electrode has two C-shaped silver-coated contact areas with a diameter of 2.5 mm. The electrode contacts of each electrode are placed on both sides of a corresponding printed circuit board (PCB) with a thickness of 1 mm and a diameter of 9 mm. The PCBs are mounted into isolating plastic electrode housings which are sealed with epoxy resin. The plastic housings have a diameter of approximately 14 mm and are approximately 8 mm thick. The inner electrode contacts connect to the subject's scalp via conductive electrode gel (scalp layer) and the outer electrode contacts connect to a grid made of silicone tubes which is filled with physiological saline solution (reference layer). For a schematic representation of an electrode see figure 1 panel C. The reference layer is galvanically isolated from the scalp layer, only at the common ground/reference electrode both layers are galvanically connected to each other, see figure 1 panel C and D. All electrode contacts (scalp layer and reference layer) are equipped with 5 k Ω non-magnetic current limiting resistors which are built in the electrodes. Wire pairs run from each electrode pair to a coupling board allowing the connection of the cap to the EEG recording system. Each wire at the coupling board is also equipped with a 5 k Ω current limiting resistor. The distance between the coupling board and the cap is about 50 cm (see figure 1 panel B). Two additional leads run from the coupling board to the cap

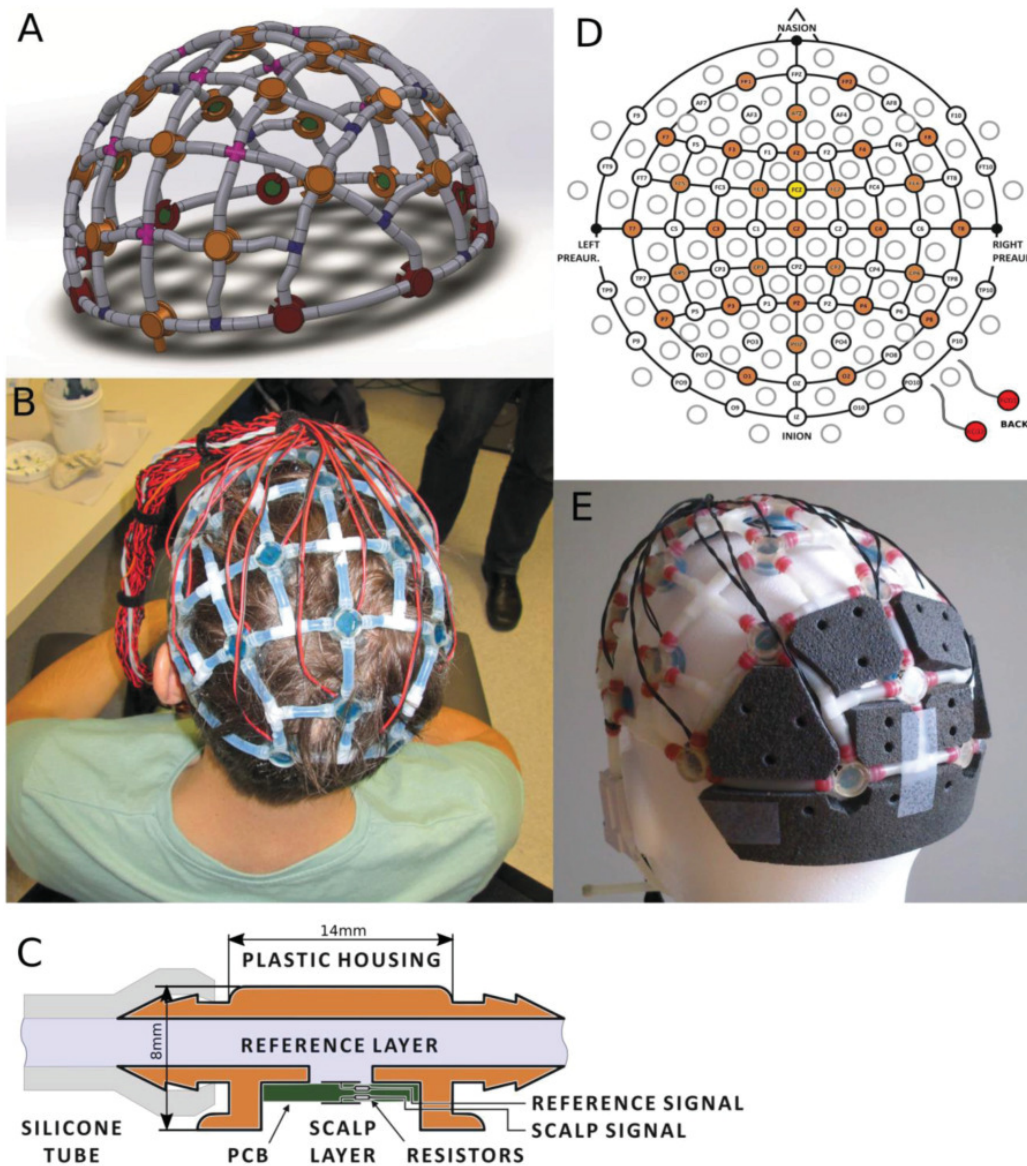


Figure 1. Reference layer cap prototype. Panel A: rendering of the reference layer cap prototype. Panel B: actual cap with cabling. Panel C: principle of a reference layer electrode pair. Panel D: cap layout with electrode positions in the extended 10/20 system. The common ground/reference electrode is colored yellow. The ECG electrodes are colored red. Panel E: cap equipped with foam pads for comfort.

and down to the back of study participants to connect to two self-adhesive MRI compatible ECG electrodes (see figure 1 panel D). The complete positioning of electrodes according to the international extended 10/20 system is shown at figure 1 panel D. To prevent pain resulting from head weight resting on a few electrodes, we putted foam pads in between of the occipital electrodes to distribute the weight, see figure 1 panel E. Temperature measurements were conducted before the cap was used on human. The cap was mounted on a spherical, electrode gel covered fMRI phantom. fMRI compatible heat sensors measured the temperature directly in the connecting gel between phantom surface and electrode. No heating above

1 °C was found during SAR intensive sequences. Hence, we consider the construction as safe concerning the heating due to the switching magnetic fields.

fMRI scanner and EEG recording system

Functional MRI data were acquired on a Siemens Skyra 3.0 T (Siemens, Erlangen, Germany) at the MRI-Lab Graz (Austria) using a 20 channel head coil. The helium pump was active, ventilation was set to lowest level possible. A standard EPI sequence was implemented (TR = 2000 ms, TE = 24 ms, base resolution = 64, $3.5 \times 3.5 \times 3.5$ mm³ voxel size, no gap,

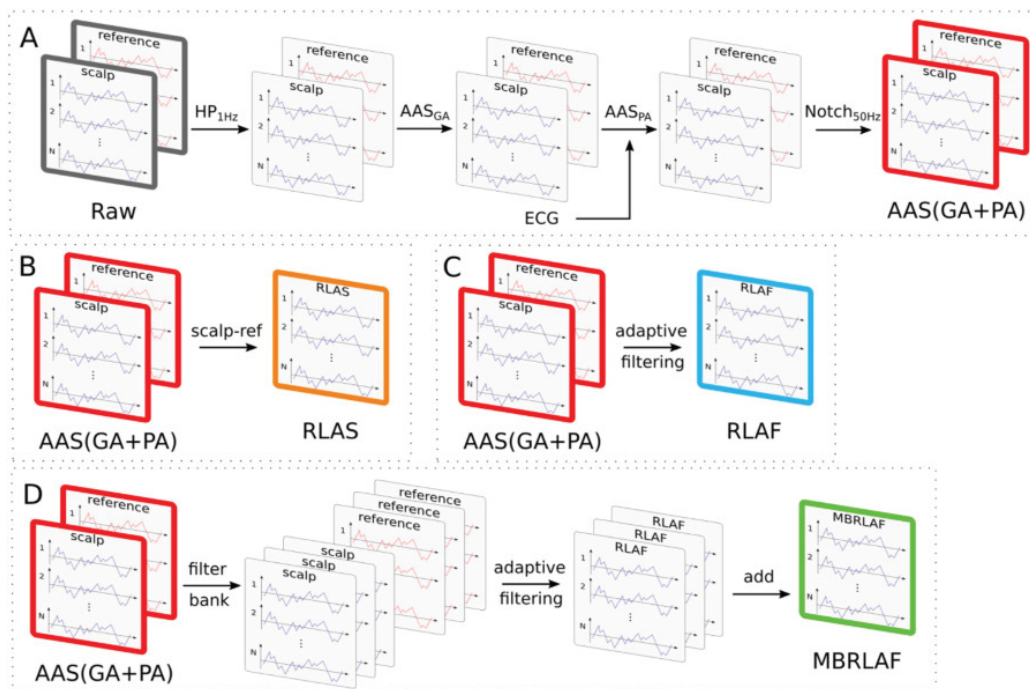


Figure 2. Signal processing chain. Panel A: the pre-processing chain included high pass filtering (HP), average artifact subtraction (AAS) of the gradient artifact (GA), AAS of the pulse artifact (PA) with support of electrocardiogram (ECG) data and notch filtering. Panel B: in RLAS, reference channels were subtracted of scalp channels. Panel C: in RLAF, reference channels were adaptively scaled before being subtracted from the scalp channels. Panel D: in MBRLAF, reference channels and scalp channels were decomposed into frequency components by a filter bank. Reference channel components were adaptively scaled and subsequently subtracted of respective scalp channel components. Full bandwidth MBRLAF data were recomposed by adding up filtered components.

34 slices, field of view = 224×224). The fMRI data are not reported in this work.

EEG and ECG were recorded with a 64 channel MRI compatible EEG system (BrainAmp MR plus, Brain Products GmbH, Gilching, Germany). The EEG amplifier was positioned inside the borehole at the head end of the scanner on a wooden panel. Cables and amplifier were fixed with sand bags. All settings of the amplifier were according the manufacturer's recommendations. The sampling rate was 5 kHz, cutoff frequency of the hardware high pass filter was set to 0.016 Hz and cut off frequency of the hardware low pass filter to 250 Hz. The voltage range was ± 16.384 mV, resulting in a resolution of $0.5 \mu\text{V}/\text{bit}$. The EEG system clock was synchronized with the gradient clock of the MRI scanner via the Brain Products SyncBox device to ensure a highly accurate GA sampling. Sync status was monitored. BrainVision Recorder (Brain Products GmbH, Gilching, Germany) software version 1.20.0802 was used for data recording. All data processing was performed offline, after the recording.

EEG data preprocessing

All 29 possible electrode pairs of the reference layer cap were recorded for each participant, but one pair of participant 1 (position Cz) and two pairs of participant 2 (position FC6 and CP2) had to be rejected due to electrode lift off during the experiment. Hence, signals of 55 of the 58 electrode pairs

were taken for further analysis. In line with Chowdhury *et al* and Jorge *et al* but also due to our own pre-analysis, AAS was used as pre-processing step to reference layer methods (Chowdhury *et al* 2014, Jorge *et al* 2015b). Pre-processing was carried out offline for each electrode signal separately using BrainVision Analyser software (Brain Products GmbH, Gilching, Germany) version 2.1.1.327 and MATLAB (Mathworks Inc., Natick, MA, USA) version 2012b. Figure 2 panel A presents a schematic overview on the pre-processing. Pre-processing included the following steps: (i) Signal offsets were removed by applying a high pass filter (Butterworth zero phase) with a cut-off of 1 Hz and 48 dB/oct damping. (ii) The next step was GA reduction with AAS as implemented in BrainVision Analyser. During data recording the MRI scanner was sending markers whenever a new volume and hence a new GA started. These markers were used to divide the signal into GA epochs. A sliding average artifact template approach was chosen, which calculated GA templates separately for each epoch from 100 adjacent artifact epochs, 50 before and 50 after. This approach can be beneficial if slight changes in the artifact epochs occur. GA templates were subsequently subtracted from signals and all signals were down sampled to 250 Hz. (iii) PA reduction, the third step, was carried out with AAS as implemented in BrainVision Analyser software. The software supports a semiautomatic mode, where R-peaks are detected automatically in dedicated ECG recordings, manually adjusted and then used to divide

the signals into PA epochs. Like in the GA reduction step, a dedicated template for subtraction was computed for each PA epoch separately. A sliding window with 50 adjacent PA epochs, 25 epochs before and 25 epochs after each PA, was taken for calculating PA templates, which were subsequently subtracted. (iv) As the last step in pre-processing the data were exported to MATLAB and a 50 Hz notch filter (0.5 Hz bandwidth, 8th order, IIR) was applied. After preprocessing one reference channel and one EEG channel per electrode pair was left.

Reference layer artifact subtraction (RLAS)

After pre-processing, reference electrode signals were subtracted sample-by-sample from scalp electrode signals, separately for each electrode pair as in Chowdhury *et al* (2014). Hence, after RLAS, one EEG channel per electrode pair was left, see figure 2 panel B.

Reference layer adaptive filtering (RLAF)

In RLAF, artifact subtraction was replaced by adaptive filtering. Each electrode pair was treated separately and was thus filtered with its own adaptive filter. Respective reference electrode signals and scalp electrode signals were fed into first order least-mean-square (LMS) adaptive filters (Haykin 1986). The least-mean-square algorithm was chosen since it is the most common. The first order model restricted the adaptive filters to act like adaptive scalars. One can interpret this process as scaling of the artifact until the residual after subtraction has minimum power (Haykin 1986). The adaptation rate, which is the maximum change in scaling per step, is a crucial parameter. On the one hand, a restricted, thus small adaptation rate prevents overfitting, because the filter cannot follow changes in signals instantly. On the other hand, we want the adaptive filter to follow changes in the scaling, this is why we use adaptive filters. Further, the adaptation rate is crucial to guarantee a stable adaptation process. Small adaptation rates increase the stability, whereas high adaptation rates can lead to unstable behavior. We calculated an individual adaptation rate for each adaptive filter. We thus multiplied the maximum value of the reference electrode signal with the maximum value of the skin electrode signal and multiplied this value by 10 for reducing residual errors and for improving stability. The inverse of this value was our adaptation rate and was between 7×10^{-6} and 1.5×10^{-4} , depending on the respective electrode pair. These small adaptation rates reduce the risk of overfitting the data. The actual adaptive filtering was performed in double pass. First, adaptive filtering was performed forward in time from beginning of the data to end of the data with initial scaling values of one. In a second pass, the scaling was initialized with final values of pass one and the adaptive signal filtering was performed backwards on the original unfiltered data. This procedure yielded a cleaner estimation of the scaling during the starting period, where the adaptive filter had not converged yet and was also used by Jorge *et al* (2015b). After RLAF, one EEG channel per electrode pair was left, see figure 2 panel C.

Multi band reference layer adaptive filtering (MBRLAF)

EEG power spectral density is known for an $1/f$ characteristic, hence, most of the power is found in low frequencies. Adaptive filters minimize total signal power after subtracting filtered reference signals from signals of interest. In case of the RLAF approach, adaptive filters minimized signal power after subtracting scaled reference signals from skin electrode signals. Thus the scalings of the reference signals were particularly fitted to low frequencies and not high frequencies. With MBRLAF, we present an improved version of RLAF which is not afflicted by that problem. In MBRLAF, adaptive filtering was not performed on the full bandwidth signal, but on bandwidth limited sub-bands of the reference and skin electrode signals (Shynk 1992). The full bandwidth signal was afterwards recomposed by adding up the adaptively filtered sub-band signals, see figure 2 panel D. MBRLAF included the following processing steps: (i) A filterbank decomposed reference electrode signal and skin electrode signal of each electrode pair into bandwidth limited sub-bands. (ii) Adaptive filtering was performed on each pair of sub-bands of reference and skin electrode signals separately. (iii) The adaptively filtered sub-band signals were added up to regain the final full bandwidth signal. In this work, we decomposed the full band spectrum into the following frequency sub-bands: from 1–16 Hz in 3 Hz broad bands and separate bands at 16–27 Hz, 27–39 Hz, 39–49.5 Hz, 49.5–50.5 Hz, 50.5–65 Hz, 65–75 Hz, 75–90 Hz and a final band at 90–120 Hz. The choice of the filter bands was motivated by the different artifact types described in the literature and visible in the signal spectra. The sub-bands are different from classical EEG bands, since we tried to define individual frequency bands for artifacts. The actual adaptive filtering was carried out in two passes, as described in the RLAF paragraph above. After MBRLAF, one EEG channel per electrode pair was left, see figure 2 panel D.

Analysis and performance metrics

In order to evaluate the RLAF and the MBRLAF approach on human EEG data, we used a procedure similar to Jorge *et al* (2015b) and included the following analyses: (i) comparison of time courses of EEG signals after artifact reduction, (ii) scaling factors of the adaptive filters, (iii) root-mean-square (RMS) voltage changes, (iv) power spectra (ratio) changes and (v) single trial VEP quality before and after artifact reduction.

Nothing can substitute a direct inspection of the EEG signals. We show a representative example of EEG time courses after applying artifact reduction methods. This specific example was chosen because it shows alpha-rhythm activity and is also afflicted by artifacts. It was taken from the eyes closed part of participant 1 at position O₂, starting 760s after the beginning of the experiment and lasts 8s.

We present scaling factors of the adaptive filters captured at half time during the forward pass to illustrate the necessity of a scaling of the reference signal before subtraction. The choice of time was arbitrary, but motivated by the idea to report representative scaling values. Further we show selected time courses of the scaling factors of adaptive filters for

representative channels over the total signal length. Changes in the scaling factors over time indicate that a onetime fit is insufficient. Scaling values different from one indicate that a straight subtraction is not optimal.

EEG RMS voltages before and after artifact reduction quantify artifact attenuation, under the condition that EEG components are preserved. EEG RMS voltage reduction is then a measure of artifact magnitude that actually was subtracted. The data of the entire experimental time course were used to calculate RMS voltages. The computation was performed separately for each EEG channel of each participant before and after applying different artifact reduction methods. Starting from these RMS voltages per channel, two measures were calculated. (i) Average RMS voltages were computed over EEG channels, hence, an average RMS voltage for raw EEG data and an average RMS voltage per artifact attenuation method. Reductions of these average RMS voltages were calculated relative to the Raw EEG in percent of Raw EEG. (ii) Per channel RMS voltage reduction were calculated in dB relative to raw EEG for each artifact reduction method separately by

$$\text{attenuation}_{\text{dB}} = 20 \cdot \log_{10} \left(\frac{\text{RMS}_i}{\text{RMS}_f} \right), \quad (1)$$

with RMS_i being the RMS voltage after artifact attenuation and RMS_f before (Raw) artifact attenuation. We report median and min/max values of these per channel reductions.

EEG is traditionally analyzed in frequency bands. These bands were classically associated with task specific changes in their power. Hence, an analysis of artifact attenuation per frequency band is of interest. The full band EEG data were decomposed into the most common frequency bands: delta (1–4 Hz), theta (4–8 Hz), alpha (8–13 Hz), beta (13–30 Hz), and gamma (30–120 Hz). These frequency bands defined 3 dB cut-off frequencies of five 12th order second-order IIR band pass filters with zero phase. The average power of frequency bands was calculated by squaring and subsequently averaging each frequency band separately over the full experimental time course of EEG channels. Hence separate band power values per method and frequency band were computed. We report the average band power over channels and the reduction in average band power relative to Raw EEG in dB. Lower power implies lower artifacts under the condition of preserved physiological EEG components.

It is known that a high spatial quality of EEG signatures is hard to obtain in simultaneous EEG-fMRI measurements. Several inside scanner artifacts are harder to deal with at lateral electrodes positions than at central positions. We show alpha power topographies during eyes closed after applying different artifact reduction methods. Better performing artifact reduction methods should show a more dipolar topography. In particular, homogeneous and low alpha power in frontal and central electrode positions and high alpha power at occipital electrode positions.

Full spectrum visualization gives a more detailed view on how well artifact attenuation methods suppress artifacts with specific spectral fingerprints. A Welch power spectral density

estimation approach was applied to EEG data of the full experimental time course. The EEG data were segmented into windows with a length of 5s and an overlap of 631 samples (~50% overlap). A 1250 point fast Fourier transformations (FFT) was applied to each window and averaged over windows. Spectra were subsequently averaged over EEG channels, leading to separate average power spectra for each method.

To illustrate that reference layer based approaches preserve task specific induced EEG activity, we calculated separate spectra of eyes closed and eyes open tasks after AAS and MBRLAF, averaged over occipital channels O1, O2, POZ, P3, P4, and PZ. The procedure of spectra estimation was the same as described in the paragraph above. Further we calculated ratios of power in alpha band between eyes closed and eyes open for occipital channels O1, O2, POZ, P9, P3, PZ, P4, and P8 with

$$\text{alpha power ratio} = \frac{P_{\text{oc}}}{P_{\text{oo}}}, \quad (2)$$

where P_{oc} is the average power in alpha band during eyes closed and P_{oo} is the average power in alpha band during eyes open. This ratio becomes higher when less noise is in the data and becomes lower when alpha power at eyes closed is removed.

To show that reference layer methods preserve evoked brain activity, we calculated separate average visual evoked responses per artifact reduction method. Before averaging a band pass filter (0.5–10 Hz bandwidth, 12th order, SOS-IIR, zero phase) was applied. We collected data of 1200 repetitions of the VEPs during the first part of our measurements. This high number allows for an accurate estimate of the true VEP, even when the artifact reduction methods are not perfect. Hence, VEPs after different artifact reduction methods should be very similar. Differences in average VEPs implies a removal of evoked responses of the respective method. In addition to check for evoked activity preservation, we used VEP homogeneity as a quality measure for artifact reduction methods, similar to Vanderperren *et al* (2010). Of course, VEPs are as a rule intrinsically variable, but if an artifact attenuation method can reduce the variability and thus increase the homogeneity of the VEPs without changing the average VEP, this then means that the method removes artifacts. To quantify VEP homogeneity, mean-squared-distances (MSD) of single VEP epochs to their corresponding average VEP were calculated before and after artifact attenuation methods were applied. Another VEP quality measure is single trial VEP classification accuracy. Equal classification accuracies indicate that physiological components, hence, the information in the EEG, were preserved. Higher classification accuracies indicate that the signal-to-noise ratio was improved. To estimate single trial classification accuracy, 100 repetitions of 5-fold cross-validations were performed. Analytical shrinkage regularized linear discriminant analysis (sLDA) was the classifier of choice (Blankertz *et al* 2011). The dataset consisted of 2 classes. Class 1 were 1200 VEPs measured at skin electrodes O1 and O2. Class 2 were 1200 windows with equal length as the VEPs also measured at skin electrodes O1 and O2, but drawn from random positions in time of the eyes closed part

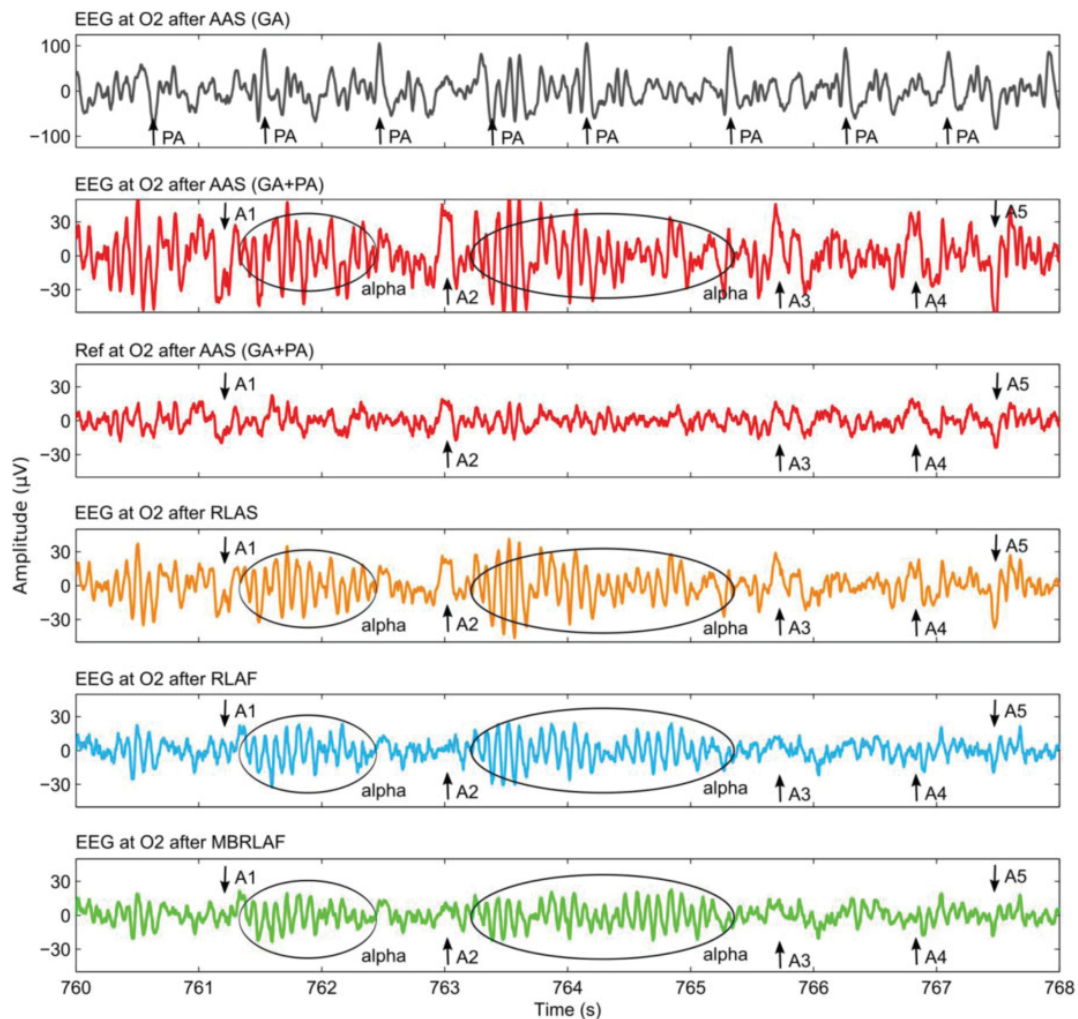


Figure 3. Representative example of EEG time courses after applying artifact reduction methods. The example is taken from channel O₂ and the corresponding reference channel (Ref) of participant 1 starting 760s after the beginning of the experiment. The participant had her eyes closed. Arrows PA mark pulse artifacts. Arrows A1 to A5 mark artifact positions. Be aware of the different scaling of the first row. Artifact reduction methods: average artifact subtraction of gradient artifact and pulse artifact (AAS of GA + PA), reference layer artifact subtraction (RLAS), reference layer adaptive filtering (RLAF), and multi band reference layer adaptive filtering (MBRLAF).

of the experiment. These class 2 data were redrawn for each repetition of the cross-validation process to not be susceptible to random variations in classification results caused by the choice of class 2 data.

Results

Figure 3 shows an eight second piece of EEG of channel O₂ of participant 1 after applying artifact reduction methods and in addition the according reference channel. The EEG piece is taken from the eyes closed part of the experiment where we anticipate increased alpha-rhythm activity. EEG after AAS of the gradient artifact is superimposed by very prominent pulse artifacts. The PAs are marked with an arrow in figure 3 top row. The repetitive nature of the PA is clearly visible with a frequency of ~ 1.1 Hz, which corresponds to a pulse rate of ~ 66 . Comparing the shape of the 1st and

2nd PA, one can recognize the PAs intrinsic variability. It is hardly possible to identify other artifacts or physiological components like alpha-rhythm. After AAS of the pulse artifact, the PA is not visible anymore in our EEG example and alpha-rhythm activity became recognizable. However, also artifacts became visible and are marked with arrows (A1 to A5) in figure 3 second row. The aforementioned artifacts (A1 to A5) are also visible in the corresponding reference channel, which is mandatory for a successful application of RLAS, RLAF, or MBRLAF. The reference channel after AAS of the GA and the PA is depicted in figure 3 third row. After RLAS, amplitudes of the EEG are generally smaller compared to the amplitudes after AAS (GA + PA), because the reference channel was subtracted. Alpha-rhythm activity is clearly visible. Although the artifacts A1 to A5 are smaller after RLAS than after AAS (GA + PA), they are still present. Figure 3 fourth row shows the EEG after RLAS.

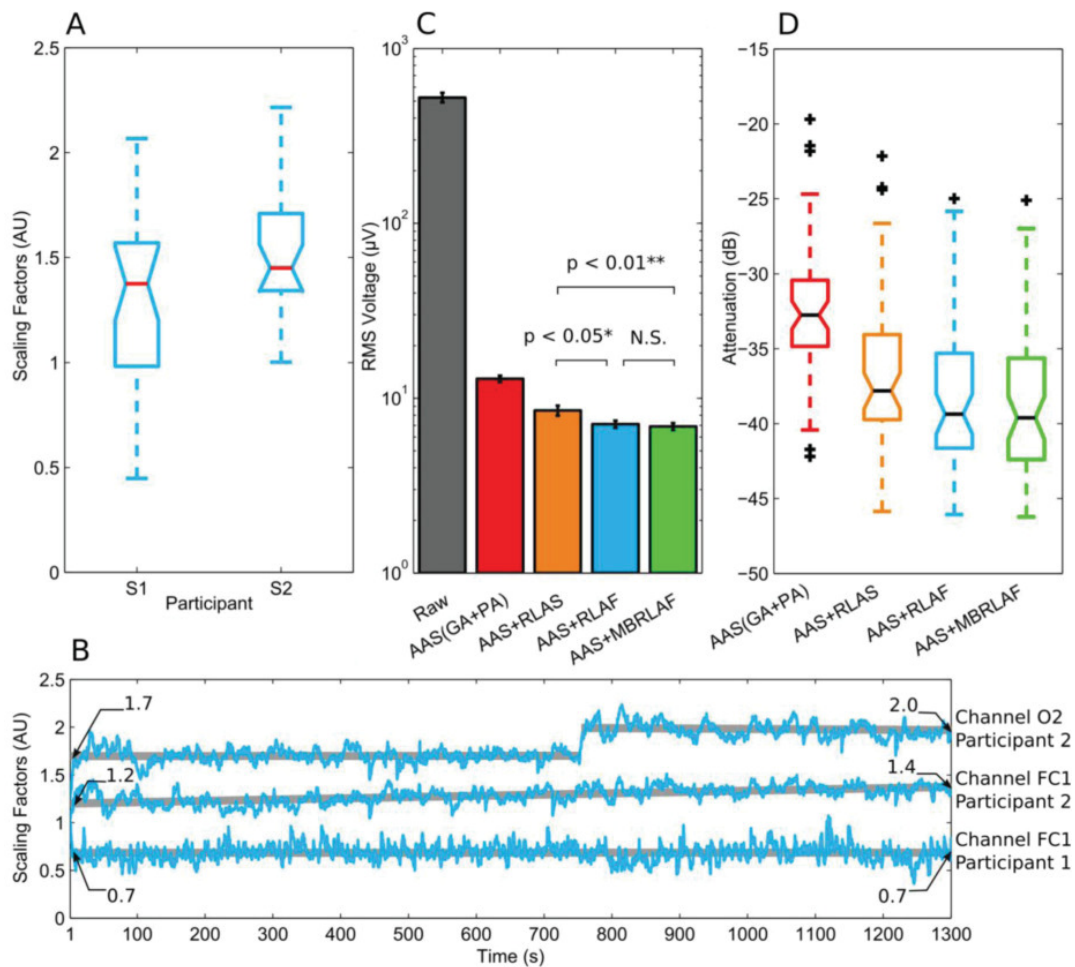


Figure 4. Scaling factors of adaptive filters after the half experiment duration (A), examples of time courses of adaptive filter scaling factors (B), root-mean-square (RMS) voltages after different artifact reduction methods (C), and attenuation by artifact reduction methods (D). A: panel A shows scaling factors of all channels for RLAF at halftime of the experiment. B: panel B shows examples of time courses of adaptive filter scaling factors in RLAF. The examples are taken from channels O₂ and FC1 of participant 2 and from channel FC1 of participant 1. The grey lines represent linear fits to the scaling factors. C: panel C shows average RMS EEG voltages. The average was computed over both participants' total experimental data of skin electrode signals before (Raw) and after artifact reduction. The error bars indicate standard error of the mean. D: panel D shows the boxplot of RMS voltages after artifact attenuation relative to Raw RMS voltages of skin electrodes in dB. Artifact reduction methods: average artifact subtraction of gradient artifact and pulse artifact (AAS of GA + PA), reference layer artifact subtraction (RLAS), reference layer adaptive filtering (RLAF), and multi band reference layer adaptive filtering (MBRLAF).

After RLAF, amplitudes are even smaller than after RLAS and after AAS (GA + PA), because the reference channel was scaled before subtraction. This scaling has direct impact on the aforementioned artifacts A1 to A5. They are greatly reduced and appear hardly visible. Alpha-rhythm activity is still clearly visible. Figure 3 fifth row displays the EEG after RLAF. After MBRLAF, amplitudes are again generally smaller than after RLAF, RLAS, or after AAS (GA + PA), since the adaptive scaling is now fitted per frequency band. Therefore, the fit of the reference channel to the EEG channel is better, which in turn leads to the smaller amplitudes after subtraction. Like after RLAF, the residuals of the artifacts A1 to A5 are small and hardly recognizable. Alpha-rhythm activity is clearly visible. See figure 3 last row for the EEG after MBRLAF.

The scaling factors of adaptive filters, which give a clue on the necessity of scaling the reference channels before subtracting them from EEG channels, were in median 1.38 and 1.45 for participant 1 and participant 2, respectively, after half time of the experiment. For participant 1 the minimum and the maximum scaling factor was 0.45 and 2.07, respectively. For participant 2 the minimum and the maximum scaling factor was 1 and 2.22, respectively. See figure 4 panel A for a boxplot of the scaling factors of all channels at half time of the experiment. Adaptive filters can change the scaling factors over time if necessary. We perceived the following three types of adapting the scaling factors: (i) merely slight or no changes over time. (ii) Steadily increasing or decreasing scaling factors. (iii) Sudden, abrupt changes in scaling factors. Examples for each of these behaviors are given in figure 4 panel B.

Table 1. Average RMS voltage over the experiment duration and channels in μV of Raw EEG and after applying artifact reduction methods. RMS voltage reduction in % relative to Raw EEG and relative to artifact reduction methods: average artifact subtraction of gradient artifact and pulse artifact (AAS of GA + PA), reference layer artifact subtraction (RLAS), reference layer adaptive filtering (RLAF), and multi band reference layer adaptive filtering (MBRLAF).

	RMS voltage (μV)	Reduction to Raw EEG	Reduction to AAS(GA + PA)	Reduction to AAS + RLAS	Reduction to AAS + RLAF
Raw EEG	524	—	—	—	—
AAS(GA + PA)	12.9	-97.5%	—	—	—
AAS + RLAS	8.5	-98.4%	-34.1%	—	—
AAS + RLAF	7.1	-98.6%	-45.0%	-16.5%	—
AAS + MBRLAF	6.9	-98.7%	-46.5%	-18.8%	-2.8%

Table 2. Median RMS voltage reduction over channels per method relative to Raw EEG in dB. Minimum and maximum RMS voltage reduction over channels per method relative to Raw EEG in dB. Artifact reduction methods: average artifact subtraction of gradient artifact and pulse artifact (AAS of GA + PA), reference layer artifact subtraction (RLAS), reference layer adaptive filtering (RLAF), and multi band reference layer adaptive filtering (MBRLAF).

Method	Median RMS voltage reduction over ch (dB)	Min RMS voltage reduction at a ch (dB)	Max RMS voltage reduction at a ch (dB)
AAS	-32.7	-19.7	-42.2
AAS + RLAS	-37.8	-22.2	-45.8
AAS + RLAF	-39.4	-25.0	-46.0
AAS + MBRLAF	-39.6	-25.1	-46.2

Table 3. Absolute (μV^2) average power over channels in frequency bands before (Raw) and after applying artifact reduction methods. Reduction in average power per frequency band relative to Raw power in dB. Artifact reduction methods: average artifact subtraction of gradient artifact and pulse artifact (AAS of GA + PA), reference layer artifact subtraction (RLAS), reference layer adaptive filtering (RLAF), and multi band reference layer adaptive filtering (MBRLAF).

Method	P in delta/red. to Raw	P in theta/red. to Raw	P in alpha/red. to Raw	P in beta/red. to Raw	P in gamma/red. to Raw
Raw	299.6 $\mu V^2/0$ dB	462.9 $\mu V^2/0$ dB	651.6 $\mu V^2/0$ dB	11 736.4 $\mu V^2/0$ dB	318 343.5 $\mu V^2/0$ dB
AAS	67.3 $\mu V^2/-13.0$ dB	33.0 $\mu V^2/-22.9$ dB	30.6 $\mu V^2/-26.6$ dB	12.8 $\mu V^2/-59.2$ dB	5.7 $\mu V^2/-94.9$ dB
AAS + RLAS	40.4 $\mu V^2/-17.4$ dB	10.7 $\mu V^2/-32.7$ dB	12.8 $\mu V^2/-34.1$ dB	6.3 $\mu V^2/-65.4$ dB	2.8 $\mu V^2/-101.1$ dB
AAS + RLAF	21.2 $\mu V^2/-23.0$ dB	6.9 $\mu V^2/-36.5$ dB	8.6 $\mu V^2/-37.6$ dB	5.2 $\mu V^2/-67.1$ dB	3.2 $\mu V^2/-100.0$ dB
AAS + MBRLAF	21.2 $\mu V^2/-23.0$ dB	6.5 $\mu V^2/-37.1$ dB	7.2 $\mu V^2/-39.1$ dB	4.9 $\mu V^2/-67.6$ dB	2.7 $\mu V^2/-101.4$ dB

Average RMS voltages and their relative reduction after applying artifact reduction methods are shown in table 1. Average RMS voltage was statistically significantly different between AAS + RLAS and AAS + RLAF (Wilcoxon rank sum test over channel RMS voltages, $p < 0.05$, average channel wise difference 1.4 μV , min/max difference 0.03 $\mu V/19.82 \mu V$). Average RMS voltage was statistically significantly different between AAS + RLAS and AAS + MBRLAF (Wilcoxon rank sum test over channel RMS voltages, $p < 0.01$, average channel wise difference 1.6 μV , min/max difference 0.12 $\mu V/19.99 \mu V$). No statistical difference was found between AAS + RLAF and AAS + MBRLAF. See figure 4 panel C.

Median RMS voltage attenuation of the applied artifact reduction methods are presented in table 2. RMS voltage reduction is given relative to the raw EEG RMS voltage. MBRLAF achieved the highest RMS voltage reduction of all methods. Artifact reduction for EEG channel FP1 of participant 1 was found to be low after any artifact reduction method and is marked as outlier in figure 4 panel D, but was not removed in analysis.

EEG signal power and artifact power are not evenly distributed over the frequency range. Table 3 and figure 5 show a

complete overview of the powers per frequency band and their reduction per artifact reduction method. In terms of classical EEG frequency bands, the average power of artifact contaminated raw EEG data is starting at 300 μV^2 in the Delta band and reaches approx. $3.2 \times 10^5 \mu V^2$ in Gamma band. After artifact attenuation, average EEG power shows the opposite characteristic. Average EEG power is falling with frequency rising. Hence the average power difference of EEG data before and after artifact reduction is rising with frequency bands. The artifact reduction methods showed varying levels of success. The least average power reductions were achieved by AAS. RLAS achieved third lowest powers in all frequency bands except in the Gamma band. In the Gamma band, RLAS achieved second lowest power. RLAF achieved second lowest average power in any frequency band, except in Gamma band. MBRLAF artifact reduction achieved lowest average signal power in any classical EEG frequency band.

Alpha power topographies for the different artifact reduction methods are presented in figure 6. Alpha power topographies should show low and homogeneous alpha power at frontal and central electrode positions and high alpha power at

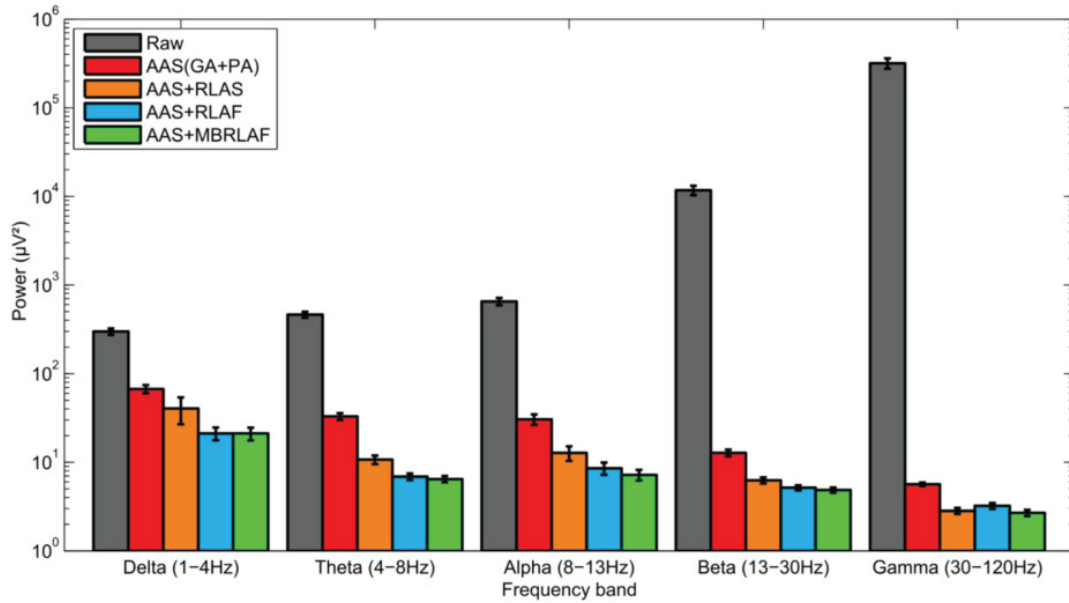


Figure 5. Average EEG power in common frequency bands. The average was computed over skin electrode signals before (Raw) and after artifact reduction. The error bars indicate standard error of the mean. Artifact reduction methods: average artifact subtraction of gradient artifact and pulse artifact (AAS of GA + PA), reference layer artifact subtraction (RLAS), reference layer adaptive filtering (RLAF), and multi band reference layer adaptive filtering (MBRLAF).

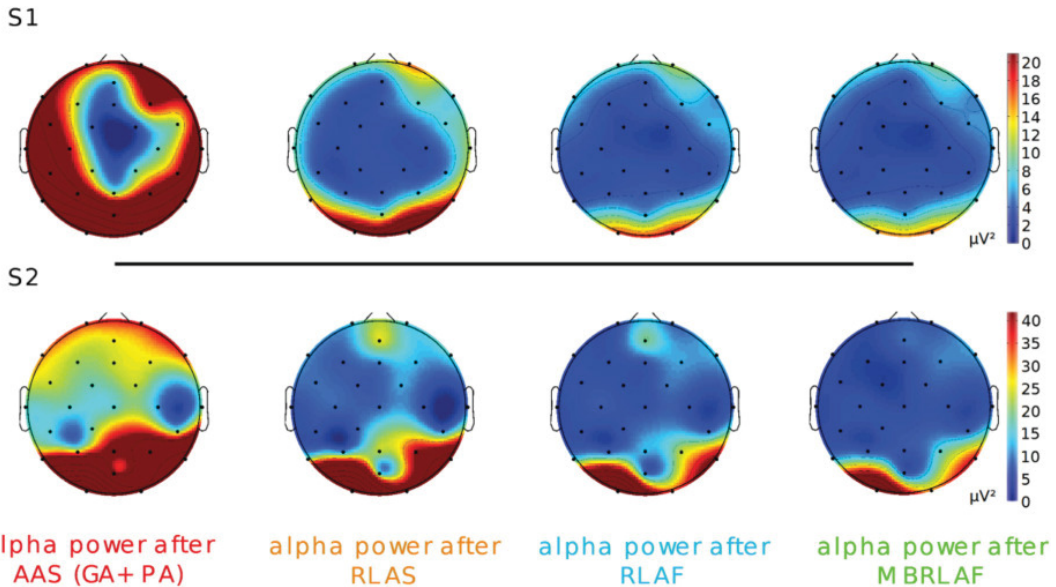


Figure 6. Average alpha power topographies during eyes closed for participant 1 (S1) and participant 2 (S2). Artifact reduction methods: average artifact subtraction of gradient artifact and pulse artifact (AAS of GA + PA), reference layer artifact subtraction (RLAS), reference layer adaptive filtering (RLAF), and multi band reference layer adaptive filtering (MBRLAF). Please note the different scaling for participant 1 and participant 2.

occipital electrode positions, when eyes are closed. The alpha power distribution after AAS is different. High alpha power at occipital positions is present, but also at frontal positions and for participant 1 also at lateral positions. In contrast, reference layer based approaches show a topography as expected. Low and homogeneous frontal and central alpha power and high occipital alpha power. For participant 1 some residuals are

still visible after RLAS, particularly at lateral positions and frontal position FP2. The residuals are smaller after RLAF and MBRLAF. For participant 2 residuals at AFZ and P4 are visible after RLAS, and are smaller after RLAF and MBRLAF.

After artifact attenuation, the typical $1/f$ shape of EEG power spectra is visible and a classical EEG alpha peak is recognizable from 10 to 12 Hz. Moreover, artifactual spectral power

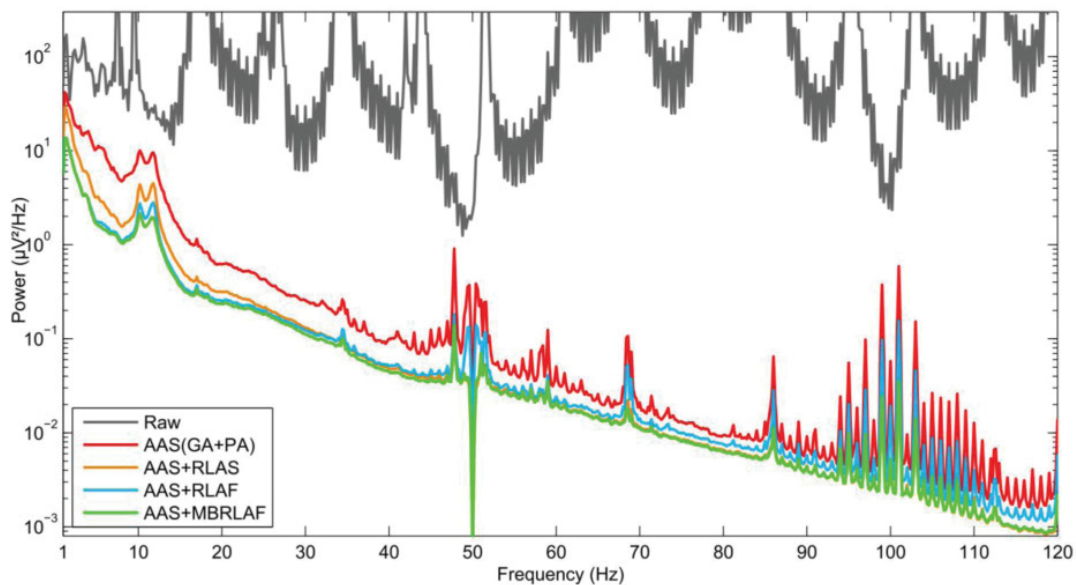


Figure 7. Average power spectra before (Raw) and after artifact reduction. Artifact reduction methods: average artifact subtraction of gradient artifact and pulse artifact (AAS of GA + PA), reference layer artifact subtraction (RLAS), reference layer adaptive filtering (RLAF), and multi band reference layer adaptive filtering (MBRLAF).

complexes are visible at around 17 Hz, 34.5 Hz, 47.8 Hz, 51.5 Hz, 59 Hz, 68.5 Hz, 86 Hz, 120 Hz, and a huge artifact complex of several peaks is ranging from 94 Hz to 113 Hz. Highest artifact power was found at 47.8 Hz with amplitudes of $0.91 \mu\text{V}^2 \text{Hz}^{-1}$, $0.15 \mu\text{V}^2 \text{Hz}^{-1}$, $0.18 \mu\text{V}^2 \text{Hz}^{-1}$, and $0.14 \mu\text{V}^2 \text{Hz}^{-1}$ after AAS, RLAS, RLAF, and MBRLAF, respectively. Highest power of the artifact complex at around 100 Hz was found at 101 Hz with amplitudes of $0.599 \mu\text{V}^2 \text{Hz}^{-1}$, $0.054 \mu\text{V}^2 \text{Hz}^{-1}$, $0.156 \mu\text{V}^2 \text{Hz}^{-1}$, and $0.035 \mu\text{V}^2 \text{Hz}^{-1}$ after applying AAS, RLAS, RLAF, and MBRLAF, respectively. Generally, reference layer methods achieved lower power per Hz than AAS. MBRLAF achieved the lowest power per Hz of all the methods within the total power spectrum. The power magnitude ranged from $1.4 \times 10^1 \mu\text{V}^2 \text{Hz}^{-1}$ at ~ 1 Hz to $8.6 \times 10^{-4} \mu\text{V}^2 \text{Hz}^{-1}$ at ~ 119 Hz. RLAF achieved the second lowest power at low frequency ranges, but starting at ~ 35 Hz, RLAS achieved lower power than RLAF. Full power spectra are presented in figure 7.

Separate spectra of eyes open and eyes closed of both participants are presented in figure 8. A clear task specific change in the spectra is visible. Participant 1, depicted in figure 8 left panel, shows a classical increase in alpha power after eyes were closed. Participant 2, figure 8 right panel, shows a pronounced peak in alpha band already before eyes were closed, but alpha power increased further after eyes were closed. The spectral changes are more pronounced after MBRLAF.

The median of alpha power ratios between eyes closed and eyes opened was highest after MBRLAF (1.84), second highest after RLAF (1.80), third highest after RLAS (1.60), and lowest after AAS (1.37), see figure 9.

Specific VEP patterns were found for both participants and are shown in figures 10 and 11, respectively. For participant 1, highest VEP amplitudes were found at position O2. VEP homogeneity was measured in mean-squared-distance of single VEP

to the respective average VEP at position O2. No specific VEP pattern was found at electrode position O1. For participant 2, highest VEP amplitudes were found at position O1. Mean-squared-distance (VEP homogeneity) of single VEPs to the corresponding average VEP were calculated at position O1. A similar VEP pattern, but with slightly lower amplitudes were found at electrode position O2. Table 4 summaries the maximum average VEP amplitudes and the mean-squared-distances to the average VEP.

Single trial VEP classification accuracies are presented in table 5. They were worst with raw EEG data and best after MBRLAF artifact reduction for both participants. For participant 1, classification accuracies ranged from a minimum of 52.8% to a maximum of 69.1%. For participant 2, accuracies ranged from a minimum of 54.2% to a maximum of 62.6%. Classification accuracies after AAS were higher than with raw EEG data, but never reached accuracies of reference artifact reduction methods. For participant 1, RLAF was the second best artifact reduction method while for participant 2 RLAS, RLAF and MBRLAF were practically equal.

Discussion

Reference layer cap prototype and EEG preprocessing

Our work represents a successful application of a truly reusable reference layer cap in combination with adaptive filtering to minimize residual artifacts in EEG of simultaneous EEG-fMRI in human. Our study extends and combines ideas for improving simultaneous EEG-fMRI data quality that were partly invented by work of Bonmassar *et al*, Masterton *et al* and the no longer available ‘fEEG’ system, and which were partly reinvestigated by a work of Chowdhury *et al*

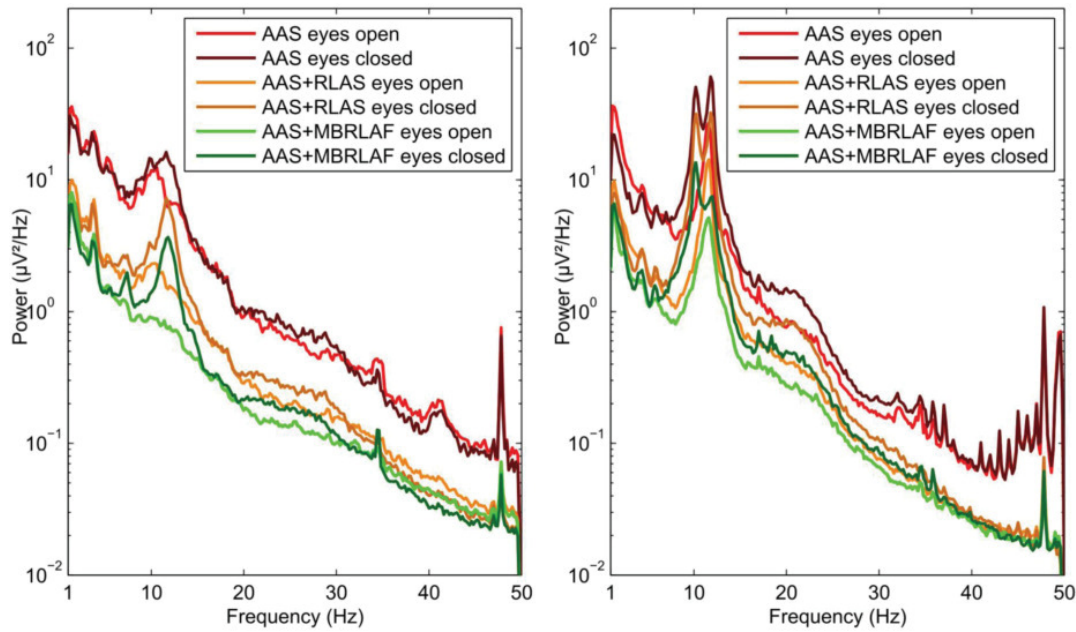


Figure 8. Power spectral density after average artifact subtraction (AAS), Reference layer artifact subtraction (RLAS), and multi band reference layer adaptive filtering (MBRLAF) of participant 1 (left panel) and participant 2 (right panel) averaged over occipital channels O1, O2, POZ, P3, P4, and PZ separately for eyes open and eyes closed.

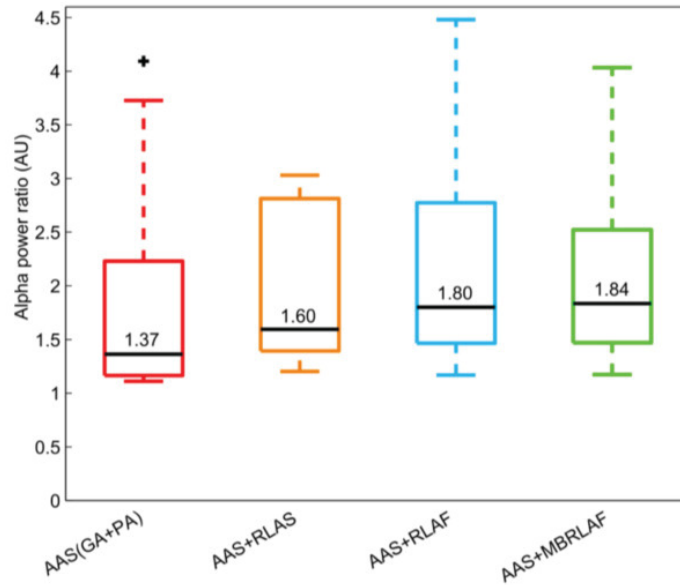


Figure 9. Alpha power ratios between eyes open and eyes closed after different artifact reduction methods at occipital channels O1, O2, POZ, P9, P3, PZ, PZ, P4, and P8. Higher is better. Artifact reduction methods: average artifact subtraction of gradient artifact and pulse artifact (AAS of GA + PA), reference layer artifact subtraction (RLAS), reference layer adaptive filtering (RLAF), and multi band reference layer adaptive filtering (MBRLAF).

(Bonmassar *et al* 2002, Masterton *et al* 2007, Dunseath *et al* 2009, Chowdhury *et al* 2014).

The reference layer cap prototype that we used in this work, is compatible with available fMRI capable EEG amplifier systems, which allows for an upgrade of systems that are already in use. Preparation and handling of the reference layer cap was

similar to standard simultaneous EEG-fMRI caps in terms of duration as well as in terms of comfort for the participants. We did not notice additional susceptibility artifacts in visual inspections of fMRI images compared to standard simultaneous EEG-fMRI caps and EEG of reasonable quality became visible after AAS. The main benefit of this cap is, however, the

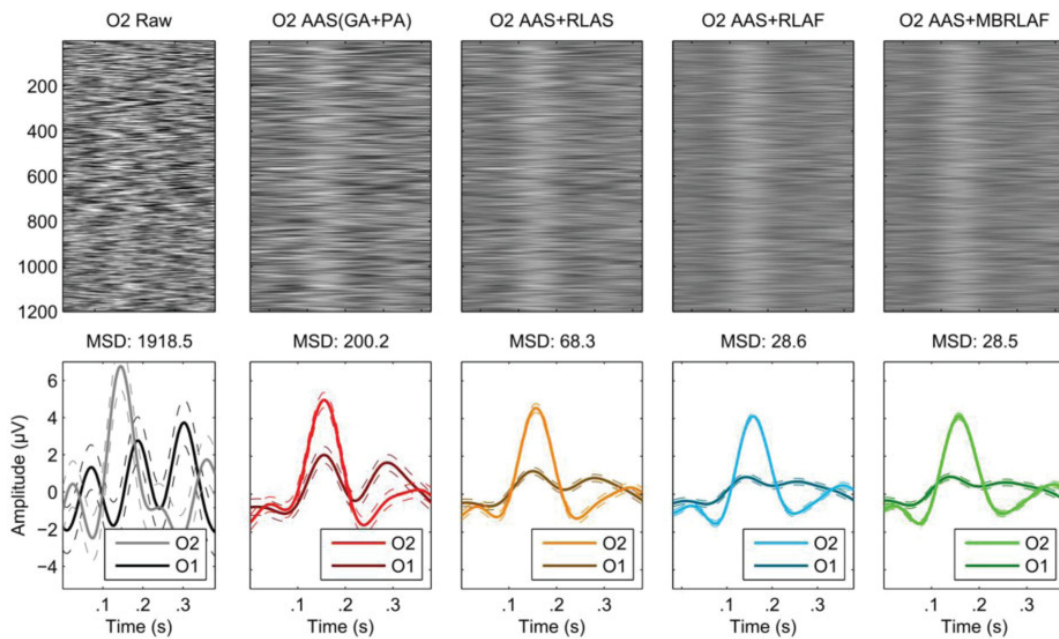


Figure 10. Visual evoked potentials (VEP) of participant 1. The upper row shows epochs of all recorded VEP at skin electrode O2 before (Raw) and after artifact reduction. Bottom row shows average VEP of skin electrodes of participant 1 at position O1 and O2. Dashed lines indicate standard error of the mean. The mean squared distance (MSD) of single VEP epochs to average VEP is a measure of VEP homogeneity and is exemplified in the middle row for participant 1 skin electrode position O2. Artifact reduction methods: average artifact subtraction of gradient artifact and pulse artifact (AAS of GA + PA), reference layer artifact subtraction (RLAS), reference layer adaptive filtering (RLAF), and multi band reference layer adaptive filtering (MBRLAF).

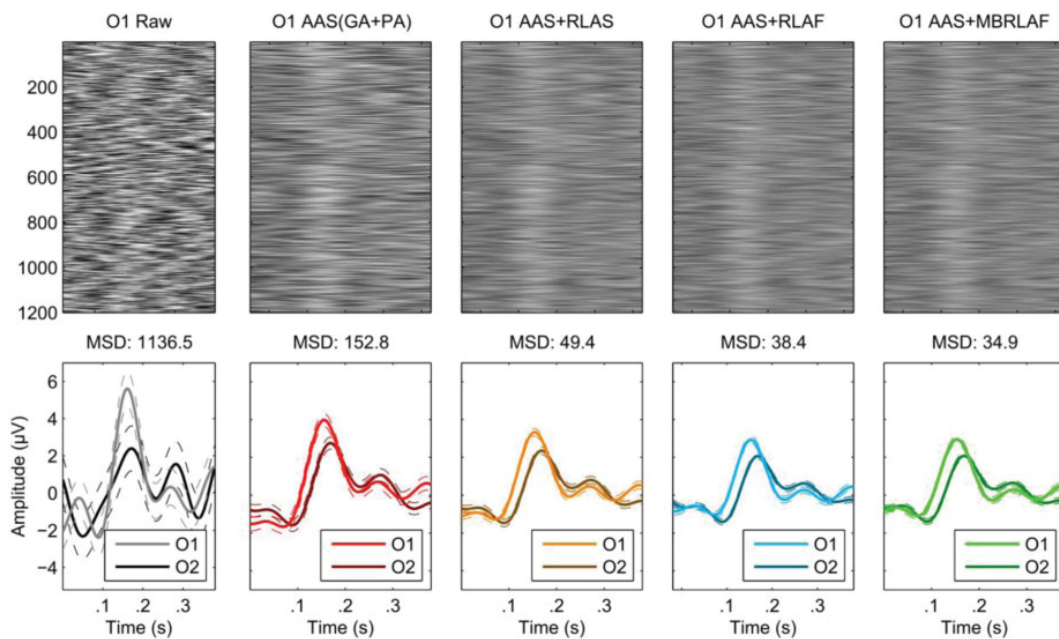


Figure 11. Visual evoked potentials (VEP) of participant 2. Upper row shows epochs of all recorded VEPs at skin electrode O1 before (Raw) and after artifact reduction. The bottom row shows average VEP of skin electrodes of participant 2 at position O1 and O2. Dashed lines indicate standard error of the mean. Mean squared distance (MSD) of single VEP epochs to average VEP is a measure of VEP homogeneity and is exemplified in the middle row for participant 2 skin electrode position O1. Artifact reduction methods: average artifact subtraction of gradient artifact and pulse artifact (AAS of GA + PA), reference layer artifact subtraction (RLAS), reference layer adaptive filtering (RLAF), and multi band reference layer adaptive filtering (MBRLAF).

Table 4. Maximum average VEP amplitudes per participant and per artifact correction method for EEG channels that showed the highest VEP amplitude. Mean-squared-distance of single VEPs to their respective average VEP. Mean-squared-distance is a measure for VEP homogeneity.

	Participant 1		Participant 2	
	Max VEP amp at O2 (μV)	MSD at O2 (μV^2)	Max VEP amp at O1 (μV)	MSD at O1 (μV^2)
Raw	6.7	1918.5	5.6	1136.5
AAS	5.0	200.2	4.0	152.8
AAS + RLAS	4.6	68.3	3.3	49.4
AAS + RLAF	4.1	28.6	2.9	38.4
AAS + MBRLAF	4.1	28.5	3.0	34.9

Table 5. Single trial visual evoked potential classification accuracies of participant 1 (S1) and participant 2 (S2) in percent before (Raw EEG) and after applying artifact reduction methods. Analytic shrinkage regularized linear discriminant analysis was applied in 100 repetitions of 5 fold cross-validation to estimate the accuracies and the standard deviations. Artifact reduction methods were: average artifact subtraction of gradient artifact and pulse artifact (AAS of GA + PA), reference layer artifact subtraction (RLAS), reference layer adaptive filtering (RLAF), and multi band reference layer adaptive filtering (MBRLAF).

ID	Raw EEG (%)	AAS(GA + PA) (%)	AAS + RLAS (%)	AAS + RLAF (%)	AAS + MBRLAF (%)
S1	52.8 \pm 2.3	57.0 \pm 2.2	62.1 \pm 2.3	68.4 \pm 2.1	69.1 \pm 2.1
S2	54.2 \pm 2.3	58.8 \pm 2.2	61.7 \pm 2.1	61.5 \pm 2.2	62.6 \pm 2.0

optional use of reference layer based approaches to improve EEG quality further, namely RLAS and the two methods that we introduced with this work, RLAF and MBRLAF. Visual inspection of EEG after applying artifact reduction methods indicate the benefits of reference layer based approaches, namely reducing residual artifacts, while preserving physiological EEG components. We found that MBRLAF reduces artifact components most, followed by RLAF and RLAS.

Preprocessing is crucial for the efficacy of reference layer based approaches. Our experience within this work support the findings of Chowdhury *et al* and Jorge *et al* about the sequence when combining AAS and RLAS (Chowdhury *et al* 2014, Jorge *et al* 2015b). AAS before RLAS was most effective, while altering the pre-processing sequence impaired the efficacy of RLAS. We observed a similar behavior with RLAF and MBRLAF.

RLAS

In line with Chowdhury *et al* and Jorge *et al* we observed reduced residual artifacts in visual inspections of EEG data after applying RLAS, while physiological EEG activity was preserved (Chowdhury *et al* 2014, Jorge *et al* 2015b). In the present work, RLAS achieved an overall RMS voltage reduction of -37.8 dB compared to the Raw EEG, which is an improvement over AAS by -5.1 dB. Average power in common EEG frequency bands was lower after RLAS than after AAS. Topographical plots of alpha power during eyes closed show reduced residual artifacts at frontal and lateral electrode positions after RLAS compared to AAS. RLAS was also effective in reducing artifacts in higher frequency bands, as visible in the full power spectrum. Further, higher median alpha power ratios as well as more pronounced VEPs with smaller MSD to the average VEP, indicate the preservation of physiological EEG components and underlines the

effectiveness of RLAS. However, as mentioned in the introduction, there are several causes why artifacts at the reference layer can be different from artifacts at scalp, which implies that a straightforward subtraction of reference layer signals from scalp layer signals, as applied in RLAS, might be improved. Practically observed scaling values of the adaptive filters demonstrate that for optimal (in the LMS sense) artifact attenuation reference layer signals need to be scaled by factors between ~ 0.5 and ~ 2 . Theoretical considerations based on Faraday's law justify a linear relationship assumption between reference and scalp layer artifacts, although, the linear relationship can change over time, for example due to motion or due to changes in electrode impedances (Jorge *et al* 2015b). The time courses of the adaptive filters scaling factors provide evidence for that assumption. We perceived three prototypical courses of scaling factors: (i) no change in scaling factors over time. The linear approximation of our example in figure 3 showed practically no change over time with scaling factors of 0.7 in the beginning and in the end. (ii) Linear change over time. In our example the scaling factors increased from 1.2 to 1.4, which is a relative change of 16.7% over ~ 20 min. We assume that slow drifts in the electrode impedances are the cause for that changes. (iii) Abrupt change in scaling factors. We perceived that the scaling factors can also change abrupt, in our example from 1.7 to 2.0. That is a relative change of $\sim 18\%$. We attribute this fast changes to slight motions which change the orientation of the electrodes and therefore the relationship between the scalp and reference electrode. Motions can also change the pressure on electrodes and therefore the impedance. Particularly time courses like (ii) and (iii) are problematic when the scaling factors are time invariant. Errors of up to 20% can be introduced within 20 min. The problems of changing impedances and of motion were for example already brought up in Masterton *et al* (2007) and Jorge *et al* (2015b). The theoretical considerations, combined

with our practical experiences with RLAS and the aforementioned discussions give the justification why we replaced subtraction by adaptive filtering in our RLAF approach.

Reference layer adaptive filtering (RLAF)

Any artifact reduction in simultaneous EEG-fMRI experiments is highly appreciated, since it is still challenging to achieve high EEG quality in these experiments, which in turn is a necessity for a broader field of application of simultaneous EEG-fMRI. Within our work, we found adaptive filtering potentially superior to straight forward subtraction. Visual inspection of EEG after RLAF artifact reduction shows mitigated residual artifacts compared to EEG after RLAS. Residual artifacts after RLAF are visually hardly noticeable. RLAF outperforms RLAS in terms of RMS voltage reduction, while maintaining physiological signals. RLAF achieved significantly lower RMS voltages compared to RLAS (on average 16.5% lower), which is equal to 1.6 dB lower median power when analyzing the full bandwidth EEG. The computational effort of the RLAF approach is easily manageable. One adaptive filter per electrode pair, hence 29 in our experiment, is not at all a problem for modern computers. Back in 2007 Masterton *et al* used already more complex adaptive filters (Masterton *et al* 2007). Hence, an online application is conceivable.

Adaptive filters commonly take into account current and past samples of a signal. The number of past samples is reflected by the model order of the adaptive filter and represent a learned and adaptively tuned FIR filter (Haykin 1986, Shynk 1992). We chose a first order model which restricts an adaptive filter to adaptive scaling of the current sample. One can argue that a higher order model would be beneficial since the optimal filter would be learned too. However, preliminary unpublished investigations by ourselves suggests that higher order models have only a marginal effect. We attribute that behavior to the combination of the LMS optimization criterion of our adaptive filters and the spectral power distribution of EEG. LMS adaptive filters aim to minimize the overall residual power after filtering. Most EEG power is present in low frequency ranges and less power in higher frequency ranges, which is well known as $1/f$ characteristic. Hence, adaptive filters find an optimal scaling for the lower frequency components since lower frequency components contribute most to the overall residuals. Adaptive filters with higher order models, still have the same LMS optimization criterion and still most power is present in lower frequency bands. Hence, we experienced that a low pass filter is learned and the adaptive filter again optimizes the scaling for low frequency ranges, which only marginally improved the adaptive filter quality compared to the first order model.

An EEG power analysis per frequency band indicate that RLAF potentially outperforms RLAS from Delta to Beta band, but is less effective in the Gamma band. This behavior is also visible in the full spectra. RLAF achieves lower power than RLAS up to ~35 Hz, but in higher frequency ranges, RLAF is less effective than RLAS. This is a consequence of

the aforementioned adaptation of the scalings to lower frequency ranges because of their higher power.

The topological alpha power plots show lower residual artifacts after applying RLAF when compared to topo plots after RLAS. Particularly frontal channels can benefit from RLAS. Higher median alpha power ratios as well as VEPs with small MSD to the average VEP, indicate the preservation of physiological EEG components and also indicate a higher effectiveness of RLAF compared to RLAS. All together, these results point at a potentially improved effectiveness of RLAF over RLAS, at least in lower frequency ranges of up to ~35 Hz.

Multi band reference layer adaptive filtering (MBRLAF)

We enhanced the RLAF approach by restricting the frequency range of reference and scalp signals to multiple sub-bands and performed a separate adaptive filtering per sub-band (Shynk 1992). Therefore, we named this approach MBRLAF. As a consequence of the frequency range restriction to sub-bands, each adaptive filter minimized the LMS residuals separately for each band. This resulted in a method that achieves lowest RMS voltages over all, but also lowest power over the whole frequency range and was the best performing method over all. MBRLAF achieved significantly lower RMS voltages compared to RLAS, on average 18.8% lower and achieved also lower RMS voltages than RLAF. However, the reduction of power distribution dependency comes at the cost of computational power. A lot more adaptive filters are necessary (one per sub-band) and computational cost increases linearly with the number of adaptive filters. Luckily, the adaptive filtering can be parallelized on channel level, hence, a real time application of a modified MBRLAF algorithm is conceivable in future. The improvement of MBRLAF over RLAS is significantly, however, the improvement over RLAF is rather marginally, on average 0.2 μ V less RMS voltage. Topological alpha power plots are comparable to RLAF, maybe with a small advantage for MBRLAF. MBRLAF achieved in median the highest alpha power ratio between eyes closed and eyes open and the lowest MSD of single VEPs to the average VEP. These potentially higher effectiveness of MBRLAF is particularly important in higher frequency ranges where signals of interest are already very small and where every possible improvement in signal quality is very welcome.

Preservation of physiological components in the EEG

Reductions in RMS voltage and EEG power are characteristics for artifact reduction only if physiological components are not removed from EEG. Four facts indicate that reference layer based methods preserve physiological components. (i) The shape of EEG spectra: a $1/f$ decay in EEG spectral power is clearly visible after all artifact reduction methods (Schomer and da Silva 2011). (ii) A peak in spectral power at 10 Hz to 12 Hz, the alpha peak, is also clearly visible (Schomer and da Silva 2011). (iii) The dedicated spectra and also the alpha power ratios demonstrate that occipital alpha power is increasing with eyes closed compared to eyes opened, as it

is expected (Schomer and da Silva 2011). The alpha power ratios are higher with reference layer based approaches, indicating better preservation. (iv) VEPs are preserved and average VEPs are very similar after applying different artifact reduction methods (Schomer and da Silva 2011). Hence, a removal of evoked potentials can be ruled out. Concluding these four facts, we do not see a removal of physiological EEG components.

Evoked potentials quality improvement and practical implications

Mean-squared-distance of single evoked potentials to their respective average evoked potential is a measure of variance in EEG that is not related to evoked potentials. This variance consists of ongoing, spontaneous EEG and artifacts. One wants of course to reduce exclusively artifacts. However, when reduced MSD measures are computed, one cannot distinguish which of these two components was removed. Nevertheless, we found induced activity (alpha peak) which is in coincidence with eyes open and eyes closed episodes, and indicate that artifacts were reduced and not ongoing EEG. Hence, a low MSD of evoked potentials to their average evoked potential implies a reduction in artefacts. RLAF and MBRLAF are both capable to reduce the MSD by up to 58% compared to RLAS.

EEG quality improvement has practical implications for simultaneous EEG-fMRI experiments. An improved VEP homogeneity directly impacts experimental design, since a lower number of VEPs is necessary for the same quality of average VEPs. The experiments can thus be of shorter duration, which in turn is beneficial to avoid tiredness of study participants. On single trial level, VEPs are more pronounced. Single trial classification of VEPs benefit as well from MBRLAF. In our single trial accuracy estimation via cross validation, we obtained highest average classification accuracies after MBRLAF. Classification accuracies of participant 1 improved up to 12% from baseline (AAS). Classification accuracies of participant 2 were practically identical after RLAS, RLAF and MBRLAF, which implies only marginal improvement, but indicates that no information, hence VEP, was removed. Classification accuracy is important in many experiments for the accurate detection of brain patterns (Lotte *et al* 2007, Steyrl *et al* 2016).

Limitations

By concept this setup needs two EEG channels per later-to-be-derived EEG signal. For example, a 64 channel setup is necessary to bring the later-to-be-derived channel count to 32. With currently available hardware, 128 or even higher numbers of channels are possible, but comes with the caveat of introducing more technical equipment into the scanner bore, which can be impractical. However, we assume that this caveat should become less important in future, since the number of available channels in EEG hardware steadily increased over the past years. Further we are aware of many experiments

where high quality EEG is more important than the pure number of channels, especially when it comes to analysis of brain signals with a very bad signal-to-noise-ratio, like it is the case for gamma band activity.

In addition to these conceptual limitations, we also perceived practical restrictions. Although no major problems arose during the actual use of the reference layer cap prototype, we found the durability of the silver coated electrodes limited over the long term. The abrasive gel removed the silver coating, which made the cap unusable after several measurements. Future caps need to be equipped with sintered Ag/AgCl pellets, which are more robust (Schomer and da Silva 2011).

The RLAF/MBRLAF approach should in principle be able to cope with motion artifacts, since this was shown already for the RLAS approach by Chowdhury *et al* and we further improved the motion dependent behavior by using the mechanically tightly coupled electrode pair (Chowdhury *et al* 2014). We, however, did not test for these artifacts explicitly in this work. This is future work.

And finally, although EEG quality was improved, residual artifacts are still present after applying AAS, RLAS, RLAF, or MBRLAF. The spectra show remaining artifacts of non-negligible magnitudes. Particularly the huge artifact complex at about 100 Hz is prominent, which is presumably caused by the helium pump. However, it is not yet clear why this artifact is still present after the application of RLAF or MBRLAF. We speculate that more than one source emits interfering electromagnetic fields which are not in phase and therefore the adaptive filter is not able to find a scaling that eliminates this artifact. For illustration, if the adaptive filter finds a scaling that removes one part of the artifact, the other is still present and vice versa, although both components are present in the reference layer. However, this artifact will need further investigations.

Summary

We showed that, based on theoretical considerations, there is potential to increase EEG quality by combining a reference layer with adaptive filtering. We brought practical evidence that EEG quality is potentially improved after applying RLAF or MBRLAF compared to previous methods. We observed reduced artifacts in visual inspections of EEG data after RLAF or MBRLAF artifact reduction. RMS voltage and spectral power were reduced, while physiological EEG components were preserved, even when the coolant system of the scanner was active. RLAF was effective in reducing artifact components up to ~35 Hz, while MBRLAF was the most effective method in all frequency ranges. Nevertheless, residual artifact components above 40 Hz are still present and must be kept in mind when analyzing simultaneous EEG-fMRI data.

In conclusion, we see RLAF and MBRLAF as a potential step forwards to the goal of achieving high quality EEG in simultaneous EEG-fMRI measurements over the full frequency range and particularly for high EEG quality in classical EEG frequency ranges.

Acknowledgments

This work was partly supported by the ERC Consolidator Grant 681231 'Feel Your Reach'. The authors wish to thank Martin Seeber and Prof. Hermann Scharfetter for fruitful discussion and comments.

References

- Abbott D F, Masterton R A J, Archer J S, Fleming S W, Warren A E L and Jackson G D 2014 Constructing carbon fiber motion-detection loops for simultaneous EEG–fMRI *Front. Neurol.* **5** 260
- Abolghasemi V and Ferdowsi S 2015 EEG–fMRI: dictionary learning for removal of ballistocardiogram artifact from EEG *Biomed. Signal Process. Control* **18** 186–94
- Abreu R, Leite M, Jorge J, Grouiller F, van der Zwaag W, Leal A and Figueiredo P 2016 Ballistocardiogram artefact correction taking into account physiological signal preservation in simultaneous EEG–fMRI *NeuroImage* **15** 45–63
- Acharjee P P, Phlypo R, Wu L, Calhoun V D and Adali T 2015 Independent vector analysis for gradient artifact removal in concurrent EEG–fMRI Data *IEEE Trans. Biomed. Eng.* **62** 1750–8
- Allen P J, Josephs O and Turner R 2000 A method for removing imaging artifact from continuous EEG recorded during functional MRI *NeuroImage* **12** 230–9
- Allen P J, Polizzi G, Krakow K, Fish D R and Lemieux L 1998 Identification of EEG events in the MR scanner: the problem of pulse artifact and a method for its subtraction *NeuroImage* **8** 229–39
- Blankertz B, Lemm S, Treder M, Haufe S and Müller K-R 2011 Single-trial analysis and classification of erp components—a tutorial *NeuroImage* **56** 814–25
- Bonnmassar G, Hadjikhani N, Ives J R, Hinton D and Belliveau J W 2001 Influence of EEG electrodes on the BOLD fMRI signal *Hum. Brain Mapp.* **14** 108–15
- Bonnmassar G, Purdon P L, Jääskeläinen I P, Chiappa K, Solo V, Brown E N and Belliveau J W, 2002 Motion and ballistocardiogram artifact removal for interleaved recording of EEG and EPs during MRI *NeuroImage* **16** 1127–41
- Briselli E, Garreffa G, Bianchi L, Bianciardi M, Macaluso E, Abbafati M, Marciani M G and Maraviglia B 2006 An independent component analysis-based approach on ballistocardiogram artifact removing *Magn. Reson. Imaging* **24** 393–400
- Brookes M J, Mullinger K J, Stevenson C M, Morris P G and Bowtell R 2008 Simultaneous EEG source localisation and artifact rejection during concurrent fMRI by means of spatial filtering *NeuroImage* **40** 1090–104
- Chowdhury M E, Mullinger K J, Glover P and Bowtell R 2014 Reference layer artefact subtraction (RLAS): a novel method of minimizing EEG artefacts during simultaneous fMRI *NeuroImage* **84** 307–19
- Debener S, Mullinger K J, Niazzy R K and Bowtell R W 2008 Properties of the ballistocardiogram artefact as revealed by EEG recordings at 1.5, 3 and 7 tesla static magnetic field strength *Int. J. Psychophysiol.* **67** 189–99
- Debener S, Strobel A, Sorger B, Peters J, Kranczioch C and Engel A K 2007 Improved quality of auditory event-related potentials recorded simultaneously with 3 T fMRI: removal of the ballistocardiogram artefact *NeuroImage* **34** 587–97
- Dunseath W J R and Alden T A 2009 Electrode Cap for Obtaining Electrophysiological Measurement Signals from Head of Subject, has Measurement Signal Electrodes Extended through Electrically Conductive Layer and Insulating Layer for Contacting Head of Subject *US Patent Specification* 2009/0099473 USA
- Ferdowsi S, Sanei S, Abolghasemi V, Nottage J and O'Daly O 2013 Removing Ballistocardiogram artifact from EEG using short- and long-term linear predictor *IEEE Trans. Biomed. Eng.* **60** 1900–11
- Haykin S 1986 *Adaptive Filter Theory* 5th edn (Englewood Cliffs, NJ: Prentice-Hall)
- He B, Yang L, Wilke C and Yuan H 2011 Electrophysiological imaging of brain activity and connectivity—challenges and opportunities *IEEE Trans. Biomed. Eng.* **58** 1918–31
- Huster R J, Debener S, Eichele T and Herrmann C S 2012 Methods for simultaneous EEG–fMRI: an introductory review *J. Neurosci.* **32** 6053–60
- Jorge J, Grouiller F, Gruetter R, van der Zwaag W and Figueiredo P 2015b Towards high-quality simultaneous EEG–fMRI at 7 T: detection and reduction of EEG artifacts due to head motion *NeuroImage* **120** 143–53
- Jorge J, Grouiller F, Ipek Ö, Stoermer R, Michel C M, Figueiredo P, van der Zwaag W and Gruetter R 2015a Simultaneous EEG–fMRI at ultra-high field: artifact prevention and safety assessment *NeuroImage* **105** 132–44
- Laufs J 2012 A personalized history of EEG–fMRI integration *NeuroImage* **62** 1056–67
- Liu Z, de Zwart J A, Van Gelderen P, Kuo L W and Duyn J H 2012 Statistical feature extraction for artifact removal from concurrent fMRI–EEG recordings *NeuroImage* **59** 2073–87
- Lotte F, Congedo M, Lécuyer A, Lamarche F and Arnaldi B 2007 A review of classification algorithms for EEG-based brain-computer interfaces *J. Neural. Eng.* **4** 1–13
- Luo Q and Glover G H 2012 Influence of dense-array EEG cap on fMRI signal *Magn. Reson. Med.* **68** 807–15
- Luo Q, Huang X and Glover G H 2014 Ballistocardiogram artifact removal with a reference layer and standard EEG cap *J. Neurosci. Methods* **233** 137–49
- Mantini D, Perrucci M G, Cugini S, Ferretti A, Romani G L and Del Gratta C 2007 Complete artifact removal for EEG recorded during continuous fMRI using independent component analysis *NeuroImage* **34** 598–607
- Masterton R A, Abbott D F, Fleming S W and Jackson G D 2007 Measurement and reduction of motion and ballistocardiogram artefacts from simultaneous EEG and fMRI recordings *NeuroImage* **37** 202–11
- McGlone F, Dunseath R and Stern J 2009 Simultaneous EEG and functional MRI employing novel noise reduction *Epilepsia* **50** 82–2
- Michel C M and Murray M M 2012 Towards the utilization of EEG as a brain imaging tool *NeuroImage* **61** 371–85
- Mulert C and Lemieux L 2010 *EEG-fMRI Physiological Basics, Technique, and Applications* (Heidelberg: Springer)
- Mullinger K J and Bowtell R 2011 Combining EEG and fMRI ed M Modo and J W M Bulte *Magnetic Resonance Neuroimaging, Methods in Molecular Biology* vol 711 (Springer) pp 303–26
- Mullinger K J, Castellone P and Richard Bowtell R 2013b Best current practice for obtaining high quality EEG data during simultaneous fMRI *J. Vis. Exp.* **76** 50283
- Mullinger K J, Havenhand J and Bowtell R 2013a Identifying the sources of the pulse artefact in EEG recordings made inside an MR scanner *NeuroImage* **7** 75–83
- Mullinger K J, Morgan P S and Bowtell R W 2008 Improved artifact correction for combined electroencephalography/functional mri by means of synchronization and use of vectorcardiogram recordings *J. Mag. Res. Imaging* **27** 607–16
- Mullinger K J, Yan W X and Bowtell R 2011 Reducing the gradient artefact in simultaneous EEG–fMRI by adjusting the subject's axial position *NeuroImage* **54** 1942–50

- Niazy R K, Beckmann C F, Iannetti G D, Brady J M and Smith S M 2005 Removal of fMRI environment artifacts from EEG data using optimal basis sets *NeuroImage* **28** 720–37
- Niedermeyer E and Lopes da Silva F H 2005 *Electroencephalography: Basic Principles, Clinical Applications, and Related Fields* 5th edn (Philadelphia: Williams & Wilkins)
- Nierhaus T, Gundlach C, Goltz D, Thiel S D, Pleger B and Villringer A 2013 Internal ventilation system of MR scanners induces specific EEG artifact during simultaneous EEG-fMRI *NeuroImage* **74** 70–6
- Norris D G 2006 Principles of magnetic resonance assessment of brain function *J. Magn. Reson. Imaging* **23** 794–807
- Ogawa S, Lee T M, Kay A R and Tank D W 1990 Brain magnetic resonance imaging with contrast dependent on blood oxygenation *Proc. Natl Acad. Sci. USA* **87** 9868–72
- Ritter P and Villringer A 2006 Simultaneous EEG-fMRI *Neurosci. Biobehav. Rev.* **30** 823–38
- Ritter P, Becker R, Graefe C and Villringer A 2007 Evaluating gradient artifact correction of EEG data acquired simultaneously with fMRI *Mag. Res. Imaging* **25** 923–32
- Rothlübbers S, Relvas V, Leal A, Murta T, Lemieux L and Figueiredo P 2014 Characterisation and reduction of the EEG artefact caused by the helium cooling pump in the MR environment: validation in epilepsy patient data *Brain Topogr.* **28** 208–20
- Schomer D L and da Silva F L 2011 *Niedermeyer's Electroencephalography: Basic Principles, Clinical Applications and Related Fields* (Philadelphia: Williams & Wilkins)
- Shynk J J 1992 Frequency-domain and multirate adaptive filtering *IEEE Signal Process. Mag.* **9** 14–37
- Srivastava G, Crottaz-Herbette S, Lau K M, Glover G H and Menon V 2005 ICA-based procedures for removing ballistocardiogram artifacts from EEG data acquired in the MRI scanner *NeuroImage* **24** 50–60
- Steyrl D, Patz F, Krausz G, Edlinger G and Müller-Putz G R 2015 Reduction of EEG artifacts in simultaneous EEG-fMRI: reference layer adaptive filtering (RLAF) *2015 37th Annual Int. Conf. of the IEEE Engineering in Medicine and Biology Society (EMBC)* pp 3803–6
- Steyrl D, Scherer R, Faller J and Müller-Putz G R 2016 Random forests in non-invasive sensorimotor rhythm brain-computer interfaces: a practical and convenient non-linear classifier *Biomed. Eng.-Biomed. Tech.* **61** 77–86
- Uludag K and Roebroeck A 2014 General overview on the merits of multimodal neuroimaging data fusion *NeuroImage* **102** 3–10
- van der Meer A P, Van Someren E J W, Ramautar J R, van der Werf Y D, Gomez-Herrero G, Lepsien J, Hellrung L, Hinrichs H, Möller H E and Martin Walter M 2016 Carbon-wire loop based artifact correction outperforms post-processing EEG/fMRI corrections—a validation of a real-time simultaneous EEG/fMRI correction method *NeuroImage* **125** 880–94
- van der Meer J N, Tijssen M A J, Bour L J, Van Rootselaar A F and Nederveen A J 2010 Robust EMG-fMRI artifact reduction for motion (FARM) *Clin. Neurophysiol.* **121** 766–76
- Vanderperren K et al 2010 Removal of BCG artifacts from EEG recordings inside the MR scanner: a comparison of methodological and validation-related aspects *NeuroImage* **50** 920–34
- Wu X, Wu T, Zhan Z, Yao L and Wen X 2016 A real-time method to reduce ballistocardiogram artifacts from EEG during fMRI based on optimal basis sets (OBS) *Comput. Methods Programs Biomed.* **127** 114–25
- Xia H, Ruan D and Cohen M S 2013 BCG Artifact removal for reconstructing full-scalp EEG inside the MR scanner *2013 Int. Workshop on Pattern Recognition in Neuroimaging (PRNI)* pp 178–81
- Yan W X, Mullinger K J, Geirsdottir G B and Bowtell R 2010 Physical modeling of pulse artefact sources in simultaneous EEG/fMRI *Hum. Brain Mapp.* **31** 604–20



Online Reduction of Artifacts in EEG of Simultaneous EEG-fMRI Using Reference Layer Adaptive Filtering (RLAF)

David Steyrl^{1,4} · Gunther Krausz² · Karl Koschutnig^{3,4} · Günter Edlinger² · Gernot R. Müller-Putz^{1,4} 

Received: 9 July 2017 / Accepted: 31 October 2017 / Published online: 9 November 2017
© The Author(s) 2017. This article is an open access publication

Abstract Simultaneous electroencephalography (EEG) and functional magnetic resonance imaging (fMRI) allow us to study the active human brain from two perspectives concurrently. Signal processing based artifact reduction techniques are mandatory for this, however, to obtain reasonable EEG quality in simultaneous EEG-fMRI. Current artifact reduction techniques like average artifact subtraction (AAS), typically become less effective when artifact reduction has to be performed on-the-fly. We thus present and evaluate a new technique to improve EEG quality online. This technique adds up with online AAS and combines a prototype EEG-cap for reference recordings of artifacts, with online adaptive filtering and is named reference layer adaptive filtering (RLAF). We found online AAS + RLAF to be highly effective in improving EEG quality. Online AAS + RLAF outperformed online AAS and did so in particular online in terms of the chosen performance metrics, these being specifically alpha rhythm amplitude ratio between closed and opened eyes (3–45% improvement), signal-to-noise-ratio of visual evoked potentials (VEP) (25–63% improvement), and VEPs variability (16–44% improvement). Further, we found that EEG quality after online AAS + RLAF is occasionally even comparable with the offline variant of AAS at a 3T MRI scanner. In conclusion RLAF is a very effective add-on tool to enable high quality EEG in simultaneous

EEG-fMRI experiments, even when online artifact reduction is necessary.

Keywords Simultaneous electroencephalography (EEG) and functional magnetic resonance imaging (fMRI) · Artifact reduction · Reference layer adaptive filtering (RLAF) · Online processing

Introduction

Non-invasive neuroimaging techniques offer the unique opportunity to investigate the active human brain without surgery. The two most popular non-invasive neuroimaging techniques are electroencephalography (EEG) and functional magnetic resonance imaging (fMRI) (Michel and Murray 2012; Norris 2006). EEG measures electrical brain activity, whereas fMRI measures blood oxygenation level changes in the brain (Niedermeyer and Lopes da Silva 2005; Ogawa et al. 1990). These two techniques have partly complementary properties. For example, the time resolution of EEG is in the millisecond range, whereas it is in the range of seconds for fMRI. A second example is the spatial resolution of the techniques, which is commonly in the range of millimeters for fMRI and in the range of centimeters for EEG (Laufs 2012; He et al. 2011). The combing of EEG and fMRI was proposed to benefit from the best of both worlds. The combined simultaneous application of these two techniques allows comprehensive studies of the same brain activity from the electrophysiological and from the metabolic/vascular point of view. Examples of such studies include the combined or joint analysis of EEG and fMRI data such as e.g. in EEG-informed fMRI, the localization of transient brain activity, and also the analysis of the interaction of electrophysiology and metabolism (Huster et al.

✉ Gernot R. Müller-Putz
gernot.mueller@tugraz.at

¹ Laboratory of Brain-Computer Interfaces, Institute of Neural Engineering, Graz University of Technology, 8010 Graz, Austria

² GUGER TECHNOLOGIES OG, Graz, Austria

³ Department of Psychology, University of Graz, Graz, Austria

⁴ BioTechMed-Graz, Graz, Austria

2012; Uludag and Roebroeck 2014; Debener et al. 2006; Ritter and Villringer 2006). This combination is often referred to as simultaneous EEG-fMRI.

Unfortunately, these two techniques influence each other and deteriorate the data quality of the respective other. The additional EEG equipment inside the MRI scanner interferes with the static magnetic field and with the radio frequency field of the scanner. This interference generates field inhomogeneities and signal losses, which in turn degrade the fMRI data quality. Studies demonstrate that the data quality loss in fMRI varies between negligible and severe, but is never prohibitive (Bonmassar et al. 2010; Luo and Glover 2012; Jorge et al. 2015a). The effect of fMRI data acquisition on the EEG data quality is however critical (Mulert and Lemieux 2010; Mullinger and Bowtell 2011a). Over the past years, a variety of fMRI related artifacts in EEG of simultaneous EEG-fMRI have been described. Below, we give an overview, sorted by the usual magnitudes of the artifacts.

The most prominent artifact is the so-called gradient artifact (GA), sometimes also referred to as the scanner artifact (Allen et al. 2000). It has amplitudes up to 1000 times higher than the EEG (Allen et al. 2000; Mullinger et al. 2011b). The switching of the scanner gradient during fMRI data acquisition causes this artifact by electromagnetic induction in the leads of the EEG electrodes. It repeats whenever a new volume acquisition starts. Although techniques to reduce this artifact are known, it is not possible yet to avoid it completely (Mullinger et al. 2011b; Jorge et al. 2015a; Asseconi et al. 2016). Various signal processing based methods have thus been developed to reduce the impact of this artifact. Average artifact subtraction (AAS) is one of them and probably the most widely used one (Allen et al. 2000). AAS exploits the repetitive and deterministic nature of the GA. A separate artifact template is compiled for each single artifact epoch of each EEG channel by averaging over adjacent epochs. This template is subsequently subtracted from the EEG. By averaging over adjacent artifact epochs, AAS can cope with slow changes of the GA, but not with brisk changes, due to e.g. motion of the study participant. Hence, although AAS reduces the GA largely, residuals of the GA are still present and they can be in the same order of magnitude as the EEG.

Reducing the GA unveils a second artifact, the pulse artifact (PA), which is repetitive with the cardiac-pulse cycle. PA amplitudes have the same order of magnitude as the EEG amplitudes and they increase with the strength of the static magnetic field (Allen et al. 1998; Debener et al. 2007, 2008). The PA itself is mainly caused by motion of EEG electrodes, due to cardiac-pulse driven head nodding and due to expansion of blood vessels below the respective EEG electrode (Bonmassar et al. 2002). A second contributor to this artifact is voltage induction in EEG electrodes due to the acceleration of blood below the electrode.

Blood is electrically conductive and therefore surrounded by an electromagnetic field, when accelerated in a static magnetic field. The proportion of this second contributor is relatively small, however, when compared to the first motion related component (Mullinger et al. 2013a). Signal processing based methods are the only option to reduce the artifact and its impact on EEG. AAS is again the most common method to tackle this artifact (Allen et al. 1998). PA epochs are defined by additional electrocardiogram recordings. An individual pulse artifact template per PA epoch and EEG channel is computed by averaging over adjacent PA epochs and subsequently subtracted from the current PA epoch. The cardiac cycle is, however, inherently varying. Hence, the artifact template is only an approximation of the PA and significant PA residuals are often present, particularly at higher static magnetic field strengths of 3T or more. The frequency range of these residuals is usually including the alpha and beta range of EEG and can completely obscure these important brain rhythms.

Other known artifacts in EEG of simultaneous EEG-fMRI are vibration related artifacts like the helium pump artifact (HPA) and the ventilation artifact (VA) (Mullinger et al. 2013b; Nierhaus et al. 2013). Both are caused by MRI scanner systems and are therefore presumably specific to a scanner model. The HPA is mainly generated by vibrations from the cooling system of the MRI scanner, in particular from the helium pump (Nierhaus et al. 2013; Rothluebbers et al. 2014). The VA is caused by vibrations of the patient ventilation system of the MRI scanner (Nierhaus et al. 2013). Both artifacts can be circumnavigated by disabling the systems temporarily. However, both systems are important for a safe and comfortable usage of the MRI scanner and disabling them can be unwanted or not possible. Further, both artifacts are so far not well investigated and artifact reduction techniques are available for the HPA only (Rothluebbers et al. 2014; Kim et al. 2015).

The motion artifact (MA) is another very problematic artifact. It is caused by EEG electrode and cable motion in the static magnetic field of the MRI scanner (Van Der Meer et al. 2010). It is problematic in two senses. First, it is non-repetitive, non-stationary, and typically not predictable. Hence, there is no way to reduce the MA with signal processing based methods that exploit repetitive structures in the artifact. Second, motions change the shape of the GA and the PA. Hence, the AAS approach fails to reduce these artifacts well, since the AAS template is not a good representation of the respective artifact anymore. Many MA reduction techniques have been proposed (Bonmassar et al. 2002; Masterton et al. 2007, Van Der Meer et al. 2010; Abbott et al. 2014; Jorge et al. 2015b). However, best practice is to prevent them by restricting possible motions of the study participants.

These variety of artifacts in EEG of simultaneous EEG-fMRI recordings and the need to improve EEG quality, have led to the development of many different methods for reducing artifacts. Beside the standard AAS approach, particularly the optimal basis set (OBS) approach and the independent component analysis (ICA) approach are frequently used (Niazy et al. 2005; Srivastava et al. 2005; Briselli et al. 2006; Mantini et al. 2007; Ritter et al. 2007; Vanderperren et al. 2010; Abreu et al. 2016). Other methods, for example based on beam former, singular value decomposition, linear predictors, independent vector analysis and dictionary learning, were introduced too and can outperform the aforementioned methods under certain conditions (Brookes et al. 2008; Liu et al. 2012; Ferdowsi et al. 2013; Acharjee et al. 2015; Abolghasemi and Ferdowsi 2015).

Apart from the interest in techniques that improve EEG quality of simultaneous EEG-fMRI in general, there is also growing interest in special techniques that reduce the above-mentioned artifacts on-the-fly. Specifically, in order to carry out experiments, where online processing of the measured data is required. In this context, online processing of data means timely signal processing without knowing the future data, hence signal processing that relies on the past data only, also known as causal signal processing. Some examples for experiments of this kind are: (1) Triggering visual stimulation depending on ongoing EEG and investigating the effects with fMRI (Becker et al. 2011). (2) Locating cerebral generators of epilepsy spikes online (Gotman et al. 2006). (3) Investigating brain activity with fMRI during the use of EEG neurofeedback (Zotев et al. 2014; Zich et al. 2014, 2015). (4) The construction of a new type of brain-computer interfaces (BCIs) that rely on the online feedback of two neuroimaging modalities, hence simultaneous EEG and fMRI feedback, to generate control signals for an application or for the paradigm itself (Brunner et al. 2015; Mano et al. 2017; Perronnet et al. 2017). Unfortunately, most of the MRI artifact reduction methods rely on non-causal signal processing, hence knowledge of upcoming data is required and they can therefore only be applied offline, after the experiment. This situation led to the development of online applicable artifact reduction techniques. Brain Products (Brain Products GmbH, Gilching, Germany) provide an online version of AAS for GA and PA reduction in their commercial RecView tool. Other online artifact reduction methods, for example based on windowed versions of OBS and ICA, have also been developed (Wu et al. 2016; Mayeli et al. 2016; Wen et al. 2016).

The EEG data quality of simultaneous EEG-fMRI is often mediocre. For example, Zich et al. carried out a BCI experiment based on the classification of sensorimotor rhythms and they report a drop in average classification accuracy by approximately 10% when moving from outside the scanner to inside the scanner (Zich et al. 2015).

In a similar experiment with a single participant, we found the classification accuracy to be 22% lower inside the scanner compared to outside the scanner (Steyrl et al. 2013). One reason for the poorer EEG data quality can be found in the artifact reduction methods. Both studies used AAS and as mentioned above, AAS is susceptible to brisk artifact changes and inherently varying artifacts. Moreover, AAS also depends on reliable detection of artifact periods. And naturally, AAS is only able to reduce repetitive artifacts such as the GA and the PA. Unfortunately, switching to another artifact reduction method is not necessarily a solution. The limitations of AAS also hold for the OBS method. ICA based methods on the other hand are partly able to reduce other artifact types too, however, they rely on the basic assumption that artifacts, or components, are stationary in space, which is particularly violated for PAs (Debener et al. 2007).

We recently presented a new add on technique for artifact reduction in EEG of simultaneous EEG-fMRI, which uses a completely different approach. This technique is based on the idea of recording artifacts independently of, but simultaneously with EEG, at a reference layer that is isolated from the scalp. Adaptive filters use those independent reference recordings to reduce the artifacts in the EEG. This technique is therefore named reference layer adaptive filtering (RLAF) (Steyrl et al. 2015, 2017; Chowdhury et al. 2014; Dunseath and Alden 2009; McGlone et al. 2009). In our previous works, we presented a reusable EEG-cap prototype that is equipped with a saline-water based reference layer to allow the aforementioned independent reference recordings (Steyrl et al. 2017). We showed that RLAF is most effective when artifacts have already been reduced using another technique such as AAS in a pre-processing step. We reported on artifact reduction results of data recorded at a spherical fMRI phantom, as well as on artifact reduction results of human EEG (Steyrl et al. 2015, 2017). Our results demonstrate that RLAF tackles all artifacts that occur, as long as they are represented in the reference layer, which leads to a substantially improved EEG quality compared to predecessor techniques (Steyrl et al. 2017).

In this work, we introduce RLAF for the online artifact reduction in EEG of simultaneous EEG-fMRI. As in our previous work, RLAF is applied as an add on after AAS and in this case after online AAS. The evaluation of EEG artifact reduction techniques is generally tricky, since a basic truth in this issue remains an unknown factor. Several suggestions for evaluation strategies have been made, but despite this a gold standard has not emerged yet. For this work, we decided to focus on the evaluation of what can be assumed as the best known and most widely analyzed EEG phenomena. We analyze alpha rhythm amplitude differences between opened and closed eyes, and visual evoked potentials (VEP). We compare the online version of AAS+RLAF with: the

online version of AAS, the offline version of AAS, and EEG recorded outside the MRI scanner.

Materials and Methods

Participants

The experiment was performed in accordance with the Declaration of Helsinki and was approved by the local ethics committee. Seven participants (all male, students, age 21–26 years) volunteered in this experiment. One was excluded, because he felt uncomfortable inside the scanner and aborted the experiment. Participants had medical histories free of neurological abnormalities and gave written informed consent for participation before the experiment. They received a monetary compensation of 20 €.

Experiment Description

The aim of the present work was to record EEG, specifically alpha rhythm amplitude differences and evoked brain responses and to compare those from measurements inside and outside the MRI scanner. Hence, each participant performed the experiment twice. First, recordings were performed outside the MRI scanner, in the room where the EEG cap was prepared and then a second time inside the MRI scanner. We used a modified version of the experiment in our last RLAf work (Steyrl et al. 2017). The experiment itself was divided into two parts. During the first part, evoked brain responses were recorded. Participants had their eyes opened and were looking at a computer monitor, where a checkerboard was presented. The checkerboard had 8 × 8 black and white square fields with a small red dot in the center. The black and white fields were inverted every 0.5–0.6 s to trigger visual evoked potentials (VEP). 600 VEPs were collected per experiment. In the second part of the experiment, participants closed their eyes and were instructed to relax, but not to fall asleep, to provoke changes in the alpha rhythm. The experiments outside and inside the scanner differed in three points: (1) Outside the scanner, participants were upright sitting in a chair. Inside the scanner, participants were lying in supine position. (2) The distance between monitor and eyes was about 1 m in the experiments outside the scanner (visual angle 20°), and approximately 2.5 m in the experiments inside the scanner (visible angle 15°). (3) Outside the scanner, the environment was quiet. Inside the scanner, we used earplugs to reduce the scanner noise. One experiment lasted in total about 12 min with approximately 6 min opened eyes and 6 min closed eyes. The overall time per participant was about 2 h with 20 min for instructions and information, 40 min cap preparation and testing, 12 min experiment outside, 20 min preparation

inside scanner, 10 min testing inside scanner, 12 min experiment inside scanner, and 5 min for removing the equipment from the participant.

Reference Layer Cap Prototype

In this work, we used the second version of a reference layer cap prototype, developed by GUGER TECHNOLOGIES OG, Austria (patents pending). This prototype cap offers the opportunity of dedicated reference recordings from a separate layer. The new cap version has Ag/AgCl sinter-pellets as electrode contact areas instead of pure Ag. For a description and an evaluation of the first version please see (Steyrl et al. 2015, 2017). A rendering of the cap is depicted in Fig. 1a and see Fig. 1b for a photo of the new cap version. The cap size is optimized for a head circumference of about 58 cm. However, the cap is flexible enough for head circumferences between 56 and 58 cm. To use this cap with larger heads is not recommended, because in that case the cap can cause pain due to high contact pressure. The cap is equipped with 29 double-layer EEG electrode pairs, a common ground/reference electrode, and connectors for two additional self-adhesive MRI compatible electrocardiogram (ECG) electrodes at the participants back. Each double-layer EEG electrode is made of a pair of Ag/AgCl sinter-pellets with a diameter of approximately 2 mm and a thickness of approximately 1 mm. The pellets are glued with conductive epoxy to both sides of an approximately 1 mm thick printed circuit board (PCB). One pellet connects to the scalp via conductive EEG gel and the other to the reference layer. The PCB with sinter-pellets is fixed into an isolating plastic housing. The whole electrode is about 8 mm thick and has a diameter of approximately 14 mm. For a schematic of a double layer electrode see Fig. 1c. The reference layer itself is a grid of silicon tubes filled with physiological saline solution and is electrically isolated from the scalp, except at the common ground/reference electrode. At this electrode, the scalp is connected to the reference layer to pull them at the same potential. Electrodes are connected to the EEG amplifier via thin copper cables. 5kOhm current limiting resistors were placed between the sinter-pellets and the cables, and additional 5kOhm resistors were placed at the end of the cables before a coupling board connects to the EEG amplifiers via a flat ribbon cable. ECG connectors are equipped with 10kOhm current limiting resistors at the electrodes. The cable length is approximately 50 cm. The electrode arrangement is according to the international 10/20 system and depicted in Fig. 1d. We put foam pads between the occipital EEG electrodes to prevent pain from lying on a few small electrodes, see Fig. 1e. Temperature measurements were carried out during SAR intensive sequences to rule out a harmful heating of the electrodes.

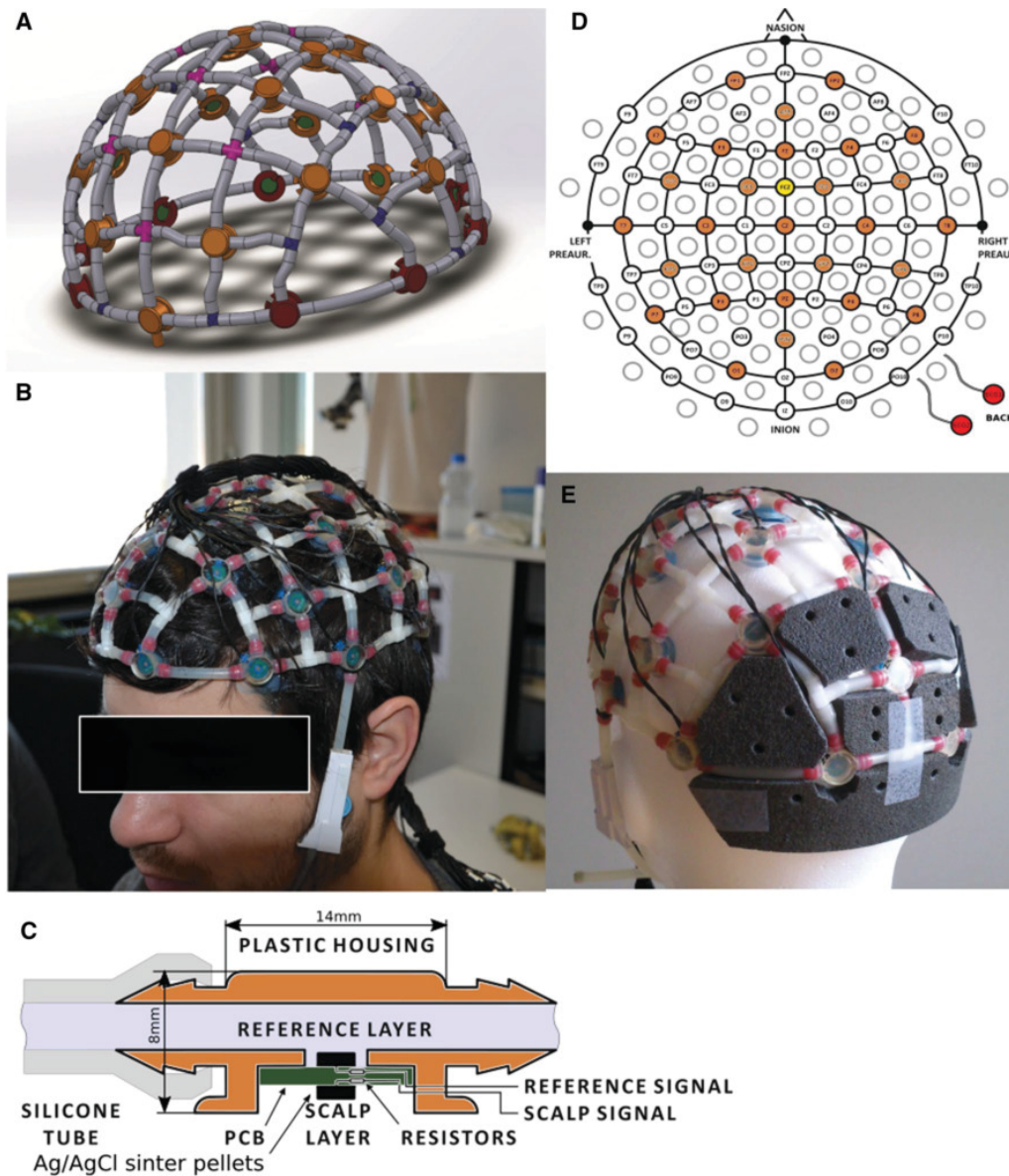


Fig. 1 Reference layer cap prototype. **a** Rendering of the cap prototype, **b** cap mounted on a head, **c** schematics of a reference layer electrode pair, **d** cap layout with electrode positions in the extended

10/20 system. Available electrode positions are colored orange. The common ground/reference electrode is colored yellow. The ECG electrodes are colored red, **e** cap equipped with foam pads for comfort

fMRI Scanner and EEG Recording System

Functional MRI data were acquired at a Siemens Skyra 3.0T (Siemens, Erlangen, Germany) at the MRI-Lab Graz (Austria) using a 20 channel head coil. The helium pump was active and the ventilation was set to the lowest level possible. A standard EPI sequence was implemented (TR = 2250 ms, TE = 28 ms, base resolution = 64, $3.5 \times 3.5 \times 3.5\text{mm}^3$ voxel

size, 0.4 mm gap, 36 slices, field of view = 224×224). EEG and ECG was recorded with a 64 channel MRI compatible EEG system (BrainAmp MR plus, Brain Products GmbH, Gilching, Germany). The EEG system was positioned inside the borehole at the head end of the MRI scanner on a wooden panel. Cables and amplifiers were fixed with sand bags. All amplifier settings were chosen according to the manufacturer’s recommendations. Hence, the sampling

rate was set to 5 kHz, the cut-off frequency of the hardware high pass filter to 0.016 Hz and the cut-off frequency of the hardware low pass filter to 250 Hz. The voltage range was set to ± 16.384 mV, resulting in a resolution of 0.5 $\mu\text{V}/\text{bit}$. The EEG system clock was synchronized with the gradient clock of the MRI scanner via the Brain Products SyncBox device to ensure a highly accurate GA sampling. Sync status has been monitored. BrainVision Recorder (Brain Products GmbH, Gilching, Germany) software version 1.21.0102 was used for EEG data recording. The two ECG channels were treated like EEG channels, hence, EEG settings also apply to ECG recordings. We carefully prepared the electrode skin contact with abrasive electrode gel, but we were not able to control the skin impedances. It would appear that separate ground and reference electrodes must be mandatory to measure impedances with that EEG system.

Pre-processing Procedure of Outside-MRI-Scanner EEG

After the experiments, outside-MRI-scanner EEG recordings were down-sampled from 5000–250 Hz, using the “Change sampling rate” transformation in the BrainVision Analyzer software (Brain Products GmbH, Gilching, Germany, version 2.1.1.327). That included a 112.5 Hz low-pass anti-aliasing filter with 24 dB/oct damping before the down-sampling. The down-sampling itself is based on spline interpolation. See also Fig. 2a for a summary of the pre-processing procedure. We refer to the EEG after this procedure of outside-MRI-scanner EEG recording and offline EEG pre-processing, when we write of “outside EEG” in upcoming chapters.

Offline AAS Artifact Reduction Procedure of Inside-MRI-Scanner EEG

BrainVision Analyzer was used to perform artifact reduction offline and included the following steps: (1) Removing signal offsets with a high-pass filter (Butterworth zero phase, cut-off at 1 Hz, 4th order). (2) The next step was GA reduction with AAS as implemented in BrainVision Analyzer. The MRI scanner was sending TTL level triggers during the data recording, to mark new volumes. These markers were used to divide the EEG recordings into GA epochs. GA templates have been calculated separately for each epoch by averaging over 100 adjacent artifact epochs, 50 before and 50 after the current epoch. Subsequently, GA templates were subtracted from EEG recordings and all recordings were down sampled to 250 Hz (low-pass anti-aliasing filter, 112.5 Hz cutoff frequency, 24dB/oct damping). (3) AAS was carried out a second time for PA reduction. To divide the EEG recordings into PA epochs, the semiautomatic R-peak detection mode of the BrainVision Analyzer software was used. In that

mode, R-peaks are detected automatically in separate ECG recordings, manually readjusted and subsequently used as markers. As in the GA reduction step, a separate template for subtraction was computed for each PA epoch. 50 adjacent PA epochs, 25 epochs before and 25 epochs after each PA, have been averaged to obtain the PA templates. The procedure is summarized in Fig. 2b. The number of epochs for averaging is a crucial parameter in AAS. It determines the adaptiveness of AAS templates as well as the EEG residuals in the AAS templates. Unfortunately, no gold standard has emerged yet for determining the number of epochs. We base our choice on the following argument: In one of the original papers on AAS (Allen et al. 2000), the aim was to obtain a clean artifact template, in which small events in the EEG are not covered by EEG residuals. They authors assumed that small EEG events have an amplitude of 10 μV and large EEG events have an amplitude of 250 μV , which leads to the use of 25 epochs (Allen et al. 2000). Beside the events argument, using 25 epochs implies that the RMS amplitude of the residual EEG in the template is reduced to 20% of the original RMS amplitude of the EEG, since the RMS amplitude is reduced by a factor of $\sqrt{\text{number of epochs}}$. Our goal was to at least maintain that level of residual EEG in two subsequent applications of AAS. Therefore, a reduction to 14% of the original RMS amplitude is necessary in each single step to maintain an overall reduction to 20%. 50 epochs for averaging are necessary to achieve that reduction to 14% and was therefore our choice for the minimum number of epochs. We name the EEG after this procedure of inside-MRI-scanner EEG recording and subsequent offline AAS, as “offline AAS EEG” throughout this work.

Online AAS Artifact Reduction Procedure of Inside-MRI-Scanner EEG

Inside-MRI-scanner EEG recordings were stored with BrainVision Recorder and were simultaneously sent to BrainVision RecView with the remote data access option of the BrainVision Recorder. Online artifact reduction in RecView included the following steps: (1) High-pass filtering to remove offsets (Butterworth filter, 1 Hz cut-off frequency, 24 dB/oct damping). (2) Online GA reduction with AAS. The TR was used to divide the past EEG into artifact epochs. The first 10 epochs per channel were averaged to compute initial individual GA templates. New epochs were added to the templates if the correlation of the new epoch with the current template exceeded a predefined threshold of 0.975. Subsequently, the current templates were subtracted online from the artifact afflicted EEG. (3) Subsequently, the EEG was down-sampled to 250 Hz (Butterworth low-pass anti-aliasing filter, 112.5 Hz cutoff, 24 dB/oct damping). (4) PAs were tackled with online AAS too. The past EEG was divided into epochs of PAs via online R-peak detection.

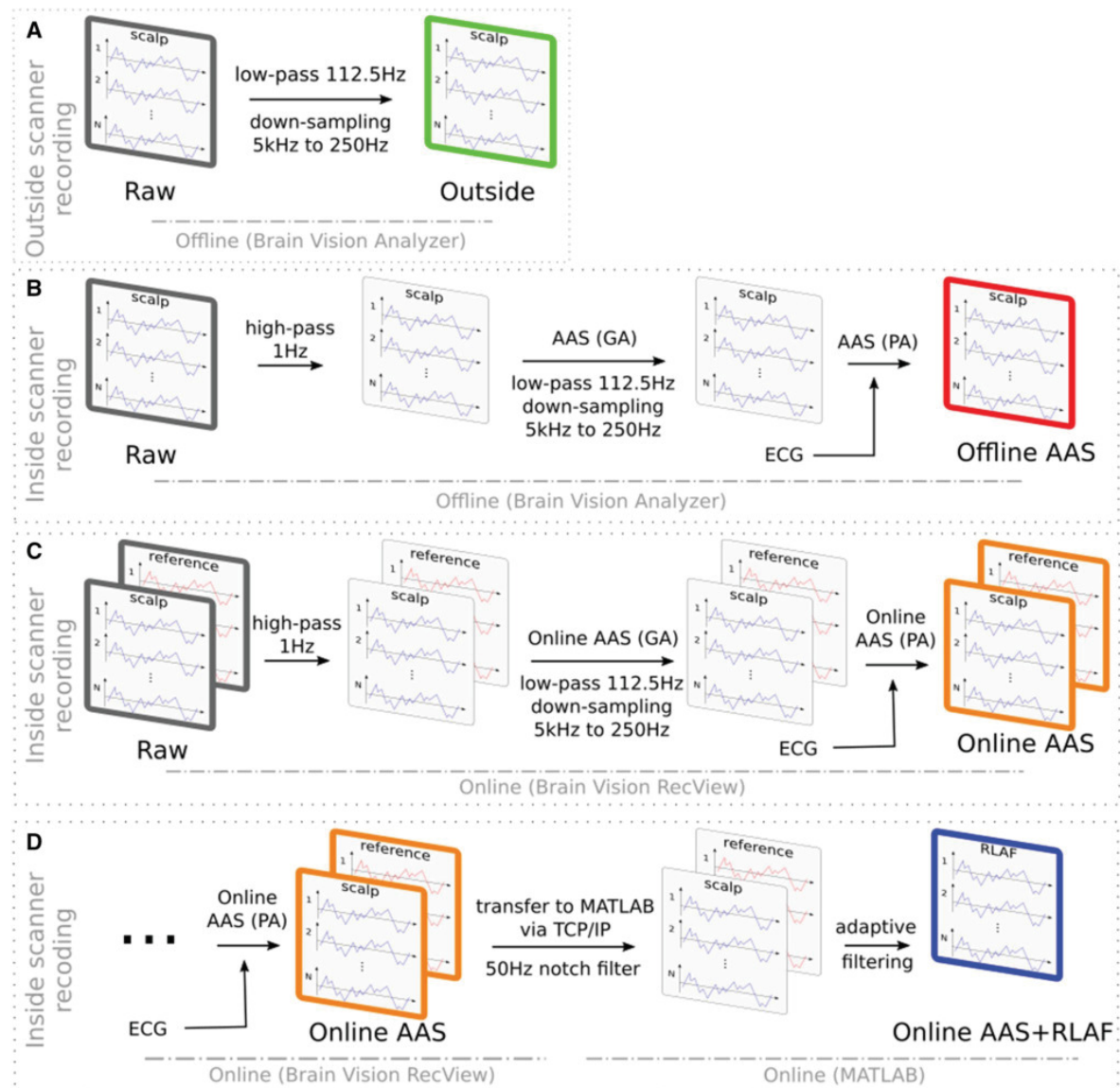


Fig. 2 Signal processing overview. **a** Outside-MRI-scanner EEG was low-pass filtered and down-sampled, **b** processing of inside-MRI-scanner EEG to reduce fMRI related artifacts. Average artifact subtraction (AAS) was applied twice. First to reduce the gradient artifact

(GA) and second to reduce the pulse artifact (PA), **c** Processing pipeline to reduce fMRI related artifacts online by applying online AAS twice, **d** Additional adaptive filtering step after online AAS to reduce fMRI related artifacts further

Online R-peak detection in RecView is based on a template correlation approach. The method searches for a prototypical ECG epoch and subsequently compares it with the ongoing EEG. If certain thresholds are exceeded an epoch is found (settings: minimal pulse period 650 ms, minimal correlation 0.6, minimal amplitude 0.6, maximal amplitude 1.2). Separate PA templates were computed per channel by averaging

over the last 50 PA epochs of the respective channel. The current templates were subtracted online from the artifact afflicted EEG. For an overview of this procedure see Fig. 2c. It can be assumed that this online artifact reduction procedure has a maximum delay of 150 ms. It takes 80–100 ms until the EEG data are available in RecView, including the hardware delay of the EEG system, transport of the EEG

data via USB and the delay of the BrainVision Recorder software. The actual online artifact reduction in RecView is carried out sample-by-sample and hence, only a small additional delay is added. We assume that this delay is below 50 ms. We abbreviate the EEG after this artifact reduction procedure of inside-MRI-scanner recording and online AAS, with “online AAS EEG” in the following chapters.

Online AAS + RLAF Artifact Reduction Procedure of Inside-MRI-Scanner EEG

In accordance with previous works, we implemented the adaptive filtering as an additional processing step after GA and PA reduction with AAS (Chowdhury et al. 2014; Steyrl et al. 2017). Online AAS artifact reduction was carried out in BrainVision RecView (see description above). Subsequently, EEG data were transmitted to MATLAB (Mathworks Inc., Natick, MA, USA, Version 2012b) via the BrainVision RecView BCI2000 bridge. This bridge opens a TCP/IP server and the data can be received with any TCP/IP client. Brain Products recommends the pnet TCP/IP client from the TCP/UDP/IP Toolbox for receiving the data in MATLAB. Brain Products provide sample code on their homepage on how to use pnet. In MATLAB, the EEG data were adaptively filtered. The adaptive filtering was directly implemented in MATLAB with the following equations,

$$\text{Subtraction step } eeg(n)_{adaptive} = eeg(n) - weight(n) \cdot ref(n) \tag{1}$$

$$\text{Weight update step } weight(n + 1) = weight(n) + step \cdot eeg(n)_{adaptive} \cdot ref(n) \tag{2}$$

where “n” is the current time sample, “eeg” is the signal of a scalp electrode, “ref” is the signal of the respective reference electrode, “weight” is the respective scaling factor, which we initialized with 1, and “eeg_{adaptive}” is the adaptively filtered EEG. “weight” can change its value over time, whereas “step” defines the speed of change. Finding a suitable value for “step” is a trade-off between speed of adaptation (large value) and preventing over-fitting (small value). Based on our experience, we choose a rather small value for “step” of $8 \times 10e-7$. Our implementation establishes first order models, hence the reference signals are scaled, but no bandwidth limiting filters are learned. The procedure is depicted in Fig. 2d. From here on we term the EEG after this procedure of inside-MRI-scanner recording and online AAS combined with online RLAF as “online AAS + RLAF EEG”.

Analysis and Performance Metrics

After a visual inspection of an EEG example, we analyze two very common EEG phenomena that were already used

as performance criteria for artifact reduction methods in other publications (Chowdhury et al. 2014; Vanderperren et al. 2010). Namely, alpha rhythm amplitude changes and evoked potentials (EPs).

Alpha Rhythm Amplitude Changes

Oscillatory EEG components often show a brain activity related relative difference in their amplitude compared to a baseline. A prominent example is the occipital alpha rhythm. The amplitude at occipital EEG electrodes rises when one closes his/her eyes. The typical frequency range of that rise is 8–13 Hz. To visualize the amplitude changes, we computed spectra for the opened eyes period and the closed eyes period of the experiment respectively (Welch approach, window length 5 s, overlap 50%). We report the average spectra over the occipital channels (P3, Pz, P4, POz, O1, O2) separate for each participant.

To obtain a performance metric that describes the amplitude change of the alpha rhythm, we calculated the ratios of alpha amplitude between closed and opened eyes with the following equation

$$ratio_{\alpha} = \frac{A_{close8-13Hz}}{A_{open8-13Hz}} \tag{3}$$

in which $A_{close8-13Hz}$ is the amplitude during the closed eyes period and $A_{open8-13Hz}$ is the amplitude during the opened

eyes period. We report the average of the alpha amplitude ratio over occipital EEG channels (P3, Pz, P4, POz, O1, O2) separate for each participant.

Artifacts or noise in the EEG can cover the amplitude change. Hence, one expects that clean EEG shows a higher alpha amplitude ratio than artifact afflicted EEG. This is generally the case, however, the ratio metric can be distorted by artifacts that (1) have the same frequency range and (2) change with closed and opened eyes. This may apply to PAs. Their frequency range is overlapping with the alpha rhythm and if the PA detection rate is different between opened eyes and closed eyes, then omitted PA artifacts distort the alpha ratio metric. One can avoid this problem in offline PA reduction with AAS, since it is possible to manually search for omitted PAs and to mark them for PA reduction. However, it becomes a problem in online AAS, where a manual intervention is not possible. Therefore, we analyzed the PA detection rate in the online EEG data, and computed the percentage of detected PAs during opened eyes and closed eyes separately for each participant.

With regard to the alpha amplitude ratio metric, it is important to assess its topological distribution. We show the spatial distribution of the metric in separate topo-plots for each participant.

Visual Evoked Potentials

Evoked potentials are often investigated with respect to their amplitude. We computed the average visual evoked potential (VEPs) of each participant for all different artifact reduction procedures. The depicted channels were selected by the highest outside EEG VEP amplitude of the respective participant.

The VEP signal-to-noise-ratio (SNR) and the similarity of single VEPs to the respective mean VEP are important metrics to quantify VEP quality. We calculated both metrics. The SNR was calculated for each EEG channel separately using

$$VEPSNR_{db} = 20 \cdot \log_{10} \left(\frac{A_{signal}}{A_{noise}} \right) \tag{4}$$

where $VEPSNR_{db}$ is the signal-to-noise-ratio in dB, A_{signal} is the amplitude of the signal, and A_{noise} is the amplitude of the noise. We defined the signal amplitude (A_{signal}) as the peak-to-peak amplitude of the first and the second peak in the average VEP. Average VEPs were calculated by averaging band-limited (1–15 Hz) EEG over the VEP trials of the respective EEG channel. We defined the noise amplitude (A_{noise}) as the root-mean-square (RMS) amplitude of the band-limited (1–15 Hz) plus-minus (\pm) reference of the EEG signal of the respective EEG channel (Schimmel 1967). For the (\pm) reference, odd and even VEPs were averaged separately and subsequently, the average odd VEP was subtracted from the average even VEP. This difference is an estimator of the residual noise in the EEG (Schimmel 1967). The RMS amplitudes of A_{signal} and A_{noise} and therefore the SNR too, are dependent on the bandwidth of the EEG. A smaller bandwidth implies a smaller RMS amplitude and hence a higher SNR, as long as the EP amplitude stays constant. However, the choice of the bandwidth is not crucial as long as it is the same for all calculations, since our intention is to unveil relative differences between the methods. We report the average SNR over occipital EEG channels (POz, O1, O2) separately for each participant.

The root-mean-square (RMS) distance of single VEPs to the average VEP measures the similarity of single VEPs to the respective average VEP. This similarity to the average VEP is equivalent to the variability of single VEPs. The variability has two causes: noise in EEG and the inherent variability of VEPs. One cannot separate these two. However, offline AAS EEG, online AAS EEG and online AAS + RLAF EEG used the same raw EEG data, hence, the

underlying inherent VEP variability was the same. Which means that a variability reduction was caused by the artifact reduction method that either reduces the noise in EEG or the inherent VEP variability, or both. It is important to keep in mind, that comparing the RMS distances of inside MRI scanner recordings with outside EEG is problematic since changes in distance could be caused by differences in the inherent VEP variability. RMS distances were normalized to the amplitude of the respective average VEP, since RMS distances are dependent on the absolute signal amplitudes. The distances were calculated per participant and per EEG channel with

$$RMS\ distance_j = \sqrt{\frac{1}{N} \sum_{n=1}^N (avgVEP(n) - VEP_j(n))^2} \tag{5}$$

$$NRMS\ distance = \frac{avgRMS\ distance}{VEP_{amplitude}} \tag{6}$$

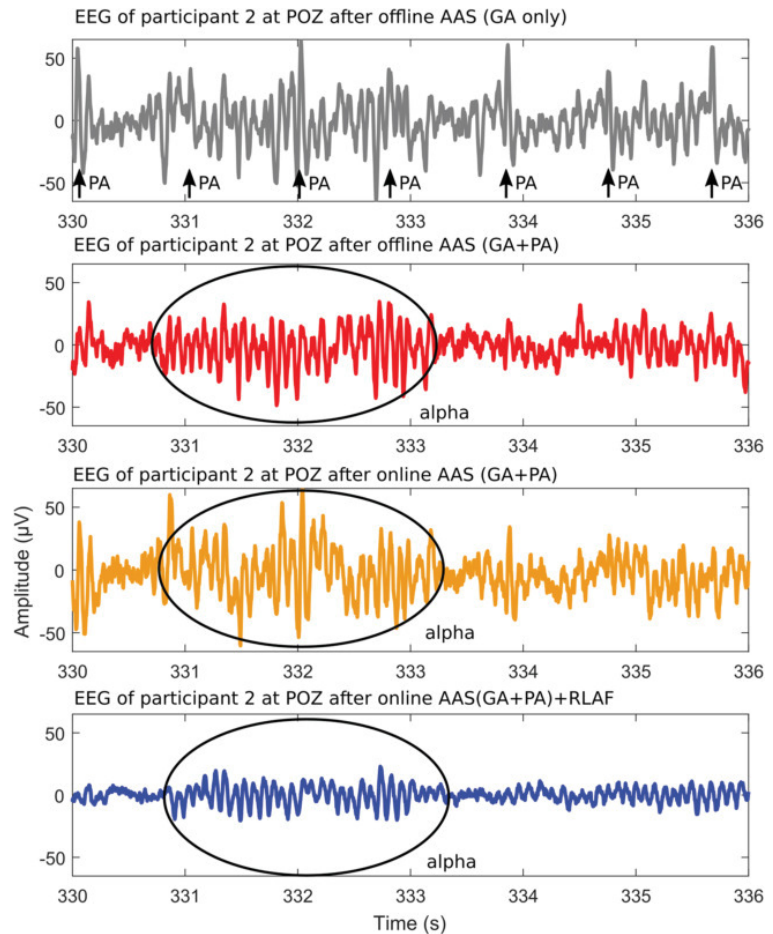
where NRMS distance is the average RMS distance divided by the amplitude of the respective average VEP. The “RMS distance” of the j th VEP to the average VEP was calculated using Eq. (5), where “ n ” is the n th time sample and “ N ” is the total number of time samples of the EEG data epochs. EEG data epochs had a length of half a second. We report the average NRMS distance over occipital EEG channels (POz, O1, O2) separate for each participant.

Results

EEG Example

Figure 3 shows a representative example of what EEG of simultaneous EEG-fMRI looks like after the different artifact reduction procedures. The example was taken from participant 3 at electrode POZ and covers the time from 330 to 336 s after starting the paradigm, hence, from the closed eyes part of the experiment. EEG after offline AAS(GA) is depicted in the upper row. GAs were removed and are no longer visible, but PAs are clearly identifiable. Maximum PA amplitudes are higher than the usual amplitudes of the EEG. The remaining three rows depict EEG after PA reduction procedures. All procedures are effective to some extent. PA residuals are noticeable after online AAS (GA + PA) e.g. PA residual at second 334. PA residuals are less present after offline AAS (GA + PA) and are hardly noticeable after online AAS + RLAF. The EEG example includes a period of increased alpha activity, which is highlighted in Fig. 3. The period is visible after any of the three artifact reduction procedures. EEG amplitudes differ between the artifact reduction procedures. Highest amplitudes are usually

Fig. 3 Six second EEG example of participant 3 at electrode POZ, recorded inside the MRI scanner during the closed eyes part of the experiment, 330 to 336 seconds after the start of the paradigm. Pronounced alpha rhythm activity is highlighted. Upper row: EEG after offline average artifact subtraction (AAS) of the GA. Arrows mark pulse artifacts. Second row: EEG after offline AAS of the GA and the PA. Third row: EEG after online AAS (GA+PA). Bottom row: EEG after online AAS (GA+PA) and subsequent online reference layer adaptive filtering (RLAF)



present in online AAS EEG, and smallest amplitudes in online AAS(GA + PA) + RLAF EEG.

Alpha Rhythm Amplitude Changes

Figure 4 presents spectra in the frequency range of 1–30 Hz, the alpha range of 8–13 Hz is highlighted. In the spectra of outside EEG, a clear alpha peak with closed eyes and a smaller or no alpha peak with opened eyes are the expected results, but the characteristics of the participants' alpha peaks vary.

During closed eyes sessions, the alpha peaks vary in terms of magnitude (e.g. factor of 4 between participants 4 and 6) and latitude (factor of 5 between participants 2 and 4). Nevertheless, the alpha peak, at least a small one, is recognizable for all six participants in the outside EEG during closed eyes sessions. This is not the case for inside the scanner EEG. In offline AAS EEG, distinct alpha peaks are hardly noticeable in participants 5 and 6 and are very

small in participants 1 and 2. Only participants 3 and 4 show clear alpha peaks. In online AAS EEG, participants 2, 3 and 4 all appear to have a distinct alpha peak. The alpha peak is hardly noticeable in EEG of participants 1, 4, and 5. In online AAS + RLAF EEG, it seems that there are distinct alpha peaks in EEG of participants 2, 3, 4, and 5, while the alpha peak is hardly noticeable for participants 1 and 6.

During opened eyes, only participant 5 shows the alpha peak in the outside EEG. Small alpha peaks are noticeable in participants 1, 2, 3, and 6. No alpha peak is noticeable in participant 4. Again the results are different in inside the scanner EEG. In offline AAS EEG, small alpha peaks are noticeable in participants 1, 3, and 5. In the other participants, almost no alpha peak is present. In online AAS EEG, participants 1, 3, and 4 seems to have a distinct alpha peak. In participants 2, 5, and 6, an alpha peak is scarcely noticeable. In online AAS + RLAF EEG, it appears that there are distinct alpha peaks in EEG of participants 2, 3, 4, and 5.

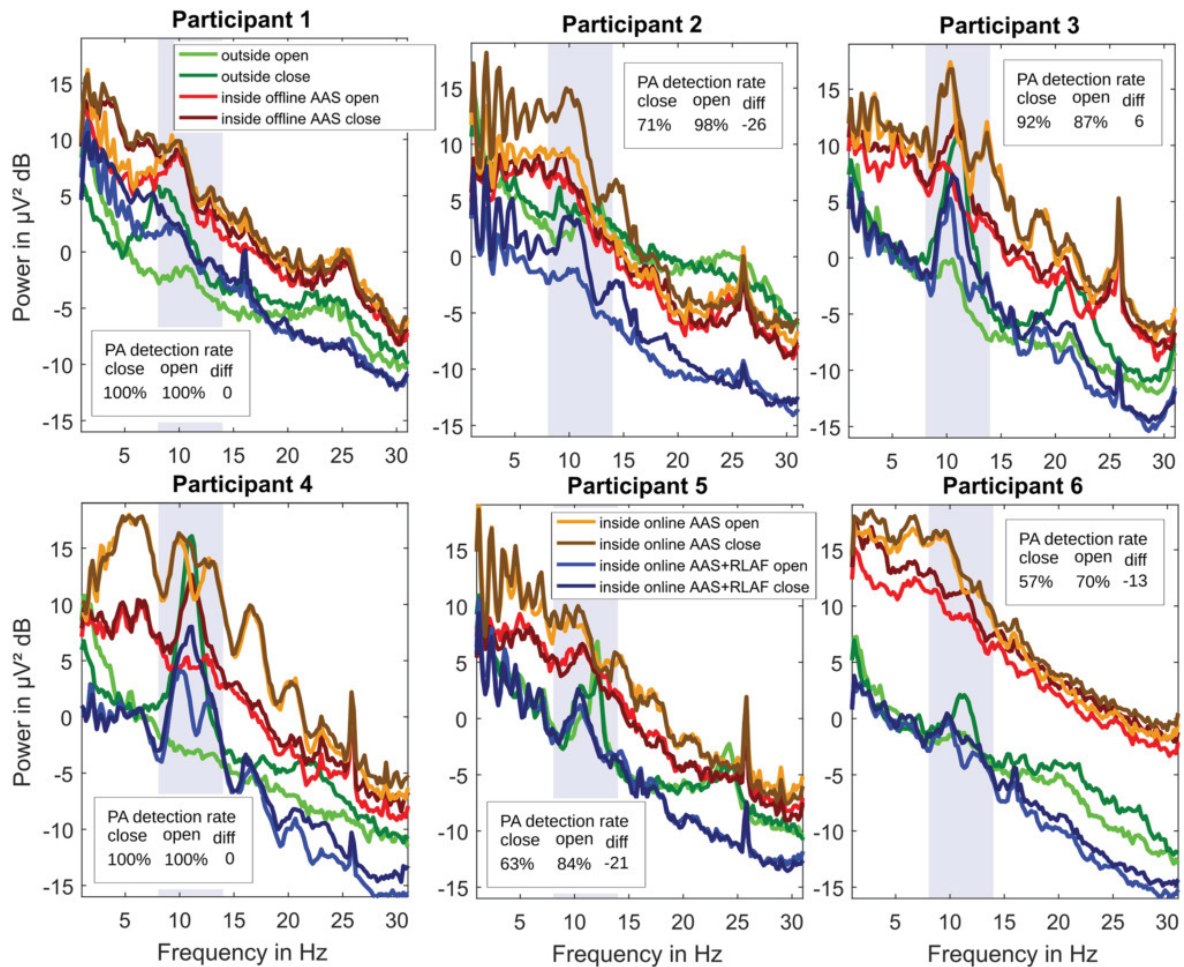


Fig. 4 Per participant individual average spectra of EEG at occipital electrode positions (P3, Pz, P4, POz, O1, O2) for opened eyes and closed eyes after different pre-processing and artifact reduction methods (average artifact subtraction AAS, reference layer adaptive

filtering RLAF). In boxes, pulse artifact (PA) detection rates of online AAS relative to the pulse artifact detection of offline AAS, separately for opened eyes and closed eyes and the respective difference. The 8–13 Hz frequency range is highlighted

Table 1 Average alpha amplitude ratio of closed eyes to opened eyes at occipital EEG channels (P3, Pz, P4, POz, O1, O2)

Alpha ratio (AU)	Outside EEG	Inside offline AAS EEG	Inside online AAS EEG	Inside online AAS+RLAF
Participant 1	1.71	1.06	1.01	1.04
Participant 2	1.12	1.10	1.61	1.50
Participant 3	2.53	1.36	1.06	1.39
Participant 4	3.62	1.57	1.09	1.58
Participant 5	1.04	0.96	1.08	1.02
Participant 6	1.27	1.22	1.08	1.12

EEG was recorded outside the scanner (outside) and inside the MRI scanner simultaneously with fMRI. Different artifact reduction procedures were applied to the inside-MRI-scanner EEG. Average artifact subtraction (AAS) was applied to the EEG after the recording (offline) or online during the recording (online). Reference layer adaptive filtering (RLAF) was applied online as an additional step after online AAS. Higher values are better

Again, in participants 1 and 6 there is almost no alpha peak noticeable.

Alpha rhythm amplitude changes between closed eyes and opened eyes are also different in terms of artifact reduction procedures and participants. Table 1 lists the alpha amplitude ratios for all participants and all artifact reduction procedures. The outside EEG alpha ratios are the highest among methods in participants 1, 3, 4, and 6, second-highest in participant 5 and they are third-highest in participant 2. The offline AAS EEG alpha ratios are second-highest for participants 1 and 6, third-highest for participants 3 and 4, and they are lowest for participants 2 and 5. The online AAS EEG alpha ratios are the highest among methods for participants 2 and 5, and are lowest for participants 1, 3, 4, and 6. Alpha ratios of online AAS+RLAF EEG are second-highest among methods for participants 2, 3, and 4, and they are third-highest for participants 1, 5, and 6.

The online PA detection rate was not stable in all participants. In Fig. 4, the differences in online PA detection rate between opened eyes and closed eyes are noted in extra boxes. Negative differences of -26 , -21 , and -13 percent points were found in participants 2, 5, and 6. A negative difference implies that the PA detection rate was higher during opened eyes and it is likely that the respective alpha ratio is increased by artifacts that are not reduced. It can be assumed that the increase of the alpha ratio is proportional to the difference in percent points. No differences in the PA detection rate was found in participants 1, and 4. A small positive difference was found in participant 3. A positive difference implies that the PA detection rate was higher during closed eyes and hence it is likely that the alpha ratio is decreased by artifacts that are not reduced.

To visualize the topographic distribution of alpha amplitude ratios, we mapped the ratios to 2D electrode positions in Fig. 5. The first column depicts the alpha amplitude ratios of outside EEG for all six participants. As expected the alpha amplitude ratios at occipital electrode positions are commonly larger than those on central or frontal positions. However, differences between participants in ratio sizes and spatial distribution are obvious. Column two shows the alpha ratio topo-plots of offline AAS EEG. The aforementioned pattern is not present in all participants anymore. For example, participant 1 and participant 5 shows only small changes in alpha amplitude between closed and opened eyes and participant 6 shows a pattern where the highest alpha ratios are present in central electrodes. Online AAS EEG alpha ratio topo-plots are presented in column 3. No participant has the expected pattern of higher ratios at occipital electrodes. For example, participants 2, 5 and 6 have their highest alpha ratios at central or frontal electrodes. The topo-plots of the online AAS+RLAF alpha ratios in the last column shows higher occipital alpha ratios in participants that exhibited almost no changes in alpha amplitude in online AAS EEG

(participants 1, 3, 4). In those participants with highest alpha ratios in central or frontal electrodes (participants 2, 5, 6), online AAS+RLAF was able to reduce those ratios. It appears that the topo-plots of online AAS+RLAF are often more similar to the topo-plots of offline AAS EEG than to the topo-plots of online AAS EEG.

Visual Evoked Potentials

Figure 6 shows single participant VEPs for all different pre-processing and artifact reduction procedures. The respective channel was selected because of the highest outside EEG VEP amplitude of the participant. The VEP amplitudes were normalized by the RMS noise amplitudes of the (\pm) reference. VEP amplitudes are highest in outside EEG among all 6 participants. In offline AAS EEG VEP amplitudes are second-highest in participants 1 and 6 and third-highest in participants 3, 4, and 5. In online AAS EEG, VEP amplitudes are third-highest in participant 2. In online AAS+RLAF EEG, VEP amplitude are second-highest in participants 2, 3, 4, and 5, and they are third-highest in participants 1 and 6. In all 6 participants, VEP amplitudes in online AAS+RLAF EEG are higher than in online AAS EEG.

For VEPs, the signal-to-noise-ratio describes the ratio of the VEP amplitude to the respective residual noise amplitude, hence, the distinctness of the VEPs. Table 2 collects the SNRs of all pre-processing and artifact reduction procedures and all participants. All SNRs are positive, indicating that VEP amplitudes are higher than the residual noise. In outside EEG, the VEP SNR is highest for all 6 participants. In offline AAS EEG, the SNR is second-highest in participants 1, 4, 5, and 6 and third-highest in participants 2 and 3. In online AAS EEG, the SNR is lowest for all 6 participants. In online AAS+RLAF EEG, the SNR is second-highest in participants 2, 3, and 5 and third-highest in participants 1, 4, and 6. A pattern is noticeable. Highest SNRs in outside EEG, second-highest SNRs in offline EEG or in online AAS+RLAF EEG with small differences only, and lowest SNRs in online AAS EEG. SNRs in online AAS+RLAF EEG are higher than in online AAS EEG for each participant.

Another performance metric that describes VEP quality is VEP variability. This criterion describes how similar single VEPs are to the respective average VEP. Similarity is measured with the normalized root-mean-square distance of single VEPs to the respective average VEP. Table 3 presents the average VEP distance (NRMS distance) at occipital EEG channels for all pre-processing and artifact reduction procedures and all participants. A smaller value denotes a smaller distance, hence a lower variability or a higher similarity. Offline EEG showed the lowest NRMS distance, hence, VEP variability in all 6 participants. Offline AAS EEG showed the second-lowest variability in participants 1 and 5 and

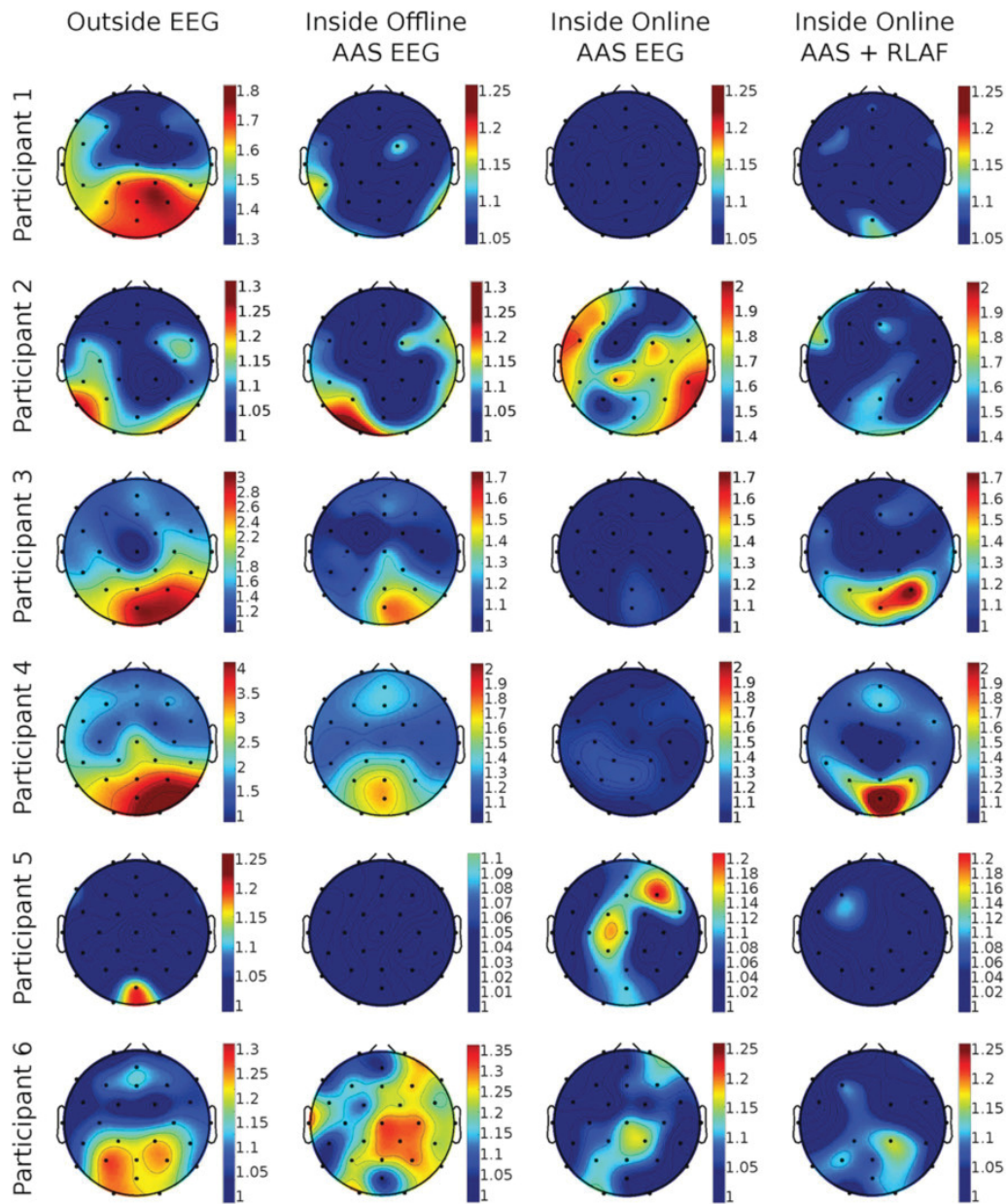


Fig. 5 Per participant topological mapping of the respective alpha amplitude ratios (8–13 Hz) after different pre-processing and artifact reduction methods (average artifact subtraction AAS, reference

layer adaptive filtering RLAf). Alpha ratios were calculated between closed and opened eyes, hence, higher values imply higher changes. Please note the different scalings

the third-lowest in participants 2, 3, 4, and 6. Online AAS EEG showed the highest variability in all single participants. Online AAS + RLAf EEG showed the second-lowest variability in participants 2, 3, 4, and 6, and the third-lowest in participants 1 and 5. The same pattern as with VEP SNR is visible. Lowest variability in outside EEG, second-lowest

variability in offline EEG or in online AAS + RLAf EEG, and highest variability in online AAS EEG. Variability in online AAS + RLAf EEG is lower than in online AAS EEG for each participant.

We exemplify VEP similarity in Fig. 7. The upper row depicts the single VEPs of participant 4 at electrode POZ for

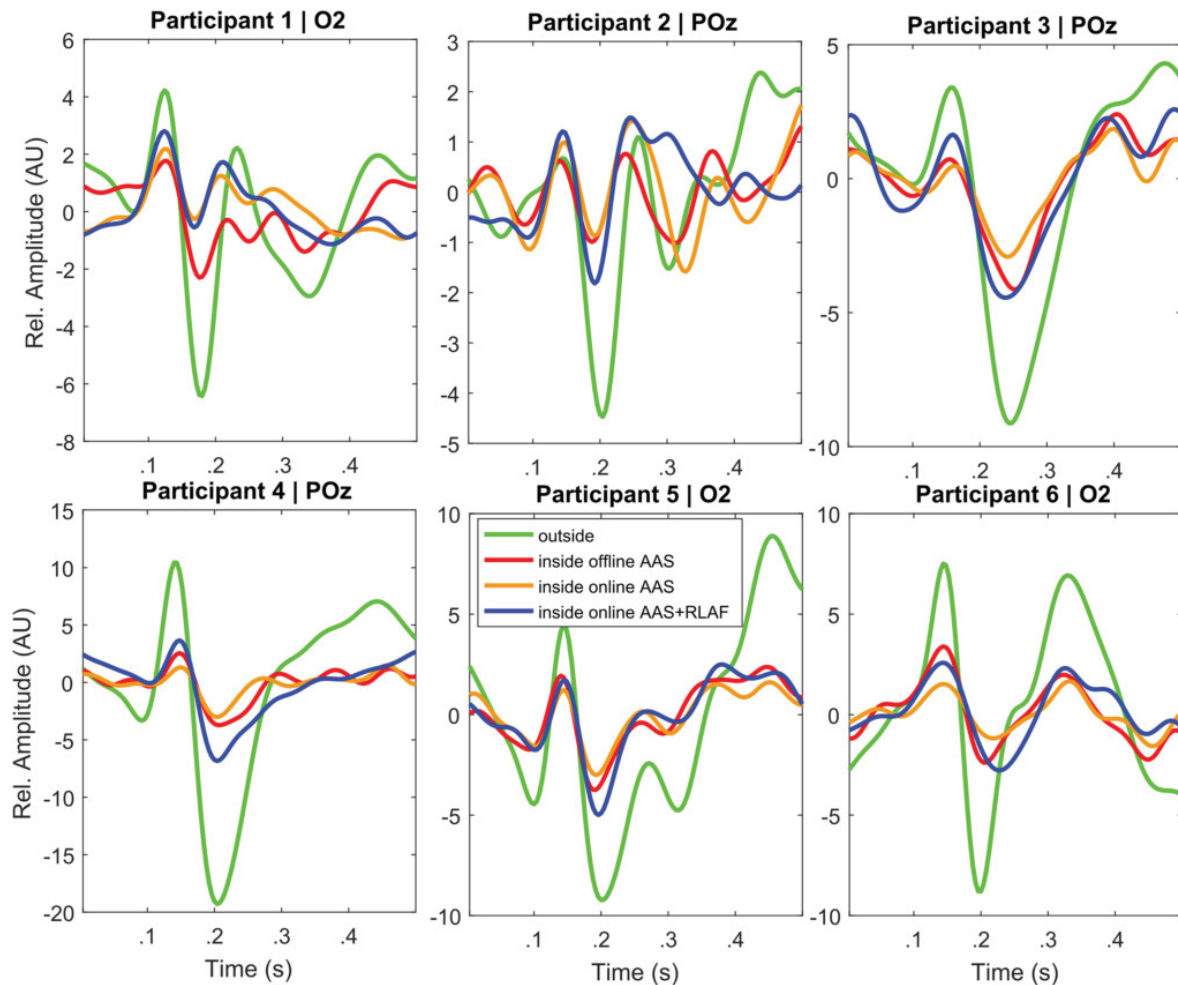


Fig. 6 Single participant VEPs for different EEG recording and pre-processing procedures [average artifact subtraction (AAS), reference layer adaptive filtering (RLAF)]. Channels were selected by the high-

est VEP amplitude of outside EEG. All VEPs were normalized by the RMS amplitudes of the respective (\pm) reference. Please be aware of the different scaling of the y axis

all pre-processing and artifact reduction procedures. In our example, single VEPs are most distinctive in outside EEG, followed by online AAS + RLAF EEG and offline AAS EEG. In online AAS EEG, single VEPs are hardly noticeable. These differences are also present in the average VEPs in the bottom row of Fig. 7. The peak-to-peak amplitude of the normalized average VEP is highest in outside EEG, followed by online AAS + RLAF EEG and offline AAS EEG. It is lowest in online AAS EEG.

Discussion

We start the discussion with a comparison of online AAS artifact reduction with its offline variant, hence a diagnosis

of the state-of-the-art. Subsequently, we discuss improved EEG quality through the additional RLAF step after online AAS in the main part of the discussion. Thereafter, we comment on EEG quality differences between inside and outside the MRI scanner recorded EEG, we share our experience with the new EEG-cap prototype and finally, we discuss limitations of this work.

Current State: Offline AAS Versus Online AAS

Effective artifact reduction in EEG of simultaneous EEG-fMRI is hard to achieve in general. It is even harder to achieve, when the artifact reduction has to be performed online. We have included offline AAS in this work to

Table 2 Average signal-to-noise-ratio (SNR) of visually evoked potentials (VEP) at occipital EEG channels (POZ, O1, O2)

SNR in dB	Outside EEG	Inside offline AAS EEG	Inside online AAS EEG	Inside online AAS +RLAF EEG
Participant 1	20.7	10.2	6.9	8.6
Participant 2	13.7	5.7	3.6	6.6
Participant 3	20.1	15.5	12.4	17.4
Participant 4	24.2	14.7	8.9	14.5
Participant 5	23.1	15.5	12.0	15.5
Participant 6	23.6	11.5	7.3	11.1

EEG was recorded outside the scanner (outside) and inside the MRI scanner simultaneously with fMRI. Different artifact reduction procedures were applied to the inside-MRI-scanner EEG. Average artifact subtraction (AAS) was applied after the recording (offline) or online during the recording (online). Reference layer adaptive filtering (RLAF) was applied online as an additional step after online AAS. Higher values are better

Table 3 Average normalized root-mean-square-distances (NRMSD) of single visual evoked potentials (VEP) to the respective mean VEP at occipital EEG channels (POZ, O1, O2)

NRMSD AU	Outside EEG	Inside offline AAS EEG	Inside online AAS EEG	Inside online AAS +RLAF EEG
Participant 1	1.2	3.1	4.5	3.8
Participant 2	2.8	7.0	9.5	5.3
Participant 3	0.7	2.3	3.1	2.1
Participant 4	0.8	2.0	3.5	1.9
Participant 5	0.9	2.2	3.6	2.4
Participant 6	0.7	6.9	9.6	3.0

EEG was recorded outside the MRI scanner (outside) and inside the MRI scanner simultaneously with fMRI. Different artifact reduction procedures were applied to the inside-MRI-scanner recorded EEG. Average artifact subtraction (AAS) was applied after the recording (offline) or online during the recording (online). Reference layer adaptive filtering (RLAF) was applied online as an additional step after online AAS. Smaller values are better

illustrate the performance differences between offline and online AAS.

In the visual inspection of the EEG example, we found larger artifact residuals in online AAS EEG than in offline

AAS EEG. The artifact at second 334 gives a good impression of the difference. Changes in the alpha range showed two different patterns. (1) Participants that showed a stable PA artifact detection rate in online AAS (participants 1, 3, 4) have larger changes in the alpha range of offline AAS EEG than of online AAS EEG. This visual finding is supported by the alpha amplitude ratios and also depicted in the topoplots, where we find the same pattern. Participant 6 exhibits also larger changes in the alpha range of offline AAS EEG although the PA detection rate between closed and opened eyes was different, however, the topo-plots shows that these are presumably caused by artifacts. (2) Participants with differences in the PA detection rate (participants 2 and 5) show a different pattern. They have smaller changes in the alpha range of offline AAS EEG than of online AAS EEG. These smaller changes do not imply, however, that online AAS performed better than offline AAS in those participants, but mean that omitted PAs had a stronger influence than the change in alpha rhythm. In the context of VEPs, the SNR is higher in offline AAS EEG than in online AAS EEG and the NRMS distance of VEPs is smaller in all participants. That relation is also visible in the VEP similarity example in Fig. 7, where single VEPs are noticeable in offline AAS EEG, but not in online AAS EEG.

Both offline and online AAS, are based on the same idea, namely to create an artifact template through averaging over adjacent artifact epochs and to subtract the template from the EEG to remove the artifact. However, offline and online AAS naturally differ due to the available EEG data in the respective technique. In offline AAS, it is possible to consider future artifact epochs to construct templates. Those future artifact epochs are also useful to detect PA epoch onsets and it is possible to adjust epoch onsets manually. This is not possible in online AAS. We have been observing periods of up to a minute without working PA epoch detection in online AAS EEG of participant 6. Omitted PAs, however, cannot fully explain the performance differences found between offline and online AAS, since the online PA detection worked almost perfectly in participants 1 and 4 and the online AAS performance was still lower than the offline AAS performance. Hence, the difference in artifact template construction must also be responsible.

In summary, a clear pattern is present in our data, namely that online AAS is less effective than offline AAS.

Online AAS EEG Quality Improvement Through Additional Online RLAF

In our last work on EEG artifact reduction in simultaneous EEG-fMRI, we compared reference layer adaptive filtering with (1) its direct predecessor, which is termed reference layer artifact subtraction (RLAS), and with (2) plain AAS

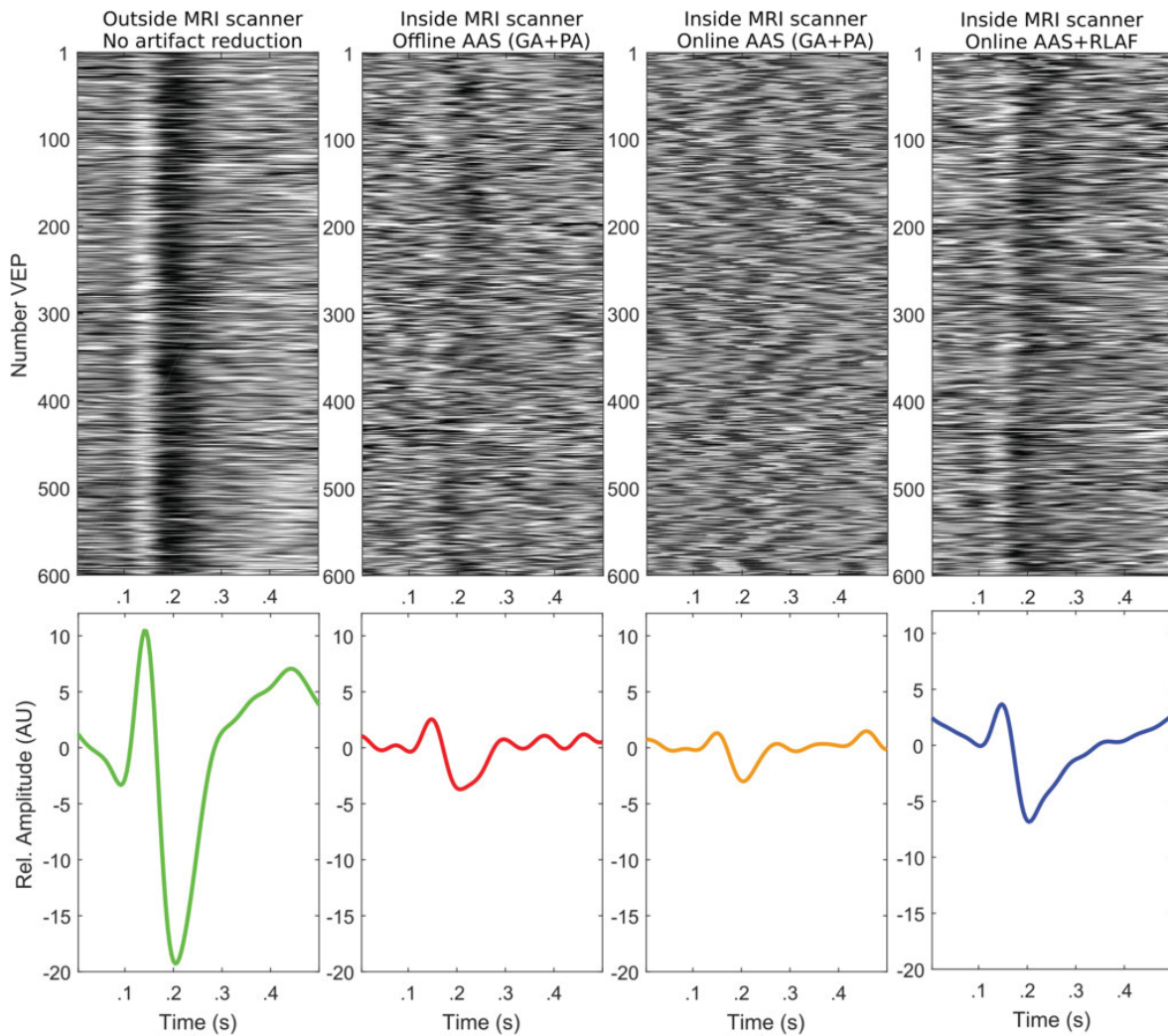


Fig. 7 Representative examples of visually evoked potentials (VEPs) for different pre-processing and artifact reduction procedures (average artifact subtraction AAS, reference layer adaptive filtering RLAF). Examples are from participant 4 at electrode POZ. Upper row: sin-

gle VEPs at electrode POZ (1–15 Hz). Bottom row: average VEPs at electrode POZ scaled to the EEG noise amplitude. Hence, VEP amplitude divided by the root-mean-square value of the (\pm) reference

as the assumed most common artifact reduction technique (Steyrl et al. 2017). Among these techniques, we found that RLAF is the most effective one, if RLAF is applied as an additional signal processing step after AAS. This result concerning the order of technique combination has also been reported by Chowdhury et al. for RLAS (Chowdhury et al. 2014). Due to this experience and due to the need for higher EEG quality in online artifact reduction, we extended RLAF to be applicable online.

The EEG example illustrates the effect of online RLAF on EEG. Three main effects are visible: (1) Generally, smaller amplitudes are an obvious effect of RLAF. Peak-to-peak

amplitudes dropped from approximately ± 50 to ± 0 μ V. This effect comes from the adaptive subtraction and was already reported by Chowdhury et al. in their work about RLAS and in our last work on RLAF (Chowdhury et al. 2014; Steyrl et al. 2017). (2) Residual artifacts are hardly identifiable in online AAS + RLAF EEG, but are visible in online AAS EEG. (3) The period of enhanced alpha activity is present in both online AAS EEG and online AAS + RLAF EEG.

In the spectra, we once again found two patterns of amplitude changes in the alpha range and they are the same as for offline AAS versus online AAS. (1) Participants with a stable PA artifact detection rate in online AAS (participants

1, 3, 4) exhibit larger changes in the alpha range of online AAS + RLAF EEG than of online AAS EEG. Participant 6 again showed the same pattern. (2) Participants with an unstable PA detection rate (participants 2 and 5) again showed the opposite pattern, hence smaller changes in the alpha range of online AAS + RLAF EEG than of online AAS EEG. This visual finding is reflected in the alpha amplitude ratios in Table 1 too. Both the larger and smaller alpha amplitude ratio results, however, imply that RLAF is removing residual artifacts and is improving the EEG quality for those participants. RLAF shows a different behavior because the main cause of the amplitude changes differs in those participants. In participants 1, 3, 4, and 6, the PA detection ratio between closed and opened eyes was stable or relatively stable and the main cause for amplitude changes was thus the alpha rhythm. RLAF was able to sharpen that amplitude change by removing residual artifacts and therefore, alpha amplitude ratios are larger in online AAS + RLAF EEG than in online AAS EEG for those participants. On the other hand, in participants 2 and 5, the PA detection ratio between closed and opened eyes was not stable, and hence omitted PAs were the main cause for amplitude changes. RLAF is reducing these artifacts, and hence the alpha amplitude ratios are smaller in online AAS + RLAF EEG than in online AAS EEG for those participants. These considerations are supported by the offline AAS results. Alpha amplitude ratios of offline AAS EEG are not afflicted by the stability of the PA detection rate, since we manually corrected omitted PAs. The following pattern can be seen: RLAF improves the alpha amplitude ratio towards the alpha ratios of offline AAS for all participants, with improvements from 3 to 45%.

A change in alpha amplitude at occipital EEG channels between closed and opened eyes is expected in the topoplots, hence a larger alpha amplitude ratio at these channels. Such patterns are hardly noticeable, however, in online AAS EEG. Nonetheless, they are visible in offline AAS EEG, which indicates, that changes actually do occur in alpha amplitudes as expected. In online AAS + RLAF EEG on the other hand, alpha amplitude changes are visible and in single participants even more pronounced than in offline AAS EEG. These patterns are often more similar to the patterns of offline AAS EEG than to the patterns of online AAS EEG and as a result these topo-plots give the impression that online RLAF is able to unveil the alpha amplitude changes from online AAS EEG.

We found a straight-forward pattern in the single participants VEPs. The VEP amplitudes are larger for all participants in online AAS + RLAF EEG than in online AAS EEG, whereby the VEP shapes are hardly changed. The shapes are also similar to outside EEG VEP shapes, but with lower amplitudes.

The VEP SNRs of online AAS + RLAF EEG are also higher in all single participants than the VEP SNRs of online

AAS EEG, with SNR gains between 25 and 63%. (V)EP experiments typically require numerous repetitions, since averaging is commonly the method of choice for getting rid of the ongoing EEG and residual artifacts and consequently to make EPs visible. The starting SNR and the number of repetitions define the resulting EP quality, hence the final SNR after averaging. A higher starting SNR makes it possible to reduce the number of repetitions while maintaining a specific (V)EP SNR or it allows for higher (V)EP SNR within the same experiment duration. Both options are greatly welcomed by neuroscientists.

Normalized-root-mean-square-distances of single VEPs are lower in online AAS + RLAF EEG than in online AAS EEG for each single participant, with differences between -16 and -44% . The variability reduction is caused by either noise reduction, including artifact residuals, or reduction of the inherent VEP variability, or both. A reduction of the inherent VEP variability implies a loss in VEP signals and is therefore unwanted. However, since VEP shapes are not altered in online AAS + RLAF and VEP SNRs are simultaneously improved, we argue that the VEP signal loss is only minor and that online RLAF is mainly reducing noise and artifacts.

Single VEPs are hardly noticeable in online AAS EEG of Fig. 7. The variability in this EEG is too high. In contrast, single VEPs are visible in online AAS + RLAF EEG, because of the lower variability. It is noteworthy that the bandwidth was the same for both.

Several possible causes are apparent as to why RLAF improves EEG quality over online AAS EEG. (1) RLAF is able to reduce PAs that were omitted by the online PA detection, and hence, were not reduced in AAS. (2) Residual PAs are present after AAS and they mask the EEG. For example, participant 4 had an exceptionally high alpha power ratio, as unveiled with offline AAS. However, this high ratio is not visible in online AAS EEG and for this participant in particular, we observed significant PA residuals over the whole experiment duration, although the PA detection rate was about 100%. RLAF reduced the PA residuals and unveiled the alpha power changes. (3) RLAF reduces other artifacts or residuals of other artifacts too, as long as they are represented in the reference layer of the cap. None of these possible causes alone can explain all of the EEG quality improvements. Hence, we assume that a combination of them is responsible for the observed quality improvement.

Occasionally, online AAS + RLAF can even compete with offline AAS. e.g. in participants 1, 3, and 4, alpha amplitude ratios in online AAS + RLAF EEG are on eye level with ratios in offline AAS EEG. In participants 2, 3, 4, 5, and 6, the VEP SNRs in online AAS + RLAF EEG are on eye level with SNRs in offline AAS EEG. Online AAS + RLAF can keep up with offline AAS even at 3T MRI scanners, also

when comparing the example of raw EEG, the alpha power ratio mapping, and the VEP variability.

A practical advantage of the RLAF technique is its low demand on computing power. The complete system consists of (1) the BrainProducts software that takes on the recording and the online AAS, (2) a Matlab script that handles the paradigm control and the adaptive filtering and (3) the communication required between these components. The system was running on a laptop with an Intel Core i7 mobile CPU at 2.4 GHz and 8 GB RAM. Windowing or storing of old data is not required in the online RLAF part, adaptive filtering steps are computed sample-by-sample. Hence, the additional RLAF step only adds a delay of one sample for processing and the delay of the network communication to the artifact reduction process of the BrainProducts system. However, a block processing scheme is also entirely feasible, that would be able to speed up the computation at higher sampling rates.

In summary, our performance metrics document that online RLAF is able to effectively reduce residual MRI related artifacts in online AAS.

EEG of simultaneous EEG-fMRI compared to EEG from outside the MRI

We did not yet comment on the general EEG quality loss of simultaneous EEG-fMRI compared to EEG that was recorded outside the MRI scanner. Such comparisons have been made already, particularly in the papers of Allen et al. in which they invented the AAS technique (Allen et al. 1998, 2000). However, such a comparison was still missing for the reference layer cap prototype and in addition we are not aware of a comparison between outside EEG and online AAS EEG.

Our performance metrics show that in any terms of comparison, the inside MRI scanner EEG quality never reaches that of outside EEG. The differences are substantial. For example, alpha amplitude ratios are higher in outside EEG than in any EEG of simultaneous EEG-fMRI if the alpha amplitude changes were not caused by artifacts. Other examples are SNRs of VEPs and NRMS distances of VEPs, where we see the same: Simultaneous EEG-fMRI recording comes at the cost of EEG quality. Nevertheless, simultaneous EEG-fMRI enables us to address new research questions about the human brain, which cannot be answered without this combination of techniques. Hence, this gap in EEG quality demonstrated how important new techniques are that improve the quality of inside MRI scanner recorded EEG, such as the one we present here in this work with the RLAF technique.

Reference Layer Cap Prototype

The old reference layer cap prototype, that was used in our last work on RLAF, became unusable after several applications (Steyrl et al. 2017). The electrode contact areas were made of copper and coated with silver. Unfortunately the abrasive electrode gel removed the silver coating and the underlying copper was revealed. The copper formed a half cell potential with the remaining silver, leading to a high offset voltage that caused permanent saturation at the amplifier. The new reference layer cap prototype overcomes this major drawback by using Ag/AgCl sinter pellets as electrode contact areas. The pellets are about 1 mm thick and as a result can resist the abrasive gel much longer. We did not notice a degradation of the pellets after 20+ (test) measurements. We assume that the durability of the electrodes of the new prototype cap will be similar to standard EEG electrodes. The advantages of the old cap prototype are valid for the new cap too. It is compatible with available EEG amplifier systems, which allows the upgrading for existing systems, its preparation and handling times are similar to standard EEG caps, no additional susceptibility artifacts are noticeable in fMRI recordings, and EEG of reasonable quality became visible after AAS.

Limitations

It is not possible to compare our results statistically, due to the limited number of participants. Hence, all comparisons imply a numerical difference only. Nevertheless, as described above, our results show very similar patterns in the performance metrics among all participants: (1) online AAS + RLAF superior to online AAS and (2) occasionally at eye level with offline AAS. (3) outside MRI scanner recordings superior to all inside scanner techniques. These patterns were stable among participants, with only two exceptions. The alpha amplitude ratios of participant 2 and 5 were highest in online AAS EEG, and lowest in offline AAS EEG. We assume that the reason for this deviation from the pattern is the unstable detection of PA epoch onsets. The onset detection failed more often during the eyes closed part of the experiment. This was visible in the spectrum as a higher power in lower frequency ranges, including the alpha range. We thus attribute the deviation of participants 2 and 5 to the higher number of PAs that are not reduced in the eyes closed part of the experiment. This behavior of the alpha amplitude ratios demonstrates one weakness of this metric, it is depending on a constant performance of the artifact reduction over the whole experiment duration.

Regarding our choice of the number of epochs for averaging in AAS, it is important to note that another number

possibly leads to better results of AAS. We did not optimize that number via e.g. a pre-study.

The online artifact reduction procedure is not of course instantaneous. The maximum delay of online AAS can be assumed to be 150 ms and RLAF adds a marginally delay only. Nevertheless, the overall delay needs to be determined accurately in a future work, since this delay is crucial for experiment design.

Another limitation of this work concerns the inside/outside MRI EEG comparison. It must be noted that although the experiment was the same inside and outside the MRI scanner and the cap stayed in place between the two experiments, the recordings are not necessarily comparable, since the environment parameters changed. For example, the distance to the screen was different inside and outside the scanner, participants were in sitting position outside and in lying position inside and outside it was quiet but inside it was loud. Hence, natural changes of the EEG over time cannot be ruled out as a source of differences, since the order of inside and outside EEG measurements was not randomized.

Conclusion

EEG quality is generally impaired when simultaneously acquired with fMRI. This impairment is even more pronounced, when artifact reduction techniques have to be performed online. Our results document this behavior for AAS, namely that online AAS is less effective than offline AAS. We extended the technique RLAF from offline to online use in order to improve online artifact reduction. We showed that online AAS + RLAF achieves higher numerical performance in all metrics when compared to online AAS. Further, we demonstrated that online AAS + RLAF is occasionally even comparable with the offline AAS artifact reduction technique at 3T MRI scanners. Based on these results, we believe online RLAF to be an add on technique after AAS, which has the potential to become a very important tool in the field of simultaneous EEG-fMRI and that will allow us to carry out simultaneous EEG-fMRI experiments at a new level of EEG quality.

Acknowledgements Open access funding provided by Graz University of Technology. This work was partly supported by the ERC Consolidator Grant 681231 ‘Feel Your Reach’.

Open Access This article is distributed under the terms of the Creative Commons Attribution 4.0 International License (<http://creativecommons.org/licenses/by/4.0/>), which permits unrestricted use, distribution, and reproduction in any medium, provided you give appropriate credit to the original author(s) and the source, provide a link to the Creative Commons license, and indicate if changes were made.

References

- Abbott DF, Masterton RAJ, Archer JS, Fleming SW, Warren AEL, Jackson GD (2014) Constructing carbon fiber motion-detection loops for simultaneous EEG–fMRI. *Front Neurol* 5:260. <https://doi.org/10.3389/fneur.2014.00260>
- Abolghasemi V, Ferdowsi S (2015) EEG–fMRI: dictionary learning for removal of ballistocardiogram artifact from EEG. *Biomed Signal Process Control* 18:186–194. <https://doi.org/10.1016/j.bspc.2015.01.001>
- Abreu R, Leite M, Jorge J, Grouiller F, van der Zwaag W, Leal A, Figueiredo P (2016) Ballistocardiogram artefact correction taking into account physiological signal preservation in simultaneous EEG–fMRI. *NeuroImage*. <https://doi.org/10.1016/j.neuroimage.2016.03.034>
- Acharjee PP, Phlypo R, Wu L, Calhoun VD, Adali T (2015) Independent vector analysis for gradient artifact removal in concurrent EEG–fMRI data. *IEEE Trans Biomed Eng* 62(7):1750–1758. <https://doi.org/10.1109/TBME.2015.2403298>
- Allen PJ, Polizzi G, Krakow K, Fish DR, Lemieux L (1998) Identification of EEG events in the MR scanner: the problem of pulse artifact and a method for its subtraction. *Neuroimage* 8(3):229–239. <https://doi.org/10.1006/nimg.1998.0361>
- Allen PJ, Josephs O, Turner R (2000) A method for removing imaging artifact from continuous EEG recorded during functional MRI. *Neuroimage* 12(2):230–239. <https://doi.org/10.1006/nimg.2000.0599>
- Asseondi S, Lavallee C, Ferrari P, Jovicich J (2016) Length matters: improved high field EEG–fMRI recordings using shorter EEG cables. *J Neurosci Methods* 269:74–87. <https://doi.org/10.1016/j.jneumeth.2016.05.014>
- Becker R, Reinacher M, Freyer F, Villringer A, Ritter P (2011) How ongoing neuronal oscillations account for evoked fMRI variability. *J Neurosci* 31(30):11016–11027. <https://doi.org/10.1523/JNEUROSCI.0210-11.2011>
- Bonmassar G, Purdon PL, Jääskeläinen IP, Chiappa K, Solo V, Brown EN, Belliveau JW (2002) Motion and ballistocardiogram artifact removal for interleaved recording of EEG and EPs during MRI. *NeuroImage*, 16:1127–1141. <https://doi.org/10.1006/nimg.2002.1125>
- Bonmassar G, Hadjikhani N, Ives JR, Hinton D, Belliveau JW (2010) Influence of EEG electrodes on the BOLD fMRI signal. *Hum Brain Mapp* 14:108–115. <https://doi.org/10.1002/hbm.1045>
- Briselli E, Garreffa G, Bianchi L, Bianciardi M, Macaluso E, Abbafati M, Marciani MG, Maraviglia B (2006) An independent component analysis-based approach on ballistocardiogram artifact removing. *Magn Reson Imaging* 24(4):393–400. <https://doi.org/10.1016/j.mri.2006.01.008>
- Brookes MJ, Mullinger KJ, Stevenson CM, Morris PG, Bowtell R (2008) Simultaneous EEG source localisation and artifact rejection during concurrent fMRI by means of spatial filtering. *NeuroImage*. 40(3):1090–1104. <https://doi.org/10.1016/j.neuroimage.2007.12.030>
- Brunner C, Birbaumer N, Blankertz B, Guger C, Kübler K, Mattia D, del Millán JR, Miralles F, Nijholt A, Opisso E, Ramsey N, Salomon P, Müller-Putz GR (2015) BNCI horizon 2020: towards a roadmap for the BCI community. *Brain Comput Interfaces* 2(1):1–10. <https://doi.org/10.1080/2326263X.2015.1008956>
- Chowdhury ME, Mullinger KJ, Glover P, Bowtell R (2014) Reference layer artefact subtraction (RLAS): a novel method of minimizing EEG artefacts during simultaneous fMRI. *Neuroimage* 84:307–319. <https://doi.org/10.1016/j.neuroimage.2013.08.039>
- Debener S, Ullsperger M, Siegel M, Engel AK (2006) Single-trial EEG–fMRI reveals the dynamics of cognitive function. *Trends Cogn Sci* 10(12):558–563. <https://doi.org/10.1016/j.tics.2006.09.010>

- Debener S, Strobel A, Sorger B, Peters J, Kranczioch C, Engel AK (2007) Improved quality of auditory event-related potentials recorded simultaneously with 3-T fMRI: removal of the ballistocardiogram artefact. *Neuroimage* 34:587–597. <https://doi.org/10.1016/j.neuroimage.2006.09.031>
- Debener S, Mullinger KJ, Niazy RK, Bowtell RW (2008) Properties of the ballistocardiogram artefact as revealed by EEG recordings at 1.5, 3 and 7 T static magnetic field strength. *Int J Psychophysiol* 67(3):189–199. <https://doi.org/10.1016/j.ijpsycho.2007.05.015>
- Dunseath WJR, Alden TA (2009) Electrode Cap for Obtaining Electrophysiological Measurement Signals from Head of Subject, has Measurement Signal Electrodes Extended through Electrically Conductive Layer and Insulating Layer for Contacting Head of Subject (USA, US 2009/0099473)
- Ferdowski S, Sanej S, Abolghasemi V, Nottage J, O'Daly O (2013) Removing ballistocardiogram artifact from EEG using short- and long-term linear predictor. *IEEE Trans Biomed Eng* 60(7):1900–1911. <https://doi.org/10.1109/TBME.2013.2244888>
- Gotman J, Kobayashi E, Bagshaw AP, Bénar CG, Dubeau F (2006) Combining EEG and fMRI: a multimodal tool for epilepsy research. *J Magn Reson Imaging* 23(6):906–920. <https://doi.org/10.1002/jmri.20577>
- He B, Yang L, Wilke C, Yuan H (2011) Electrophysiological imaging of brain activity and connectivity—challenges and opportunities. *IEEE Trans Biomed Eng* 58(7):1918–1931. <https://doi.org/10.1109/TBME.2011.2139210>
- Huster RJ, Debener S, Eichele T, Herrmann CS (2012) Methods for simultaneous EEG-fMRI: an introductory review. *J Neurosci* 32(18):6053–6060. <https://doi.org/10.1523/JNEUROSCI.0447-12.2012>
- Jorge J, Grouiller F, Gruetter R, van der Zwaag W, Figueiredo P (2015a). Towards high-quality simultaneous EEG-fMRI at 7 T: detection and reduction of EEG artifacts due to head motion. *NeuroImage* 120:143–153. <https://doi.org/10.1016/j.neuroimage.2015.07.020>
- Jorge J, Grouiller F, Ipek Ö., Stoermer R, Michel CM, Figueiredo P, van der Zwaag W, Gruetter R (2015b) Simultaneous EEG-fMRI at ultra-high field: artifact prevention and safety assessment. *NeuroImage* 105:132–144. <https://doi.org/10.1016/j.neuroimage.2014.10.055>
- Kim H, Yoo S, Lee J (2015) Recursive approach of EEG-segment-based principal component analysis substantially reduces cryogenic pump artifacts in simultaneous EEG-fMRI data. *Neuroimage* 104:437–451. <https://doi.org/10.1016/j.neuroimage.2014.09.049>
- Laufs H (2012) A personalized history of EEG-fMRI integration. *NeuroImage* 62:1056–1067. <https://doi.org/10.1016/j.neuroimage.2012.01.039>
- Liu Z, de Zwart JA, Van Gelderen P, Kuo LW, Duyn JH (2012) Statistical feature extraction for artifact removal from concurrent fMRI-EEG recordings. *NeuroImage* 59(3):2073–2087. <https://doi.org/10.1016/j.neuroimage.2011.10.042>
- Luo Q, Glover GH (2012) Influence of dense-array EEG cap on fMRI signal. *Magn Reson Med* 68:807–815. <https://doi.org/10.1002/mrm.23299>
- Mano M, Lécuyer A, Bannier E, Perronnet L, Noorzadeh S, Barillot C (2017) How to build a hybrid neurofeedback platform combining EEG and fMRI. *Front Neurosci*. <https://doi.org/10.3389/fnins.2017.00140>
- Mantini D, Perrucci MG, Cugini S, Ferretti A, Romani GL, Del Gratta C (2007) Complete artifact removal for EEG recorded during continuous fMRI using independent component analysis. *Neuroimage* 34(2):598–607. <https://doi.org/10.1016/j.neuroimage.2006.09.037>
- Masterton RA, Abbott DF, Fleming SW, Jackson GD (2007) Measurement and reduction of motion and ballistocardiogram artefacts from simultaneous EEG and fMRI recordings. *Neuroimage* 37:202–211. <https://doi.org/10.1016/j.neuroimage.2007.02.060>
- Mayeli A, Zotev V, Refai H, Bodurka J (2016) Real-time EEG artifact correction during fMRI using ICA. *J Neurosci Methods* 274:27–37. <https://doi.org/10.1016/j.jneumeth.2016.09.012>
- McGlone F, Dunseath R, Stern J (2009) Simultaneous EEG and functional MRI employing novel noise reduction. *Epilepsia* 50(Suppl. 11):82–82. <https://doi.org/10.1111/j.1528-1167.2009.02377.x>
- Michel CM, Murray MM (2012) Towards the utilization of EEG as a brain imaging tool. *NeuroImage* 61:371–385. <https://doi.org/10.1016/j.neuroimage.2011.12.039>
- Mulert C, Lemieux L (2010) EEG-fMRI physiological basics, technique, and applications. Springer, Heidelberg, ISBN:978-3-540-87918-3. <https://doi.org/10.1007/978-3-540-87919-0>
- Mullinger KJ, Bowtell R (2011) Combining EEG and fMRI. In Mado M, Bulte JWM (eds), *Magnetic resonance neuroimaging, methods in molecular biology*, vol 711, Springer Science + Business Media, Germany, pp 303–326. https://doi.org/10.1007/978-1-61737-992-5_15
- Mullinger KJ, Yan WX, Bowtell R (2011) Reducing the gradient artefact in simultaneous EEG-fMRI by adjusting the subject's axial position. *Neuroimage* 54(3):1942–1950. <https://doi.org/10.1016/j.neuroimage.2010.09.079>
- Mullinger KJ, Castellone P, Richard Bowtell R (2013a) Best current practice for obtaining high quality EEG data during simultaneous fMRI. *J Vis Exp* 76:50283. <https://doi.org/10.3791/50283>
- Mullinger KJ, Havenhand J, Bowtell R (2013b) Identifying the sources of the pulse artefact in EEG recordings made inside an MR scanner. *Neuroimage* 7:75–83. <https://doi.org/10.1016/j.neuroimage.2012.12.070>
- Niazy RK, Beckmann CF, Iannetti GD, Brady JM, Smith SM (2005) Removal of FMRI environment artifacts from EEG data using optimal basis sets. *Neuroimage* 28(3):720–737. <https://doi.org/10.1016/j.neuroimage.2005.06.067>
- Niedermeyer E, Lopes da Silva FH (2005) *Electroencephalography: basic principles, clinical applications, and related fields*, 5th edn. Lippincott Williams & Wilkins, Philadelphia, ISBN-13: 978-0781789424\$4
- Nierhaus T, Gundlach C, Goltz D, Thiel SD, Pleger B, Villringer A (2013) Internal ventilation system of MR scanners induces specific EEG artifact during simultaneous EEG-fMRI. *Neuroimage* 74:70–76. <https://doi.org/10.1016/j.neuroimage.2013.02.016>
- Norris DG (2006) Principles of magnetic resonance assessment of brain function. *J Magn Reson Imaging* 23:794–807. <https://doi.org/10.1002/jmri.20587>
- Ogawa S, Lee TM, Kay AR, Tank DW (1990) Brain magnetic resonance imaging with contrast dependent on blood oxygenation. *Proc Natl Acad Sci USA* 87:9868–9872
- Perronnet L, Lécuyer A, Mano M, Bannier E, Lotte F, Clerc M, Barillot C (2017) Unimodal versus bimodal EEG-fMRI neurofeedback of a motor imagery task. *Front Hum Neurosci*. <https://doi.org/10.3389/fnhum.2017.00193>
- Ritter P, Villringer A (2006) Simultaneous EEG-fMRI. *Neurosci Biobehav Rev* 30(6):823–838. <https://doi.org/10.1016/j.neubiorev.2006.06.008>
- Ritter P, Becker R, Graefe C, Villringer A (2007) Evaluating gradient artifact correction of EEG data acquired simultaneously with fMRI. *Magn Reson Imaging* 25(6):923–932. <https://doi.org/10.1016/j.mri.2007.03.005>
- Rothlübbers S, Relvas V, Leal A, Murta T, Lemieux L, Figueiredo P (2014) Characterisation and reduction of the EEG artefact caused by the helium cooling pump in the MR environment: validation in epilepsy patient data. *Brain Topogr* 28(2):208–220. <https://doi.org/10.1007/s10548-014-0408-0>

- Schimmel H (1967) The (+/-) reference: accuracy of estimated mean components in average response studies. *Science* 157:92–94. <https://doi.org/10.1126/science.157.3784.92>
- Srivastava G, Crottaz-Herbette S, Lau KM, Glover GH, Menon V (2005) ICA-based procedures for removing ballistocardiogram artifacts from EEG data acquired in the MRI scanner. *NeuroImage* 24(1):50–60. <https://doi.org/10.1016/j.neuroimage.2004.09.041>
- Steyrl D, Wriessnegger SC, Müller-Putz GR (2013) Single trial Motor Imagery classification in EEG measured during fMRI image acquisition—a first glance. *Biomed Eng/Biomedizinische Technik*. <https://doi.org/10.1515/bmt-2013-4450>
- Steyrl D, Patz F, Krausz G, Edlinger G, Müller-Putz GR (2015) Reduction of EEG artifacts in simultaneous EEG-fMRI: reference layer adaptive filtering (RLAF). In: proceedings of the 37th Annual International Conference of the IEEE Engineering in Medicine and Biology Society, EMBC15, Milano, Italy, August 25–29, pp. 3803–3806. <https://doi.org/10.1109/EMBC.2015.7319222>
- Steyrl D, Krausz G, Koschutnig K, Edlinger G, Müller-Putz GR (2017) Reference layer adaptive filtering (RLAF) for EEG artifact reduction in simultaneous EEG-fMRI. *J Neural Eng* 14(2):1–20. <https://doi.org/10.1088/1741-2552/14/2/026003>
- Uludag K, Roebroek A (2014) General overview on the merits of multimodal neuroimaging data fusion. *Neuroimage* 102:3–10. <https://doi.org/10.1016/j.neuroimage.2014.05.018>
- Van der Meer JN, Tijssen MAJ, Bour LJ, Van Rootselaar AF, Nederveen AJ (2010) Robust EMG-fMRI artifact reduction for motion (FARM). *Clin Neurophysiol* 121(5):766–776. <https://doi.org/10.1016/j.clinph.2009.12.035>
- Vanderperren K, De Vos M, Ramautar JR, Novitskiy N, Mennes M, Assecondi S, Vanrumste B, Stiers P, Van den Bergh BRH, Wagemans J, Lagae L, Sunaert S, Van Huffel S (2010) Removal of BCG artifacts from EEG recordings inside the MR scanner: a comparison of methodological and validation-related aspects. *NeuroImage*. 50(3):920–934. <https://doi.org/10.1016/j.neuroimage.2010.01.010>
- Wen X, Kang M, Yao L, Zhao X (2016) Real-time ballistocardiographic artifact reduction using the k-teager energy operator detector and multi-channel referenced adaptive noise cancelling. *Int J Imaging Syst Technol* 26:209–215. <https://doi.org/10.1002/ima.22178>
- Wu X, Wu T, Zhan Z, Yao L, Wen X (2016). A real-time method to reduce ballistocardiogram artifacts from EEG during fMRI based on optimal basis sets (OBS). *Comput Methods Progr Biomed*. <https://doi.org/10.1016/j.cmpb.2016.01.018>
- Zich C, Debener S, De Vos M, Kranczioch C, Gutberlet I (2014) Real-time artifact correction enables EEG-based feedback inside the fMRI scanner. In: proceedings of the 6th International Brain-Computer Interface Conference 2014, Verlag der Technischen Universität Graz. <https://doi.org/10.3217/978-3-85125-378-8-25>
- Zich C, Debener S, Kranczioch C, Bleichner MG, Gutberlet I, De Vos M (2015) Real-time EEG feedback during simultaneous EEG-fMRI identifies the cortical signature of motor imagery. *NeuroImage* 114:438–447. <https://doi.org/10.1016/j.neuroimage.2015.04.020>
- Zotov V, Phillips R, Yuan H, Misaki M, Bodurka J (2014) Self-regulation of human brain activity using simultaneous real-time fMRI and EEG neurofeedback. *NeuroImage* 85:985–995. <https://doi.org/10.1016/j.neuroimage.2013.04.126>

SINGLE TRIAL MOTOR IMAGERY CLASSIFICATION IN EEG MEASURED DURING fMRI IMAGE ACQUISITION - A FIRST GLANCE

Steyrl D¹, Wriessnegger S C¹, Müller-Putz G R¹,

¹Institute for Knowledge Discovery, BCI Lab, Graz University of Technology, Austria

david.steyrl@tugraz.at

Abstract: *Non-invasive electroencephalogram (EEG) based Brain-Computer Interfaces (BCIs), which rely on event related desynchronization (ERD), are often affected by large fluctuations of their accuracy. We want to overcome this drawback by using simultaneous EEG and functional magnetic imaging (fMRI). The question we are addressing in this work is if ERD is still classifiable in EEG on a single trial basis after the removal of fMRI related artefacts. In a first single participant recording we found the classical ERD distribution and were able to compute a leave-one-out-cross-validation (LOOCV) accuracy of 78%, which is significantly higher than chance level.*

Keywords: *Brain-Computer Interface (BCI), EEG, fMRI, Motor Imagery (MI), classification*

Introduction

The simultaneous measure of the electroencephalogram (EEG) and functional magnetic resonance imaging (fMRI), is on the edge to make the breakthrough and to become a broader used neuroscience tool. EEG-fMRI offers the unique opportunity to measure two different brain activity related signals simultaneously. First, the electrical activity and second, the oxygen consumption of the brain. Although the relationship between these two brain signals is not clear yet, the bimodal view allows new insights into the brain functionality [1].

Brain-Computer Interfaces (BCIs) are devices which provide control signals out of brain activity signals. One common brain signal used for EEG based non-invasive BCIs, is the event related desynchronization (ERD) of sensory motor rhythms (SMR). This desynchronization can be induced by the imagery of limb movements, called motor imagery (MI) [2]. Unfortunately this kind of BCIs are often unreliable. Reasons for that can be found in the data; noise and outliers, high dimensionality, time information, non-stationarity, poor signal-to-noise ratio (SNR) and small training-sets for the machine learning algorithms.

We want to study the processes of MI by measuring EEG and fMRI simultaneously for future improvements of existing BCI systems. This work addresses the question if MI induced ERD is classifiable on a single trial basis in EEG measured with fMRI simultaneously.

Methods

Participant: The participant (male, 23 years old), a known good MI performer, was lying in the fMRI scanner and was

looking at a screen via a mirror. He got instruction for MI by a paradigm similar to the classical Graz-BCI [3].

Exp. paradigm: At the start of each trial a white cross appeared. At second 3, a white arrow was added, indicating the kind of MI and removed after 1.25 s. Right hand and feet MIs were used in a randomized order. In this work we reported only the right hand imagery data. The participant was asked to perform sustained MI until the white cross disappeared (at second 10). Following there was a break (black screen) with a random length between 6 s and 8 s. We measured 5 runs with 10 right hand MI trials each, but we had to reject the last 2 runs due to movement artefacts. Finally, we got 30 trials of right hand MI for further analysis.

Data acquisition: We used a "BrainCap-MR" electrode system by EasyCap (EASYCAP GmbH, Herrsching, Germany), which consists of 66 MRI compatible Ag/AgCl pin electrodes with safety resistors. One ground, one reference, one electrocardiogram (ECG) and 63 EEG electrodes. The EEG electrodes were rectangularly arranged with distances of 2.5 cm. The rectangular grid was centred on the 10-20 system positions C3, Cz and C4. The electrodes and the cables were fixed on the cap to prevent looping, which would be a safety risk because of eddy currents and therefore, heating. We recorded the EEG with a "BrainAmp MR" amplifier system, an fMRI compatible shielded EEG amplifier by BrainProducts (Brain Products GmbH, Gilching, Munich, Germany). The amplifiers and the batteries were positioned directly in the MRI scanner, in the near of the subject's head. Recording settings: Low pass filter at 1000 Hz, high pass filter at 0.1 Hz, sampling rate 5 kHz. The EEG recording was performed in a Siemens Skyra 3T (Siemens AG, Munich, Germany), during a fMRI echo planar imaging (EPI) sequence with a TR of 3000 ms. We used a head coil for sending and receiving. For this work we did not report the fMRI data.

Data analysis: The simultaneous EEG-fMRI measurement is highly contaminated by two types of fMRI related artefacts. First, the gradient artefact due to gradient switching during the image acquisition and second, the cardiac related artefact, due to micro movements and blood speed changes in the high static magnetic field during a cardiac cycle [1]. For both artefact types, we used the template subtraction approach invented by Allen et al. [4] [5] and as implemented in the BrainVision Analyzer2 (Brain Products GmbH, Gilching, Munich, Germany) software.

The event related desynchronization/synchronization (ERDS) time-frequency maps were computed according to [6].

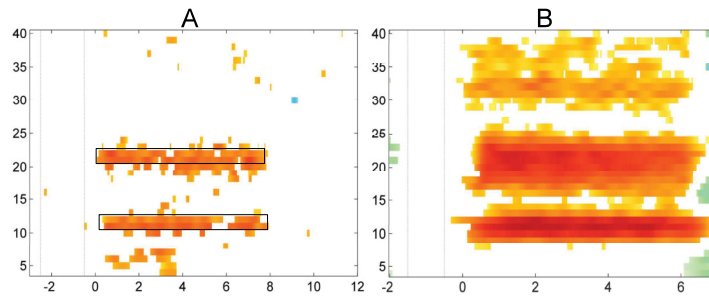


Figure 1: ERDS maps (BP). A/B: Lap C3, Trials: 30/90, classes: 1, fs: 250/512 Hz, time: [-3, 0, 12]/[-2, 0.05, 7] s, ref: [-2.5, -0.5]/[-1.5, -0.5] s, f borders: [4, 40] Hz, f bandwidths: 2 Hz, f steps: 1 Hz, Bootstrap significance test ($\alpha = 0.01$)

We used two time segments of each trial's laplacian derivation at C3 for classification. One time segment (start $t = 1$ s, length 1 s) was during reference period and is called the rest condition. The other segment (start $t = 4.5$ s, length 1 s) was during the MI period and is called the MI condition. We calculated the absolute values of the segment's Fourier transformations and used two bands of the values as features for a linear discriminant analysis (LDA). First band (11-12 Hz) was in the mu band and second band (21-22 Hz) was in the beta band. To estimate a single trial classification accuracy, we used a leave-one-out-cross-validation (LOOCV).

Results

Fig. 1 shows significant ERDS maps of the same participant with frequency bands from 4-40 Hz for position C3. Fig. 1 A was calculated with the data recorded simultaneously with fMRI (30 trials). The resulting signal patterns are highlighted. Fig. 1 B was calculated using data measured outside the scanner (90 trials).

The results of the single trial classification showed that 78,33% of the samples were correctly classified in the LOOCV. Two rest condition samples and 11 MI condition samples were wrong classified. The chance level was 64,54% according to [7].

Discussion

The observed ERD patterns (Fig. 1 A), one in the mu band (11-12 Hz) and one in the beta band (21-22 Hz), are similar to the patterns found in the measurement outside the fMRI scanner (Fig. 1 B) and are in line with other work [8]. Due to more trials the bands are more pronounced in Fig. 1 B. Our findings suggest, that the fMRI artefact correction algorithms can restore the underlying EEG and preserves the ERD phenomena, which is a requirement for a successful single trial MI classification. With these two pattern as features for an LDA, we computed an LOOCV accuracy of 78% which is significantly better than chance level (65%). In summary, ERD phenomena can be classified on single trial basis although when the raw EEG is contaminated with fMRI related artefacts.

Acknowledgement

This work was performed within the BioTechMed initiative.

Bibliography

- [1] C. Mulert and L. Lemieux, *EEG-fMRI Physiological Basis, Technique, and Applications*. Springer, Berlin, 2010.
- [2] G. Pfurtscheller and C. Neuper, "Motor imagery and direct brain-computer communication," *Proceeding IEEE*, vol. 89 no. 5, p. 1123–1134, 2001.
- [3] G. Pfurtscheller, G. R. Müller-Putz, A. Schlögl, B. Graimann, R. Scherer, R. Leeb, C. Brunner, C. Keinrath, F. Lee, G. Townsend, C. Vidaurre, and C. Neuper, "15 years of bci research at graz university of technology: current projects," *IEEE Transactions on Neural Systems and Rehabilitation Engineering*, vol. 14, pp. 205–210, 2006.
- [4] P. J. Allen, G. Polizzi, K. Krakow, D. R. Fish, and L. Lemieux, "Identification of eeg events in the mr scanner: The problem of pulse artifact and a method for its subtraction," *NeuroImage*, vol. 8, p. 229–239, 1998.
- [5] P. J. Allen, O. Josephs, and R. Turner, "A method for removing imaging artifact from continuous eeg recorded during functional mri," *NeuroImage*, vol. 12, p. 230–239, 2000.
- [6] B. Graimann, J. Huggins, S. Levine, and G. Pfurtscheller, "Visualization of significant erd/ers patterns in multichannel eeg and ecog data," *Clinical Neurophysiology*, vol. 113, p. 43–47, 2002.
- [7] G. R. Müller-Putz, R. Scherer, C. Brunner, R. Leeb, and G. Pfurtscheller, "Better than random? a closer look on bci results," *International Journal of Bioelectromagnetism*, vol. 10, pp. 52–55, 2008.
- [8] V. Kaiser, A. Kreilinger, G. R. Müller-Putz, and C. Neuper, "First steps toward a motor imagery based stroke bci: New strategy to set up a classifier," *Frontiers in Neuroscience*, vol. 5, p. 86, 2011.

David Steyrl | Curriculum Vitae

Hammer-Purgstall-Gasse 7/12
1020 Vienna, Austria
phone: +43 650 4011115
email: david.steyrl@gmail.com

Google Scholar: <https://scholar.google.at/citations?user=wtkskIUAAAAJ>
Researchgate: https://researchgate.net/profile/David_Steyrl
ORCID: <https://orcid.org/0000-0002-3215-8115>
Publons: <https://publons.com/a/1332486/>



Education

Since 2012 **PhD Student, Computer Sciences, Graz University of Technology**

Thesis title: *“Improving the quality of the electroencephalogram simultaneously recorded with functional magnetic resonance imaging”*

Adviser: Univ.-Prof. Dipl.-Ing. Dr.techn. Gernot R. Müller-Putz

Reviewer: Prof. Dr. Klaus-Robert Müller, TU Berlin

2005-2012 **Dipl.-Ing. (MSc), Biomedical Engineering, Graz University of Technology** (w. honors)

Thesis title: *“On the suitability of random forests for detecting mental imagery for non-invasive brain-computer interfacing”*

Adviser: Assoc.-Prof. Dipl.-Ing. Dr.techn. Reinhold Scherer

1998-2003¹ **Higher Engineering School, Automation Engineering, Neufelden** (w. honors)

(German: Höhere Technische Bundeslehranstalt Neufelden)

Graduation project: *“Development of a fully automatic assembly unit”*

Professional Experience

Since 2018 **Tieto Austria GmbH**, Data Scientist

I am the technical leader in a project on sensor fusion to reconstruct the tracks of vehicles on the street.

2012-2018 **Graz University of Technology**, Teaching and Research Assistant, Project Assistant

I was member of the Institute of Neural Engineering, until 2015 known as Institute for Knowledge Discovery, and of its affiliated Laboratory of Brain-Computer Interfaces at Graz University of Technology. My teaching duties included lectures, exercises, seminars and thesis (co-)supervision at Bachelor and Master level. My research focused on adaptive (bio-) signal processing and machine learning, with application to simultaneous EEG-fMRI and EEG based Brain-Computer Interfaces. I worked with disabled and healthy study participants and in the course of this work, I performed about 100 measurement sessions. I presented scientific findings at numerous international conferences and published in high ranked scientific engineering journals. I co-organized the 6th and 7th Graz Brain-Computer Interfaces Conference and I am one of the founders of the Graz BCI Racing Team, a student team that participated at the worldwide first Cybathlon. The Cybathlon is a competition for handicapped people supported by the latest assistance systems, organized by the ETH Zurich.

2005 **Global Hydro Energy GmbH**, Mechanical drafter

My tasks included the design and engineering of hydro power plants, the preparation of blueprints, and the monitoring of the construction progress.

¹ Followed by obligatory military service

Involvement in International Research Projects

2012 **EU project “BrainAble”** (Autonomy and social inclusion through mixed reality brain-computer interfaces: Connecting the disabled to their physical and social world; FP7-STREP-247447, 2010-2012), Project Assistant

Teaching

Lectures

2017 **Neuroprosthetics**, Lecture, WS2017/18

(German: Neuroprothesen)

Institute of Neural Engineering, Graz University of Technology

Taught selected chapters, 25 graduate students per semester, in English

2014-2016 **Interdisciplinary Team-Taught Lecture Series: Trends in Neurorehabilitation**, Lecture, SS2014-SS2016

(German: Interuniversitäre Ringvorlesung: Trends in der Neurorehabilitation)

Institute of Neural Engineering, Graz University of Technology

Assisted in course management and exams, 20 graduate students per semester, in German

2013-2015 **Foundations of Computer Science**, Lecture, WS2013/14-WS2015/16

(German: Grundlagen der Informatik)

Institute of Neural Engineering, Graz University of Technology

Taught selected chapters, assisted in exams, 290 undergraduate students per semester, in German

2012-2016 **Rehabilitation Engineering**, Lecture, WS2012/13-WS2016/17

(German: Rehabilitationstechnik)

Institute of Neural Engineering, Graz University of Technology

Taught selected chapters, assisted in exams, 50 graduate students per semester, in English since 2015

Seminars

2013-2017 **Neuroimaging with EEG, fNIRS and fMRI**, Seminar, WS2013/14-WS2017/18

(until 2015 referred to as Neuroimaging with fMRI and NIRS)

Institute of Neural Engineering, Graz University of Technology

Partly responsible for organization, taught selected chapters, up to 25 graduate students per semester, in English

Laboratory and Construction Exercises

2017-2018 **Biomedical Sensor Systems**, Laboratory exercise, SS2017-SS2018

Institute of Health Care Engineering, Graz University of Technology

Partly responsible for organization, taught selected exercises, 30 graduate students per semester, in German

2016-2017 **Non-Invasive Brain-Computer Interfaces 2**, Construction exercise, WS2016/17-WS2017/18

Institute of Neural Engineering, Graz University of Technology

Fully responsible, 15 graduate students per semester, in English

2013-2017 **Non-Invasive Brain-Computer Interfaces**, Construction exercise, SS2013-SS2017

Institute of Neural Engineering, Graz University of Technology

Fully responsible, 20 graduate students per semester, in English

2013-2017 **Fundamentals of Biomedical Engineering**, Laboratory exercise, SS2013-WS2017/18
(German: Grundlagen der Biomedizinischen Technik)
Institute of Medical Engineering, Graz University of Technology
Partly responsible for organization, taught selected exercises, assisted in exams, 100 undergraduate students per semester, in German

2013-2016 **Neurophysiology**, Laboratory exercise, SS2013-SS2016
(German: Neurophysiologie)
Institute of Neural Engineering, Graz University of Technology
Fully responsible, up to 45 graduate students per semester, in German

Thesis and Project Supervision

2017-2018 **Bachelor Thesis (Co-) Supervision**
Thesis title: “*Redesign of the functional electric stimulation laboratory exercise*”
Institute of Neural Engineering, Graz University of Technology

2016-2018 **Master’s Thesis (Co-) Supervision**
Thesis title: “*Optimization of filter bank parameters in combination with common spatial patterns and multiclass hierarchical brain computer interface for rest class detection*”
Institute of Neural Engineering, Graz University of Technology

2016-2017 **Master’s Thesis (Co-) Supervision**
Thesis title: “*Data Transfer Methods for Calibration Time Reduction in Sensorymotor Rhythm based Brain-Computer Interface*”
Institute of Neural Engineering, Graz University of Technology

2014 **Project in Medical Informatics and Neuroinformatics (Co-) Supervision**
(German: Seminar/Projekt Medizinische Informatik und Neuroinformatik)
Project topic: “*Common spatial patterns filtering combined with a random forests classifier*”
Institute of Neural Engineering, Graz University of Technology

Publications

Journal Publications First Author

- 2018 **Steyrl D**, Müller-Putz GR (2018) Simultaneous EEG-fMRI: Average artifact subtraction adds noise to the EEG due to residual artifacts in the subtraction template. *Journal of Neural Engineering*. In revision
- 2018 **Steyrl D**, Krausz G, Koschutnig K, Edlinger G, Müller-Putz GR (2018) Online reduction of artifacts in EEG of simultaneous EEG-fMRI using reference layer adaptive filtering (RLAF). *Brain Topography* 31(1):129-149. <https://doi.org/10.1007/s10548-017-0606-7>
- 2017 **Steyrl D**, Krausz G, Koschutnig K, Edlinger G, Müller-Putz GR (2017) Reference layer adaptive filtering (RLAF) for EEG artifact reduction in simultaneous EEG-fMRI. *Journal of Neural Engineering* 14(2):026003. <https://doi.org/10.1088/1741-2552/14/2/026003>
- 2016 **Steyrl D**, Kobler RJ, Müller-Putz GR (2016) On similarities and differences of invasive and non-invasive electrical brain signals in brain-computer interfacing. *Journal of Biomedical Science and Engineering* 9(8):393-398. <https://doi.org/10.4236/jbise.2016.98034>
- 2016 **Steyrl D**, Scherer R, Faller J, Müller-Putz GR (2016) Random forests in non-invasive sensorimotor rhythm brain-computer interfaces: A practical and convenient non-linear classifier. *Biomedical Engineering / Biomedizinische Technik* 61(1):77-86. <https://doi.org/10.1515/bmt-2014-0117>

Journal Publications Co-Author

- 2018 Schulz L, Ischebeck A, Wriessnegger SC, **Steyrl D**, Müller-Putz GR (2018) Action affordances and visuo-spatial complexity in motor imagery: an fMRI study. *Brain and Cognition* 124:37-46. <https://doi.org/10.1016/j.bandc.2018.03.012>
- 2017 Statthaler K, Schwarz A, **Steyrl D**, Kobler RJ, Höller MK, Brandstetter J, Hehenberger L, Bigga M, Müller-Putz GR (2017) Cyathlon experiences of the Graz BCI racing team Mirage91 in the brain-computer interface discipline. *Journal of NeuroEngineering and Rehabilitation* 14(129):1-16. <https://doi.org/10.1186/s12984-017-0344-9>
- 2016 Wriessnegger SC, **Steyrl D**, Koschutnig K, Müller-Putz GR (2016) Cooperation in Mind: Motor imagery of joint and single actions is represented in different brain areas. *Brain and Cognition* 106:19-25. <https://doi.org/10.1016/j.bandc.2016.08.008>
- 2014 Wriessnegger SC, **Steyrl D**, Koschutnig K, Müller-Putz GR (2014) Short time sports exercise boosts motor imagery patterns: implications of mental practice in rehabilitation programs. *Frontiers in Human Neuroscience* 8(469). <https://doi.org/10.3389/fnhum.2014.00469>

Conference Publications First Author – Peer Reviewed

- 2016 **Steyrl D**, Schwarz A, Müller-Putz GR (2016) The MIRAGE91 Brain-Computer Interface. In: Gassert R, Lamercy O (Eds.), *Cyathlon Symposium Booklet*, ETH, SWISS Arena, Zurich/Kloten, Switzerland, October 6, p.77.
- 2015 **Steyrl D**, Patz F, Krausz G, Edlinger G, Müller-Putz GR (2015) Reduction of EEG Artifacts in Simultaneous EEG-fMRI: Reference Layer Adaptive Filtering (RLAF). In: *Proceedings of the 37th Annual International Conference of the IEEE Engineering in Medicine and Biology Society, EMBC15*, Milano, Italy, August 25-29, pp.3803-3806. <https://doi.org/10.1109/EMBC.2015.7319222>
- 2014 **Steyrl D**, Scherer R, Förstner O, Müller-Putz GR (2014) Motor Imagery Brain-Computer Interfaces: Random Forests vs Regularized LDA – Non-linear Beats Linear. In: Müller-Putz GR, Bauernfeind G, Brunner C, Steyrl D, Wriessnegger SC, Scherer R (Eds.), *Proceedings of the 6th International Brain-Computer Interface Conference 2014*, Graz, Austria, September 16-19, pp.241-244. <https://doi.org/10.3217/978-3-85125-378-8-61>
- 2013 **Steyrl D**, Wriessnegger SC, Müller-Putz GR (2013) Single trial Motor Imagery classification in EEG measured during fMRI image acquisition – a first glance. *Biomedical Engineering / Biomedizinische Technik* 58(Suppl.1):1-2. <https://doi.org/10.1515/bmt-2013-4450>
- 2013 **Steyrl D**, Scherer R, Müller-Putz GR (2013) Random Forests for Feature Selection in Non-invasive Brain-Computer Interfacing. In: Holzinger A, Pasi G (Eds.), *Lecture Notes in Computer Science vol.7947, Human-Computer Interaction and Knowledge Discovery in Complex, Unstructured, Big Data, Third International Workshop HCI-KDD 2013, Held at SouthCHI 2013*, Maribor, Slovenia, July 1-3, pp.207-216. https://doi.org/10.1007/978-3-642-39146-0_19
- 2013 **Steyrl D**, Scherer R, Müller-Putz GR (2013) Using random forests for classifying motor imagery EEG. In: Millán NL, Guechoul N, Leeb R, Millán JdR (Eds.), *Proceedings of TOBI Workshop IV*, EPFL, Sion, Switzerland, January 23-25, pp.89-90.

Conference Publications Co-Author – Peer Reviewed

- 2016 Schwarz A, **Steyrl D**, Müller-Putz GR (2016) Brain-Computer Interface adaptation for an end user to compete in the Cyathlon. In: *Proceedings of the 2016 IEEE International Conference on Systems, Man, and Cybernetics*, SMC2016, Hotel Intercontinental, Budapest, Hungary, October 9-12, pp.1803-1808. <https://doi.org/10.1109/SMC.2016.7844499>

- 2016 Schwarz A, **Steyrl D**, Höller MK, Statthaler K, Müller-Putz GR (2016) BCI adaption for end user – The GRAZ-BCI approach. In: Gassert R, Lamercy O (Eds.), *Cyathlon Symposium Booklet*, ETH, SWISS Arena, Zurich/Kloten, Switzerland, October 6, p.74.
- 2016 Statthaler K, **Steyrl D**, Schwarz A, Höller MK, Müller-Putz GR (2016) Optimized individual mental tasks to control BCIs. In: Gassert R, Lamercy O (Eds.), *Cyathlon Symposium Booklet*, ETH, SWISS Arena, Zurich/Kloten, Switzerland, October 6, p.23.
- 2016 Höller MK, Schwarz A, **Steyrl D**, Statthaler K, Müller-Putz GR (2016) First contact screening of a BCI Pilot. In: Gassert R, Lamercy O (Eds.), *Cyathlon Symposium Booklet*, ETH, SWISS Arena, Zurich/Kloten, Switzerland, October 6, p.72.
- 2016 Müller-Putz GR, Schwarz A, **Steyrl D** (2016) Mirage91: The Graz BCI-Racing Team – making students familiar with BCI research. In: Müller-Putz GR, Huggins JE, Steyrl D (Eds.), *Proceedings of the 6th International Brain-Computer Interface Meeting*, Asilomar Conference Center, Pacific Grove, California, USA, May 30-June 3, p.63. <https://doi.org/10.3217/978-3-85125-467-9-63>
- 2015 Schwarz A, Scherer R, **Steyrl D**, Faller J, Müller-Putz GR (2015) A Co-adaptive Sensory Motor Rhythms Brain-Computer Interface Based on Common Spatial Patterns and Random Forest. In: *Proceedings of the 37th Annual International Conference of the IEEE Engineering in Medicine and Biology Society*, EMBC15, Milano, Italy, August 25-29, pp.1049-1052. <https://doi.org/10.1109/EMBC.2015.7318545>
- 2015 Scherer R, Faller J, Opisso E, Costa U, **Steyrl D**, Müller-Putz GR (2015) Bring mental activity into action! An enhanced online co-adaptive brain-computer interface training protocol. In: *Proceedings of the 37th Annual International Conference of the IEEE Engineering in Medicine and Biology Society*, EMBC15, Milano, Italy, August 25-29, pp.2323-2326. <https://doi.org/10.1109/EMBC.2015.7318858>
- 2014 Bauernfeind G, Pokorny C, **Steyrl D**, Wriessnegger SC, Pichler G, Schippinger W, Noirhomme Q, Real RG, Kübler A, Mattia D, Müller-Putz GR (2014) Improved Classification of Auditory Evoked Event-Related Potentials. In: Müller-Putz GR, Bauernfeind G, Brunner C, Steyrl D, Wriessnegger SC, Scherer R (Eds.), *Proceedings of the 6th International Brain-Computer Interface Conference 2014*, Graz, Austria, September 16-19, pp.245-248. <https://doi.org/10.3217/978-3-85125-378-8-62>
- 2014 Müller-Putz GR, **Steyrl D**, Faller J (2014) Adaptive hybrid Brain-Computer Interaction: Ask a Trainer for Assistance!. In: *Proceedings of the 36th Annual International Conference of the IEEE Engineering in Medicine and Biology Society*, EMBC14, Chicago, Illinois, USA, August 26-30, pp.1493-1496. <https://doi.org/10.1109/EMBC.2014.6943884>
- 2014 Bauernfeind G, **Steyrl D**, Brunner C, Müller-Putz GR (2014) Single Trial Classification of fNIRS-based Brain-Computer Interface Mental Arithmetic Data: A Comparison Between Different Classifiers. In: *Proceedings of the 36th Annual International Conference of the IEEE Engineering in Medicine and Biology Society*, EMBC14, Chicago, Illinois, USA, August 26-30, pp.2004-2007. <https://doi.org/10.1109/EMBC.2014.6944008>

Editor of Conference Proceedings

- 2017 Müller-Putz GR, **Steyrl D**, Wriessnegger SC, Scherer R (Eds.) (2017) Proceedings of the 7th Graz Brain-Computer Interfaces Conference 2017 From Vision to Reality. *7th Graz Brain-Computer Interface Conference 2017*, Graz, Austria, September 18-22, ISSN: 2311-0422, ISBN: 978-3-85125-533-1. <https://doi.org/10.3217/978-3-85125-533-1>
- 2016 Müller-Putz GR, Huggins JE, **Steyrl D** (Eds.) (2016) Proceedings of the 6th International Brain-Computer Interface Meeting: BCI Past, Present, and Future. *6th International Brain-Computer Interface Meeting*, Asilomar Conference Center, Pacific Grove, California, USA, May 30-June 3, ISBN: 978-3-85125-467-9. <https://doi.org/10.3217/978-3-85125-467-9>

- 2014 Müller-Putz GR, Bauernfeind G, Brunner C, **Steyrl D**, Wriessnegger SC, Scherer R (Eds.) (2014) Proceedings of the 6th International Brain-Computer Interface Conference 2014 The Future of Brain-Computer Interaction: Basics, Shortcomings, Users. *6th International Brain-Computer Interface Conference*, Graz, Austria, September 16-19, ISSN: 2311-0422, ISBN: 978-3-85125-378-8. <https://doi.org/10.3217/978-3-85125-378-8>

Acknowledged in Publications

- 2017 Pereira J, Ofner P, Schwarz A, Sburlea AI, Müller-Putz GR (2017) EEG neural correlates of goal-directed movement intention. *NeuroImage* 149:129-140. <https://doi.org/10.1016/j.neuroimage.2017.01.030>
- 2015 Brunner C, Birbaumer N, Blankertz B, Guger C, Kübler A, Mattia D, Millán JdR, Miralles F, Nijholt A, Opisso E, Ramsey N, Salomon P, Müller-Putz GR (2015) BNCI Horizon 2020: towards a roadmap for the BCI community. *Brain-Computer Interfaces* 2(1):1-10. <https://doi.org/10.1080/2326263X.2015.1008956>
- 2015 Scherer R, Faller J, Friedrich EVC, Opisso E, Costa U, Kübler A, Müller-Putz GR, Individually Adapted Imagery Improves Brain-Computer Interface Performance in End-Users with Disability. *PLoS ONE* 10(5):1-14. <https://doi.org/10.1371/journal.pone.0123727>

Presentations

Talks / Speaker

- 2017 **Steyrl D** (2017) Brain-Computer Interface: New Perspectives (“Cybathlon”). At: *1st Special Interest Day Electrotherapy*, Vienna, Austria, June 24. (German: Brain-Computer Interface: Neue Perspektiven (“Cybathlon”), am 1. Fachtag Elektrotherapie)
- 2015 **Steyrl D** (2015) Reduction of EEG Artifacts in Simultaneous EEG-fMRI: Reference Layer Adaptive Filtering (RLAF). At: *37th International Conference of the IEEE Engineering in Medicine and Biology Society*, EMBC15, Milano, Italy, August 25-29.
- 2014 **Steyrl D** (2014) Motor Imagery Brain-Computer Interfaces: Random Forests vs Regularized LDA – Non-linear Beats Linear. At: *6th International Brain-Computer Interface Conference 2014*, Graz, Austria, September 16-19.
- 2014 **Steyrl D** (2014) Single Trial Classification of fNIRS-based Brain-Computer Interface Mental Arithmetic Data: A Comparison Between Different Classifiers. At: *36th International Conference of the IEEE Engineering in Medicine and Biology Society*, EMBC14, Chicago, Illinois, USA, August 26-30.

Poster Presentations

- 2017 **Steyrl D**, Müller-Putz GR (2017) Reference layer adaptive filtering (RLAF) in simultaneous EEG-fMRI. At: *3rd Alpine Chapter Symposium of the OHBM*, Inselspital Bern, Switzerland, November 3-4.
- 2017 **Steyrl D**, Müller-Putz GR (2017) Reference layer adaptive filtering (RLAF) in simultaneous EEG-fMRI. At: *2nd TU Graz Fields of Expertise Day Human & Biotechnology*, Graz, Austria, October 18.
- 2016 **Steyrl D**, Schwarz A, Müller-Putz GR (2016) The MIRAGE91 Brain-Computer Interface. At: *Cybathlon Symposium*, SWISS Arena, Zurich/Kloten, Switzerland, October 6.
- 2014 **Steyrl D**, Wriessnegger SC, Müller-Putz GR (2014) Single trial Motor Imagery classification in EEG measured during fMRI image acquisition – a first glance. At: *Austrian Computer Science Day 2014*, Graz, Austria, June 6.

- 2013 **Steyrl D**, Wriessnegger SC, Müller-Putz GR (2013) Single trial Motor Imagery classification in EEG measured during fMRI image acquisition – a first glance. At: *Three Countries Meeting of the German, Swiss and Austrian Society for Biomedical Engineering*, BMT2013, (German: BMT (Biomedizinische Technik) 2013 – Dreiländertagung der Deutschen, Schweizerischen und Österreichischen Gesellschaft für Biomedizinische Technik), Graz, Austria, September 19-21.
- 2013 **Steyrl D**, Scherer R, Müller-Putz GR (2013) Using random forests for classifying motor imagery EEG. At: *TOBI Workshop IV, Practical Brain-Computer Interfaces for End-Users: Progress and Challenges*, Sion, Switzerland, January 23-25.

Posters Co-Author

- 2016 Schwarz A, **Steyrl D**, Höller MK, Statthaler K, Müller-Putz GR (2016) BCI adaption for end user – The GRAZ-BCI approach. At: *Cyathlon Symposium*, SWISS Arena, Zurich/Kloten, Switzerland, October 6.
- 2016 Höller MK, Schwarz A, **Steyrl D**, Statthaler K, Müller-Putz GR (2016) First contact screening of a BCI Pilot. At: *Cyathlon Symposium*, SWISS Arena, Zurich/Kloten, Switzerland, October 6.
- 2016 Wriessnegger SC, **Steyrl D**, Müller-Putz GR (2016) Improving the vividness of motor imagery tasks for future application in Brain-Computer Interfaces. At: *10th FENS Forum of Neuroscience*, Copenhagen, Denmark, July 2-6.
- 2016 Müller-Putz GR, Schwarz A, **Steyrl D** (2016) Mirage91: The Graz BCI-Racing Team – making students familiar with BCI research. At: *6th International Brain-Computer Interface Meeting: BCI Past, Present, and Future*, Asilomar Conference Center, Pacific Grove, California, USA, May 30-June 3.
- 2015 Schwarz A, Scherer R, **Steyrl D**, Faller J, Müller-Putz GR (2015) A Co-adaptive Sensory Motor Rhythms Brain-Computer Interface Based on Common Spatial Patterns and Random Forest. At: *37th International Conference of the IEEE Engineering in Medicine and Biology Society*, EMBC15, Milano, Italy, August 25-29.
- 2014 Bauernfeind G, Pokorny C, **Steyrl D**, Wriessnegger SC, Pichler G, Schippinger W, Noirhomme Q, Real RG, Kübler A, Mattia D, Müller-Putz GR (2014) Improved Classification of Auditory Evoked Event-Related Potentials. At: *6th International Brain-Computer Interface Conference 2014*, Graz, Austria, September 16-19.

Conference, Symposium, Workshop and Competition Participation

Member of the Organizing Committee

- 2017 7th Graz Brain-Computer Interface Conference, Graz, Austria, September 18-22
- 2014 6th International Brain-Computer Interface Conference, Graz, Austria, September 16-19

Attendee

- 2017 3rd Alpine Chapter Symposium of the OHBM, Inselspital Bern, Switzerland, November 3-4
- 2017 2nd TU Graz Fields of Expertise Day Human & Biotechnology, Graz, Austria, October 18
- 2017 ARS Electronica – AI Artificial Intelligence – The other I, Booth of the Graz BCI Racing Team MIRAGE91, Linz, Austria, September 7-11
- 2017 1st Special Interest Day Electrotherapy, Vienna, Austria, June 24 (German: 1. Fachtag Elektrotherapie)

- 2016 Austrian Neuroscience Association – Opening Event of the Local Chapter Graz – Connecting Regional Neuroscientists powered by ANA and INGE St., Graz, Austria, November 24
- 2016 1st TU Graz Fields of Expertise Day Human & Biotechnology, Graz, Austria, November 3
- 2016 CYBATHLON Championship for Athletes with Disabilities 2016, Zurich/Kloten, Switzerland, October 8
- 2016 CYBATHLON Symposium, SWISS Arena, Zurich/Kloten, Switzerland, October 6
- 2016 1st Center of Knowledge Interchange (CKI) Conference – Graz University of Technology in Cooperation with SIEMENS, Graz, Austria, May 19
- 2015 1st Computational Life Sciences Day at the 15th International Conference on Knowledge Technologies and Data-Driven Business (i-KNOW2015), Graz, Austria, October 21
- 2015 Symposium on the 10th Anniversary of INGE St., (German: INGE St. Symposium zum 10-jährigen Bestehen), Graz, Austria, October 12
- 2015 37th International Conference of the IEEE Engineering in Medicine and Biology Society, EMBC15, Milano, Italy, August 25-29
- 2015 CYBATHLON Championship for Athletes with Disabilities Rehearsal 2015, Zurich/Kloten, Switzerland, July 13-15
- 2015 BioTechMed-Graz Symposium 2015, Graz, Austria, June 11
- 2014 10th Austrian Curriculum “Functional Brain-Imaging” – Basics, (German: 10. Österreichisches Curriculum "Funktionelle Bildgebung des Gehirns" – Grundkurs), Graz, Austria, December 12
- 2014 36th Annual International Conference of the IEEE Engineering in Medicine and Biology Society, EMBC14, Chicago, Illinois, USA, August 26-30
- 2014 Austrian Computer Science Day 2014, Graz, Austria, June 6
- 2014 BioTechMed-Graz Symposium 2014, Graz, Austria, June 3
- 2014 3rd Styrian Spring School of Neuroscience, Graz, Austria, April 28-30
- 2014 BNCI Horizon 2020 Retreat, Hallstatt, Austria, March 24-26
- 2013 Three Countries Meeting of the German, Swiss and Austrian Society for Biomedical Engineering, BMT2013, (German: BMT (Biomedizinische Technik) 2013 – Dreiländertagung der Deutschen, Schweizerischen und Österreichischen Gesellschaft für Biomedizinische Technik), Graz, Austria, September 19-21
- 2013 TOBI Workshop IV, Practical Brain-Computer Interfaces for End-Users: Progress and Challenges, Sion, Switzerland, January 23-25
- 2012 BBCI Summer School 2012: Brain-Computer Interfacing and Neurotechnology, Berlin, Germany, September 20-28
- 2011 5th International Brain-Computer Interface Conference, Graz, Austria, September 22-24
- 2008 VDE Kongress 2008, Munich, Germany, November 3-5

Referee / Reviewer Activity

Journals

Biomedical Engineering/Biomedizinische Technik, DeGruyter

Biomedical Signal Processing and Control, Elsevier

Human Brain Mapping, Wiley

IEEE Transactions on Biomedical Engineering, IEEE-TBME

IEEE Transactions on Human-Machine Systems, IEEE-THMS

Journal of Neural Engineering, IOP

Neuroimage, Elsevier

Conferences

2018 7th International Brain-Computer Interface Meeting, Asilomar Conference Center, Pacific Grove, California, USA, May 21-25

2017 7th Graz Brain-Computer Interface Conference, Graz University of Technology, Graz, Austria, September 18-22

2016 IEEE International Conference on Systems, Man, and Cybernetics, SMC 2016, Hotel Intercontinental, Budapest, Hungary, October 9-12

2016 6th International Brain-Computer Interface Meeting, Asilomar Conference Center, Pacific Grove, California, USA, May 30-June 3

2014 6th International Brain-Computer Interface Conference, Graz University of Technology, Graz, Austria, September 16-19

2014 36th International Conference of the IEEE Engineering in Medicine and Biology Society, EMBC14, Chicago, Illinois, USA, August 26-30

Membership in Scientific Societies, Associations and Teams

2016-2018 Member of the Austrian Neuroscience Association, Local Chapter Graz

2014-2017 Founding member of the Graz BCI Racing Team Mirage91

2014-2016 Member of IEEE, Engineering in Medicine and Biology Society

2009-2017 Member of OVE, Austrian Electrotechnical Association

Additional Professional Training

2015 Didactics 2: Holding Courses in the Academic Sector
Continuing Education, Graz University of Technology
(German: Didaktik 2: Durchführen von Lehrveranstaltungen im akademischen Bildungsbereich)

2013 Didactics 1: Basics of Teaching and Learning in the Academic Sector
Continuing Education, Graz University of Technology
(German: Didaktik 1: Grundlagen des Lehrens und Lernens im akademischen Bildungsbereich)

- 2013 Organization of Conferences and Meetings
Continuing Education, Graz University of Technology
(German: Organisation von Kongressen und Tagungen)
- 2013 The TU Graz Teach Center: The TU Graz Teaching and Learning Platform
Continuing Education, Graz University of Technology
(German: Das TU Graz Teach Center – Einsatz der TU Graz Lehr- und Lernplattform in der universitären Lehre)
- 2012 Basics of Effective Time Management
Continuing Education, Graz University of Technology
(German: Grundlagen effektiven Zeitmanagements)
- 2012 Welcome Day for New Employees
Continuing Education, Graz University of Technology
(German: Einführungstag für neue Mitarbeiterinnen und Mitarbeiter der TU Graz)
- 2010 Training to Medical Laser Safety Officer according to EN60825
AUVA and Institute of Healthcare Engineering, Graz University of Technology

Media Appearance

- 2017 Cybathlon with support of robots
Thema, ORF, Vienna, Austria, March 27
(German: Cybathlon mit Roboterunterstützung)
- 2016 Human, machine and swiss competition atmosphere
"Talking about..." - TU Graz blog, Graz, Austria, October 13
(German: Mensch, Maschine und Schweizer Wettkampfstimmung)
<https://www.tugraz.at/tu-graz/services/news-stories/talking-about/einzelansicht/article/mensch-maschine-und-schweizer-wettkampfstimmung/>
- 2016 "Cybathlon": Human-machine-competition in Zurich as audience magnet
Tiroler Tageszeitung, Innsbruck, Austria, October 8
(German: "Cybathlon": Menschmaschinen-Wettbewerb in Zürich als Publikumsmagnet)
<http://www.tt.com/home/12109528-91/cybathlon-menschmaschinen-wettbewerb-in-z%C3%BCrich-als-publikumsmagnet.csp>
- 2016 With the power of thoughts through all barriers
Kleine Zeitung, Graz, Austria, October 7
(German: Mit der Kraft der Gedanken durch alle Hindernisse)
http://www.kleinezeitung.at/steiermark/steirerdestages/5097681/Steirer-des-Tages_Muehsam-zurueck-ins-Leben
- 2016 Using thought power for competition
Die Presse, Vienna, Austria, October 7
(German: Mit Gedankenkraft den Wettkampf bestreiten)
<https://diepresse.com/home/science/5098382/Mit-Gedankenkraft-den-Wettkampf-bestreiten>
- 2016 Cybathlon: Competition of the Human-Machines in Zurich
Austria Presse Agentur, Vienna, Austria, October 6
(German: "Cybathlon": Wettkampf der Menschmaschinen in Zürich)
https://www.science.apa.at/rubrik/natur_und_technik/Cybathlon_Wettkampf_der_Mensch_maschinen_in_Zuerich/SCI_20161006_SCI39391351432349876
- 2016 Brain controls computer: Students of TU Graz start at the Cybathlon in Zurich
Ausseer Regionalfernsehen, Bad Aussee, Austria, October 3
(German: Gehirne steuern Computer: Studierende der TU Graz starten am 8. Oktober beim Cybathlon in Zürich)

- 2016 VAMED and Team Mirage 91 of TU-Graz at Cybathlon 2016
 Promo video of VAMED, Vienna, Austria, August 2
 (German: VAMED und Team Mirage 91 der TU-Graz am Cybathlon 2016)
<https://www.youtube.com/watch?v=AxUWNM6BS0E>
- 2016 Brain controls computer: Styrian starts at “Cybathlon” in Swiss
 Austria Presse Agentur, Graz, Austria, July 19
https://www.science.apa.at/rubrik/natur_und_technik/Gehirn_steuert_Computer_Steirer_tritt_bei_Cybathlon_in_Schweiz_an/SCI_20160719_SCI39391351430917142
 Shortened and/or renamed versions of this article where published in:
 - Austria.com, Schwarzach, Austria, July 19
 - Futter, Graz, Austria, July 19
 - Kleine Zeitung, Graz, Austria, July 19
 - Krone, Vienna, Austria, July 19
 - Neues Volksblatt, Linz, Austria, July 20, p. 16
 - ORF Science, Vienna, Austria, July 19, <http://science.orf.at/stories/2786506/>
 - ORF Steiermark, Vienna, Austria, July 20, <http://steiermark.orf.at/news/stories/2786558/>
 - Salzburger Nachrichten, Salzburg, Austria, July 19
 - Tiroler Tageszeitung, Innsbruck, Austria, July 19
 - UnserTirol24.com, Neumarkt, Austria, July 19
 - Vorarlberg Online, Schwarzach, Austria, July 19
 - economy, Wagram, Austria, September 30, <http://economy.at/forschung/human-machine>
 (German: Gehirn steuert Computer: Steirer tritt bei “Cybathlon” in Schweiz an)
- 2016 The countdown is running (Cybathlon)
 Radio Soundportal & Uni Webradio, Graz, Austria, July 1
 (German: Der Countdown läuft)
- 2016 A Life-Science-Tour de Force through Graz
 Medical Tribune, No. 23, Vienna, Austria, June 8, p. 12
 (German: Eine Life-Science-Tour de Force durch Graz)
- 2016 The human-machine becomes reality
 derStandard, Vienna, Austria, May 27
 (German: Die Mensch-Maschine wird Realität)
<https://derstandard.at/2000037587773/Die-Mensch-Maschine-wird-Realitaet>
- 2015 They "control" games with thoughts
 Kleine Zeitung, Graz, Austria, October 22, p. 30
 (German: Sie “steuern” Spiele mit Gedanken)
- 2015 TU Graz-students with full speed ahead
 TU Graz people, No. 54/2015-2, Graz, Austria, pp. 4-5, ISSN: 2076-748X
 (German: TU Graz-Studierende geben Vollgas)
https://www.tugraz.at/fileadmin/user_upload/tugrazInternal/News_Stories/Print/people/pdf/tugrazpeople_54.pdf
- 2015 TU Austria – Austria's engineering students are world class
 TU Austria, Mai, pp. 6-7
 (German: TU Austria – Österreichs Technik-Studierende sind Weltklasse)
http://www.tuaustria.ac.at/fileadmin/shares/tuaustria/docs/TU_Austria_Studierendeninit-Web3.pdf
- 2014 Find the liar – Science fiction
 Galileo TV Magazine, ProSieben, August 19
 (German: Finde den Lügner – Science Fiction)
<http://www.prosieben.at/tv/galileo/videos/6219-finde-den-luegner-science-fiction-clip>

Vienna, Oct 2018